Mechanism of Collision-Induced Decomposition of Gaseous Multiatomic Ions

Caroline Davina Bradley

Submitted for the qualification of Doctor of Philosophy

University of Warwick
Department of Chemistry

March 1992

Contents

Chapter 2: INSTRUMENTATION AND EXPERIMENTAL METHODS

List of Tables

List of Figures

Acknowledgements

I am deeply grateful to Professor Peter Derrick, my academic supervisor, for his guidance and assistance throughout the course of this work.

Kratos Analytical sponsored my work as part of a Science and Engineering Council CASE award. I am grateful to Mr S. Evans, my industrial supervisor, for his constructive criticisms and suggestions, and also to Dr B. Wright, for his help and enthusiasm during my industrial project.

Dr Einar Uggerud and Bal Dhesi helped me with the normal mode analysis.

For his practical help and suggestions with the experiments on the large-scale mass spectrometer (and the many opportunities to unwind at social events at his home!) my many thanks go to Alex Colburn.

Jonathan Curtis assisted me with the four-sector mass spectrometry. I am also particularly grateful for his skills in shaping several publications.

Dominic Chan, Desmond Yau, Dr David Reynolds, Dr John Trainor and Anastassios Giannakopulos, my work colleagues, have been good companions, inspiring both enthusiasm and helpful discussions .

My family and friends have been a constant source of support throughout my research. I particularly wish to thank my parents, Rosemary and Geoff Bradley, for their continuous encouragement throughout my education, and my partner, Phil Edwards, for his advice concerning the statistical elements of this thesis, his help with the preparation of figures, and many patient hours of proof reading.

Declaration

I hereby declare that this thesis is my own work and that, to the best of my knowledge and belief, it contains no material previously published or written by another person, nor material which to a substantial extent has been accepted for the award of any other degree or diploma of a university or other institute of higher learning, except where due acknowledgement is made in the text.

Caroline Davina Bradley

"For we are as treetrunks in the snow. They appear to lie flat on the surface, and with one little push one should be able to shift them. No, one cannot, for they are fixed firmly to the ground. But look, even that is mere appearance."

"The Trees" by Franz Kafka, Betrachtung; written between 1904 and 1912.

List of abbreviations and frequently used terms

Ala	**Alanine**
CID	**Collision-induced decomposition**
Da	**Daltons**
EHC	**Field desorption emitter heating current**
EI	**Electron impact ionisation**
ESI	**Electrospray ionisation**
FAB	**Fast-atom bombardment**
FD	**Field desorption**
Gly	**Glycine**
Hyv or H	**Hydoxyisovaleric acid**
ICT	**Impulsive collision theory**
Lac or L	**Lactic acid**
Leu	**Leucine**
MALDI	**Matrix-assisted laser desorption/ionisation**
Met	**Methionine**
MIKES	**Mass-analysed ion kinetic energy spectroscopy**
MS/MS	**Tandem mass spectrometry**
m/z	**Mass-to-charge ratio**
PD	**Plasma desorption**
Phe	**Phenylalanine**
QET	**Quasi-equilibrium theory**
RMM	**Relative molecular mass**
Trp	**Tryptophan**
Tyr	**Tyrosine**

Val or V	Valine
a_n, b_n, c_n, x_n, y_n, z_n, w_n, v_n, d_n	Abbreviations to describe the fragment ions of linear peptides (see Section 1.6.1)
$k(E)$	Microcanonical rate constant
E	Internal energy available to a reactant ion
E_o	Critical energy for a reaction
ΔE	Translational energy lost by incident/parent ions during collision with the target gas
Q	Internal energy uptake by the incident ion as as result of collision with the target gas
E_R	Recoil energy of target gas atom
V_c	Calculated electric sector analyser potential required for transmission of fragment ions formed by CID based on a proportion of the incident ion energy
V_m	Measured electric sector analyser potential required for transmission of fragment ions formed by CID.
V_i	Electric sector analyser potential required for transmission of incident ions with translational energy E_i.
m_i	Mass of incident ion
m_f	Mass of fragment ion
ΔV	Difference between calculated and measured electric sector analyser potentials required for transmission of fragment ions formed by CID.
E_i	Translational energy of parent ions prior to collision - incident ion energy/laboratory frame collision energy
E_{cm}	Centre-of-mass frame collision energy
m_g	Mass of target gas
ΔE_{max}	Maximum possible translational energy loss as a result of collision

θ_l	Angle to the original ion beam path through which incident ions are scattered (in the laboratory frame of reference)
m_a	Mass of atom within the ion which is directly hit by the target gas atom
m_{int}	Mass of part of the ion which is directly involved in the collision with the target gas atom
n_f	Total number of detected fragment ions
n_p	Total number of detected parent ions

Abstract

The mechanism of collision-induced decomposition (CID) has been studied for ions with masses up to 2000 Da. Mass-analysed ion kinetic energy spectroscopy (MIKES) on a large-scale reverse-geometry mass spectrometer was used to measure translational energy losses (ΔE) by parent ions in collision with inert gas atoms during CID. To avoid ambiguities in mass assignments due to these energy losses, these assignments were made using a four-sector mass spectrometer.

Translational energy losses were found to have different dependencies on collision gas pressure depending on the fragment ion formed. The results suggest that tens of electronvolts of translational energy are lost during each collision between ion and target gas, which is consistent with energy uptake via direct momentum transfer. Multiple collisions are thought not to play a major role in CID of large organic ions. Increasing the incident ion energies from 8 to 25 keV resulted in considerable improvements in fragmentation efficiency, suggesting increased internal energy uptakes. These were more dramatic with increasing incident ion mass.

Comparisons of four-sector tandem mass spectra of the peptides valinomycin and valine-gramicidin A show how additional structural information may be obtained by using a number of different ionisation methods and also different molecule-ions. The use of collision energies of up to 400 eV with argon as target gas on a hybrid mass spectrometer have produced tandem mass spectra which closely resemble those obtained with keV collision energies on the four-sector mass spectrometer using helium as target.

Quasi-equilibrium theory (QET) has been used to calculate the dependence of rate constants on internal energy as the sizes of molecule-ions increase. For an ion of mass approximately 1900 Da, QET predicts that internal energies of the order of many tens of eV are required for dissociation to take place within the experimental time-scale.

Chapter 1 : INTRODUCTION

1.1 OVERVIEW

The potential of collision-induced decomposition (CID) as an analytical technique has been recognised since the 1960's, when it was observed that the introduction of a gas into a mass spectrometer could increase the abundance of metastable ions.[1] Ideally, ions of interest, referred to as incident ions or parent ions, are mass-selected into a collision region into which a gas has been introduced. The most commonly employed collision/target gases are the inert gases. Collision of the incident ions with gas atoms/molecules results in an uptake of internal energy by the incident ion which may subsequently dissociate. If dissociation takes place within the time-scale of the experiment, the resulting fragment ions may be mass-analysed and the tandem mass spectrum recorded (i.e. two stages of mass analysis have taken place).

Until the development of the ionisation techniques of field desorption (FD),[2] fast-atom bombardment (FAB) [3] and plasma desorption (PD),[4] tandem mass spectrometry (MS/MS) had been limited to volatile substances and hence had been restricted for the most part to small polyatomic ions with masses of up to a few hundred Daltons (Da). Since the development of these techniques for ionisation of non-volatile substances, the mass range of tandem mass spectrometry has been extended to a few thousand Daltons. Tandem mass spectrometry has been applied to a wide range of analytical problems,[5] the most well known of which are the biochemical applications,[6,7] such as determination of peptide sequences.[6-9] Over the past few years another revolution has taken place in the ionisation methods available. With the development of the

techniques of electrospray (ESI) [10-12] and matrix-assisted laser desorption / ionisation (MALDI),[13] molecules with masses in excess of 100,000 Da have been successfully ionised and mass-analysed. Concern has been expressed in the past as to the decreasing efficiency of CID with increasing incident ion mass.[14] At present the upper limit for the successful use of CID is generally agreed to be at best around 3000 Da. Hence the usefulness of CID in conjunction with MALDI and ESI is questionable. To improve the efficiency of CID a better understanding of the mechanism involved is required. The energetics and dynamics of CID have been more thoroughly investigated for small polyatomic ions and several reviews have been published which outline the current understanding of the mechanisms of CID,[16-18] but for ions with masses > 500 Da the mechanisms involved are still not at all certain.[19]

1.2 DISSOCIATION OF IONS :- QUASI-EQUILIBRIUM THEORY

Collision-induced decomposition (CID) is usually considered to occur in two steps separated in time: excitation as a result of collision followed by unimolecular dissociation. The ion and target are considered to have had sufficient time to separate prior to dissociation, since the time scale of their interaction is of the order of 10^{-14} s (for kiloelectronvolt (keV) incident ion energies of an ion of mass 2000 Da and assuming an interaction length of 10 Å) compared to the fastest possible dissociation rate of $\sim 10^{-14}$ s i.e. the shortest vibrational period. Since dissociation is treated as a unimolecular process, the rate can be calculated using quasi-equilibrium theory (QET).[20-22] QET was developed at the same time as Rice, Ramsperger, Kassel and Marcus (RRKM) theory.[22,23] The two theories are similar, both being statistical in nature and based upon the same assumptions. QET assumes rapid randomisation of the internal energy over the vibrational and rotational states of the ion, and the dissociation step is therefore independent of the detailed mechanism of energy

uptake. QET had been successfully applied to decomposition reactions observed in electron impact (EI) mass spectra. It was suggested that QET would also be applicable to the reactions observed in CID due to the similarities between EI mass spectra and CID spectra.[1,24] The microcanonical rate constant $k(E)$ is given by

$$k(E) = \frac{\alpha\, G^{\ddagger}(E - E_o)}{h\, N(E)} \qquad (1.1)$$

where E is the internal energy of the reactant ion and E_o the critical energy for the reaction. h is Planck's constant, α is the reaction path degeneracy, $G^{\ddagger}(E - E_o)$ is the total number of vibrational and rotational states available to the transition state in the energy range $E - E_o$ and $N(E)$ is the density of quantum states, i.e. the number of states per unit energy at the internal energy E. Calculations of $k(E)$ are usually simplified by consideration of vibrational states only. A description of the use of Equation 1.1 for calculating $k(E)$ is described later in Chapter 2.

QET assumes that the rate of dissociation is slower than the rate of internal energy randomisation over the vibrational modes of the ion. The excitation energy is therefore presumed to be statistically distributed over all the internal modes. For small polyatomic ions randomisation of energy has been proposed to take place on the time scale of 10^{-12} s.[25] As the mass of the incident ion increases (and correspondingly the number of vibrational modes increases) then for a fixed internal energy and critical energy, the energy per vibrational mode will fall. The rate of dissociation will then be slow compared to a small ion and will decrease with increasing number of internal modes. This has important implications for CID of very large ions in that the rate of dissociation may become too slow to be observed within the time-scale of the mass spectrometer. Schlag and Levine [26] found that a faster than QET rate was required to describe the

dissociations of large molecules. This was said to be due to bottlenecks to energy randomisation and the available phase space being too large to allow dissociation from a statistical distribution of internal energy over all vibrational modes. Bunker and Wang [27] have also discussed the limiting behaviour of QET rate constants. Rates of dissociation were found to approach zero for bond breaking near the middle of a long-chain molecule, but were finite near the ends of the molecule and for ring-opening reactions. The experimental results of Craig and Derrick [28] show agreement with these theoretical results. Polystyrene chains with masses >100 Da were shown to fragment near the ends of the chain.[28] For peptide ions with ~50 positive charges, Loo *et al.*[29] also found that the majority of fragment ions formed corresponded with dissociations occurring near the ends of the molecules. Theoretical calculations with considerations of the Coulombic forces involved for multiply charged ions, suggest that as the number of charge states increases, rates of dissociation increase and cleavages near the centre of the molecules will become more important.[30]

1.3 Mechanisms of Energy Transfer

The collisions of interest between incident ions and target gas atoms/molecules are inelastic and involve a loss of translational energy ΔE. A proportion of this translational energy loss ΔE results in the internal energy uptake Q of the system (ion and target) and the remainder, assuming no internal energy is taken up by the target, is imparted as recoil energy of the target gas, E_R, such that

$$\Delta E = Q + E_R \qquad (1.2)$$

It is generally assumed that target gas excitation does not occur when inert gases are employed. The two most important questions concerning the energetics of CID are how much internal energy is taken up by the incident ion and what is the mechanism of this energy uptake. For small polyatomic ions

much work has been carried out recording translational energy loss spectra.[31] Reverse-geometry mass spectrometers have been used to measure the translational energies of the product ions of CID by the so-called mass analysed ion kinetic energy (MIKE) technique, which makes use of the energy analysing properties of a cylindrical electric field.[32,33] The electric sector analyser (ESA) potential required to produce the electric field strengths necessary for transmission of product ions V_m differ from the expected values V_e by an amount ΔV. The expected ESA potentials assume zero translational energy loss and are given by

$$V_e = V_i (m_f / m_i) \qquad (1.3)$$

where V_i is the ESA potential required to transmit undissociated incident ions and m_f and m_i are the masses of the fragment and incident ions respectively. ΔV was related to the translational energy loss of the incident ions by[32,34,35]

$$\Delta E = (m_i / m_f) (\Delta V / V_i) E_i \qquad (1.4)$$

where E_i is the laboratory frame translational energy of the incident ion. Translational energy losses for small polyatomics have been measured of up to 20 eV for certain high energy decomposition pathways.[31,36] In the ideal case of no scattering of the incident ion and negligible recoil energy of the target the translational energy loss is approximated to the internal energy uptake of the incident ion.[16,32,37]

The mechanisms for conversion of translational energy to internal energy were outlined by Durup [38] for diatomic and small polyatomic ions and have been discussed further elsewhere.[5,16-18] The mechanisms of internal energy uptake for these small ions can be divided into the following categories: electronic excitation, direct vibrational excitation, and vibrational excitation involving a long-lived ion-molecule complex.

1.3.1 Electronic excitation

Electronic excitation involves a vertical transition between the electronic ground state and an excited state of the ion. Rapid radiationless transitions may then occur to leave the ion in a vibrationally excited state from which dissociation may occur. The cross-section for electronic excitation is high, i.e. electronic excitation is most likely to occur, when the interaction time between ion and target is appropriate. This has been described using the Massey criterion:[16,17,39]

$$R_M = t_c / \tau \qquad (1.5)$$

where t_c is the interaction time and τ the period of the motion being excited. t_c is the ratio of v the velocity of the ion to a the interaction distance (adiabatic parameter) and τ the ratio of h, Planck's constant to the difference in energy between the initial and final states of the ion. If $R_M >> 1$ the interaction time is relatively long and the electrons have time to adjust adiabatically during the collision making electronic excitation improbable. If $R_M \leq 1$ collisions are non adiabatic and the probability for energy transfer via electronic transitions is large.[39-41] Electronic excitation is most likely for small ions with keV incident ion energies, for example, an ion of mass 100 Da and with 8 keV translational energy will have an interaction time with an atomic target of approximately 4×10^{-15} s (assuming an interaction length of 4 Å). This compares with the time for electronic motion which is of the order of 10^{-15} s and hence electronic excitation is favourable. As the mass of the incident ion increases then at a fixed translational energy the velocity is correspondingly lower, making this mechanism of excitation less probable.

1.3.2 Direct vibrational excitation

There are two models describing energy transfer via conversion of translational energy to the vibrational/rotational modes of the ion. The impulse model involves

direct momentum transfer to the vibrational/rotational states of the ion. One atom or a part of the ion is considered to undergo a collision with one atom or a part of the target, with the remaining parts acting as spectators to the collision event.[42,43] Such a mechanism is associated with a small impact parameter and will be associated with large scattering angles due to the repulsive potentials involved. This model was developed further by Mahan [44] to give closer agreement with experiment at higher energies. An impulsive mechanism of excitation is expected to occur when the interaction time between ion and target is > 10^{-14} s, and hence the electrons have time to adjust adiabatically.

A second mechanism for vibrational excitation is the Russek mechanism.[45] An induced dipole in the target interacts with a permanent or induced dipole in the incident ion, resulting in vibrational/rotational excitation. The impact parameter associated with this mechanism is large, resulting in negligible scattering and small translational energy losses.

1.3.3 Vibrational excitation involving a long-lived ion-molecule complex

If the interaction between ion and target involves a deep potential well in the potential energy surfaces then the formation of an ion-molecule complex may occur if the collision energy is sufficiently low.[46] The cross-sections for the formation of ion-molecule complexes have been described by a number of theories. The classic Langevin theory neglects polarisation of the interacting molecules.[47] Other theories have been developed which consider the interaction between ion and dipole [48-52] and have been summarised recently by Castleman and Hsieh.[53]

1.3.4 Mechanism of CID of large ions

The above mechanisms have been used for describing CID of diatomic and small polyatomic ions. The suitability of using these mechanisms to describe excitation

of large ions has been the subject of much debate in recent years. Most sector mass spectrometers operate with laboratory frame collision energies of 4 - 10 keV. On the basis of the Massey criterion, collisional activation of small polyatomic ions is most likely to occur via electronic excitation. It was generally assumed that the same mechanism of excitation would be extended to larger ions. As the mass of the incident ion is increased, however, the interaction time between ion and target increases and electronic excitation becomes less probable. The interaction time between a biological ion of mass 2000 Da and an atomic target is of the order of 10^{-14} s for an incident ion energy of 8 keV, assuming an interaction length of 10 Å. The collision interaction time is therefore on the time-scale of molecular vibrations 10^{-12} - 10^{-14} s. There is now a trend towards describing the mechanism of internal energy uptake for CID of large ions with masses > 1000 Da at keV incident ion energies, as being via vibrational excitation.[17,18] Uggerud and Derrick [54] have developed an impulsive collision theory for large ions (based on conservation of energy and momentum) which gives a relationship between the internal energy uptake Q and the translational energy loss ΔE (discussed further in Section 1.4.5).

1.4 CID OF LARGE IONS AT keV TRANSLATIONAL ENERGIES

1.4.1 Nature of target gas

The maximum energy available to an ion in collision with a target is limited by their relative translational energies, known as the centre-of-mass collision energy E_{cm}. The laboratory frame translational energy of the target is assumed to be zero and E_{cm} is then given by

$$E_{cm} = \frac{m_g}{m_i + m_g} E_i \qquad (1.6)$$

where E_l is the translational energy of the incident ion and m_l and m_g are the masses of the incident ion and target gas respectively. The decreasing efficiency of CID as the mass of the incident ion increases is attributed to the decreasing centre-of-mass collision energy, assuming that all other factors remain equal. Table 1 shows a comparison of the centre-of-mass collision energies for ions of various masses with 8 keV incident ion energy in collision with some of the most commonly employed targets.

TABLE 1

TARGET	CENTRE-OF-MASS COLLISION ENERGIES / eV (For a laboratory frame incident ion energy E_l= 8 keV)			
	acetone m_l=58 Da	valine gramicidin A m_l=1882 Da	bovine insulin m_l=5733 Da	cytochrome C m_l=12360 Da
Helium (m_g=4Da)	516.1	17.0	5.6	2.7
Argon (m_g=40Da)	3265.3	166.4	55.4	25.8
Xenon (m_g=131Da)	5545.0	520.6	178.7	83.9

The centre-of-mass collision energies for large ions are relatively small compared to small polyatomic ions yet QET predicts that larger ions will require more internal energy in order to dissociate with a similar rate. Schlag and Levine [26] estimate that an ion with 1000 vibrational modes would require 70 eV of internal energy to dissociate with a rate of 10^6 s^{-1}. This number of vibrational modes would correspond to a biological molecule with a mass of approximately 2000 Da. Unless heavier targets are employed, ions of mass > 1000 Da may have insufficient centre-of-mass collision energy available for conversion to internal energy Q in order to dissociate on the experimental time-scale. The use of heavier targets has the obvious disadvantage of increased scattering of the incident ions which may result in the fragment ions being scattered outside the acceptance angle of the second stage of mass analysis, and thus resulting in decreased

sensitivity. The option of electrically floating the collision cell to positive potentials (kV) although reducing the incident ion energy, helps re-focus some of the scattered ions and results in less discrimination against low-mass fragment ions.[55]

For small polyatomic ions, helium was the preferred target due to reduced ion losses from scattering and charge exchange.[56,57] Studies of larger ions have often found heavier targets to be preferable. Curtis *et al.*[58] report argon or xenon to be preferential to helium as targets for incident ions with masses 1500 - 2500 Da. Increased relative intensities of low-mass fragment ions were shown. In the range of incident ion masses of 500 - 1500 Da, a mixture of both gases is recommended, to produce both intense high and low mass fragment ions.[58] Bordas-Nagy *et al.*[59] in a study of over 20 peptides on a 4-sector tandem mass spectrometer with an electrically floated collision cell, found that argon was a preferable target to helium for ions with masses > 1500 Da, except in the cases where the peptide contained a basic amino acid when helium was equally as good. Use of argon as a target gave increased sensitivity and gave relative increases in the intensity of some structurally important fragment ions.

1.4.2 Translational energy losses ΔE

In the early 1980's Derrick *et al.*[60,61] reported very large translational energy losses of the order of many tens of electronvolts for singly charged peptide ions with masses 500 -1650 Da in collision with helium. For large ions, these large translational energy losses manifested themselves as considerable apparent mass shifts (several Da) in the MIKE spectrum. There was some question as to the accuracy of these measurements due to the low resolution of the MIKE technique i.e. neighbouring fragment ion peaks may have been contributing to the mass shifts. The occurrence of these large energy losses was later confirmed by other workers.[62,63] The question as to how much of this translational energy loss

manifests itself as internal energy of the ion has been the subject of much speculation. Derrick and co-workers [60] attribute the energy losses to large amounts of internal energy uptake resulting from a single collision between ion and target. In contrast Russell [64] has argued that they result from multiple collision processes and that target gas excitation is the predominant sink for this energy.[62] The results of these studies will be discussed in more detail below.

Derrick *et al.*[60,61] showed that the average translational energy losses increased with increasing incident ion mass in a study of incident ions with masses up to 1618 Da. The optimum collision gas pressure for producing maximum fragment ion abundances was found to be independent of the fragment ion mass, but decreased as the mass of the incident ions increased despite the transmission (the ratio of the incident ion intensity before and after addition of collision gas) remaining the same. It was argued that these findings weighed against the likelihood of multiple collisions.

Bricker and Russell [62] in a study of the chlorophyll-*a* molecular ion (RMM = 892.5) showed ΔE to decrease as the target was changed from He to Ne, Ar and Kr. ΔE decreased with increasing ionisation energy of the target and it was concluded that target gas excitation and CID were in competition.[62,65] Correspondingly, internal energy uptake by the incident ion as a result of CID would represent only a small proportion of the overall energy loss ΔE. This interpretation has also been used to explain the observed decrease in the efficiency of CID with increasing incident ion mass since the cross-section for charge transfer to the target increases as the mass or velocity of the incident ion increases. This work has since been re-investigated by Alexander *et al.*[66] who found the earlier work to be in error due to the contributions to the peaks used for measuring the translational energy losses from metastable fragment ions. The use of an electrically floated collision cell ensured separation of the metastable component of the fragment ion peaks and it was shown that the relationship was

with target gas mass rather than ionisation energy. Translational energy losses for helium and deuterium were similar despite the ionisation energy of deuterium being closer to that of argon.[66,67]

A later study by Sheil and Derrick [68] of the peptide valine-gramicidin A (RMM = 1881.2) showed measurements of the translational energy losses ΔE associated with individual fragment ions. ΔE was shown to differ depending on the fragment ion used to measure its value, and in general was found to increase as the mass of the fragment ion decreased. That ΔE should vary depending on the fragment ion studied, is consistent with the different critical energies associated with different dissociation pathways. Extremely large energy losses of up to 1200 eV were measured for some very low-mass fragment ions. These energy losses were far in excess of the maximum possible energy loss ΔE_{max} as given by the laws of conservation of energy and momentum for elastic collisions ($Q = 0$)[69]

$$\Delta E_{max} = \frac{4\, m_i\, m_g\, E_i}{(m_i + m_g)^2} \qquad (1.7)$$

These extremely large energy losses were attributed to multiple and sequential collisions. Multiple collisions are defined as being when the incident ion collides a number of times with target gas atoms prior to dissociation. The observed energy loss, ΔE, is then equal to the sum of the individual energy losses associated with each collision. The term 'sequential collisions' will be used to describe when an incident ion collides with a target gas atom, dissociates and the resulting fragment ion may then collide with gas atoms and in turn undergo CID. The observed energy loss is then dependent on each intermediate energy loss amplified by the ratio of m_i/m_f and may become extremely large for small fragment ions, despite the individual energy losses being of the usual magnitude. These studies of the translational energy lost by incident ions have lead to the

conclusion that CID of large ions at keV ion energies is via vibrational excitation.[64,69-71]

The largest ions for which translational energy losses have been measured have been the molecule-ions of cytochrome C (RMM = 12360) formed by MALDI.[72] CID of these ions was performed in a time-of-flight mass spectrometer using water and helium as targets. Results were obtained by detection of undissociated parent ions and of the neutral fragments formed in the CID process. The time-of-flights of the undissociated parent ions and neutrals showed comparable translational energy losses in the case of helium as target. With water as target, the surviving parent ions showed negligible energy losses and the neutrals showed larger energy losses than in the helium case. These results imply that all collisions with water resulted in dissociation whereas only a small proportion of collisions with helium resulted in fragmentation. These results contradict those discussed above where translational energy losses were found to be largest for helium as target.

1.4.3 Multiple collisions

Multiple collisions may also be used to increase the internal energy uptake since multiple amounts of the centre-of-mass collision energy are made available to the incident ion. The disadvantages of multiple collisions are the increased possibilities of ion losses due to scattering, possibility of de-activation of the ion, and of charge-exchange between ion and target. Studies on small polyatomic ions revealed that the CID cross-section increased on increasing the incident ion energy.[73] Todd and McLafferty [74] showed that the CID spectrum of methane recorded with E_l = 9.8 keV at a transmission of 8.5% resembled that at E_l = 64 keV under single collision conditions.

A fundamental question in understanding the dynamics of CID concerns the number of collisions which occur at the optimum target gas pressure. This will

also have important consequences for the calculation of internal energy uptakes from energy loss values. For large ions the argument as to the number of collisions occurring under normal conditions of transmissions of 20 - 40% remains unresolved. Derrick and co-workers[60,61,68,75] conclude that predominantly single collisions occur at transmissions of > 40 %, however at slightly higher gas pressures multiple and sequential collisions may contribute to the extremely large energy losses that have been observed (see Section 1.4.2). In contrast Russell *et al.*[64,76,77] argue that at 40 % transmission, on average > 5 collisions occur. Kim [78,79] has predicted relative abundances of fragment ions of the methane molecular ion using Poisson statistics to calculate the probability of collisions occurring and has taken into account the effects of sequential collisions and also the cross-section for ion loss processes.

1.4.4 Incident ion energies

A further method for increasing the centre-of-mass collision energy, in an attempt to increase the internal energy uptake of large ions, is to increase the incident ion energy. Increasing the laboratory frame collision energy of the peptide valine-gramicidin A to 24 keV as compared to 8 keV would result in an increase in E_{cm} to 51 eV from 17 eV for collision with helium, making it comparable to an 8 keV collision with argon as target. Increasing incident ion energy is a less preferable method of increasing the centre-of-mass collision energy since it requires instrument modifications and the use of higher potentials results in the increased likelihood of electrical breakdowns. Shell [69] reported increased translational energy losses for this peptide as the incident ion energy was increased to 15 keV. Above this value no further significant increases were observed despite the continuing increase in the fragmentation efficiency. Fragmentation efficiency is defined as the ratio of the current of fragment ions arriving at the detector to incident ion current entering the collision region, I_f/I_o. The fragmentation efficiency increased from 0.06 to 0.19 on increasing E_l from 8 to 20 keV. This

improvement could not be entirely attributed to a decrease in ion losses resulting from scattering and charge transfer. It was therefore suggested that increases in internal energy uptake may occur on increasing the collision energy.

A study of the variation of the relative intensities of fragment ions with incident ion energy in the tandem mass spectra of peptides has been made by Martin *et al.*[80] There were no significant variations over the range of E_l = 5 - 10 keV, but at incident ion energies of only a few keV, fragment ion peaks due to sequence ions involving side-chain fragmentations decreased in relative intensity or disappeared totally. Such side-chain specific fragmentations are thought to arise as a result of charge-remote processes and to be associated with high energy requirements.[81]

1.4.5 Internal energy uptake

The internal energy Q taken up by large ions as a result of CID is yet another unknown quantity. For small polyatomic ions ΔE was often directly equated with Q, since the recoil energy of the target was assumed to be negligible (Section 1.3). With large ions, this assumption can no longer be made. No experiments have been performed which allow the exact measurement of the internal energy uptake by large ions. Various theories have been used to predict the proportion of the translational energy loss ΔE which results in internal energy of the ion. ΔE may be related to Q by consideration of the collision as involving the whole ion and target and by applying the laws of conservation of energy and momentum. This leads to the expression[43]

$$Q = [(m_i + m_g) \Delta E / m_g] - [(2 m_i E_l / m_g)(1 - [(E_l - \Delta E) / E_l]^{1/2} \cos \theta_l)] \quad (1.8)$$

where θ_l is the scattering angle of the incident ion.

Recently, an impulsive collision theory (ICT) has been developed by Uggerud and Derrick [54] which considers the binary interaction between an atom

in the ion and an atomic target. ICT relates Q to the experimentally observed quantity ΔE via

$$Q = (\mu / 2\varepsilon)\ \Delta E \qquad (1.9)$$

where μ and ε are given by

$$1/\mu = 1 - [(m_a\, m_g)/(m_i\,(m_a + m_g))] \qquad (1.10)$$

$$\varepsilon = [(m_a + m_g)/2m_g\ ][(m_i + m_a)/m_i\ ] \qquad (1.11)$$

in which m_a is the mass of the atom in the ion which is involved in the collision. Both ICT and Equation 1.8 predict that the average value of ΔE would increase with increasing incident ion energy. This is consistent with the experimental observations of Sheil.[69] The internal energy uptake Q will also be expected to increase with increasing incident ion energy. Q is expected to decrease with increasing mass of the incident ion and from Equation 1.9, ΔE would also be expected to decrease. This contradicts experimental findings, where ΔE was observed to increase with increasing incident ion mass.[60] A further prediction of ICT was that the efficiency of energy transfer, χ, to the ion would be dependent on the masses of the two interacting atoms:

$$Q_{av} = {}^1/_2\, \chi\, E_{cm} \qquad (1.12)$$

where Q_{av} is the average amount of energy transferred and χ is given by

$$\chi = 4\,(m_a\, m_g)/[(m_a + m_g)^2] \qquad (1.13)$$

Energy transfer would be most efficient when the masses of the target atom and atom of the ion involved are similar, but the observed energy losses were predicted to increase with increased target gas mass. It was suggested that for biological molecules, where the average mass of atoms is around 7 Da, helium

would compensate for the lower centre-of-mass collision energy compared to argon or xenon, by the increased efficiency of energy transfer. This latter point contradicted experimental findings which may have been due to increased scattering outside of the acceptance angle of the mass spectrometer with the heavier targets . Since Q was shown to increase with increased scattering angle the range of experimentally observed energy losses was shown to decrease with increasing target gas mass. Comparisons of ICT with molecular dynamics calculations showed good agreement but both were described as less reliable for the heavier targets. It was suggested that this may have been a consequence of the two step model being less applicable and that for very large targets a binary assumption may also be less valid; fragmentation may be immediate on collision resulting in the production of numerous small fragments. Some evidence for this suggestion has been shown by Wesdemiotis [82] who, in neutralisation-reionisation experiments of the peptide leucine-enkephalin, found that the neutrals formed were no larger than di-amino acid units whereas the charged fragments covered the whole mass range.

1.5 CID OF LARGE IONS AT eV TRANSLATIONAL ENERGIES

The mechanism of CID for large ions at electronvolt incident ion energies has been generally assumed to be similar to that of small polyatomic ions. At these energy regimes,[83] CID of small polyatomic ions has been attributed to vibrational excitation [38] due to the relatively long interaction times involved during the collision. Vibrational energy transfer may occur as a result of direct momentum transfer in an impulsive collision or via the formation of a long-lived collision complex with subsequent energy randomisation. Douglas [83] developed a statistical theory to describe collisional activation of polyatomic ions via complex formation. This theory was based on the phase space theory developed by Light [84] to describe the cross-section for reactive ion-molecule collisions. Comparison

of experimental results for the dependence of CAD cross-sections on ion translational energy with theoretical predictions, made using the momentum transfer model and the statistical model, showed cross-sections to be intermediate between both models. It was suggested that translational energy may not be completely randomised in the collision complex prior to dissociation. Eastes and Toennies [85] also developed a statistical theory to describe rotationally and vibrationally inelastic collisions but which could be applied to both the direct mechanism of excitation by an impulsive model and also to ion-molecule complex formation.

Comparison of CID spectra recorded with keV and eV incident ion energies has shown that the efficiency of low-energy CID for promoting fragmentations decreases considerably above incident ion masses of 1000 Da.[86-88] This has been attributed to insufficient internal energy uptake at electronvolt collision energies. In general, charge-remote fragmentations have not been observed in low energy CID experiments,[80,81] presumably reflecting lower internal energy uptakes. Alexander *et al.*[89], however, have reported such cleavages when the incident ion energies were raised above 100 eV.

1.6 TANDEM MASS SPECTROMETRY OF PEPTIDES

Field desorption mass spectrometry (FD-MS) of underivatised peptides was first reported by Beckey *et al.* for di- and tri-peptides.[90] Subsequently FD of larger peptides was successful [91-93], with a predicted limitation to peptides of 15 - 20 amino acids in length.[92] FD-MS of peptides yielded little structural information and it was not until FD was used with tandem mass spectrometry that complete peptide sequences could be determined.[95,96] It was with the development of fast-atom bombardment (FAB) that tandem mass spectrometry became used extensively for the structural identification of peptides. The application of tandem mass spectrometry to the analysis of biological molecules

has been discussed by numerous authors [5-9,97-99] and extensive reviews of the literature have been made.[6,8]

Due to limitations of the ionisation methods, sensitivity of instruments and the decreasing efficiency of CID, the upper mass limit for complete peptide sequence information by tandem mass spectrometry has been between 2500 and 3500 Da. For reliable mass measurement of the fragment ions formed by CID a monoisotopic beam of parent ions must be mass selected into the collision cell. As the mass of the incident ion increases, the isotopic envelope broadens, decreasing the absolute intensity of the monoisotopic peaks. The number of possible fragmentation pathways is also increased as the mass of the ion increases resulting in the fragment ion current being distributed over more peaks. Both these factors, combined with the decreased CID efficiency, result in rapidly decreasing sensitivity as the mass of the parent ion increases. Large proteins may be sequenced by being enzymatically cleaved into smaller peptide units. The most successful instruments for peptide sequencing work have been the four-sector mass spectrometers due to their high mass-range, picomole sensitivity and enhanced resolution capabilities.[8]

The relatively new electrospray ionisation technique [10-12] shows promise for the sequencing of much larger peptides and proteins which have been desorbed intact.[100] Due to the many charge states of the parent ion, assignment of fragment ions becomes complex. The presence of complementary pairs of fragment ions (both fragments can be charged, as opposed to MS/MS of singly charged ions where only one fragment is charged) makes assignments slightly less complicated. The sequence information obtained to date by ESI-MS/MS has been limited. A recent report [29] illustrates the potential of the technique and shows sequence ions obtained for serum albumins (RMM ~66000) by low-energy CID in a triple quadrupole mass spectrometer.

1.6.1 Nomenclature for peptide fragment ions

The nomenclature used for describing the fragmentations of linear peptides has been described elsewhere [8,9] but will be summarised below. The nomenclature describing the backbone cleavages common to linear peptides was originally proposed by Roepstorff and Fohlman.[101] The capital letters A, B and C were used to describe cleavages in which the charge was retained at the amide or N-terminus of the peptide. X, Y and Z were used to denote charge retention at the carboxylic acid C-terminus. The specific cleavages associated with each letter are illustrated in Figure 1.1. Subscripted numbers refer to the amino acid position along the backbone and are counted from the N- or C-terminus. The masses of fragment ions often differ from these defined structures by one or two mass units corresponding to hydrogen transfers to or from the charged fragment. These were denoted by single or double primes, preceding the letter for loss of hydrogens and after the letter for extra hydrogen attachment. Biemann [9] proposed that lower case letters should be used so as to eliminate confusion with the single letter codes used to describe amino acids and the use of +1 or +2 to describe the addition of one or two hydrogen atoms respectively. Fragmentations involving side-chain cleavages have been designated d, v and w.[81] The proposed structures of the various fragment ions are illustrated in Figure 1.2. Two further types of fragmentation commonly observed in tandem mass spectrometry of peptides are internal fragments, forming either acyl or immonium ions and also the immonium ions corresponding to individual amino acid units.

To aid in the interpretation of tandem mass spectra of peptides numerous computer programs have been developed [102,103] which either calculate the masses of all the possible fragment ions described in Figure 1.2 (i.e. predictive programs) or from a given spectrum calculate all the possible combinations of amino acids which could give rise to the observed fragment masses.

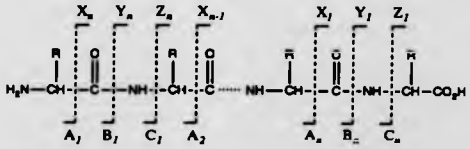

Figure 1.1 Roepstorff and Fohlman nomenclature for describing fragment ions of linear peptides. Side-chains are designated by 'R'.

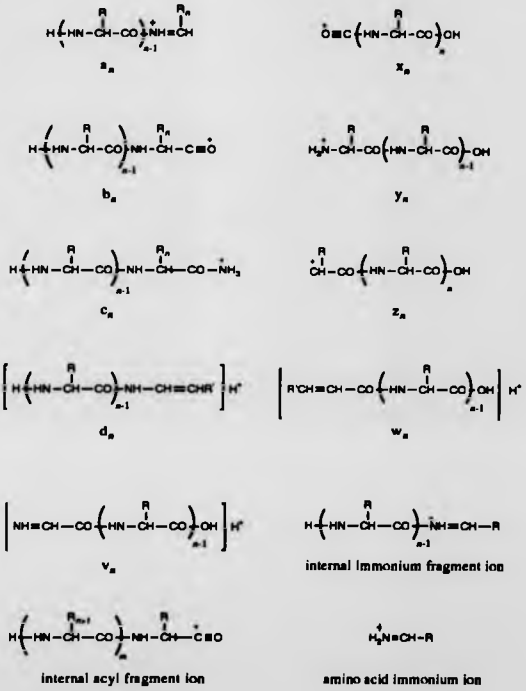

Figure 1.2 Structures of peptide fragment ions and Biemann nomenclature.[9,81]

1.7 Aims

The research discussed in this thesis has been aimed at studying the dynamics of kiloelectronvolt collision-induced decomposition of large ions, where 'large' in this case refers to ions with masses up to a few thousand Da. The ionisation method mainly employed in this work has been field desorption. Since the start of this research project a considerable change has taken place in the ionisation methods available to the mass spectrometrist. With the development of the techniques of ESI and MALDI, molecules of mass in excess of 200,000 Da have been successfully ionised.[104,105] The term 'large ion' had originally been applied with reference to ions with masses of a few thousand Da, the limit of such ionisation techniques as FAB and FD, but now appears outmoded in view of these recent developments.

The aim was to measure translational energy losses for large ions in an attempt to gain further knowledge of the mechanism of CID of large ions. Biological molecules were of the most interest, although inorganic ions have also been studied. Higher incident ion energies were of particular interest, following on from the work of Sheil [69] who reported increased translational energy losses. Determination of methods for increasing the amount of internal energy deposition into the ion is of paramount importance for improvement of the efficiency of CID as the mass of the incident ion increases. It was known that fragment ion mass assignments could be ambiguous due to translational energy losses and the low resolution of the MIKES technique. Mass assignments would then be made by comparison with spectra obtained using a 4-sector tandem mass spectrometer, where the mass assignments should be good to within 0.3 Da.

A further objective was to use QET to investigate the variation of the rate of decomposition with internal energy of the ions, with increasing ion mass and for a range of critical energies (to represent the various fragmentation pathways

available). The problems associated with obtaining a full set of fundamental vibrational frequencies for large ions would be addressed with the use of a computer program to calculate the normal modes from x-ray crystallographic data.

Chapter 2 : INSTRUMENTATION AND EXPERIMENTAL METHODS

2.1 LARGE-SCALE REVERSE-GEOMETRY MASS SPECTROMETER

The large-scale research mass spectrometer used in the majority of this work was originally designed and constructed at La Trobe University, Australia between the years of 1976 and 1981. It was then transferred to the University of New South Wales and underwent its most recent move to the University of Warwick, U. K. in 1987. The original construction of the instrument has been described in detail elsewhere.[70,106] A brief description of the instrument will be made here with particular emphasis on details relevant to this work and to any changes which have been made since the move to the U.K.

2.1.1 General

A schematic diagram of the mass spectrometer is shown in Figure 2.1 and a photograph in Figure 2.2. The instrument was double-focussing (Section 2.1.7) and of reverse-geometry configuration with the magnetic sector preceding the electric sector analyser. The unusually large size of the mass spectrometer corresponds to a flight path for the ions of length 6.5 m. The vacuum of on average 10^{-8} Torr within the instrument was maintained by eight 6" oil diffusion pumps [107a-b] backed by seven rotary pumps [108a-d]. The instrument pressure was monitored with ionisation guages [109] and the backing pressures measured with Pirani guages [110a,b,d]. The vacuum system was protected by a series of relays which would cut out the current to the diffusion pump heaters if the backing pressure became too high, the flow of cooling water became restricted or if there was an excessive draw of current.

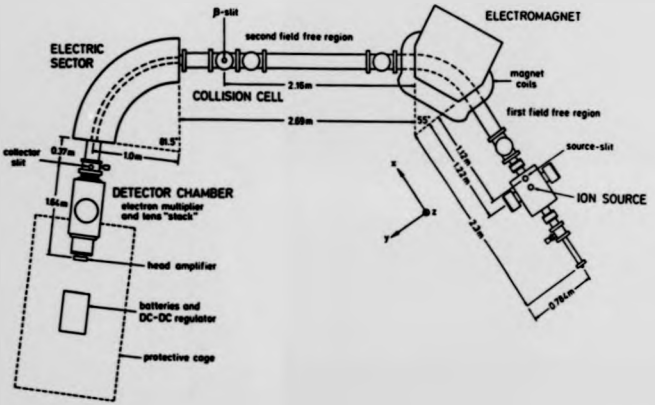

Figure 2.1 Schematic diagram of the large-scale reverse-geometry mass spectrometer

Figure 2.2 Photograph of the large-scale reverse-geometry mass spectrometer.

2.1.2 Ion source and lenses

The source chamber could be isolated from the probe airlock by a gate valve, and a second gate valve situated after the source exit slit was used to isolate the source chamber from the rest of the mass spectrometer. After insertion of the probe the airlock would be evacuated to backing pressure prior to opening of the first gate valve. The second gate valve would only be opened after the source chamber had reached a pressure of 10^{-7} Torr. The probe consisted of a vespel [111] rod for electrical insulation attached to the end of a stainless steel cylinder and was wound in and out of the source chamber by means of a rack and pinion drive. Correct positioning in the source chamber was ensured by means of a peg on the probe locating into a hole in a plate attached to the source chamber end-flange. The accelerating potential was supplied by means of a 30 kV Spellman [112] power supply via feedthroughs into the source chamber and spring contacts to brass disks on the vespel rod. Wires through the vespel rod carried the high potential to the brass sockets of the probe tip in which the field desorption (FD) emitter or fast atom bombardment (FAB) target was held by screws. In the case of field desorption experiments a small current was also passed through these wires for heating of the sample-coated emitter wires to aid the desorption and ionisation process.

In FAB experiments, sample-coated copper targets were used. A description of sample handling and experimental technique is given in Section 2.4.2. Beams of xenon atoms with keV energies bombarded the target from an Ion Tech [113] fine-beam fast atom saddle field gas gun. The gun was mounted onto a linear motion drive on the source housing. This enabled alignment of the gun and also for it to be wound back out of position when other ionisation methods were to be employed. A cylindrical barrel with a small spherical aperture at the base was fixed to the front of the FAB gun at the point of exit of the atom beam.

This so-called 'top hat' improved the performance of the gun allowing up to 6 keV atom beams to be generated without electrical breakdown occurring. The FAB gun was controlled from an Ion Tech B50 power supply.[113]

Ion beams generated by FAB or FD were focussed by a series of electrostatic lenses. Individual lens stacks had been designed by previous workers [114] to provide optimum performance for each individual ionisation method. Lens stacks were aligned in the source using scribe marks on the inside of the source housing and were held in position by screws. A schematic diagram and photograph of the field desorption lens stack are shown in Figures 2.3 and 2.4 respectively. This lens stack was specially designed for use with potentials of up to 30 kV.[114] The first lens through which the ion beam would pass was the 'counter electrode' which was usually held at ground potential. The lens was made from 2 mm thick stainless steel and contained a vertical slit measuring 30 mm high by 4 mm wide. To reduce the likelihood of electrical discharges between counter electrode and emitter, the lens was maintained in a clean and highly polished condition. The second lens provided focussing in the *xy*-plane of the instrument (*y*-focussing) and was split into two halves to provide *y*-deflection. Plates were made from 6 mm thick aluminium alloy separated by 8 mm. The potential applied to these plates was approximately 80 - 90 % of the emitter potential and a deflection of ± 20 - 50 V was usually required. The *y*-focus electrodes were followed by a grounded plate constructed from 1 mm thick stainless steel. Behind this plate was another split lens which provided focussing in the *xz*-plane of the mass spectrometer and also *z*-deflection. These plates were made from stainless steel with a plate separation of 7 mm. Individual lenses were mounted on macor [115] (machinable glass ceramic) rods and spacers which had an overall diameter of 21 mm and were held in place on a base plate by vespel screws. The base plate was made from 9.26 mm thick aluminium alloy with a 60 mm diameter hole in the centre. Mounted in this hole on four screws was a circular plate of stainless

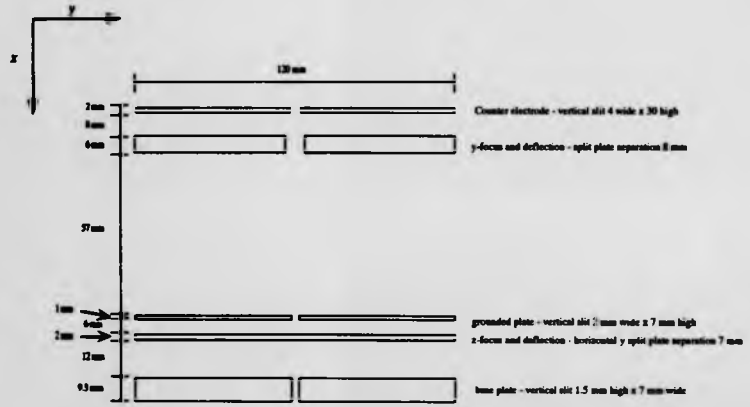

Figure 2.3 The lens stack used with field desorption/ionisation on the large-scale reverse-geometry mass spectrometer. Diagram shows a horizontal cross section (*xy*-plane) through the lens viewed from above (along *z*-axis).

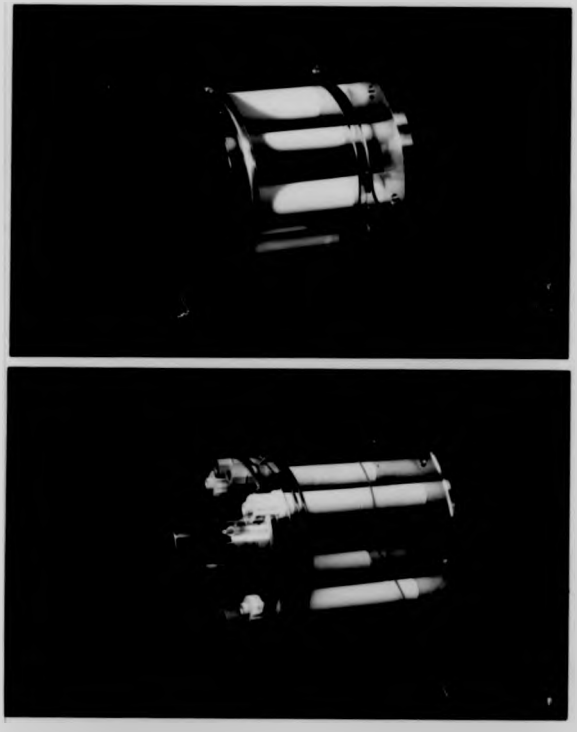

Figure 2.4 Photographs of the lens stacks used with field desorption / ionisation (top) and fast-atom bombardment (bottom) on the large-scale reverse-geometry mass spectrometer.

steel with a vertical slit of 1.5 mm wide by 7 mm high. The base plate was held at ground potential by contact with the source housing. The potentials for the focus electrodes were supplied by two 30 kV Spellman power supplies [112] and the deflection voltages by two differential ion beam deflectors. The deflector supplies constructed by Dawson [116] floated at the focus potential and could provide ± 250 V with respect to the other half of the lens.

A photograph and schematic diagram of the lens stack for use with FAB ionisation are shown in Figures 2.4 and 2.5 respectively. The ion optical design and construction of this lens stack have been described in detail elsewhere.[114] Immediately in front of the probe was a 3 mm thick plate floated at the probe potential. Mounted on this plate was a half cylinder which shielded the FAB target from the grounded casing of the FAB gun. An extraction electrode was positioned 3 mm behind this first plate and was floated to a potential below that of the probe/accelerating potential V_{acc}. Penetration of the field through the aperture of the first plate extracted ions formed at the FAB target. A grounded plate followed by two sets of split plates providing *y*-focussing and deflection were positioned behind the extraction electrode. These focussing electrodes were constructed from 1 mm thick copper. The other plates were constructed from stainless steel and all had spherical apertures 4 mm in diameter. All plates with the exception of the first plate and the extraction plate were mounted on four teflon rods held into the thick base plate by teflon screws. The first two plates were held in place by teflon nuts, bolts and spacers to the grounded plate. The base plate was of similar construction to that of the FD lens but with a copper disc in the centre.

The distance from the base plates of the lens stacks to the point of focus at the source exit slit (α-slit) was approximately 5 mm.

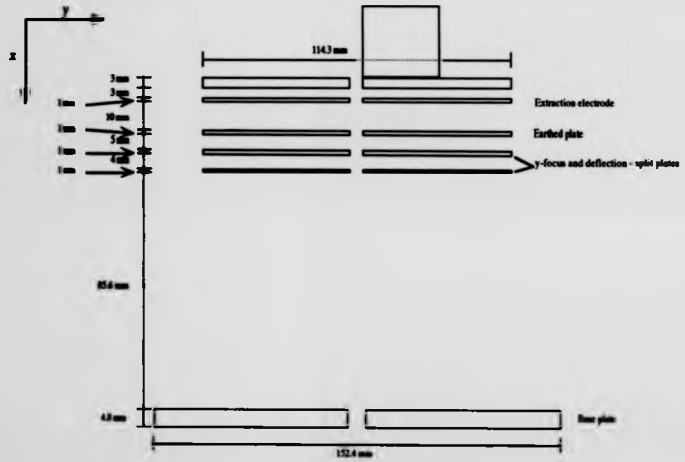

Figure 2.5 Schematic diagram of the lens stack used with fast-atom bombardment ionisation on the large-scale reverse-geometry mass spectrometer. Diagram shows a horizontal cross section (*xy*-plane) through the lens viewed from above (along *z*-axis).

2.1.3 Magnetic sector

The magnetic sector in the large-scale instrument was designed and constructed to provide high mass-range and high resolution through its sheer physical size producing a large dispersion of ions according to their momenta-to-charge ratios.[117,118] The magnet was a conventional soft-iron cored 'C-shaped' electromagnet with a pole gap of 22 mm. The sector angle was 55° with a radius of 780 mm. A 1.5 Tesla field was provided using an 80 A power supply [119] giving a range of up to m/z = 8000 for 8 kV accelerating potential. Both power supply and magnet were water cooled. A magneto resistor positioned in the pole gap provided a monitor of the field and in conjunction with a sweep generator was used to control the magnetic field in either stationary or sweeping mode. The output from the field sensor was also converted by a microprocessor [69,70,120] to provide a digital mass readout. To record a mass spectrum the magnetic field was swept as a function of time under the control of the sweep generator. To sweep from zero to full field required a minimum of 40 s. The magnetic field would be held constant during tuning-up procedures and for collision-induced decomposition (CID) experiments, when only one momentum-to-charge ratio ion would be required to be focussed into the collision cell .

2.1.4 Collision cell

The collision cell was positioned at the focal point of the magnet in the second field-free region of the instrument (β-focus). The cell was composed of two 64 mm diameter stainless steel discs attached to the end of a 10 mm long cylinder made from paclene (machinable plastic). The dimensions of the entrance and exit slits were 2 mm wide (*xy*-plane) and 10 mm high (*yz*-plane). An adjustable β-slit (0 - 10 mm) controlled by a micrometer drive could be positioned either in front of or behind the collision cell. For all experiments described in this work the β-slit was positioned after the collision cell and used with widths 1.0 - 2.0 mm. Both

the cell and β-slit were mounted on an aluminium support attached to the flange of the collision cell T-piece. In order to restrict the flow of collision gas into the rest of the mass spectrometer, the collision cell T-piece and neighbouring T-pieces were fitted with baffles at either end containing apertures of 6 mm wide by 20 mm high and 20 mm square respectively.

Collision gas was admitted to the cell via a precision variable leak valve.[121] The type of collision gas used could be readily changed by means of quickconnect valves [122] attached in the gas lines from the regulator valves of the gas cylinders to the leak valve. One disadvantage of this set up was the lack of a facility for evacuating the line between the precision leak valve and the quickconnect valve. Therefore on changing to a different target a relatively high pressure of gas (i.e. that which would correspond to a transmission of 5 %) was passed through to the collision cell for 15 minutes or more in order to flush out traces of the previous gas. The pressure in the cell has been calculated to be around 80 times that measured on the ion guage monitoring pressure outside of the cell in the T-piece.[69]

2.1.5 Electric sector analyser

The electric sector was of cylindrical design and consisted of two parallel curved plates. The plates were 149.5 mm high and separated by 33.5 mm. The radius of the central path of the ion beam through the electric sector was 1000 mm. Fringing fields were reduced by the use of Herzog plates [123] at either end of the sector plates and inhomogeneities in the field corrected using Matsuda plates [124] above and below. Potentials applied to the sector plates were from two 3 kV Fluke power supplies [125] and were equal but of opposite signs (the inner plate was negative for positive ions). These potentials passed through voltage dropping resistors prior to reaching the electric sector analyser (ESA) plates. These resistors were controlled by a transistor which was in turn controlled by

an amplified signal from a sweep generator (ESA drive amplifier). This ESA drive amplifier differed from that used previously in that it had the facility for all channels from the 16 bit DAC, from which it was driven, to be placed across a desired voltage range. Hence where previously all 2^{16} DAC channels were placed permanently across 1000 V (corresponding to the maximum ESA potential desirable) the new electronics allowed these channels to be placed across almost any range. For example, in a mass analysed ion kinetic energy spectroscopy (MIKES) experiment where the parent ion energy was 14.9 keV, all channels were set across 5 - 505 V of the ESA. Alternatively, for a high resolution study of an individual peak, all the channels could be set across a small range corresponding to the peak width.

During the course of recording a mass spectrum the electric sector plate potentials were held at a constant value corresponding to the energy of the ions and served to re-focus ion beams after the velocity dispersion of the magnetic sector (described in Section 2.1.7). As the magnetic field was swept, ion beams of different mass to charge ratios were brought to focus at the collector slit (y-slit).

For tuning purposes the magnetic field would be held at a constant value corresponding to the transmission of a particular molecular ion, but a small voltage sweep would be applied to the electric sector plates (usually of 0.54 V or 1.12 V) resulting in a small mass window being viewed. Source lens stack potentials and the accelerating potentials would then be adjusted to provide maximum signal intensity.

MIKES experiments involved the use of a fixed magnetic field to select ions of interest into the collision cell and also sweeping the ESA potential to energy analyse the fragment ions formed. This will be discussed in more detail in Section 2.1.8.

2.1.6 Detection system and computer control

Ions passing through the y-slit were accelerated and focussed onto the first dynode of an ETP electron multiplier [126] by a lens stack [114]. The potential applied to this lens stack was supplied by a 100 kV Spellman power supply and in the experiments described in this work was used with the last plate before the multiplier being floated at -30 kV. High-mass ions have relatively low momenta compared to small polyatomic ions at similar ion energies. This may lead to insufficient secondary electron emission when such ions impinge upon the first dynode of the electron multiplier. Also, very low mass fragment ions formed by CID may be discriminated against due to their correspondingly low momenta. Hence the use of post acceleration serves to increase detection sensitivity for high mass ions and their fragment ions.

The potential on the multiplier itself was 2.7 kV corresponding to a theoretical gain in current of the order of 10^6. This voltage was supplied by two deep cycle lead acid batteries and associated electronics mounted in a Faraday cage and floated to the post acceleration potential. The Faraday cage was insulated from the floor by means of a large ceramic insulator. The amplification electronics were situated on a teflon cylinder fitted to the outside of the end flange of the instrument. High impedance electronics resulted in nanosecond pulses from the electron multiplier being converted into optical signals and conveyed to a counter via optical fibres. The computer (PDP11/23)[127] sampled the counter at certain time intervals depending on the nature of the experiment and the information was stored in the appropriate signal array. This method of ion detection is referred to as ion-counting whereas the more frequently used method in commercial instruments is that of analogue detection (see Section 2.2.7). An account of the ion-counting electronics used here has been given previously by Davis.[114]

The computer was used to control the ESA potential and accelerating potential via two 16 bit DACs and a fast serial bus driver. A 12 bit DAC was used to provide output to an oscilloscope which was used to view peaks for tuning-up purposes. The computer programs controlling the various parts of the mass spectrometer and output devices were written in assembler language in 56 individual modules and have been described in detail by Shell.[69] For MIKES experiments the 16 bit DAC was incremented in steps of two least significant bits and data from four such steps would be entered into each channel of the data array stored in the computer. The size of the least significant bit was governed by the range set on the ESA drive amplifier and hence a parent ion energy of 14.9keV would correspond with 0.0076 V (500 ESA volts / 2^{16}). Therefore each channel stored in the computer corresponded to eight times this, *i.e.* to a width of 0.0608 V. Hard-copies of the MIKE spectra could be plotted [128] as raw data with discrete channels being drawn or the spectrum could be smoothed. The smoothing coefficients used for all spectra are given in Table 2.1.

TABLE 2.1

Coefficients used in the weighted average smoothing routine for plotting of MIKE spectra

Channel number	Coefficient
1,17	0.000078
2,16	0.000124
3,15	0.009324
4,14	0.043512
5,13	0.141414
6,12	0.339394
7,11	0.622222
8,10	0.888889
9	1

2.1.7 The double-focussing principle

Consider two ions with masses m_a and m_b generated in the source of the mass spectrometer with a small range of velocities. These ions follow circular paths of different radii through the magnetic field according to their momenta and different mass ions will be brought to focus along an image curve (at the focal point of the magnet), as shown in Figure 2.6a. Ions with mass m_a but a small range of velocities will be brought to focus at differing points along the image curve and are said to have been velocity dispersed. The magnetic sector is direction focussing in that a divergent beam of ions with the same mass and velocity will be re-focussed to one point on the image curve.

Secondly consider the case when two ions m_a and m_b with a small range of energies, for example E_1 and E_2, are produced from a point source and enter a radial electric field (Figure 2.6b). Ions will follow circular paths through the field with radii dependent on their energies. In the case of a single ion of mass m_a it can be said to have been velocity dispersed by the electric field. The electric sector is also direction focussing in that a divergent beam of ions will be re-focussed.

With a suitable choice of magnetic and electric fields the velocity dispersion effects of one can compensate for that of the other. Ions with mass m_a and a range of velocities v_1, v_2 and v_3 will be brought to the same focal point on the image curve at the γ-focus of the mass spectrometer. Ions of different masses will be focussed at different points along this velocity focussing curve. However due to the angular spread of the ion beam, the image on the velocity focussing curve will be blurred. Only the central rays of each velocity dispersed group will coincide on the velocity focussing curve (Figure 2.6c). Each velocity group will be focussed at a different point along the direction focussing curve. Hence at the direction focussing curve the images are blurred by the velocity spread of the

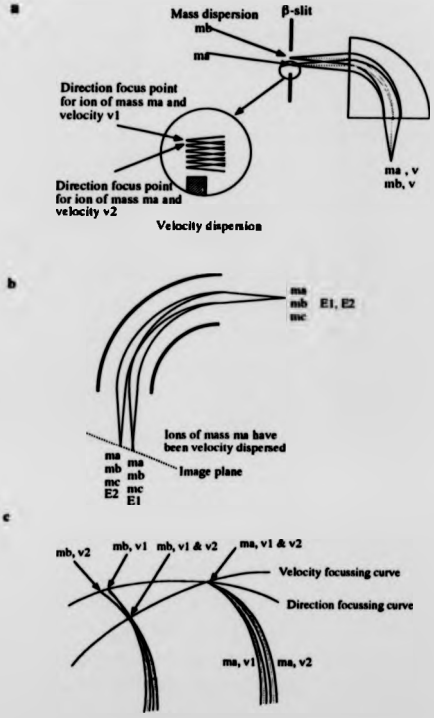

Figure 2.6 Principle of double focussing
a) Mass and velocity dispersive effects of magnetic sector
b) Velocity dispersion and direction focussing of ESA
c) Point of double focus at the collector slit

ions, whereas at the velocity focussing curves images are blurred due to the directional spread. With a suitable combination of magnetic and electric fields these two focussing curves can be made to coincide to produce a sharp image, the point of double focus.[33]

The y-displacement of the final image after exiting all fields is given by an expression of the form [33,129]

$$y = a_m (B_1\alpha_e + B_2\beta + B_{11}\alpha_e^2 + B_{12}\alpha_e\beta + B_{12}\beta^2 \ .....) \qquad (2.1)$$

where a_m is the radius of the magnetic sector, α_e the initial angular divergence and β the velocity spread. The B_{xx} terms correspond to the 'image aberration coefficients'. These are defined by the geometry of the instrument and have been given by Hintenberger and König.[130] When $B_1 = B_2 = 0$ first order double focussing occurs, and when also $B_{11} = B_{12} = B_{22} = 0$, the condition for second order double focussing is satisfied.

2.1.8 Collision-induced decomposition experiments

Slit widths were maintained at α = 0.3 - 0.6 mm and $\beta = \gamma$ = 1 - 1.5 mm so as to resolve the isotope distributions of the molecule-ions formed in the source and to admit only one mass-to-charge ratio ion into the collision cell, thus avoiding ambiguities in the mass assignments of fragment ions. The larger slit widths were used for parent ions with masses below 1500 Da but above this mass these slit widths were insufficient to separate the purely ^{12}C containing molecule-ion peak from that containing one ^{13}C. Further restriction of the slit widths in order to resolve isotope peaks for higher mass molecule-ions decreased the intensity of the parent ion beam and, combined with the increased number of dissociation channels, resulted in poorer signal-to-noise ratios for the resulting CID spectrum.

For the recording of a complete CID spectrum electric sector scan rates of either 5 or 10 V/s were used. 10 V/s was generally used with higher accelerating potentials where the scan range of the electric sector was necessarily larger. Some experiments required the scanning of small voltage ranges corresponding to individual peaks or small ranges of peaks. In this case scan rates ≤ 1 V/s were used.

a) Setting of transmission

For standardisation of procedures collision gas pressures have generally been reported in terms of attenuation, suppression or transmission. Transmission (T) was briefly defined in Section 1.4.2 and corresponds to $T = I_t/I_o$, the ratio of the intensity of parent ions reaching the detector after addition of collision gas to that prior to gas addition. Two other frequently used terms are attenuation and suppression and refer to $(1 - T)$. The control software used during the instrument tuning-up procedure had the facility for a static ion count (no small ESA sweep) and hence transmission could be set from the rate of incident ions arriving at the detector before and after admission of collision gas. Transmissions were checked during and after the experiment, and the pressure outside of the collision cell was monitored throughout.

b) Measurement of fragmentation efficiencies

Fragmentation efficiencies have been quoted on all spectra herein and correspond to the ratio of the total number of fragment ions detected, n_f, to the total number of incident ions entering the collision cell, n_o. Since n_o was not directly measurable, it was assumed to correspond to the number of surviving parent ions, n_t, arriving at the detector multiplied by 1/T. n_f and n_t were obtainable from the final spectrum using the plotting software routine. On entering ESA voltage

ranges the total number of ions counted within that window was displayed. Quoting of n_f was also found to be valuable for comparison of spectral quality.

c) Measurement of translational energy losses, ΔE

As discussed in Chapter 1, parent ions may lose considerable translational energy ΔE during the collisional activation process which manifests itself as translational energy losses ΔE of the fragment ions and can be measured by the MIKES technique. The magnetic field was held at a constant value corresponding to transmission of ions of interest into the collision cell. Sweeping of the electric field from close to zero to that corresponding to the parent ion energy resulted in transmission of the various fragment ions at field strengths corresponding to their energies, and if ΔE = 0 the masses of these ions can be calculated from Equation 1.3. Since ΔE is non-zero, mass assignments must be made from independent methods, in this case by 4-sector tandem mass spectrometry, and can then be used to calculate the expected ESA potentials V_e. Shifts in the ESA potential required for transmission of the fragment ions in the MIKE experiment (V_m - V_e) can be measured and used to calculate the translational energy lost by the parent ion ΔE as a result of CID (Section 1.3 and Equation 1.4).

V_m values corresponding to the fragment ion peak centroids were measured manually from the MIKE spectra. Fragment ion peaks were plotted individually onto A3 paper, usually over a 15 V range for accelerating potentials of 15 kV and with gain factors sufficient to be at least 15 cm high. Centres of peaks at their half-heights were then found manually with the use of a compass and ruler. The ESA voltage corresponding to the peak centroid would then be measured from the plotted scale using a ruler accurate to ± 0.25 mm. The most accurate and reliable ΔV measurements would be made for smooth Gaussian shaped peaks. Very often when scanning the whole CID spectrum, the number of ion-counts making up an individual peak would only be of the order of a few thousand, and

hence the peak shapes, despite the applied smoothing, would sometimes have shoulders. In this case a more symmetrical portion of the peak would be taken to find the centroid rather than the half-height; in some cases the peak top would be used. Unless otherwise stated, ΔE measurements reported in this thesis correspond to the half-height measurement. For helium as target gas, ΔE measurements made using the half-height have been reported as being larger than those corresponding to peak top measurements due to the skewed nature of the peaks whereas argon tends to produce more symmetrical peaks.[66]

d) Errors in measurements of translational energy losses

Possible sources of error in measurement of ΔE arise from instrumental errors in the ion energies measured by the electric sector and from human error when manually finding peak centroids. For metastable ions, translational energy losses should be zero and hence the measured ESA voltages V_m should be equal to those which have been calculated V_c. A MIKE spectrum was recorded for each of the samples, dodecane, iodoethane, iodopropane and iodobutane with parent ion energies of 14.9 keV. The metastable fragment ions of these small organic ions were chosen since good ion statistics could be obtained due to the relatively intense FI and FD ion currents achieved for the parent ions. Each metastable fragment ion peak was plotted nine times with different scaling each time and V_m measured for each (as described in Section 2.1.8c), so as to test the accuracy of the manual centroiding method. A plot of the differences between the measured and expected ESA voltages (V_m - V_c) is shown in Figure 2.7. The mean error of V_m from V_c was 0.022 V and represents the instrument bias. The mean standard deviation resulting from each set of nine values was 0.008 V. The ΔE values reported in this thesis for peptide and inorganic molecule-ions were calculated from the measured V_m values minus the instrument bias (0.022 V). The range of error in the calculated ΔE values is given as ± two standard deviations (0.016V),

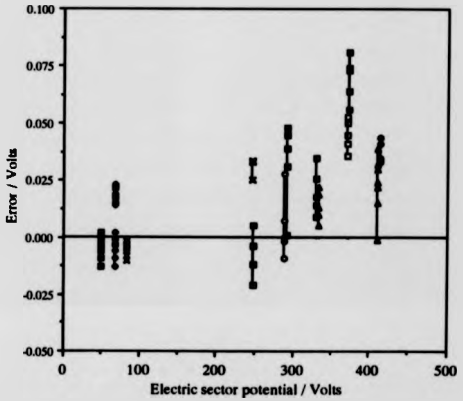

Figure 2.7 Plot showing the deviation of metastable peak centroids from the calculated ESA voltages corresponding to the ion energies

since the fragment ion peaks for these ions will have comparatively worse signal-to-noise ratios.

e) Artifacts and discrimination effects in MIKES

Artifact peaks can arise in MIKE spectra from decompositions in the source of intense ions higher in mass than the parent ion being studied, if the following conditions are met: ions will be transmitted through the magnet if $m_f^2 / m_p' = m_p$, and through the ESA if $m_f^2 / m_p' = m_p / m_f$. The origins of such artifacts have been discussed in greater detail elsewhere.[131,132] Rumpf *et al.*[133] have considered the mass discrimination effects during MIKES for the instrument used in this present work. They suggest that for a peptide ion of m/z 5000 with 8 keV ion energy, very low mass fragment ions may be discriminated against by a factor as high as 10^3 compared with fragment ions close in mass to the parent ion.

2.2 FOUR-SECTOR MASS SPECTROMETER

2.2.1 General

The 4-sector mass spectrometer used in this study was a Kratos Concept II HH.[134] The instrument was effectively composed of two double-focussing forward geometry (ESA (E) preceding magnetic sector(B)) mass spectrometers linked together by a collision cell and associated electrostatic lenses (the Flexicell). The instrument layout was 'C' shaped and the geometry is described by the term 'EBEB'. Other suitable combinations of 4-sectors are BEEB, EBBE and BEBE. The latter two geometries have not been constructed to date. Tandem mass spectrometry on a 4-sector instrument involves mass selection of the ions of interest into the collision region by a suitable combination of the electric and magnetic fields of the first two sectors (MS1). The fragment ions formed are mass analysed by linked scanning of the second ESA and magnet

(MS2). A discussion of the linked scanning of MS2 and of the option of electrically floating the collision cell is given in Section 2.2.5. The use of MS1 to mass select parent ions removes the possible artifacts from metastable decompositions of other ions formed in the source, as might be observed during linked scanning of a two-sector tandem instrument. Such artifacts are limited to occurring only from peaks close in mass to the parent and are dependent on resolution. In principle the parent ions may be mass selected with high resolution, although in practice sensitivity is important so a resolution of 1000 - 1500 is more commonly used.

A schematic diagram of the Concept II HH mass spectrometer is shown in Figure 2.8 and shows ion trajectories exemplifying the double focussing operation of the two parts of the instrument. Photographs of the instrument are shown in Figure 2.9.

2.2.2 The vacuum system and source chamber

The vacuum within the instrument of 10^{-7} Torr was maintained by 7 turbomolecular pumps. These turbo pumps were backed by 4 rotary pumps. The instrument was vacuum protected and all turbo pumps, high voltages, etc., would be shut down in the event of too high an increase in pressure, overheating or electrical power failure. Pressures inside the instrument were monitored by flange-mounted ion guages and backing pressures by thermocouple guages.

Samples for FAB and FD experiments were introduced into the source via a direct insertion lock. The probe would be entered into the first section of the air lock and this would then be evacuated to backing pressure prior to insertion further into the air lock. A ball valve was used to isolate the air lock from the source chamber. Solid samples for electron impact ionisation were admitted into the source on a 'solids probe' via a second direct insertion lock positioned at 90°

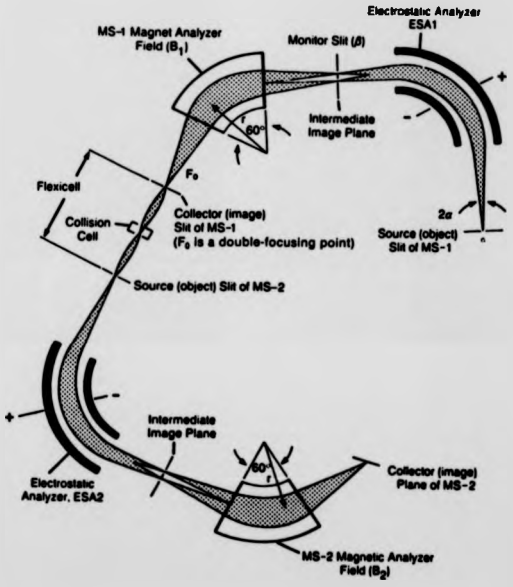

Figure 2.8 Schematic diagram of the Concept II HH four-sector tandem mass spectrometer.

Figure 2.9 Photographs of the Kratos Concept II HH four-sector tandem mass spectrometer.

to the ion optical axis of the instrument. The source chamber was isolated from the rest of the instrument by an electronically controlled valve.

2.2.3 Ion sources and lenses

a) Field desorption

The lens stack used for FD experiments on the 4-sector mass spectrometer was constructed 'in house' based on the original manufacturers design.[134] To improve performance, modifications have been made to the original design and a schematic is shown in Figure 2.10. A photograph of the lens is shown in Figure 2.11. A z-lens has been added in the place of a cylindrical earthed barrel which was part of the mounting block. An earthed plate was also added in front of the mounting block to help define the beam at that point by reducing stray fields. A further modification was the shield electrode. This was held at the same potential as the FD emitter which was positioned 1.5 mm from the counter electrode. Ion beam trajectories have been calculated by Davis;[114,135] Figure 2.12 shows a schematic of the effect of a shield electrode in enhancing focussing of ions through the counter electrode slit. A shield electrode also has the effect of lowering the electric field at the emitter. In the case of the 4-sector FD lens stack the shield electrode comprised two separate plates with the emitter positioned parallel to them. It was anticipated that this arrangement would result in similar focussing effects to those shown in Figure 2.12.

All lenses were made from stainless steel and mounted on stainless steel rods sheathed in ceramic tubing for insulation. The distances between lenses were set with 6 mm diameter quartz spacers of various thickness. The posts of the emitters were pushed fully into sockets in the end of the probe. A rod on the probe handle located into a hole on the outside of the source airlock to ensure vertical alignment. The emitter potential was supplied via contact of the probe tip

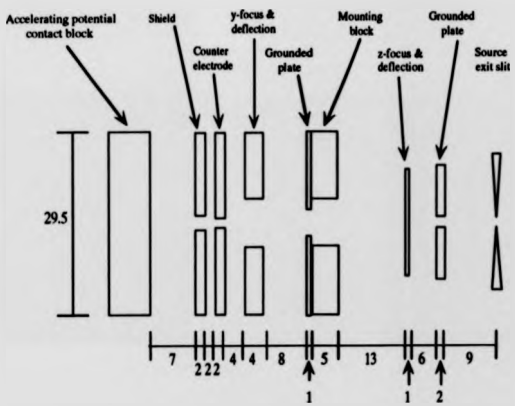

Slit widths:

Shield 3 mm
Counter electrode 2 mm
y-focus 10 mm
First grounded plate 5 mm
z-deflector 5 mm
Second grounded plate 2 mm

Figure 2.10 Schematic of the 4-sector field desorption lens stack. All dimensions are in mm.

Figure 2.11 Photograph of the lens stack used with field desorption on the 4-sector mass spectrometer.

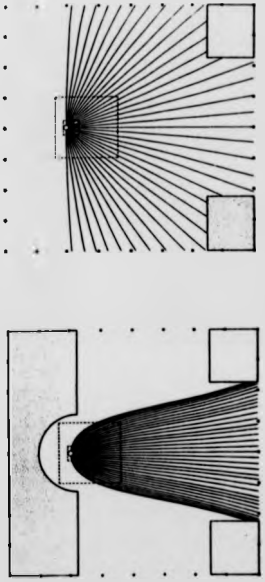

Figure 2.12 Effect of a shield electrode behind the emitter in a field desorption ion source. Ion trajectories calculated by Davis.[114]

with a spring fitted in the aperture of the accelerating potential contact block. The emitter heating current was supplied via wires inside the probe handle and shaft. The shield electrode was connected directly to the contact block and hence was held at the emitter potential. All voltages apart from those for the *z*-lens were supplied through the usual source feedthroughs. The *z*-lens was supplied separately by a 30 kV Spellman power supply [112] and a differential ion beam deflector [116] (See Section 2.1.2). For an accelerating potential of 8.03 kV typical voltages on the various lenses were: counter electrode -1 to -3.5 kV, *y*-focus 7.83 V ± 20 V deflection, *z*-focus 1.84 kV with ±20 V deflection.

b) Fast atom bombardment source and lens

The fast atom bombardment ion source was the standard Kratos design.[134] The accelerating potential was applied to the probe tip by a contact block similar to that described for the FD lens above. 8 keV xenon atoms bombarded the FAB target from an Ion Tech fine-beam saddle field FAB gun powered from an Ion Tech B50 supply.[113]

2.2.4 MS1

Ions exiting the source chamber via the α-slit passed into the first electric sector analyser. The ESA was of radial design and the fields produced were sufficient to transmit ions with 8 keV ion energy which corresponded to the full accelerating potential of the instrument. An indication of the magnitude of the ion current passing through the first field-free region was given by a measurement of the ion current hitting the β-slit. Calibration of MS1 was carried out from the mass spectrum of caesium iodide cluster ions formed by FAB.

2.2.5 Collision cell and MS2

Figure 2.13 shows the ion optical configuration of electrostatic lenses before and after the collision cell. Floating of the collision cell to positive potentials has been

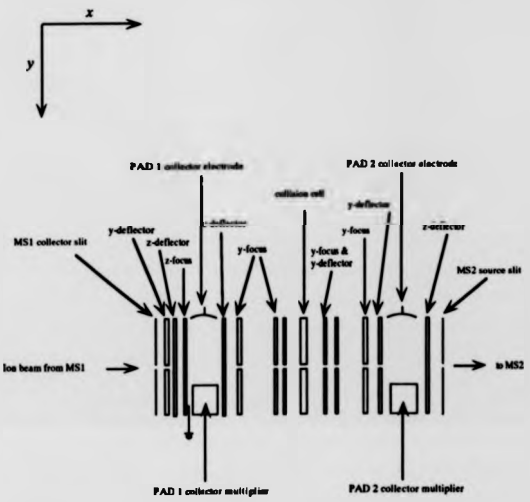

Figure 2.13 Arrangements of lenses and slits before and after the collision cell (the Flexicell) of the 4-sector tandem mass spectrometer.

shown to result in increased resolution and reduced discrimination against lower mass fragment ions.[55,136] The increased resolution observed is a direct result of reduced peak broadening due to kinetic energy release.[55] The 4-sector instrument used in this work could be used with collision cell potentials, V_{cell}, of up to 8 kV. On leaving the cell, ions are re-accelerated through V_{cell} resulting in a lower limit for fragment ion energies of eV_{cell}. With these increased energies the transmission of lower mass fragment ions through the instrument is improved.

For $V_{cell} = 0$, fragment ions formed from a chosen parent may be recorded by linked scanning of the second ESA and magnet using the standard B/E linked scan law (i.e. for recording spectra of fragment ions formed in the first field-free region of an EB geometry two sector instrument).[137,138] If the collision cell is floated, fragment ions leaving the cell will have kinetic energies E_f given by

$$E_f = (m_f / m_i).e.(V_{acc} - V_{cell}) + eV_{cell} \qquad (2.2)$$

where V_{acc} is the potential used in the source for acceleration of the parent ions. A detailed derivation of Equation 2.2 has been described by Boyd.[139] The linked scan law must be modified accordingly and is shown in Equation 2.3.

$$\frac{B_f^2}{B_p^2} = \left(\frac{V_{ESAf}}{V_{ESAp}}\right)\left(\frac{V_{ESAf} - V_{cell}}{V_{ESAp} - V_{acc}}\right)\Big/\left(1 - \frac{V_{cell}}{V_{acc}}\right) \qquad (2.3)$$

where V_{ESAp} and V_{ESAf} are the ESA potentials required to enable transmission of the parent and fragment ions respectively and B_f and B_p are the corresponding magnetic field strengths. If $V_{cell} = 0$ then Equation 2.3 reduces to the usual linked scan law where B/E is a constant.

The double-focussing combination of an electric sector analyser and magnetic sector results in ions with slightly lower kinetic energies, due to

translational energy losses, being re-focussed (velocity focussed) and hence the mass assignment problems associated with the MIKES technique are not present. If the translational energy losses are very large the exact linked-scan locus of points may not pass through the maximum intensity region for the fragment ion peaks, hence leading to a loss in sensitivity. Floating the collision cell results in a lower laboratory frame collision energy and ΔE is assumed to be correspondingly reduced, hence reducing this problem. Also, calibration of the linked scan law with a known compound is assumed to cancel out the effect of such energy losses, but this makes the assumption that the magnitudes of ΔE are similar for all compound types.

Artifacts, although reduced using a 4-sector mass spectrometer with a floated collision cell, can still arise. Broad but weak peaks observed alongside higher mass fragment ions have been attributed to dissociations of parent ions in the second ESA.[55]

Calibration of MS2 was carried out by using the collision cell as the ion source. This involved insertion of a Phraser direct insertion probe into the collision cell airlock. This probe had a built-in FAB gun, gas line and sample target. Generation of beams of caesium iodide cluster ions by FAB were then used for the magnet DAC calibration of MS2, and the mass-time (LRP) calibration.

In order to record the masses of fragment ions formed in the flexicell a 'metastable' calibration was required. This involved conversion by the datasystem of the apparent masses m^* obtained in the time/mass (LRP) calibration to the real masses of the fragment m_f and parent ions m_i using

$$m^* = (m_f^2/m_i) + (V_{cell}/V_{acc})[m_f - (m_f^2/m_i)] \qquad (2.4)$$

The ESA2 values corresponding to these masses are then calculated using Equation 2.3. This calibration was checked by recording the 4-sector tandem mass spectrum of caesium iodide cluster ions selected into the cell using MS1.

2.2.6 Detection and recording of spectra

There were four detectors in the instrument; i) after MS1 and pre-flexicell, ii) post-flexicell, iii) after ESA2, and iv) after the second magnetic sector. All four detectors were of the same design and high voltages applied only to the one in use. Ion beams were then deflected to hit an aluminium electrode held at a potential of -8 kV. The resulting electron emission from this electrode was attracted to the electron multiplier positioned opposite (see PAD1 and 2 in Figure 2.15), the last dynode of which was held at a potential of up to +4 kV providing a variable gain of up to 10^6. The current output from the multiplier was passed through a current to voltage converter and various filters and the final signal was detected as a voltage. Pulses of voltage of the order of μs were produced. This system is known as 'analogue detection'.

Signals were passed to a Data General Computer [140] running the Kratos DS90 [134] data system software. The instrument could be used in two modes: under computer control, known as autoconsole or under combined computer and manual control. The latter required the operator to manually switch between detectors, scanning rates, etc., on the console. This mode of operation was generally the one used. A later addition to the computer system was an ethernet link to a Sparc Station IPC [141] running the Kratos Mach 3 [134] data system. The software had not yet been developed for the running of the 4-sector mass spectrometer, but was used for off-line processing of data. Use of Mach 3 resulted in much faster data processing.

2.2.7 Interpretation of spectra

Peptide fragment ion assignments in the present work were made with the aid of a predictive program called MacProMass.[142,143]

2.3 HYBRID MASS SPECTROMETER

2.3.1 General

A Kratos Concept hybrid IHQ mass spectrometer was used during a period of study on-site at Kratos Analytical.[134] A schematic of the EBqQ instrument is shown in Figure 2.14. MS1 was of the similar construction and design to MS1 of the 4-sector mass spectrometer described above, whereas MS2 consisted of two quadrupole filters. The first quadrupole was used as a collision cell with only radio frequency (RF) voltages applied and therefore acted as a focussing device with no mass analysis capabilities. The second quadrupole had both RF and DC voltages applied, and was used for mass-analysis of fragment ions formed by CID. The instrument was controlled by the Mach 3 [134] data system running on a Sun 3/80 [141] workstation.

2.3.2 Source and MS1

The ionisation method employed in the hybrid experiments was FAB, using an ion source and methods identical to those described for the 4-sector mass spectrometer (Sections 2.2.3b and 2.4.2). MS1 could be used to record mass spectra in the usual manner using a detector situated prior to MS2. MS1 was calibrated from the mass spectrum of caesium iodide cluster ions formed by FAB.

Figure 2.14 Schematic diagram of the Kratos Concept Hybrid 1HQ mass spectrometer

2.3.3 Collision quadrupole and mass analysing quadrupole (MS2)

Both quadrupoles were approximately 200 mm in length and the rods were hyperbolic in shape, providing an inscribed radius of approximately 4 mm. Turbo pumps situated before and after the collision quadrupole prevented leakage of collision gas into the rest of the instrument. 2 kV peak-to-peak RF voltage was supplied to the quadrupole rods at a frequency of 1.1 MHz. The DC potential applied to the second quadrupole was ± 1000 V.

2.3.4 Tandem mass spectrometry using a hybrid mass spectrometer

Ions generated in the source had 8 keV translational energy and ions of interest were mass-selected with high resolution, using the sector part of the instrument (MS1). Since quadrupole mass filters function for electronvolt ion energies, the ion beam must be decelerated and also shaped from a slit image to a beam of circular cross-section. This was performed by floating of the deceleration optics and quadrupoles at kV potentials. The collision quadrupole was floated at a potential equivalent to the source accelerating potential minus the desired collision energy. The analytical quadrupole was floated with a variable offset so as to provide optimum transmission for all ions by maintaining a constant ion energy for all masses and thus compensating for fragment ions being formed with reduced energies. The RF-voltage applied to the collision quadrupole was varied with that of the analytical quadrupole, referred to as 'tracking', so that each ion was transmitted with equal efficiency. Scanning of the voltages of the second quadrupole resulted in mass analysis of the ions, which were then detected after post-acceleration of 8 kV into an electron multiplier.

The upper mass limit of the hybrid instrument was limited to 2000 Da by the range of the quadrupole assembly. Calibration of tandem mass spectra was carried out using the CID spectrum of caesium and rubidium iodide cluster ions formed by FAB. Calibrations were generally valid for several days if no

instrument failures occurred. The resolution for ions of mass > 1000 Da gave peak widths at half-height of 1.5 Da.

2.4 IONISATION METHODS

2.4.1 Field desorption

The technique of field desorption for the ionisation of substances of low volatility deposited onto the surface of an emitter was first reported by Beckey in 1969.[144] Since then the technique has been used for ionisation of a wide range of sample types from biological to environmental to polymeric materials.[94,145,146]

a) Field desorption emitter activation

The FD emitters used in this work were made by the high-temperature activation method described by Beckey.[147] The FD emitters used on the large-scale mass spectrometer were composed of two nichrome posts supported in a base of vespel with a separation of 6 mm. The emitters used on the 4-sector mass spectrometer were purchased from MSE [148] and were also composed of nichrome posts but mounted in a ceramic base with a 5 mm separation. 25 μm diameter tungsten wire [136] was spot welded to the top of the support posts with sufficient tension to produce a straight wire. Welds which resulted in a flattening of the wire into a leaf shape were desirable for minimum resistance and hence were checked under a microscope for consistency. Batches of five or six emitters were loaded into the vacuum chamber of the activation unit. A schematic of the activation unit is shown in Figure 2.15. The vacuum was maintained by a diffusion pump [107c] backed by a rotary pump [108a]. Emitter wires were positioned 2 mm from a grounded counter electrode made from stainless steel. The counter electrode was removable and was cleaned after each activation process to remove all carbon deposits. Occasionally counter electrodes were sand-blasted

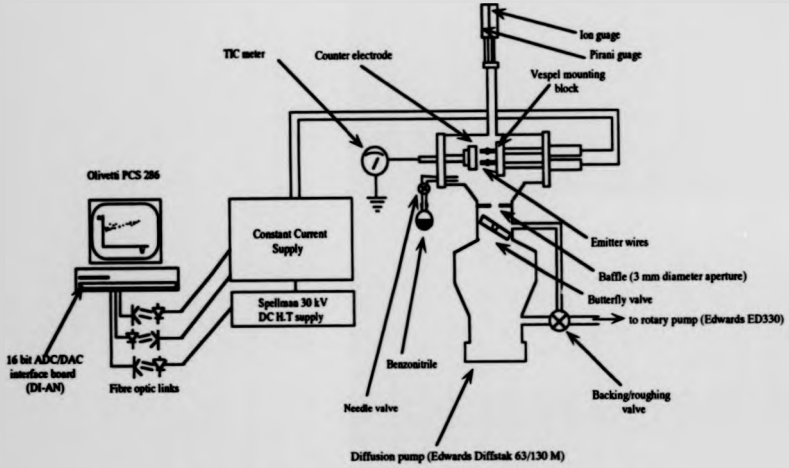

Figure 2.15 Schematic diagram of the field desorption emitter activation unit.

to remove any lingering deposits and periodically the surface was skimmed to remove raised areas produced from such cleaning processes. Benzonitrile purchased from the Aldrich Chemical Co.[150] was contained in a glass flask and leaked into the vacuum chamber via a needle valve. The benzonitrile was degassed by freezing with liquid nitrogen and then allowing the liquid to thaw, freezing again and pumping away any evolved gases. This freeze and thaw cycle was repeated until no further gases evolved from the liquid, as observed by the pressure reading on the Pirani [110c,e,f] and ion guages.[109] The chamber was flushed a number of times with nitrogen gas to aid the removal of oxygen which would otherwise have been detrimental to the activation process. In general the chamber was left to evacuate overnight where possible or until the pressure inside the chamber was of the order of 4×10^{-5} Torr. High tension was applied to the emitters with a Brandenburg high voltage supply,[151] and heated via a home-built constant current supply. Both power supplies were under computer control via a commercial digital to analogue converter.[152] The control programs written by Chan have been described elsewhere.[153] Prior to the activation process, wires were pre-activated or carburised [147] using a constant power of ~0.19 W per emitter (0.18 W for 4-sector emitters) in a benzonitrile pressure of $\sim 1 \times 10^{-2}$ mbar for 30 - 40 minutes. This process converted tungsten into tungsten carbide and resulted in an increase in the total resistance of the wires from on average 4 - 6 Ω. Occasionally the power was incremented or decremented if the emitter wires were observed to be either too bright or too dim as viewed through an optical telescope. A wire temperature of around 1600 K was necessary for carburisation. Carburisation was then followed immediately by the activation process for which the benzonitrile pressure was reduced to $\sim 6 \times 10^{-3}$ mbar. A high potential was then applied between emitter wires and counter electrode with an initial power per emitter of ~0.15 W. For the first five hours of the 40 hour activation process the high potential was held constant at 14 kV and also constant power was maintained. This ensured complete carburisation and

initiated the growth of carbon deposits as protrusions. After this initial 5 hour period, the high potential was gradually decreased and the power adjusted under computer control to maintain a pre-set power-resistance isotherm. This power-resistance isotherm has been described in reference 153 and has been used to produce emitters with uniform quality. The isotherm was originally determined via a series of manual activations and it has not been necessary to adjust it since the original setting. Computer control removed the necessity for constant manual adjustment of the current as the resistivity of the emitters changed during the activation procedure. The stages of activation are: growth of protrusions, 5 - 10 hours after commencement of the procedure, initiation of branching of these protrusions and the formation of microneedles (10 - 25 hours), and finally elongation of the microneedles. Figure 2.16 shows scanning electron micrographs taken of one of the emitters with various magnifications. In general the microneedles produced were 50 μm in length but occasionally it was desirable to produce shorter microneedles, ~30 μm, and hence the activation procedure would be terminated early (after 30 - 35 hours).

b) Sample loading

Peptide samples were purchased from the Sigma Chemical Company Ltd.[154] and used without any further purification. μg quantities of sample were placed in a small glass dish (cut off sample vial) and dissolved in ~5 μl of either methanol, ethanol or propanol. These solvents were spectroscopic grade and purchased from Aldrich.[150] Spectroscopic grade dimethylformamide used by previous workers as a solvent for FD of peptides [69] was found to contain contaminants which produced erratic emissions during FD experiments. Where production of alkali cationated molecule-ions was desired sodium or potassium iodide were added to the solution in a 1 : 100 mass ratio to the peptide. FD emitters were then repeatedly dipped into this solution and excess solvent evaporated between dippings by blowing with a hot air blower. Between each dipping emitters were

a)

b)

Figure 2.16 Scanning electron micrographs of one of the FD emitters.
a) magnification x 15 showing emitter posts, wire and activated region
b) magnification x 200 showing length of microneedles to be 55 - 60μm

c)

d)

Figure 2.16 continued Scanning electron micrographs of one of the FD emitters.
c) magnification x 900 of microneedles, showing branching
d) magnification x 2700 of microneedles at the periphery of the activated region

observed under a microscope to check for sufficient quantities of sample deposited on the microneedles and also for an even coating. In most cases a fairly heavy loading of sample was desirable so as to maintain strong long-lasting ion currents. A sufficiently heavy loading was deemed to be when either a white or silvery layer could be observed under the microscope. Excess sample adhered to the tops of emitter posts was removed by washing with solvent, usually by dropping from a syringe. Attempts were made to load emitters from droplets of the solution from a μl syringe but failed to produce the desired heavy loadings. This may have been a result of insufficient wetting of the emitter by the solvent.

Loaded emitters were then positioned on the probe tip so as to be approximately 1.5 mm away from the counter electrode of the lens stack when the probe was wound fully into the source chamber of the mass spectrometer. In the case of the large-scale instrument, this was carried out with the aid of an optical jig and emitters could also be checked for alignment in the *z* and *y* directions. Misalignment was corrected for by bending the nichrome posts below the vespel base. When emitter potentials above 15 kV were to be used the emitter-counter electrode distance was increased, up to 4 mm. On the 4-sector mass spectrometer, the emitter-counter electrode distances were set by means of insertion of an unactivated emitter base, perpendicular to the usual positioning on the probe, into the source chamber until it reached the counter electrode. A micrometer attached to the probe handle was then used to retract the probe and set the desired distance. Due to the method of mounting of emitters onto the probe tip (Section 2.1.2), no facility was available for correcting any *z* or *y* direction misalignment caused by variation in the emitter bases.

c) Emitter heating and desorption of samples

On the large-scale mass spectrometer, emitters were heated by a constant current supply. The emitter heating current (EHC) was slowly manually adjusted until the total ion current (TIC) measured at the counter electrode increased. For most peptide samples an EHC of greater than 80 mA was required to promote desorption of molecule-ions. Initial increases in the TIC generally subsided and were found not to correspond with ion currents reaching the detector of the instrument. The most stable ion currents and successful experiments resulted when the EHC was increased gradually over a period of up to 1 hour. Any rapid fluctuations in the TIC were allowed to settle before further increases in the EHC were made. Rapid increases in the EHC were found to result in unstable ion currents and usually resulted in discharge. Such sparks had the effect of removing all the sample from the emitter, or of breakage of the emitter wire, and very often resulted in contamination of the counter electrode. A contaminated counter electrode also increased the likelihood of discharge and was usually accompanied by rapid fluctuations in the TIC reading or an unusually high TIC, very often off-scale, even with zero EHC. Hence a clean counter-electrode was of the utmost importance. Successful experiments corresponded with TIC readings of 20 - 100 nA lasting for periods of up to 5 hours and corresponded with an unattenuated parent ion current of ≥ 125,000 ions/s arriving at the detector. Different emitters were found to be associated with different source lens focussing conditions. Continual checking of the source lens tuning was necessary so as not to overlook an emission site producing strong ion currents. *Z*-deflection was most critical and corresponded to searching the length of the emitter for suitable emission sites. General observations concerning the use of field desorption for ionisation of peptides are discussed in Section 5.1.2.

2.4.2 Fast atom bombardment

The large-scale mass spectrometer was used with FAB ionisation for measurement of translational energy losses of caesium iodide cluster ions. A choice of targets was available with a range of angles to the probe tip and varying off-axis alignments to the source slit. Optimum signal intensities were found using a copper target of diameter of 4 mm with a 45° angle to the probe and positioned in line with the central axis of the mass spectrometer. A 5 - 10 μl droplet of a saturated solution of caesium iodide in distilled water was deposited onto the target and the solvent was then evaporated with a hot air blower. An even layer of caesium iodide was desirable, covering most of the surface area of the probe tip. The FAB gun would not operate with potentials above 6 kV without discharge occurring. Such discharges resulted in large noise spikes being recorded and incorporated into the spectrum. Therefore experiments were carried out with xenon beam energies of ≤ 6 kV. Various unsuccessful attempts were made to find the cause of the electrical discharging, and it was the use of the so-called 'top-hat' (section 2.1.2) which improved the accessible beam energy considerably from the previous restriction to a 4.5 keV xenon beam. Molecule-ion beams of caesium iodide could be maintained for several hours.

On the 4-sector mass spectrometer calibration experiments were carried out using caesium iodide applied to the stainless steel probe tips in the same manner as described above. These tips were not angled but were concave in design. Peptide samples were dissolved in a suitable solvent (usually methanol) to a concentration of approximately 1 mg/ml. A few μl of the solution would be deposited on the probe tip and a droplet of a suitable FAB matrix added. A matrix of a 1:1 mixture of glycerol and thioglycerol was used for valinomycin. For gramicidin D the sample solution in methanol was acidified with trifluoroacetic acid and a 1:3 mixture of dithioerythritol and dithiothreitol (referred to as 'magic

bullet') was used as the FAB matrix. For production of [M + cation]$^+$ molecular ions a small quantity of alkali salt was added to the sample solution in the same manner as for FD experiments. In the case of valine-gramicidin A, the sample solution no longer required acidification when alkali salt was added. The FAB gun used in these experiments produced 8 keV xenon atoms. Ion beams generated from biological samples were maintained for periods of a few minutes.

2.5 THEORETICAL WORK

2.5.1 Vibrational analysis

Vibrational frequencies for use with the QET calculations were determined with the aid of a computer program, 'vib'.[155] The program uses classical mechanics to calculate the vibrational frequencies from the cartesian co-ordinates and force constants associated with the possible vibrations of a given molecule. The cartesian co-ordinates were taken from x-ray crystallographic data and the internal co-ordinates were defined by consideration of all possible stretching, bending and torsional modes within the molecule. Force constants associated with these vibrations were estimated from literature values for small molecules. The program performs a series of matrix operations to find the normal vibrational modes via the so-called GF-matrix method. A detailed treatment of the mathematics involved has been given by Wilson *et al.*[156] and by Woodward.[157]

2.5.2 Quasi-equilibrium theory calculations

As described in Chapter 1 a simplification of Equation 1.1 is necessary for the practical calculation of $k(E)$. The calculation of $k(E)$ is limited to consideration of the vibrational states of the molecule. The computer program used for the calculation of rate constants by quasi-equilibrium theory was originally written by Nordholm [158] and later developed further by Uggerud [155] for use with large

molecules. It was necessary to make further changes for it to run successfully on the University of Warwick Unix system. The program was written in Fortran and the final version called RRKM7 is listed in Appendix 1.

Input data for RRKM7 consisted of a list of the fundamental vibrational frequencies for the reactant (NF = 3N - 6) followed by the vibrational frequencies of the transition state (NF - 1). The frequency removed for the transition state was estimated from known vibrational frequencies for the type of bond being broken. Other variables required for the calculations were: the critical energy for the reaction E_0, the number of energy steps NN to be taken to reach E_0, the total number of energy steps NM to be calculated (i.e. the maximum internal energy to which the calculation should be performed), and the grain size ES. The grain size was the energy interval used for the smoothing of $k(E)$. The choice of a classical or quantum mechanical calculation was available. The latter is really a semi-classical approach and calculates a value for the zero point energy and incorporates this in the calculation of $k(E)$. A purely classical calculation with no zero point energy treatment results in rates which are too low, particularly at low energies.[159] A description of the formatting of the input data is given at the beginning of the program. Typical values of NN were chosen to give energy step sizes of 17 cm^{-1} and the value of the grain size ES was usually set at 10 cm^{-1}. A discussion of the effect of these variables on the calculated rate constants is given in Chapter 7. The normal method for counting densities of vibrational states is to count the number of ways in which an energy E can be distributed amongst the available energy levels. This method of counting becomes very time consuming as the size of the molecule under consideration increases. Both programs calculate the density of states using the Beyer and Swinehart algorithm.[160] This method considers each energy state individually and counts the number of ways that the state can accept the given energy.

Chapter 3 : FOUR-SECTOR TANDEM MASS SPECTROMETRY OF PEPTIDES

3.1 INTRODUCTION

The use of a four-sector mass spectrometer with an electrically floated collision cell for collision-induced decomposition (CID) experiments has the advantages over the use of mass-analysed ion kinetic energy spectroscopy of increased resolution and improved sensitivity particularly for low-mass fragment ions. Linked-scanning of the second electric and magnetic sector combination results in re-focussing of fragment ions formed with slightly lower kinetic energies resulting from the translational energy lost ΔE by parent ions during CID. Whereas in MIKES these energy losses result in considerable shifts in the fragment ion peaks' positions, and hence the mass assignments may become ambiguous since the mass-scale is calculated assuming a proportioning of translational energy with mass, $m_f = m_i(V_e/V_i)$, (see Section 1.3, Equation 1.3). These translational energy losses are used as indicators of the internal energy uptake during CID and their dependence on other factors, such as target gas pressure, may give important clues concerning the mechanism of CID. Chapters 5 and 6 are concerned with studies of these energy losses, but to reduce the uncertainties in their measurements the ambiguities in the fragment ion mass assignments need to be overcome, and in this case a 4-sector mass spectrometer has been used to identify the fragment ion masses to within ± 0.3 Da. The work presented in this chapter was therefore primarily concerned with identifying the masses of fragment ions of peptides to be used in subsequent studies of CID dynamics, however, also of interest was the dependence of tandem mass spectra on the ionisation method employed. This latter work follows a previous study made by

Sheil [69] who reported variations in the tandem mass spectra of molecule-ions of the peptide bradykinin and cyclic depsipeptide valinomycin, formed by FAB and FD. This earlier study made use of the MIKES technique and hence was subject to some ambiguity in fragment ion mass assignments as a result of translational energy losses of parent ions.[69] In this chapter, 4-sector tandem mass spectra are reported and compared for valinomycin $[M+H]^+$ ions formed by FAB, $[M+Na]^+$ ions formed by FAB and FD, and $M^{+\cdot}$ ions formed by FD and electron impact ionisation (EI). One explanation for differences, which may arise in the tandem mass spectra, is the formation of different structural isomers or mixture of isomers when different ionisation techniques are used. It is generally assumed that the structure of a molecule-ion is the same as that of the neutral molecule (excepting the addition of a proton, removal of an electron or whatever) and tandem mass spectrometry is used as a probe to identify that structure. Hence comparison of the tandem mass spectra of molecule-ions formed by a number of ionisation methods is of fundamental interest.

3.1.1 Field desorption experiments on the 4-sector mass spectrometer

As described in Section 2.2.3, the field desorption lens stack for use on the 4-sector mass spectrometer was constructed 'in-house'. Preliminary field ionisation experiments with acetone and field desorption experiments with the cyclic depsipeptide valinomycin produced molecule-ion beams arriving at the detector of the order of 10^{-14} A. These ion currents were at least an order of magnitude lower than those obtained by FAB, and were found to be fairly short-lived compared with ion beams generated during FD experiments on the large-scale mass spectrometer. This can be explained in terms of the use of higher emitter heating currents in an attempt to provide an ion beam of sufficient intensity to be used for tandem mass spectrometry. Modifications were made to the original FD lens stack design and a z-focussing lens was added. This resulted in a five-fold increase in sensitivity. Ion beams, however, were still of relatively low intensity,

even with cholesterol and valinomycin samples, which were known to ionise relatively well by FD. Although some 4-sector tandem mass spectra are shown, poor signal-to-noise ratios make comparisons of the relative intensities of fragment ions less reliable. FD-4-sector tandem mass spectra have only been recorded for the sample valinomycin. A further modification proposed for the FD lens stack, in an attempt to further improve sensitivity, is to supply the high-potential for the shield electrode from a separate supply to the contact block. Since the shield electrode was split in two halves, a deflection voltage could also be applied. These adjustments might result in additional focussing of the ion beam through the counter electrode slit and compensate for any misalignment of the emitters. These modifications had not been made prior to the completion of this thesis and currently ion optical calculations are being made to further improve the design of the lens stack.

3.2 VALINE-GRAMICIDIN A

3.2.1 Tandem mass spectrometry of valine-gramicidin A $[M+H]^+$ ions formed by FAB

Valine-gramicidin A (RMM = 1881.1) is the major component of the mixture gramicidin D; its amino acid sequence is shown in Figure 3.1. The 4-sector tandem mass spectrum of valine-gramicidin A $[M+H]^+$ ions (m/z 1882.1) formed by fast-atom bombardment is shown in Figure 3.2 and is similar to that obtained by Biemann.[81] All the 4-sector tandem mass spectra shown in this thesis are presented as peak centroids. The parent ion peaks are saturated and therefore the centroiding routine of the datasystem may not assign the masses with the usual accuracy. The tandem mass spectrum of valine-gramicidin A $[M+H]^+$ ions was obtained with argon as collision gas with a pressure sufficient to attenuate the parent ion beam by 70 - 80 %. A collision cell potential of 4 kV was used

HCO-Val-Gly-Ala-Leu-Ala-Val-Val-Val-Trp-Leu-Trp-Leu-Trp-Leu-Trp-$NHCH_2CH_2OH$

Calculated molecular mass = 1881.067 Da (^{12}C, ^{1}H, ^{16}O, ^{14}N)

Figure 3.1 Amino acid sequence of the peptide valine-gramicidin A

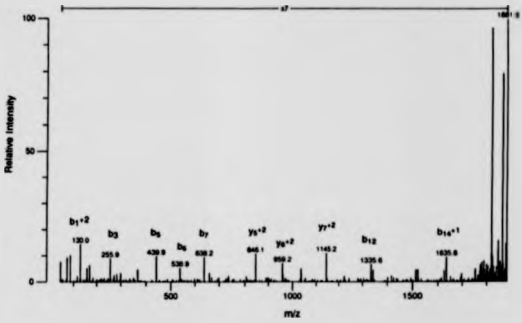

Figure 3.2 4-sector tandem mass spectrum of valine-gramicidin A $[M+H]^+$ ions (m/z 1882.1) formed by FAB.

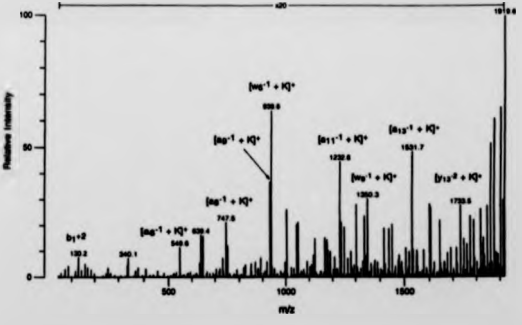

Figure 3.3 4-sector tandem mass spectrum of valine-gramicidin A $[M+K]^+$ ions (m/z 1920.2) formed by FAB.

TABLE 3.1

Assignments of the major fragment ions in the FAB-4-sector tandem mass spectrum (Figure 3.2) of valine-gramicidin A $[M+H]^+$ ions (m/z 1882.1)

Measured m/z	Relative Intensity	Fragment ion assignment
1863.5	11.4	Loss of H_2O
1847.0	2.3	
1820.6	13.8	Loss of $NH_2CH_2CH_2OH$
1799.7	1.0	
1789.0	1.2	
1781.0	1.1	x_{14}
1755.0	0.7	y_{14}^{+2}
1753.0	0.6	v_{14} (or y_{14})
1698.0	0.5	y_{13}^{+2}
1635.6	1.4	b_{14}^{+1}
1634.3	1.2	b_{14}
1626.5	0.6	y_{12}^{+2}
1521.5	0.7	b_{13}
1513.6	0.3	y_{11}^{+2}
1417.3	0.3	
1343.3	0.7	y_9^{+2}
1335.6	1.0	b_{12}
1224.2	0.3	b_{11}^{+1}
1145.2	1.6	y_7^{+2}
1036.3	0.7	b_{10}
959.2	1.0	y_6^{+2}
846.1	1.5	y_5^{+2}
737.0	0.3	b_8
659.9	0.5	y_{11}^{+2}
638.2	1.4.	b_7
538.9	0.8	b_6
439.9	1.4	b_5

TABLE 3.1 CONTINUED

Assignments of the major fragment ions in the FAB-4-sector tandem mass spectrum (Figure 3.2) of valine-gramicidin A $[M+H]^+$ ions (m/z 1882.1)

Measured m/z	Relative Intensity	Fragment ion assignment
369.0	0.7	b_4
300.0	0.5	d_4^{+1}
255.9	1.3	b_3
170.0	0.9	
159.0	0.8	Tryptophyl immonium ion
130.0	2.1	b_1^{+2}
86.1	1.5	Leucyl immonium ion
72.0	1.3	Valyl immonium ion
44.0	1.1	Alanyl immonium ion

TABLE 3.2

Assignments of the major fragment ions in the FAB-4-sector tandem mass spectrum (Figure 3.3) of valine-gramicidin A $[M+K]^+$ ions (m/z 1920.2)

Measured m/z	Relative Intensity	Fragment ion assignment
1903.4	3.3	Loss of OH or NH_3
1876.2	3.0	Loss of C_3H_8 or $[z_{15} + K]^+$
1861.3	2.6	Loss of $NHCH_2CH_2OH$
1830.4	0.8	$[a_{15}^{-2} + K]^+$
1827.9	0.7	
1818.6	1.3	$[x_{14}^{-1} + K]^+$
1789.0	1.1	Loss of C_9H_9N
1774.1	1.2	
1760.2	0.6	
1747.6	0.7	
1733.5	1.4	$[y_{13}^{-2} + K]^+$
1715.5	0.6	
1690.9	0.6	$[c_{14}^{+1} + K]^+$
1676.8	0.5	
1644.5	1.1	$[a_{14}^{-1} + K]^+$
1606.6	1.4	$[w_{12} + K]^+$ or $[v_{12}^{-1} + K]^+$
1604.8	1.1	
1602.1	1.4	$[d_{14}^{-2} + K]^+$
1577.1	0.5	$[x_{11}^{-2} + K]^+$
1550.5	0.5	$[y_{11}^{-1} + K]^+$
1535.6	0.5	$[v_{11}^{-1} + K]^+$
1531.7	2.4	$[a_{13}^{-1} + K]^+$
1506.3	0.6	$[x_{10}^{-2} + K]^+$
1478.2	0.4	$[y_{10}^{-2} + K]^+$
1449.7	1.0	$[w_{10}^{-1} + K]^+$
1436.8	0.9	$[v_{10}^{-1} + K]^+$
1416.5	1.0	$[d_{13}^{-1} + K]^+$
1350.3	1.5	$[w_9^{-1} + K]^+$

TABLE 3.2 CONTINUED

Assignments of the major fragment ions in the FAB-4-sector tandem mass spectrum (Figure 3.3) of valine-gramicidin A $[M+K]^+$ ions (m/z 1920.2)

Measured m/z	Relative Intensity	Fragment ion assignment
1345.4	0.4	$[a_{12}^{-1} + K]^+$
1337.4	1.2	$[v_9^{-1} + K]^+$
1303.4	1.4	$[d_{12}^{-1} + K]^+$
1251.5	1.0	$[w_8^{-1} + K]^+$
1238.3	1.1	$[v_8^{-1} + K]^+$
1232.6	2.2	$[a_{11}^{-1} + K]^+$
1190.3	0.5	
1181.5	0.5	$[y_7^{-1} + K]^+$
1176.5	0.7	
1166.9	0.8	$[z_7^{-1} + K]^+$
1124.6	0.7	
1117.7	0.4	$[d_{11}^{-1} + K]^+$
1052.4	1.1	$[w_7 + K]^+$
1046.7	1.0	$[a_{10}^{-1} + K]^+$
1004.5	1.3	$[d_{10}^{-1} + K]^+$
938.6	3.2	$[w_6^{-1} + K]^+$
933.4	1.8	$[a_9^{-1} + K]^+$
753.3	0.6	$[w_5 + K]^+$
747.5	1.1	$[a_8^{-1} + K]^+$
648.4	0.8	$[a_7^{-1} + K]^+$
639.4	0.8	$[w_4^{-1} + K]^+$
549.5	0.6	$[a_6^{-1} + K]^+$
340.1	0.4	$[w_2^{-1} + K]^+$
130.2	0.4	b_1^{+2}

resulting in a laboratory frame collision energy of 4 keV. The proposed fragment ion assignments are listed in Table 3.1 using the nomenclature outlined in Section 1.6.1. The spectrum contains predominantly y^{+2}- and b-type sequence ions plus the immonium ions formed from the amino acids Trp, Leu, Ala and Val. Sequence ions of the y-type are characteristic of all peptides except those containing an N-terminal arginine and b-type ions are common for peptides which contain an N-terminal acyl group or those lacking basic amino acids.[9] Hence, since valine-gramicidin A has an N-terminal acyl group and lacks basic amino acids it produces a tandem mass spectrum dominated by y- and b-type sequence ions which reflect these structural characteristics. The most intense fragment ion peak in the spectrum corresponds with the loss of 61 mass units and has been attributed to loss of the C-terminal moiety with an additional hydrogen atom. A number of fragment ion assignments are missing from the table where the structure of the fragment ion does not correspond to a common sequence ion or to an obvious side chain cleavage. In order to identify these fragment ions, more detailed tandem mass spectrometry studies would be required.

3.2.2 Tandem mass spectrometry of valine-gramicidin A $[M+K]^+$ ions formed by FAB

Figure 3.3 shows the 4-sector tandem mass spectrum of the $[M+K]^+$ ions of valine-gramicidin A (m/z 1920.2) formed by FAB of a solution of gramicidin D and KI salt in methanol, with magic bullet as matrix. The spectrum was obtained with argon collision gas at a pressure corresponding with ~70 % attenuation of the parent ion beam and with a laboratory frame collision energy of 4 keV. Suggested assignments of the more intense fragment ions are listed in Table 3.2. In contrast to the tandem mass spectrum of the $[M+H]^+$ ions, sequence ions of the b- and y-types are absent or of low intensity for $[M+K]^+$ molecule-ions. Instead, the spectrum is dominated by sequence ions of the type $[a_n^{-1} + K]^+$. In addition many

d- and w-type ions were observed which were absent in the $[M+H]^+$ case. Recently, Tomer *et al.*[161] have discussed the tandem mass spectrometry of sodiated peptides and peptide-amides. The results obtained for [M+cation]$^+$ molecule-ions of valine-gramicidin A are consistent with the results obtained by these authors. Formation of $[a_n^{-1}$ + cation$]^+$ type sequence ions of relatively high abundance was found to be characteristic of the spectra of cationised peptides.[161-164] The mechanism of formation of these ions was originally attributed to charge-remote fragmentations [162] although Gross *et al.*[163] and Teesch and Adams [164] have proposed a mechanism in which the charge site is directly involved and is illustrated by Scheme A where X represents the cation.

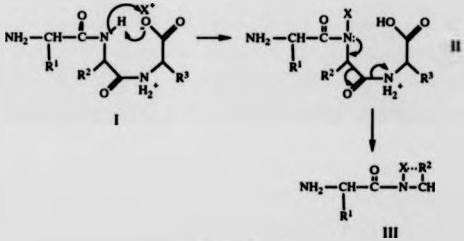

Scheme A

The relative abundances of these $[a_n^{-1}$ + cation$]^+$ was found to be dependent upon the structure of the amino acid which becomes the new C-terminus, R^2 in Scheme A.[163] The observed trends reflected the binding affinities of cations to amino acids measured in solution chemistry, with the most abundant of the $[a_n^{-1}$ + cation$]^+$ ions occurring when R^2 was aromatic.[70,163] This was attributed to the formation of stable chelate rings.[163] Other dominant fragment ions in the CID spectra of [M+cation]$^+$ molecule-ions are observed to be of the type

$[b_n+cation+OH]^+$ [161] although these sequence ions are not present in the spectrum of valine-gramicidin A shown in Figure 3.3. The absence of fragment ions of the $[b_n+cation+OH]^+$ type in this case, is consistent with the proposed mechanism of formation of these ions, where the site of cationisation is the C-terminal carboxylate group.[161] In valine-gramicidin A the C-terminus is an amide group and the alkali metal cation would be unlikely to replace this amide hydrogen in preference to any other along the peptide backbone. The tandem mass spectra of cationised molecule-ions have also been useful for identifying the C-terminal amino acid in peptides.[165] An imine, $NH=CHR_n$ and CO are eliminated after nucleophilic attack on the carbonyl group of the (n-1) amino acid by the C-terminal carboxylate anion.[163,166]

The mechanisms of formation of d- and w-type ions are thought to be via charge-remote fragmentation in the case of both $[M+H]^+$ and $[M+cation]^+$ molecule-ions.[81,161] In the case of protonated peptides abundant d- and w-type ions have been observed when amino acids with high proton affinity are present in the peptide.[81] Enhancement of these ions in the spectra of cationated peptides has been attributed to increased localisation of the charge through interactions with amino acids with high cation affinity. Valine-gramicidin A has no strongly basic amino acids, such as Arg or Lys, and therefore the absence of d- and w-type ions in the tandem mass spectrum of $[M+H]^+$ ions is expected. For the $[M+K]^+$ molecule-ions, interactions between the Trp side chain and the potassium ion may be promoting these types of fragmentations.[161] The mechanism of formation of ions of the w-type has been shown to involve cleavage of the β–γ carbon bonds of the amino acid side chain [167] and is illustrated in Scheme B for leucine.

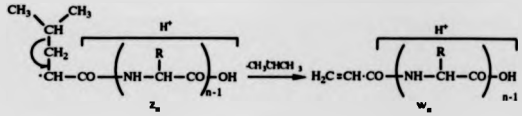

Scheme B

In the tandem mass spectrum of valine-gramicidin A $[M+K]^+$ ions, w-type ions have been observed for all Trp, Leu and Val residues (Table 3.2) but not for Gly and Ala residues which lack $\beta-\gamma$ bonds. Fragment ions of the type $[y_n^{-1}$ + cation$]^+$ were also found to be enhanced in the tandem mass spectra of $[M+cation]^+$ molecule-ions.[161] In the valine-gramicidin A case, fragment ions attributed to $[y_n^{-2} + K]^+$ were present for n=14, 13, and 10 and to $[y_n^{-1} + K]^+$ for n=11 and 7. Except in the case of $[y_{13}^{-2} + K]^+$ these fragment ions were of low relative intensities compared with the $[a_n^{-1} + K]^+$ type sequence ions.

3.3 VALINOMYCIN

Valinomycin is a cyclic depsipeptide consisting of alternate peptide and ester linkages. The structure of valinomycin is shown in Figure 3.4. This depsipeptide is composed of the residues valine, lactic acid and D-α-hydroxyisovaleric acid (Hyv) and the presence of the ester linkages make the molecule sufficiently volatile to be ionised by electron impact as well as by field desorption.

Differences in the CID-MIKE spectra of molecule-ions of valinomycin had previously been observed by Sheil [69] when field desorption and fast-atom bombardment were employed to ionise the sample. In the following sections tandem mass spectra are reported for $M^{+\cdot}$, $[M+H]^+$, $[M+Na]^+$ and $[M+K]^+$ ions of valinomycin. $M^{+\cdot}$ ions were formed by FD and EI, $[M+H]^+$ and $[M+K]^+$ ions by FAB and $[M+Na]^+$ by FAB and FD. All spectra were obtained using a

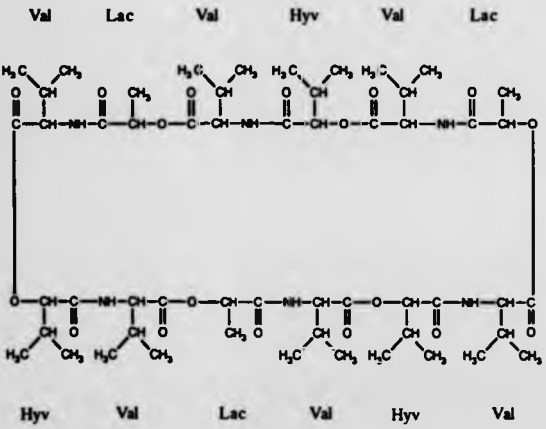

Figure 3.4 Structure of the cyclic depsipeptide valinomycin (RMM = 1110.629). Hydroxyisovaleric acid = Hyv, Lactic acid = Lac.

laboratory frame collision energy of 4 keV and with helium employed as target gas with sufficient pressure to attenuate the parent ion beam by ~70%.

3.3.1 Tandem mass spectrometry of valinomycin $M^{+\cdot}$ ions

Figure 3.5 shows the 4-sector tandem mass spectrum of valinomycin $M^{+\cdot}$ ions formed by electron impact ionisation at an electron energy of 70 eV. The masses and most probable assignments of the relatively more intense fragment ions are given in Table 3.3. Since the depsipeptide is cyclic and has no N or C terminus, the nomenclature for describing the fragment ions outlined in Section 1.6.1 cannot be used, and therefore the component amino acids of the fragment ions are listed in full. The most intense fragment ion in the spectrum is due to the loss of 42 mass units which corresponds with the loss of C_3H_6. This fragmentation is thought to occur via a McLafferty rearrangement [168] involving the side chains of the Hyv and Val residues, as illustrated in Figure 3.6. The next most intense fragment ion appears at m/z 997.6 and corresponds with loss of [Val + O] with a transfer of two H atoms from the neutral to the charged fragment. Such a cleavage may occur at the CH-O bond of either a Hyv or a Lac residue. A further cluster of fragment ions surrounding the m/z 997.6 fragment are also of relatively high intensities and have been assigned in Table 3.3. The mechanisms of fragmentation have not been studied in detail and the assignments given are therefore not proven but suggest the most probable structures. At m/z 72 the fragment ion corresponding with the formation of the valyl immonium ion can be observed. The presence of immonium ions in the tandem mass spectra of peptides is important for identifying the component amino acids.

The tandem mass spectrum of $M^{+\cdot}$ ions formed by field desorption, Figure 3.7, also shows the same dominant fragment ion corresponding with the loss of C_3H_6. The intensity of the parent ion beam formed by FD was at least two orders of magnitude lower than that obtained by EI and hence the signal-to-noise ratio of

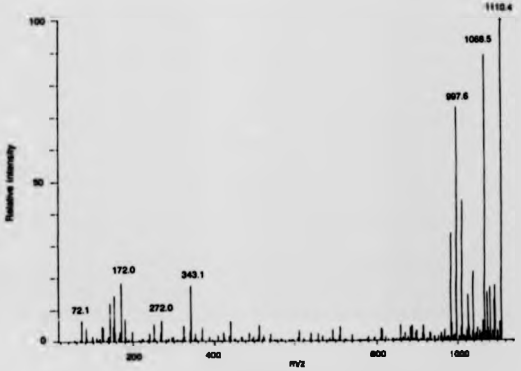

Figure 3.5 4-sector tandem mass spectrum of valinomycin $M^{+\cdot}$ ions (m/z 1110.6) formed by EI.

TABLE 3.3

Assignments of the major fragment ions in the EI-4-sector tandem mass spectrum (Figure 3.5) of valinomycin $M^{+\cdot}$ ions (m/z 1110.6)

Measured m/z	Relative Intensity	Fragment ion assignment
1095.7	2.5	Loss of CH_3
1092.4	1.9	Loss of H_2O
1086.6	0.5	
1082.5	2.4	Loss of CO
1075.3	2.2	
1068.5	12.8	Loss of C_3H_6
1064.0	1.0	Loss of HCOOH
1055.3	0.5	$[(HyvValLacVal)_2ValHyvVal + O + H]^+$
1051.5	0.6	Loss of NH_2COCH_3
1039.6	3.1	$[(HyvValLacVal)_2ValHyvVal + H]^+$
1029.5	0.6	
1027.5	2.1	$[(HyvValLacVal)_2ValLacVal + O + H]^+$
1023.9	0.5	
1011.5	6.3	$[(HyvValLacVal)_2ValLacVal + H]^+$ OR $[(HyvValLacVal)_2HyvValLac]^+$
1009.3	0.6	$[(HyvValLacVal)_2ValLacVal$ minus $H]^+$
997.6	10.5	$[(HyvValLacVal)_2HyvValLac + 2H$ minus $O]^+$
982.9	4.8	$[(HyvValLacVal)_2HyvValLac$ minus CO & $H]^+$
966.7	0.5	$[(HyvValLacVal)_2HyvVal + CO$ minus $H]^+$
912.4	0.7	$[(HyvValLacVal)_2ValLac + H]^+$
884.4	0.7	$[(HyvValLacVal)_2ValLac + H$ minus $CO]^+$
882.0	0.6	$[(HyvValLacVal)_2ValLac$ minus CO & $H]^+$
858.4	0.7	
814.4	0.5	$[(HyvValLacVal)_2Lac + 2H]^+$
812.4	0.5	$[(HyvValLacVal)_2Lac]^+$
713.4	0.6	$[(HyvValLacVal)_2 + H$ minus $CO]^+$

TABLE 3.3 CONTINUED

Assignments of the major fragment ions in the EI-4-sector tandem mass spectrum (Figure 3.5) of valinomycin $M^{+\bullet}$ ions (m/z 1110.6)

Measured m/z	Relative Intensity	Fragment ion assignment
613.1	0.5	[(HyvValLacVal)HyvValLac minus CO]$^+$
514.2	0.7	[(ValLacValHyv)ValLac + H minus CO]$^+$
443.0	0.5	[(HyvValLacVal)Lac + H]$^+$
442.0	0.9	[(HyvValLacVal)Lac]$^+$
371.0	0.6	[HyvValLacVal + H]$^+$
343.1	2.5	[HyvValLacVal minus CO + H]$^+$
325.0	0.7	[ValHyvVal + CO minus H]$^+$
324.0	0.5	[ValHyvVal + CO minus 2H]$^+$
272.0	1.0	[ValLacVal + H]$^+$ or [HyvValLacVal]$^+$
253.9	0.5	[LacValHyv minus O & H]$^+$
252.9	0.8	[LacValHyv minus O & 2H]$^+$
182.0	1.0	[ValHyv minus O & H]$^+$
181.0	0.9	[LacValHyv minus O &2H]$^+$
172.0	2.7	[ValLac + H]$^+$
155.0	0.6	[ValLac minus O]$^+$
154.0	2.1	[ValLac minus O & H]$^+$
153.0	0.6	[ValLac minus O & 2H]$^+$
144.0	1.7	[ValLac + H minus CO]$^+$
127.1	0.6	[Val-C=O]$^+$
125.1	0.7	
82.1	0.6	[Val minus NH & 2H]$^+$ OR [Hyv minus O & 2H]$^+$
72.1	1.0	Valyl immonium ion

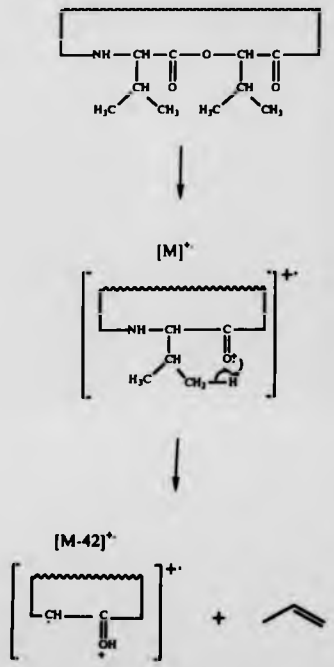

Figure 3.6 Mechanism for the loss of C_3H_6 from Hyv or Val residues in the tandem mass spectra of valinomycin $M^{+\cdot}$ ions.

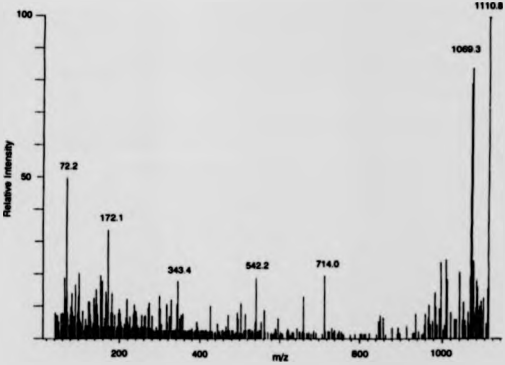

Figure 3.7 4-sector tandem mass spectrum of valinomycin $M^{+\cdot}$ ions (m/z 1110.6) formed by FD.

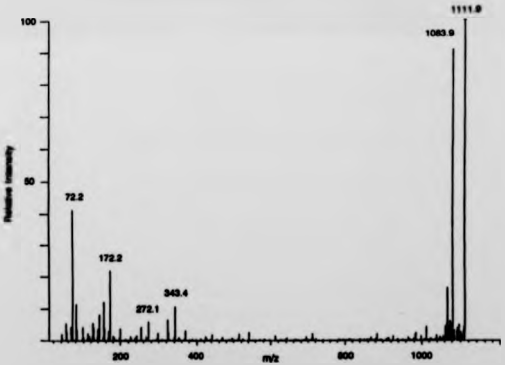

Figure 3.8 4-sector tandem mass spectrum of valinomycin $[M+H]^+$ ions (m/z 1111.6) formed by FAB.

TABLE 3.4

Assignments of the major fragment ions in the FD-4-sector tandem mass spectrum (Figure 3.7) of valinomycin $M^{+\cdot}$ ions (m/z 1110.6)

Measured m/z	Relative Intensity	Fragment ion assignment
1095.4	0.6	Loss of CH_3
1082.5	0.8	Loss of CO
1079.7	0.9	
1073.4	1.2	
1070.0	1.8	
1069.3	4.2	
1068.6	4.0	Loss of C_3H_6
1066.7	1.0	
1040.0	1.0	$[(HyvValLacVal)_2ValHyvVal + H]^+$
1011.9	0.9	$[(HyvValLacVal)_2ValLacVal + H]^+$ OR $[(HyvValLacVal)_2HyvValLac]^+$
1009.2	1.2	$[(HyvValLacVal)_2ValLacVal - H]^+$
998.4	1.1	
997.5	1.2	Loss of [Val + O minus 2H]
982.2	0.7	$[(HyvValLacVal)_2HyvValLac$ minus CO & $H]^+$
966.1	0.3	$[(HyvValLacVal)_2HyvVal$-CO minus $H]^+$
858.1	0.3	
713.9	1.0	$[(HyvValLacVal)_2$ + H minus CO$]^+$
542.2	1.0	
343.4	0.9	$[HyvValLacVal$ minus CO + $H]^+$
325.1	0.6	[ValHyvVal-C=O minus $H]^+$
298.8	0.7	
272.3	0.5	$[ValLacVal + H]^+$ or $[HyvValLacVal]^+$
253.1	0.4	[LacValHyv minus O & 2H$]^+$
172.1	1.7	$[ValLac + H]^+$
155.1	0.5	[ValLac minus O$]^+$

TABLE 3.4 CONTINUED

Assignments of the major fragment ions in the FD-4-sector tandem mass spectrum (Figure 3.7) of valinomycin $M^{+\cdot}$ ions (m/z 1110.6)

Measured m/z	Relative Intensity	Fragment ion assignment
154.2	0.9	[ValLac minus O & H]$^+$
144.2	0.8	[ValLac minus CO + H]$^+$
127.1	0.6	[Val-C=O]$^+$
125.1	0.6	
101.1	1.0	[Hyv + H]$^+$
72.2	2.5	Valyl immonium ion

TABLE 3.5

Assignments of the major fragment ions in the FAB-4-sector tandem mass spectrum (Figure 3.8) of valinomycin $[M+H]^+$ ions (m/z 1111.6)

Measured m/z	Relative Intensity	Fragment ion assignment
1096.9	1.0	Loss of CH_3
1083.9	18.2	Loss of CO
1082.5	1.0	Loss of C_2H_5 or HCO
1081.7	1.1	
1079.7	0.9	
1076.4	1.2	
1074.5	1.3	
1073.1	0.9	
1071.9	0.9	
1069.1	3.3	Loss of C_3H_7
1066.0	1.1	$[(HyvValLacVal)_2ValHyvVal + CO$ minus $H]^+$
1063.1	0.9	
1012.1	0.9	$[(HyvValLacVal)_2HyvLacVal + H]^+$
343.3	2.1	$[(HyvValLacVal) + H$ minus $CO]^+$
342.9	1.1	$[(HyvValLacVal)$ minus $CO]^+$
325.2	1.3	$[ValHyvVal + CO$ minus $H]^+$
272.1	1.2	$[HyvValLac + H]^+$
254.2	0.9	$[HyvValLac + H$ minus O & $2H]^+$
172.2	4.4	$[ValLac + H]^+$
155.2	1.1	$[(CH_3)_2CCH\text{-}O\text{-}CO\text{-}CHC(CH_3)_2]^+$
154.2	2.5	$[ValLac + H +$ minus O & $2H]^+$
144.2	1.6	$[ValLac + H$ minus $CO]^+$
126.1	1.1	$[Val\text{-}CO$ minus $H]^+$
98.2	0.9	
83.2	2.3	$[Hyv + H$ minus O & $2H]^+$ AND/OR $[Val + H$ minus NH & $2H]^+$
72.2	8.3	Valyl immonium ion
69.1	0.9	
55.2	1.1	$O{=}C^+CHCH_2$

the spectrum is much lower. Combined with poor ion statistics this makes the relative intensities of the fragment ions in the FD tandem mass spectrum less reliable. The fragment ions of significant relative intensity are listed in Table 3.4 together with their proposed assignments. In general the masses of the fragment ions correlate with those in the EI tandem mass spectrum. Overall the FD spectrum shows a lesser degree fragmentation than the EI case and is dominated by one intense fragment ion attributed to the loss of C_3H_6.

3.3.2 Tandem mass spectrometry of valinomycin $[M+H]^+$ ions

Figure 3.8 shows the tandem mass spectrum of valinomycin $[M+H]^+$ ions formed by FAB with the masses and assignments of the more intense fragment ions listed in Table 3.5. The general appearance of the spectrum is similar to that obtained for $M^{+\cdot}$ ions formed by FD, showing one intense high-mass fragment ion and several relatively intense low-mass fragment ions at m/z 72, 172 and 343 corresponding with the valyl immonium ion, $[ValLac + H]^+$ and $[(HyvValLacVal)_2 + H \text{ minus } CO]^+$ respectively. The intense high-mass fragment ion in the FAB case corresponds with the loss of 28 Da and has been attributed to the loss of CO, whereas the most intense fragment ion in the FD tandem spectrum was assigned to the loss of C_3H_6.

3.3.3 Tandem mass spectrometry of valinomycin $[M+Na]^+$ and $[M+K]^+$ ions

The 4-sector tandem mass spectrum of valinomycin $[M+Na]^+$ molecule-ions formed by FAB is shown in Figure 3.9. The general appearance of the spectrum reveals extensive fragmentation across the whole mass range. A number of fragment ions can be assigned to sequence ions of the peptide where direct cleavages of the amide or ester bonds of the molecule-ion have taken place. Also present are several series of fragment ions which appear 14 and 26 mass units below the sequence ions and also 16 and 28 mass units above. These

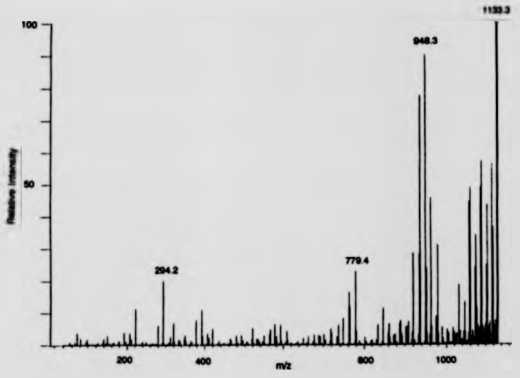

Figure 3.9 4-sector tandem mass spectrum of valinomycin $[M+Na]^+$ ions (m/z 1133.6) formed by FAB.

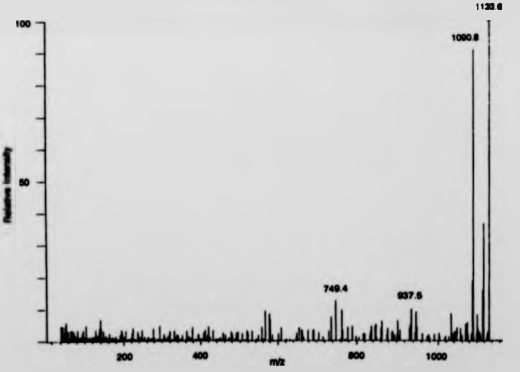

Figure 3.10 4-sector tandem mass spectrum of valinomycin $[M+Na]^+$ ions (m/z 1133.6) formed by FD.

TABLE 3.6

Assignments of the major fragment ions in the FAB-4-sector tandem mass spectrum (Figure 3.9) of valinomycin $[M+Na]^+$ ions (m/z 1133.6)

Measured m/z	Relative Intensity	Fragment ion assignment
1118.5	9.1	Loss of CH_3
1117.1	14.1	Loss of CH_4
1105.3	11.0	Loss of CO
1103.1	6.2	Loss of H_2CO
1090.5	14.3	Loss of C_3H_7
1088.8	12.3	Loss of either HCO_2 or $OCHCH_3$
1077.3	3.0	$[(HyvValLacVal)_2ValHyvVal + Na + O]^+$
1075.2	8.5	
1074.1	2.0	
1073.2	6.1	
1061.6	12.3	$[(HyvValLacVal)_2ValHyvVal + Na]^+$
1059.1	11.2	$[(HyvValLacVal)_2ValHyvVal + Na$ minus $2H]^+$
1048.9	1.0	$[(HyvValLacVal)_2ValLacVal + Na + O]^+$
1047.1	3.4	$[(HyvValLacVal)_2ValHyvVal + H + Na$ minus $NH]^+$
1045.0	1.0	
1034.4	1.1	$[(HyvValLacVal)_2HyvValLac + Na]^+$
1033.2	1.0	$[(HyvValLacVal)_2ValLacVal + Na]^+$
1031.4	4.7	$[(HyvValLacVal)_2ValLacVal + Na$ minus $2H]^+$
1020.3	1.0	$[(HyvValLacVal)_2HyvValLac + 2H + Na$ minus $O]^+$
1017.4	1.3	
1004.2	0.9	
1002.3	1.2	
989.4	1.4	
988.2	1.3	
978.4	7.8	$[(HyvValLacVal)_2HyvVal + Na + O]^+$ and/or $[(HyvValLacVal)_2ValLac + Na + O + CO]^+$

TABLE 3.6 CONTINUED

Assignments of the major fragment ions in the FAB-4-sector tandem mass spectrum (Figure 3.9) of valinomycin $[M+Na]^+$ ions (m/z 1133.6)

Measured m/z	Relative Intensity	Fragment ion assignment
974.4	2.2	
964.4	1.4	$[(HyvValLacVal)_2HyvVal + Na + 2H]^+$
962.4	11.5	$[(HyvValLacVal)_2HyvVal + Na]^+$
950.2	6.0	$[(HyvValLacVal)_2ValLac + Na + O]^+$
948.3	22.6	$[(HyvValLacVal)_2HyvVal + 2H + Na$ minus $O]^+$
936.3	19.4	$[(HyvValLacVal)_2HyvVal + 2H + Na$ minus $CO]^+$
934.3	7.1	$[(HyvValLacVal)_2ValLac + Na]^+$
920.4	7.1	$[(HyvValLacVal)_2ValLac + 2H + Na$ minus $O]^+$
908.3	1.8	$[(HyvValLacVal)_2ValLac + 2H + Na$ minus $CO]^+$
906.3	1.4	$[(HyvValLacVal)_2Val + Na + CO$ & $+ O]^+$
902.3	1.4	
890.4	1.9	$[(HyvValLacVal)_2Val + Na + CO]^+$
888.4	1.7	
863.3	1.7	$[(HyvValLacVal)_2Hyv + Na]^+$
860.3	1.0	$[(HyvValLacVal)_2Val + Na$ minus $2H]^+$
849.3	2.9	$[(HyvValLacVal)_2Hyv + 2H + Na$ minus $O]^+$
836.4	1.6	$[(HyvValLacVal)_2Val + 2H + Na$ minus $CO]^+$
781.3	1.1	$[(HyvValLacVal)_2 + 2H + Na + O]^+$
779.4	5.7	$[(HyvValLacVal)_2 + Na + O]^+$
765.3	3.0	$[(HyvValLacVal)_2 + Na + 2H]^+$
763.4	4.1	$[(HyvValLacVal)_2 + Na]^+$
749.3	2.1	$[(HyvValLacVal)_2 + 2H + Na$ minus $O]^+$
737.2	1.5	$[(HyvValLacVal)_2 + 2H + Na$ minus $CO]^+$
719.4	1.2	$[(HyvValLacVal)ValHyvVal + Na + CO]^+$
608.3	1.0	$[(HyvValLacVal)HyvVal + Na + O]^+$

TABLE 3.6 CONTINUED

Assignments of the major fragment ions in the FAB-4-sector tandem mass spectrum (Figure 3.9) of valinomycin $[M+Na]^+$ ions (m/z 1133.6)

Measured m/z	Relative Intensity	Fragment ion assignment
592.4	1.5	[(HyvValLacVal)HyvVal + Na]$^+$
578.3	1.6	[(HyvValLacVal)HyvVal + 2H + Na minus O]$^+$
566.3	1.2	[(HyvValLacVal)HyvVal + 2H + Na minus CO]$^+$
520.3	1.3	[(HyvValLacVal)Val + Na + CO]$^+$
421.3	1.2	[(HyvValLacVal) + Na + CO]$^+$
393.3	2.7	[HyvValLacVal + Na]$^+$
379.2	1.9	[HyvValLacVal + 2H + Na minus O]$^+$
321.2	1.7	[ValHyvVal + Na]$^+$
294.2	5.0	[HyvValLac + Na]$^+$
280.1	1.5	[HyvValLac + 2H + Na minus O]$^+$
222.1	2.8	[HyvVal + Na]$^+$
194.1	1.0	[ValLac + Na]$^+$
72.1	0.9	Valyl immonium ion

TABLE 3.7

Assignments of the major fragment ions in the FD-4-sector tandem mass spectrum (Figure 3.10) of valinomycin $[M+Na]^+$ ions (m/z 1133.6)

Measured m/z	Relative Intensity	Fragment ion assignment
1118.7	2.3	Loss of CH_3
1117.7	1.0	Loss of CH_4
1103.7	0.5	Loss of H_2CO
1090.8	5.7	Loss of C_3H_7
1089.9	1.2	
1075.8	0.4	
1071.5	0.3	
1048.1	0.3	$[(HyvValLacVal)_2ValHyvVal + Na + O]^+$
1033.6	0.5	$[(HyvValLacVal)_2ValLacVal + Na]^+$
950.3	0.3	
949.1	0.5	
948.7	0.6	$[(HyvValLacVal)_2HyvVal + Na + 2H$ minus $O]^+$
937.5	0.6	
936.4	0.5	$[(HyvValLacVal)_2ValLac + Na + 2H]^+$
934.4	0.3	$[(HyvValLacVal)_2ValLac + Na]^+$
932.9	0.3	
904.5	0.4	
861.6	0.3	$[(HyvValLacVal)_2Val + Na$ minus $H]^+$
849.5	0.3	$[(HyvValLacVal)_2Hyv + Na + 2H$ minus $O]^+$
847.7	0.3	
836.7	0.3	$[(HyvValLacVal)_2Val + Na + 2H$ minus $CO]^+$
789.4	0.3	
779.6	0.3	$[(HyvValLacVal)_2 + Na + O]^+$
763.4	0.5	$[(HyvValLacVal)_2 + Na]^+$
749.4	0.8	$[(HyvValLacVal)_2 + Na + 2H - O]^+$
737.4	0.5	$[(HyvValLacVal)_2 + Na + 2H$ minus $CO]^+$
657.8	0.3	

TABLE 3.7 CONTINUED

Assignments of the major fragment ions in the FD-4-sector tandem mass spectrum (Figure 3.10) of valinomycin $[M+Na]^+$ ions (m/z 1133.6)

Measured m/z	Relative Intensity	Fragment ion assignment
608.6	0.3	[(HyvValLacVal)HyvVal + Na + O]$^+$
580.3	0.4	
578.6	0.5	[(HyvValLacVal)HyvVal + Na + 2H minus O]$^+$
566.1	0.6	[(HyvValLacVal)HyvVal + Na + 2H minus CO]$^+$
559.3	0.3	
421.8	0.3	[(HyvValLacVal)+ Na + CO]$^+$
379.1	0.3	[HyvValLacVal+ Na + 2H minus O]$^+$
294.0	0.3	[HyvValLac + Na]$^+$
224.6	0.3	[HyvVal + Na + 2H]$^+$
141.1	0.4	
139.1	0.3	[Val + Na + O]$^+$
105.1	0.3	[Hyv + Na + 2H minus O]$^+$
54.3	0.4	
53.0	0.3	
47.6	0.3	
44.1	0.3	
43.2	0.3	

fragmentations can be attributed to cleavages at different positions of the peptide backbone from the amide or ester bonds. These cleavages are analogous to the a- and c-type sequence ions of linear peptides compared with b-type ions which involve cleavage of the amide bond. The fragment ions appearing 14 Da below the sequence ion have been attributed to cleavage of the O-CO bond of the Hyv or Lac residues with retention of the O atom by the neutral fragment. This reaction is accompanied by the transfer of two hydrogen atoms from the neutral to the charged fragment. The series of fragment ions which appears 16 Da above the sequence ion has been attributed to cleavage of the ester linkage but with retention of the O atom by the charged fragment. In this case there appears to be no transfer of hydrogen atoms, and hence, to retain a stable positively charged ion, some rearrangement reaction may be taking place involving the valine side chain. For detailed mechanisms to be proposed for these cleavages a more comprehensive study would be required possibly involving isotopic labelling studies and the use of high resolution tandem mass spectrometry techniques. The mechanisms outlined here are therefore speculative and aim to suggest the most likely fragmentation given the evidence available. Fragment ions which appear 26 Da below the corresponding sequence ion presumably involve cleavage of the CH-CO bond with the loss of CO to the neutral fragment and a transfer of two hydrogen atoms to the charged fragment. This type of fragmentation may occur for all possible sequence ions and has been observed for the majority of the higher mass fragment ions in the spectrum shown in Figure 3.9. Cleavage may also occur with retention of the CO group by the charged fragment, resulting in a fragment ion 28 mass units above the sequence ion assuming no transfer of hydrogen atoms occurs. Fragment ion m/z values and their corresponding assignments are listed in Table 3.6 for the more intense ions observed in the spectrum.

The 4-sector tandem mass spectrum of valinomycin $[M+Na]^+$ molecule-ions formed by FD is shown in Figure 3.10 and the fragment ion m/z values and most probable assignments given in Table 3.7. In comparison with the spectrum for the same molecule-ions formed by FAB, this spectrum shows a lesser degree of fragmentation. The decomposition pathways appear to be dominated by the loss of a C_3H_7 side chain from either the Val or Hyv residues. Domination of the tandem mass spectrum by a single fragment ion is similar to the observations made for $M^{+\cdot}$ ions formed by FD, where loss of C_3H_6 produced the most intense fragment ion. The next most intense fragmentation in the FD tandem mass spectrum of $[M+Na]^+$ molecule-ions also involves a side chain, and corresponds with the loss of CH_3.

The tandem mass spectrum of valinomycin $[M+K]^+$ molecule-ions formed by FAB is presented in Figure 3.11 and the mass assignments of the fragment ions are given in Table 3.8. The spectrum is similar to that obtained for the $[M+Na]^+$ molecule-ions formed by FAB, except for lower relative intensities of low-mass fragment ions.

3.3.4 Comparison of valinomycin tandem mass spectra and discussion of results

a) *Comparison of the tandem mass spectra of the same molecule-ions formed by different ionisation methods*

Comparisons of tandem mass spectra for both $[M+Na]^+$ and $M^{+\cdot}$ molecule-ions formed by FAB and FD, and EI and FD, respectively, reveal that FD tended to produce spectra which were dominated by a single fragmentation. In the $M^{+\cdot}$ case the spectrum was dominated by loss of C_3H_6 and in the $[M+Na]^+$ case, by loss of $\cdot C_3H_7$. In contrast, when FAB and EI were employed to ionise samples the tandem mass spectra were no longer dominated by a single fragmentation but showed many intense fragment ions, involving both backbone and side-chain

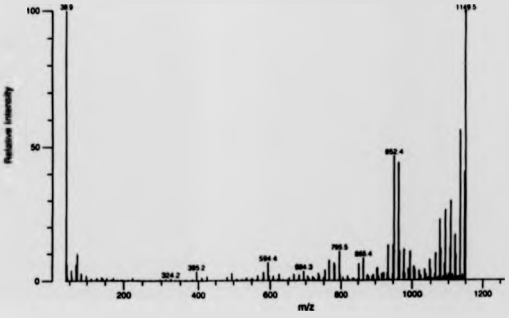

Figure 3.11 4-sector tandem mass spectrum of valinomycin $[M+K]^+$ ions (m/z 1149.6) formed by FAB.

TABLE 3.8

Assignments of the major fragment ions in the FAB-4-sector tandem mass spectrum (Figure 3.11) of valinomycin $[M+K]^+$ ions (m/z 1149.6)

Measured m/z	Relative Intenaity	Fragment ion assignment
1133.7	60.6	Loss of CH_4
1131.4	2.6	Loss of H_2O
1121.5	5.5	Loss of CO
1119.4	15.3	Loss of H_2CO
1106.6	30.1	Loss of C_3H_7
1105.2	9.0	
1103.4	2.2	
1093.6	2.0	
1091.1	27.0	
1089.3	5.3	
1077.8	9.2	$[(HyvValLacVal)_2ValHyvVal + K]^+$
1075.5	22.3	$[(HyvValLacVal)_2ValHyvVal + K$ minus $2H]^+$
1063.6	12.4	$[(HyvValLacVal)_2ValHyvVal + K + H$ minus $NH]^+$
1061.3	2.6	
1049.9	3.7	$[(HyvValLacVal)_2ValLacVal + K]^+$
1047.7	8.1	$[(HyvValLacVal)_2ValLacVal + K$ minus $2H]^+$
1036.5	2.3	$[(HyvValLacVal)_2HyvValLac + K + 2H$ minus $O]^+$
1033.5	4.0	
1022.2	2.9	
1020.4	2.7	$[(HyvValLacVal)_2ValLacVal + K$ minus H & $CO]^+$
1018.5	2.2	
1006.5	3.8	$[(HyvValLacVal)_2HyvVal + K + CO]^+$
1005.5	2.0	
1004.5	2.8	
994.6	7.2	$[(HyvValLacVal)_2HyvVal + K + O]^+$ and/or $[(HyvValLacVal)_2ValLac + K + O + CO]^+$

TABLE 3.8 CONTINUED

Assignments of the major fragment ions in the FAB-4-sector tandem mass spectrum (Figure 3.11) of valinomycin $[M+K]^+$ ions (m/z 1149.6)

Measured m/z	Relative Intensity	Fragment ion assignment
990.5	3.5	
980.4	2.0	$[(HyvValLacVal)_2HyvVal + K + 2H]^+$
978.5	7.8	$[(HyvValLacVal)_2HyvVal + K]^+$
976.5	2.9	
966.6	6.7	
964.5	46.5	$[(HyvValLacVal)_2HyvVal + K + 2H$ minus $O]^+$
952.5	50.4	$[(HyvValLacVal)_2HyvVal + K + 2H$ minus $CO]^+$
950.5	12.6	$[(HyvValLacVal)_2ValLac + K]^+$
948.6	2.1	$[(HyvValLacVal)_2ValLac + K$ minus $2H]^+$
936.6	13.7	$[(HyvValLacVal)_2ValLac + K + 2H$ minus $O]^+$
934.5	2.8	
924.6	2.9	$[(HyvValLacVal)_2ValLac + K + 2H$ minus $CO]^+$
922.5	2.7	$[(HyvValLacVal)_2Val + K + O$ & $+ CO]^+$
918.6	2.6	
908.5	2.1	
906.5	5.0	$[(HyvValLacVal)_2Val + K + CO]^+$
904.5	4.3	
894.5	2.1	
876.5	2.0	$[(HyvValLacVal)_2Val + K$ minus $2H]^+$
865.5	9.4	$[(HyvValLacVal)_2Hyv + K + 2H$ minus $O]^+$
852.5	7.0	$[(HyvValLacVal)_2Val + K + 2H$ minus $CO]^+$
819.5	2.1	
797.5	2.2	$[(HyvValLacVal)_2 + K + 2H + O]^+$
795.5	9.4	$[(HyvValLacVal)_2 + K + O]^+$
781.5	6.6	$[(HyvValLacVal)_2 + K + 2H]^+$

TABLE 3.8 CONTINUED

Assignments of the major fragment ions in the FAB-4-sector tandem mass spectrum (Figure 3.11) of valinomycin $[M+K]^+$ ions (m/z 1149.6)

Measured m/z	Relative Intensity	Fragment ion assignment
779.5	6.6	$[(HyvValLacVal)_2 + K]^+$
765.5	9.4	$[(HyvValLacVal)_2 + K + 2H$ minus $O]^+$
753.4	4.7	$[(HyvValLacVal)_2 + K + 2H$ minus $CO]^+$
735.6	3.2	$[(HyvValLacVal)_2 + K$ minus H & $C_3H_7]^+$
719.4	2.0	$[(HyvValLacVal)ValHyvVal + K + CO]^+$
694.4	4.2	
681.4	2.8	$[(HyvValLacVal)HyvValLac + K + H]^+$
666.4	3.2	$[(HyvValLacVal)HyvValLac + K + 2H$ minus $O]^+$
624.4	2.9	$[(HyvValLacVal)HyvVal + K + O]^+$
608.4	2.0	$[(HyvValLacVal)HyvVal + K]^+$
596.4	2.2	
594.4	8.0	$[(HyvValLacVal)HyvVal + K + 2H$ minus $O]^+$
582.4	4.0	$[(HyvValLacVal)HyvVal + K + 2H$ minus $CO]^+$
566.5	2.5	$[(HyvValLacVal)ValLac + K + 2H$ minus $O]^+$
495.3	4.1	$[(HyvValLacVal)Hyv + K + 2H$ minus $O]^+$
425.3	2.1	$[LacValHyvVal + K + O]^+$
395.3	4.2	$[ValHyvValLac + K + 2H$ minus $O]^+$
98.2	2.6	$[Val$ minus $H]^+$
84.2	2.2	$[Hyv$ minus $O]^+$ AND/OR $[Val$ minus $NH]^+$
83.1	3.3	$[Val$ minus N & $2H]^+$
72.1	12.0	Valyl immonium ion, $[H_2NCH\text{-}CH(CH_3)_2]^+$
69.1	7.3	
56.1	2.4	
55.1	4.7	
43.1	2.0	
38.9	93.0	K^+

cleavages. The differences between tandem mass spectra of the same molecule-ions formed by different ionisation methods were particularly striking when comparing the spectra of $[M+Na]^+$ ions formed by FAB and FD. The FAB spectrum provided a variety of relatively intense fragment ions which were related to cleavages of the backbone of the peptide, i.e. sequence ions. The FD spectrum was dominated by a single fragmentation corresponding with the loss of $\cdot C_3H_7$ but few sequence ions were observed, and those which were present were of relatively low intensity. Due to the poor signal-to-noise ratio in the FD spectrum, a detailed comparison of all fragment ions with those observed for FAB would be unreliable. Observation of the peak shapes revealed the peaks to be broken-up with very few ion counts available to provide a smooth peak which would ideally be required for centroiding.

The results imply that either the molecule-ions formed by FAB and EI have much higher internal energies after collisional activation than those formed by FD, or that the differences in initial internal energy deposition results in the formation of molecule-ions with different isomeric structures. Average internal energy uptakes during ionisation by EI are known to be of the order of a few eV[169] compared with fractions of an eV by FD[170]. If the internal energy uptake upon CID were small compared to that upon ionisation, then EI and FD with their differing amounts of initial internal energy might be expected to result in different tandem mass spectra. Studies of peptide ions in collision with helium have shown translational energy losses ΔE by the parent ions of many tens of electronvolts in magnitude. The proportion of this translational energy loss ΔE which results in internal energy deposition Q has been the subject of many studies which have been reviewed in Sections 1.4.2 and 1.4.5. An impulsive collision theory [54] (see Section 1.4.5) has been used to estimate the values of Q from ΔE values measured for valinomycin $[M+K]^+$ ions.[67] The fragment ion corresponding with loss of C_3H_7 was associated with a translational energy loss of 40 eV, and,

assuming that the mass of the atom involved in the collision corresponds with the average mass of the atoms in valinomycin, i.e.6.6 Da, internal energy uptake Q was calculated to be 15 eV. Presuming this to be a reasonable estimate, then the internal energy uptake upon collisional activation should outweigh that obtained during ionisation. Hence the tandem mass spectra of a given molecule-ion formed by different ionisation methods should not differ if the structure of the ion is the same in each case. Therefore the experimental results are perhaps better explained in terms of the formation of ions with different structures when different ionisation techniques are employed.

The results for FD are consistent with $[M+Na]^+$ and $M^{+\cdot}$ molecule-ions formed with the cyclic structure intact. Decompositions involving loss of a side chain would be expected to be energetically more favourable for a cyclic molecule, requiring the cleavage of only one bond whereas backbone fragmentations would require two bond breakages. In the tandem mass spectra of molecule-ions formed by FD the dominant fragment ions corresponded to side chain cleavages and hence the ring structure is presumably retained after ionisation. In contrast if ionisation results in molecule-ions formed with various ring-opened structures, the formation of sequence type ions from backbone cleavages would also require breakage of only one bond. This latter case is consistent with the wealth of relatively intense fragment ions in the tandem mass spectra of ions formed by FAB and EI. Therefore it is suggested that FD results in the formation of molecule-ions with the cyclic structure intact whereas FAB and EI result in the production of various ring-opened structures.

The tandem mass spectra of $[M+H]^+$ ions formed by FAB have also been compared with the spectra obtained for $[M+H]^+$ ions formed by chemical ionisation and electrospray ionisation.[171] In each case the tandem mass spectra were similar, being dominated by the loss of CO from the molecule-ion. $[M+NH_4]^+$ ions formed by ammonia-CI produced tandem mass spectra which

gave an intense fragment ion corresponding with the loss of ammonia and then similar fragmentation to that observed for the $[M+H]^+$ ions.[171] A study of the valinomycin $[M+H]^+$ ions formed by CI using FT-ICR mass spectrometry has also been reported [172] and showed similar fragmentations to $[M+H]^+$ ions formed by FAB. Increased collision energies and longer collision times (hence involving multiple collisions between ion and target) resulted in an enhanced degree of fragmentation but with little variation in the nature of the fragmentations.[172]

b) *Comparison of the tandem mass spectra of different molecule-ions formed by the same ionisation method*

Tandem mass spectrometry of $[M+H]^+$ and $[M+cation]^+$ ions of valinomycin formed by FAB (Figures 3.8, 3.9 and 3.11 respectively) resulted in quite different spectra. The spectra differ in both the nature and extent of fragmentation. The spectrum obtained for $[M+H]^+$ ions was dominated by the loss of CO and by a few low-mass fragment ions whereas the $[M+Na]^+$ spectrum showed extensive fragmentation across the whole mass range. A fragment ion corresponding with the loss of CO was still present in the $[M+Na]^+$ case but of comparable intensity to other high-mass fragment ions. In this case, the most intense fragment ion corresponded with m/z 948 and has been attributed to the loss of [ValLac-O] with transfer of two hydrogen atoms to the charged fragment. In contrast to the $[M+H]^+$ case, CID of $[M+Na]^+$ molecule-ions formed by FAB produced low-mass fragment ions of relatively low intensity with the valyl immonium ion at m/z 72 being almost too weak to be observed. Fragment ions observed at m/z 172 in the $[M+H]^+$ tandem mass spectrum, were present at m/z 194 ($[ValLac + Na]^+$) in the $[M+Na]^+$ spectrum but were also of relatively low intensity compared to other fragment ions. A fragment ion corresponding with m/z 343 ($[M+H]^+$ spectrum) was not observed in the $[M+Na]^+$ spectrum. Of the low-mass fragment ions which were present, that at m/z 294 was relatively more intense

than others, whereas the corresponding fragment ion was of relatively low intensity in the $[M+H]^+$ case.

The tandem mass spectrum of valinomycin $[M+K]^+$ molecule-ions formed by FAB was generally similar to the $[M+Na]^+$ case. The relative intensities of low-mass fragment ions were decreased relative to those at higher mass, even more so than in the $[M+Na]^+$ spectrum. The most intense fragment ion peak was due to K^+. Na^+ ions were not observed in the $[M+Na]^+$ tandem mass spectrum, since this mass was below the calibrated linked-scan and therefore outside the experimental mass range. The reduced abundances of low-mass cationised fragment ions and the observation of an intense K^+ peak implies that formation of the cation alone is energetically more favourable. Comparisons of tandem mass spectra of $[M+Li]^+$, $[M+Na]^+$ and $[M+K]^+$ ions have shown K^+ to form the most abundant cation peak, followed by Na^+ and then Li^+.[162,173] This trend follows that of increasing bond energies of the cation to the organic molecule on changing from K^+ to Li^+. The tandem mass spectrum of valinomycin $[M+K]^+$ ions was otherwise similar to that obtained for $[M+Na]^+$ ions.

A previous study involving CI of valinomycin suggested that the CO group was the predominant site of protonation.[174] That tandem mass spectrometry of $[M+H]^+$ ions formed by various ionisation methods should produce spectra dominated by the loss of CO, is therefore consistent with charge-localised fragmentation. Various authors have compared the tandem mass spectra of peptide $[M+H]^+$ and $[M+cation]^+$ molecule-ions formed by FAB and the present results are consistent with their observations.[161-164,175] Differing interactions between the peptide and alkali cation, compared with those of a proton, have been proposed to explain the variations in the spectra of $[M+H]^+$ and $[M+cation]^+$ molecule-ions. Thus mechanisms of fragment ion formation would be expected to reflect these differences. The differences in mechanisms of fragment

ion formation in the tandem mass spectra of $[M+H]^+$ and $[M+Na]^+$ ions of linear peptides have been discussed in Section 3.2.2.

Detailed comparisons of the tandem mass spectra of $M^{+\cdot}$ and $[M+Na]^+$ molecule-ions formed by FD are subject to restrictions on reliability imposed by poor signal-to-noise ratios. Comparison of the general features of the spectra, and of the more intense fragment ions, provides conclusions similar to those made when comparing $[M+H]^+$ and $[M+Na]^+$ ions formed by FAB. The $M^{+\cdot}$ tandem mass spectrum is dominated by the loss of C_3H_6 and the $[M+Na]^+$ spectrum by loss of C_3H_7. CID of $M^{+\cdot}$ ions results in several low-mass fragment ions of reasonable intensity (m/z 72, 172, 343, 542) but the corresponding fragment ions were absent or very weak in the $[M+Na]^+$ spectrum. Hence, again the results are consistent with a different mechanism of fragment-ion formation in the $[M+cation]^+$ case, presumably involving fragmentations remote from the charge site.

3.4 Conclusions

The results obtained for the peptides valine-gramicidin A and valinomycin have illustrated how additional structural information may be obtained in tandem mass spectrometry by using a number of molecule-ions and also various ionisation methods. The tandem mass spectra of $[M+H]^+$ and $[M+K]^+$ ions of valine-gramicidin A formed by FAB produced different series of sequence-ions, which provided complementary structural information. In the $[M+H]^+$ case, spectra were dominated by b- and y-type sequence-ions, which are typical of peptides containing N-terminal acyl groups and which lack basic amino acids.[9] The spectrum of the $[M+K]^+$ ions tended to be dominated by fragment ions of the type $[a_n^{-1} + K]^+$ and also $[w_n + K]^+$. These ions are characteristic of $[M + cation]^+$ molecule-ions.[161] The generation of w-type ions involving cleavages of amino acid

side chains is important for structural identification of component amino acids and their positions in the peptide. The tandem mass spectra of valinomycin were shown to vary depending on the ionisation method employed (FD, FAB or EI) to form $M^{+\cdot}$ and $[M+Na]^+$ molecule-ions. These differences were attributed to the formation of different isomeric structures or mixtures of structures. The internal energy uptake upon CID was assumed to outweigh the internal energy differences at the ionisation stage and the results supported this conclusion. For example, the tandem mass spectra of $[M+Na]^+$ ions formed by FAB and FD showed similar fragmentation pathways but the relative abundances were quite different. The FD spectrum was dominated by a fragment ion attributed to the loss of a $\cdot C_3H_7$ side chain, with fragment ions corresponding to backbone cleavages being less abundant. In contrast the FAB spectrum showed relatively intense fragment ions across the whole mass range for both side chain and backbone cleavages. These results are consistent with the formation of ring-opened structures by FAB, but in FD ions appear to have retained the cyclic structure. Valinomycin therefore illustrates a case in which the structure of an ion does not necessarily resemble that of its neutral precursor.

Chapter 4 : TANDEM MASS SPECTROMETRY USING A HYBRID MASS SPECTROMETER

4.1 INTRODUCTION

Collision-induced decomposition (CID) of large peptide ions in hybrid mass spectrometers (EBqQ) has been shown to have an apparent upper mass limit of ~1000 Da above which insufficient structural information is obtained for peptide sequencing.[86-88] Comparisons between four-sector tandem experiments with helium as target, and hybrid experiments with argon as target have shown that, for ions with masses above ~1000 Da, the low-energy CID on the hybrid fails to induce significant fragmentation above that already observed in metastable-ion spectra.[87] In general, these comparisons have been made between incident ion energies of a few eV on the hybrid and 4 - 10 keV on the 4-sector instruments and the differences in the tandem mass spectra have been attributed to the differences in centre-of-mass collision energies.[86,88] For example, an ion of mass 1133.6 Da with an incident ion energy of 50 eV colliding with an argon gas atom has a centre-of-mass collision energy of 1.7 eV, whereas the same ion with 4 keV incident ion energy in collision with helium has a value of E_{cm} = 14.1 eV. Increasing the incident ion energy on the hybrid instrument to 400 eV gives a similar centre-of-mass collision energy to the 4-sector case. Sequence-ions of the w- and v-types are generally of relatively low abundances in low-energy tandem mass spectra. These fragmentations which involve cleavages of side-chains are important for structural identification of amino acids and are believed to be formed via a charge-remote mechanism.[80,167] Presumably these higher energy pathways are not accessible under the low-energy CID regimes. Alexander *et al.*[89] have shown some success in inducing these types of fragmentations for peptide ions

by using collision energies in a hybrid mass spectrometer of at least 200 eV. Such work has shown promise for the use of higher collision energies in hybrids to give spectra more comparable with those obtained at keV collision energies in 4-sector tandem mass spectrometers. The transmission through the quadrupole assembly of high-mass ions with these higher energies, however, was much lower, and to overcome these problems the use of higher RF-voltages has been suggested.[89] Subsequently, computer modelling of the paths of ions through RF multipole fields predicted that for efficient transmission of high-mass parent and fragment ions, higher RF voltages are required, possibly as high as kV.[176]

The hybrid mass spectrometer used in the present work was designed for operation with higher incident ion energies of up to 500 eV.[134] An RF-voltage (zero-to-peak) of 1000 V was used to optimise the transmission efficiency of ions through the quadrupole assembly. Hence the potential of using higher collision energies on a hybrid mass spectrometer for obtaining improved CID spectra for large ions could be investigated. Tandem mass spectra have been recorded for valinomycin $[M+H]^+$ and $[M+Na]^+$ ions over a range of incident ion energies from 20 - 400 eV both in the presence and absence of collision gas. These CID and unimolecular spectra are compared with the 4-sector CID mass spectra presented in Chapter 3.

4.2 EFFECT OF COLLISION ENERGY ON THE TANDEM MASS SPECTRA OF VALINOMYCIN $[M+H]^+$ IONS

Figures 4.1 to 4.4 show the tandem mass spectra of valinomycin $[M+H]^+$ ions obtained using a hybrid mass spectrometer. The upper spectra in these figures are the CID spectra obtained using argon as target and with the parent ion beam attenuated by 50%. Laboratory frame collision energies of 20, 150, 250 and 400 eV were used. Beneath these CID spectra are the corresponding unimolecular

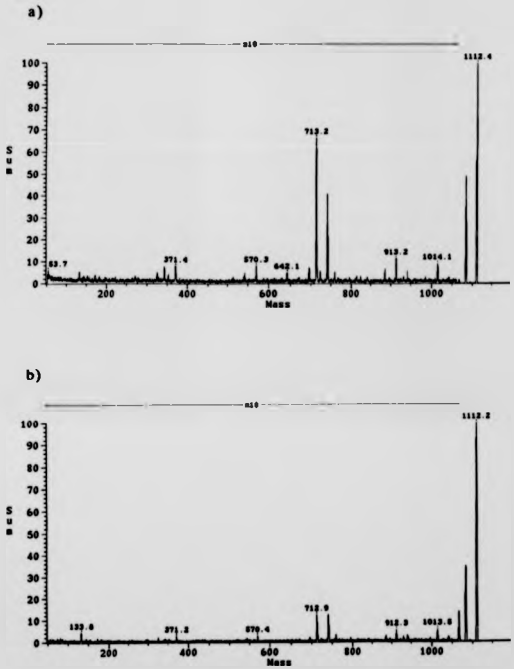

Figure 4.1 Tandem mass spectra of valinomycin $[M+H]^+$ ions (m/z 1111.6) with an incident ion energy of 20 eV obtained using a hybrid mass spectrometer. a) CID (argon target gas) b) Unimolecular

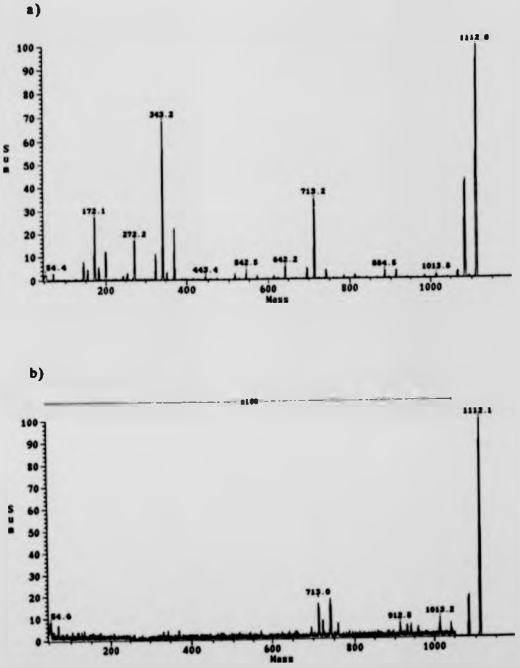

Figure 4.2 Tandem mass spectra of valinomycin $[M+H]^+$ ions (m/z 1111.6) with an incident ion energy of 150 eV obtained using a hybrid mass spectrometer. a) CID (argon target gas) b) Unimolecular

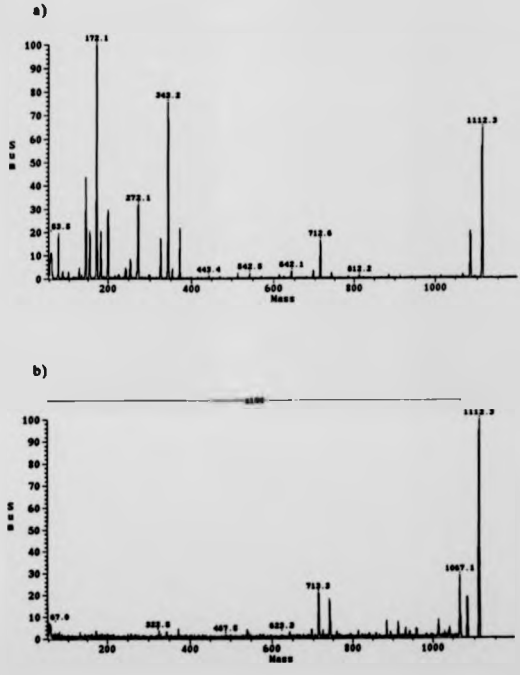

Figure 4.3 Tandem mass spectra of valinomycin $[M+H]^+$ ions (m/z 1111.6) with an incident ion energy of 250 eV obtained using a hybrid mass spectrometer. a) CID (argon target gas) b) Unimolecular

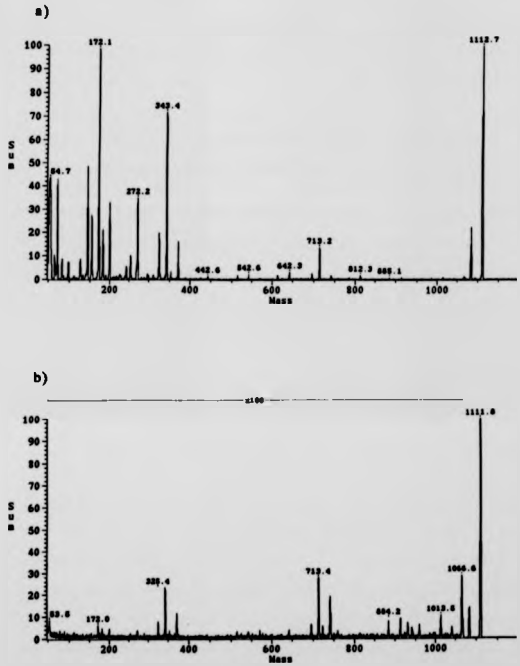

Figure 4.4 Tandem mass spectra of valinomycin $[M+H]^+$ ions (m/z 1111.6) with an incident ion energy of 400 eV obtained using a hybrid mass spectrometer. a) CID (argon target gas) b) Unimolecular

spectra recorded in the absence of collision gas which are generally similar at all ion energies. The major metastable fragment ions correspond with m/z 1084.6, 1066.6, 741.4 and 713.4. The fragment ion at m/z 1084.6 is attributed to the loss of CO from the parent ion and that at m/z 1066.6 to [(HyvValLacVal)$_2$ValHyvVal + CO minus H]$^+$. The fragment ion at m/z 741.4 corresponds with [(HyvValLacVal)$_2$ + H]$^+$ and that at m/z 713.4 with the fragment [(HyvValLacVal)$_2$ + CO minus H]$^+$. These fragment ions were all present in the 4-sector tandem mass spectrum shown in Figure 3.8.

Figure 4.1 shows the effect of addition of collision gas when the incident ion energy was 20 eV. There is very little difference between the unimolecular spectrum and the CID spectrum at this ion energy. When the incident ion energy was increased to 150 eV, addition of collision gas resulted in a spectrum which differed significantly from the unimolecular case (Figure 4.2). Fragment ions were present in the CID spectrum which were absent or of very low abundances in the unimolecular spectrum and which were also absent from the CID spectrum recorded with E_i ~ 20 eV. For example, fragment ions at m/z 642.2, 542.5, 343.2, 272.2, 199.5, and 172.1 were now of significant relative intensity. These fragment ions correspond with the following sequence type ions: fragment ions at m/z 642.2, 542.5 and 343.2 are attributed to [(HyvValLacVal)ValHyvVal + H minus CO]$^+$, [(HyvValLacVal)HyvVal + H minus CO]$^+$ and [(HyvValLacVal)+ H minus CO]$^+$ respectively, and the fragment ions with m/z 272.2, 199.5 and 172.1 formally correspond with [HyvValLac + H]$^+$, [HyvValLac + CO minus H]$^+$ and [ValLac + H]$^+$. These types of fragmentation are similar to those observed by 4-sector tandem mass spectrometry (Figure 3.8). The fragment ion at m/z 343.2 was the most relatively abundant fragment ion in the hybrid spectrum at 150 eV collision energy. In general the CID spectrum showed fragment ions across the whole mass range whereas in the 4-sector tandem mass spectrum fragment ions in the range of m/z 400 - 900 were of very low intensity. Increasing the laboratory

frame collision energy to 250 eV (Figure 4.3) further enhanced the relative abundances of fragment ions, particularly of low-mass fragment ions compared with those at higher mass. In this case, the base fragment ion peak corresponded with m/z 172.1 which was assigned to [ValLac + H]$^+$. At E_l = 400 eV (Figure 4.4), the CID spectrum was very similar to that at 250 eV, with some additional increases in the relative intensities of low-mass fragment ions.

4.3 EFFECT OF COLLISION ENERGY ON THE TANDEM MASS SPECTRA OF VALINOMYCIN [M+Na]$^+$ IONS

The [M+Na]$^+$ ions of valinomycin produced similar results at low collision energies to the [M+H]$^+$ ions. Increasing the translational energy of the parent ions had little effect on the tandem mass spectra obtained in the absence of collision gas (Figures 4.5 to 4.9). The major metastable fragment ions are found at average m/z values of 1090.2, 1062.5, 963.4 and 762.8. In the 4-sector tandem mass spectrum (obtained with helium as target gas) fragment ions are present at m/z 962.4 and 1061.6, one mass unit lower, and were attributed to [(HyvValLacVal)$_2$HyvVal + Na]$^+$ and [(HyvValLacVal)$_2$ValHyvVal + Na]$^+$. These differences are unlikely to be due to poor mass assignments, and may therefore be caused by differing fragmentation mechanisms at high and low collision energies. The fragment ions at m/z 1090.2 and m/z 762.8 correspond to loss of a C_3H_7 side chain and with [(HyvValLacVal)$_2$+ Na]$^+$ respectively. At incident ion energies of 20 eV and 50 eV, admitting collision gas into the RF-only quadrupole produced spectra similar to the unimolecular case with some slight enhancement of the relative abundances of the low-mass fragment ions compared with those at higher mass. As with the [M+H]$^+$ ions, CID at these collision energies did not promote fragmentations other than those already present in the unimolecular spectra. Increasing the incident ion energy to 150 eV and above results in spectra which are no longer dominated by unimolecular fragmentations.

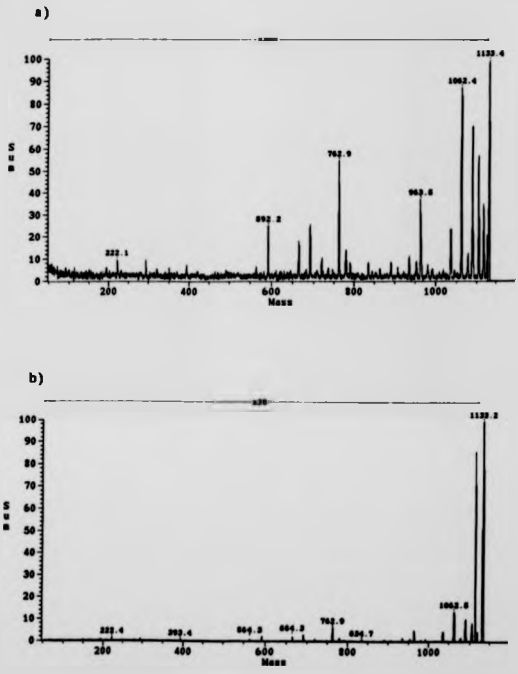

Figure 4.5 Tandem mass spectra of valinomycin [M+Na]+ ions (m/z 1133.6) with an incident ion energy of 20 eV obtained using a hybrid mass spectrometer a) CID (argon target gas) b) Unimolecular

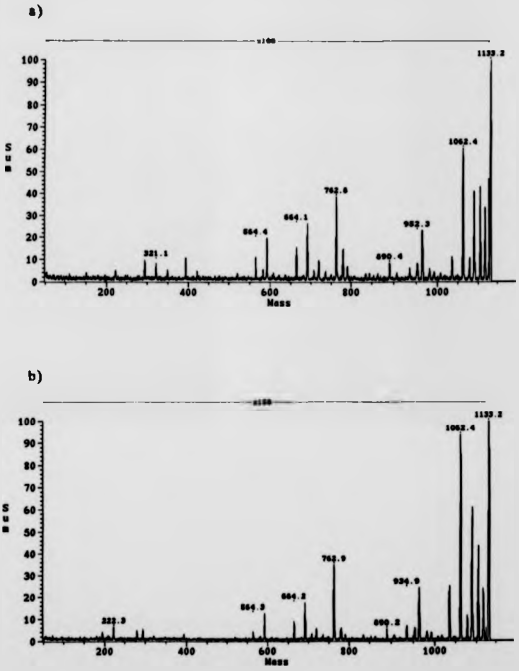

Figure 4.6 Tandem mass spectra of valinomycin $[M+Na]^+$ ions (m/z 1133.6) with an incident ion energy of 50 eV obtained using a hybrid mass spectrometer a) CID (argon target gas) b) Unimolecular

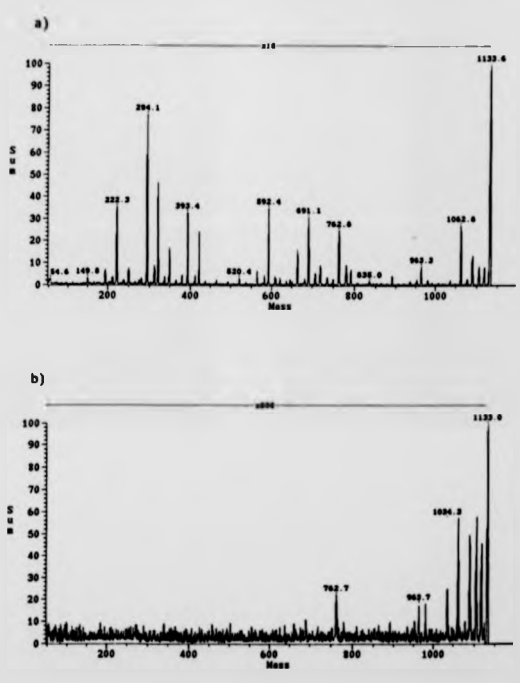

Figure 4.7 Tandem mass spectra of valinomycin [M+Na]+ ions (m/z 1133.6) with an incident ion energy of 150 eV obtained using a hybrid mass spectrometer a) CID (argon target gas) b) Unimolecular

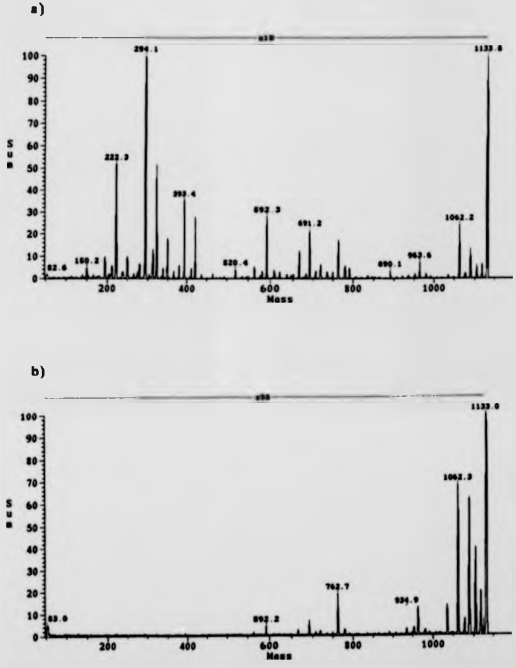

Figure 4.8 Tandem mass spectra of valinomycin [M+Na]+ ions (m/z 1133.6) with an incident ion energy of 250 eV obtained using a hybrid mass spectrometer a) CID (argon target gas) b) Unimolecular

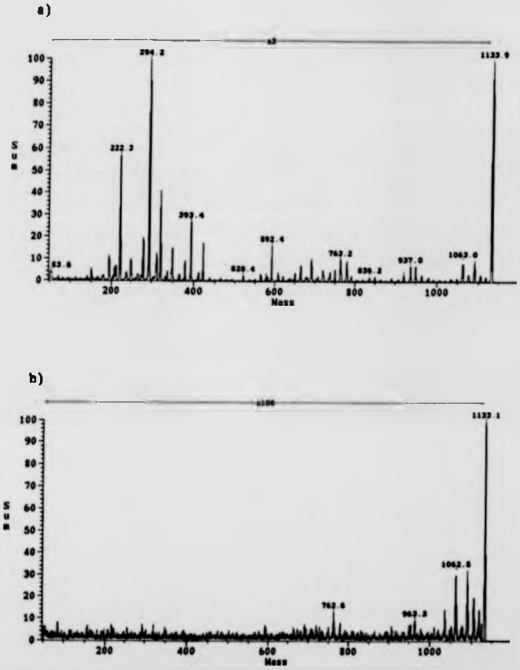

Figure 4.9 Tandem mass spectra of valinomycin $[M+Na]^+$ ions (m/z 1133.6) with an incident ion energy of 400 eV obtained using a hybrid mass spectrometer a) CID (argon target gas) b) Unimolecular

In Figure 4.7 the CID and unimolecular tandem mass spectra are compared for an incident ion energy of E_i = 150 eV. The addition of collision gas produces many fragmentation pathways previously not present in the unimolecular case, particularly at low-mass. For example, major fragment ions are observed at m/z 393.4, 321.0, 294.1 and 222.3 which correspond with [HyvValLacVal + Na]$^+$, [ValHyvVal + Na]$^+$, [HyvValLac + Na]$^+$ and [HyvVal + Na]$^+$ respectively. These ions were all present with relatively high abundances in the 4-sector tandem mass spectrum. Increasing the incident ion energy on the hybrid mass spectrometer to 250 eV (Figure 4.8) produces a CID spectrum similar to that at 150 eV. Increasing E_i further to 400 eV (Figure 4.9) produces a CID spectrum which shows quite extensive fragmentation across the whole mass range and much more closely resembles the CID spectrum obtained by 4-sector mass spectrometry (Figure 3.9).

4.4 Discussion and Conclusions

The fact that the unimolecular spectra vary very little with translational energy of the incident ion was to be expected, since the residence time in the collision quadrupole decreases only by a factor of 2.2 on changing the energy from 100 eV to 400 eV. Both the spectra obtained for [M+H]$^+$ and [M+Na]$^+$ ions of valinomycin show how the nature and degree of fragmentation varies with incident ion energy in the range of 20 - 400 eV when collision gas was present. At the lower incident ion energies, very little fragmentation was observed above that already seen in the unimolecular spectra. By using E_i = 400 eV, however, the CID spectrum resembled more closely that obtained by 4-sector mass spectrometry where the collision energy was 4 keV. The differences between the 4-sector tandem mass spectra of [M+H]$^+$ and [M+Na]$^+$ ions of valinomycin were attributed to charge remote fragmentations in the [M+Na]$^+$ case, where more extensive fragmentations were observed (Section 3.3.4 b)). These types of

fragmentation are generally associated with higher energy decomposition pathways and thus in the hybrid experiments they may have been accessible to the $[M+Na]^+$ ions only at the higher incident ion energy of 400 eV.

The results for valinomycin have shown how by increasing the incident ion energies accessible on a hybrid mass spectrometer, tandem mass spectra may be obtained which more closely resemble those obtained by 4-sector mass spectrometry. Similar work has also been carried out for the $[M+H]^+$ ion of the peptide dynorphin A fragment 1-9 (m/z 1137.5) and the $[M+H]^+$ ion of the cyclic peptide gramicidin S (m/z 1141.7).[177] These peptides were used previously in comparisons between hybrid and 4-sector tandem mass spectra, where CID on the hybrid resulted in low efficiencies for fragmenting these ions.[86,87] By increasing the collision energy to 400 eV in this more recent study,[177] additional fragmentation could be induced although a number of w-, v- and d-type fragment ions observed in the 4-sector spectrum were still absent in the low-energy case. For the $[M+H]^+$ ion of insulin A-chain (m/z 2531), only the CID spectra recorded with incident ion energies above 300 eV resulted in a significant amount of fragmentation.[177] The spectrum did not provide complete structural information, but again illustrated the potential of using higher collision energies in a hybrid mass spectrometer to promote fragmentations of ions with much higher masses. Overall, the results suggest that if incident ion energies of the order of keV could be achieved on hybrid instruments, then tandem mass spectra might be obtained which are similar to those obtained by 4-sector instruments. This would be the case provided that the efficiency of transmission through the quadrupole assembly could also be maintained with the use of increasingly higher RF-voltages. The possible use of keV collision energies in hybrid instruments should provide a means of fragmenting even larger systems, at least to the extent which can be achieved in a 4-sector mass spectrometer. However, the limitations of resolution and sensitivity which can be achieved with a quadrupole assembly will

still make 4-sector instruments more preferable for the study of peptide sequencing.

An interesting feature of the valinomycin spectra shown here was that the centre-of-mass collision energies were in fact similar to the 4-sector conditions used for the spectra shown in Figures 3.8 and 3.9, i.e. approximately 14 eV in each case. This was achieved by using argon as target in the low-energy experiments and helium for CID at keV collision energies. That there should be differences in the tandem mass spectra when the centre-of-mass collision energies are similar may be explained either by instrumental effects, such as ion optics, or alternatively may be an indication of different excitation mechanisms or differing amounts of internal energy uptake. Alexander *et al.*[87] suggested that both electronic and vibrational mechanisms of excitation were accessible at keV collision energies, whereas at eV energies only vibrational excitation was likely. These arguments were based on the Massey criterion (see Section 1.3.1) and hence the differences in velocities and interaction times were thought to be important for explaining the differences between spectra obtained on these two types of instruments. This is, however, thought to be an unlikely explanation since the interaction times involved are too long (10^{-14}s) for a high probability of electronic excitation. The differences in interaction times on increasing the incident ion from 400 eV to 4 keV are relatively small, varying only by a factor of 3.2, and would not be expected to have a significant effect on the mechanism of excitation. An alternative explanation of the results may be offered by an impulsive collision theory (ICT).[54] ICT predicts that the efficiency of energy transfer from the centre-of-mass collision energy E_{cm} to internal energy Q is dependent on the masses of the gas atom and atom within the ion (m_a) which is directly involved in the collision. Energy transfer is predicted to be most efficient when the masses of the interacting atoms are similar. The average internal energy uptake Q_{av} may be calculated from ICT using Equation 1.12. For

valinomycin ions (m_a = 6.6 Da), at an incident ion energy of 400 eV in collision with argon, the centre-of-mass collision energy is 14.1 eV and the calculated value of Q_{av} is 3.4 eV. The same ion with an incident ion energy of 4 keV, colliding with helium, has a similar centre-of-mass collision energy, 13.6 eV, but the value of Q_{av} is greater in this case, 6.4 eV. The greater internal energy uptake in the helium case, is due to closer agreement in the masses of the colliding atoms. Hence, despite the similar centre-of-mass collision energies in the hybrid and 4-sector experiments described here, a greater amount of internal energy is, on the basis of ICT, taken up in the latter case.

Chapter 5 : TRANSLATIONAL ENERGY LOST BY LARGE IONS IN COLLISION-INDUCED DECOMPOSITION. I. Variation with collision gas pressure

5.1 INTRODUCTION

5.1.1 Aims

An important question aimed towards an understanding of the mechanism of collision-induced decomposition of large ions, concerns the number of collisions which occur prior to decomposition to the detected fragment ion. This has important consequences for studies involving the measurement of translational energy losses, since ΔE is related to the internal uptake of parent ions Q by theories which make the assumption that only a single collision has taken place (Section 1.4.5). Previous studies of translational energy lost by large ions have tended to use collision gas pressures which result in parent ion attenuations of 60 - 70 %. As has been discussed in Section 1.4.3, reports concerning the numbers of collisions which occur at such transmissions are conflicting. Hence prior to using translational energy losses as a guide to the variation in internal energy uptake when a number of collision conditions were changed (Chapter 6), it was important to embark on an investigation into the question of the number of collisions which take place. This chapter presents the findings of an investigation into the variation of ΔE with collision gas pressure which was measured as a function of parent ion beam attenuation. By using extremely low collision gas pressures, where it is generally agreed that single collision conditions hold (e.g. < 40 % attenuation), the amount of energy loss per collision could be obtained. Subsequently a study of the pressure dependencies of the measured ΔE values

would be expected to provide an insight into the numbers of collisions occurring under the CID conditions generally used in tandem mass spectrometry, corresponding to attenuations of 60 - 80 %. All experiments were carried out on the large-scale reverse geometry mass spectrometer using the MIKES technique. The samples used in this study were valinomycin, valine-gramicidin A and caesium iodide cluster ions. Peptide ion beams were generated by FD and the inorganic cluster ions by FAB.

5.1.2 Field desorption of peptides

Work on the large-scale research mass spectrometer was aimed towards using higher incident ion energies (Chapter 6) and required the use of field desorption emitter (accelerating) potentials of up to +30 kV. Emitter potentials of between 8 and 15 kV were found to provide the most reliable conditions, with strongest ion currents produced at the higher potentials. Experiments which involved emitter potentials of 8 kV were accompanied by floating of the counter electrode to -4 kV in order to increase the electric field gradient. A significant improvement in parent ion beam intensity was thus achieved. Accelerating potentials above 15 kV were unpredictable and usually resulted in electrical discharges despite efforts to control carefully the conditions of the experiment. Larger emitter counter electrode distances (up to 4 mm), lighter sample loadings and floating of the counter electrode to positive potentials so as to reduce the electric field gradient, were all used in an attempt to improve the FD reliability at the higher accelerating potentials.

Parent ion currents reaching the detector of 250,000 ions per second, prior to introduction of collision gas, were found to result in the most successful CID experiments if maintained for a period of several hours. Increases in the emitter heating current (EHC) to produce stronger ion currents generally resulted in discharges, or samples were rapidly depleted. Samples tended to have an

optimum EHC at which the strongest ion currents could be maintained for long periods of time. Increasing the EHC more than a few mA above the optimum generally resulted in a reduction of the molecular ion current, possibly due to sample degradation. Hence the use of an EHC slightly higher than the optimum, for shorter periods of time, was not necessarily a viable alternative for producing the same quality spectra as compared to a slower experiment.

FD of peptides often results in the formation of $[M+H]^+$ and also $[M]^{+\cdot}$ molecule-ions. The $[M]^{+\cdot}$ ions are generally of lower intensity than the protonated molecules and thus it is preferable to use the latter for CID experiments. Contributions of the ^{13}C containing $[M]^{+\cdot}$ ions to the protonated molecule result in ambiguities in the mass assignments of the fragment ions. Hence for FD experiments on the large-scale mass spectrometer the peptide molecule-ions used were the alkali-cationated species, valinomycin $[M+Na]^+$ and valine-gramicidin A $[M+K]^+$.

5.1.3 Experiments concerning the pressure dependence of ΔE

Preliminary investigations into the pressure dependencies of ΔE revealed the changes to be small. Therefore to provide measurements with sufficient accuracy to follow such small variations it was necessary to obtain improved ion statistics for each individual fragment ion peak. This was particularly important for low-mass fragment ions which were usually of low intensities relative to the parent ion and to other higher mass fragment ions. In a complete CID-MIKE spectrum, where the whole mass range was scanned, intense fragment ion peaks usually corresponded to several thousand ion counts. Optimum ion statistics have been found to correspond with > 100,000 ion counts per fragment ion peak. This observation was made during field ionisation experiments of small organic molecules during the ESA calibration check (Section 2.1.8d). FD did not produce ion currents of sufficient intensity to provide such good ion statistics; to overcome

this limitation, the pressure dependencies of ΔE were investigated for dissociations to individual fragment ions with each peak studied in a separate series of experiments. Each ΔE value measured for an individual fragment ion peak was obtained by maintaining stable parent ion beam currents for many hours. Scanning of the ESA over only a small voltage range resulted in ion counts being collected for a particular fragment ion peak for almost the whole duration of the experiment, rather than < 3 % of the time as would occur when a complete spectrum was recorded. For the results described in the following sections, fragment ion peaks with > 10,000 ion counts were used for ΔE measurements. It was usually necessary to record spectra of these individual fragment ion peaks until the sample on the emitter was depleted. In cases where depletion of sample occurred prior to collection of sufficient data to correspond with a fairly smooth symmetrical shaped peak, the collected data were abandoned. Hence in an attempt to minimise experimental errors only data collected from one sample loading were used for each calculation of ΔE. FD emitters could be re-used for a number of separate experiments provided the same sample and alkali salt were to be used (so as to avoid contamination).

5.2 RESULTS FOR VALINOMYCIN

5.2.1 MIKES of $[M+Na]^+$ molecule-ions of valinomycin

Field desorption of valinomycin routinely resulted in stable parent ion beams of ~125,000 ions/second which could be maintained for many hours. Signal intensities stronger than this were rarely obtained. Molecule-ions were observed at an EHC above 60 mA and the optimum EHC was found to be between 84 and 96 mA, depending on the emitter used.

The MIKE spectrum of valinomycin $[M+Na]^+$ molecule-ions, m/z 1133.6, is shown in Figure 5.1. This spectrum was recorded with an incident ion energy of

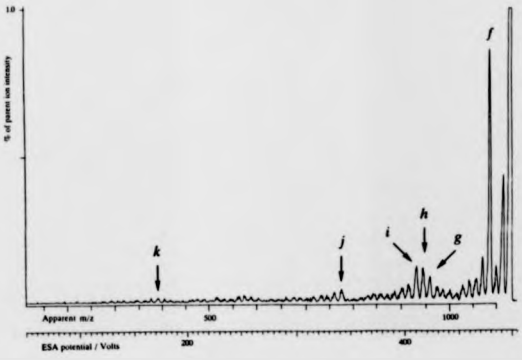

Figure 5.1 FD-MIKE spectrum of valinomycin $[M+Na]^+$ ions (m/z 1133.6); helium target gas, 60 % parent ion beam attenuation, incident ion energy E_i = 14.9 keV

TABLE 5.1

Fragment ion mass assignments in the FD-MIKE spectrum of valinomycin $[M+Na]^+$ ions (Figure 5.1). Incident ion energy = 14.9 keV and parent ion attenuated by 60% with helium target gas

V_m	Apparent m/z	Assigned mass (m_f) / Da	Fragment ion
491.906	1115.28	1118.595	Loss of CH_3
485.878	1101.61	1105.624	Loss of CO
479.715	1087.64	1090.564	Loss of C_3H_7
472.532	1071.35	1075.540	Loss of either HCO_2 or $OCHCH_3$
		1061.597	$[(HVLV)_2VHV + Na]^+$
459.963	1042.85	1047.582	$[(HVLV)_2VLV + Na + O]^+$
		1033.566	$[(HVLV)_2VLV + Na]^+$
429.754	974.36	978.585	
422.857	958.73	962.529	$[(HVLV)_2HV + Na]^+$
416.877	945.17	948.529	$[(HVLV)_2HV + 2H + Na - O]^+$
410.999	931.84	936.514	$[(HVLV)_2HV + 2H + Na - CO]^+$
404.02	916.02	920.483	$[(HVLV)_2VL + 2H + Na - O]^+$
342.106	775.64	779.368	$[(HVLV)_2 + Na + O]^+$
335.37	760.37	763.379	$[(HVLV)_2 + Na]^+$
259.8	589.03	592.320	$[(HVLV)HV + Na]^+$
		578.341	$[(HVLV)HV + 2H + Na - O]^+$
		566.341	$[(HVLV)HV + 2H + Na - CO]^+$
		409.194	$[(HVLV) + Na + O]^+$
172.863	391.93	393.199	$[HVLV + Na]^+$
166.063	376.51	379.220	$[HVLV + 2H + Na - O]^+$
		294.131	$[HVL + Na]^+$

14.9 keV and helium was used as target gas with an attenuation of 60 %. The spectrum has been plotted with a magnification such that the fragment ions may be seen, but which results in the parent ion peak being off-scale. The vertical scale represents the percentage of the parent ion signal which is on-scale. The horizontal scale shows the electric sector analyser potential required to transmit the ions and is related to the translational energy of the fragment ions by 1 V = 29.85 eV. A mass-scale is also shown which represents the calculated mass of the fragment based upon its translational energy and has been calculated using Equation 1.3. Since the parent ions may have lost translational energy as a result of collisional activation, the mass scale may not correspond to the true mass of the fragment ion and will therefore be referred to as the 'apparent mass'. The same labelling system has been applied to all MIKE spectra. The fragment ion mass assignments are given in Table 5.1 and were compiled by comparison with: the FAB and FD tandem mass spectra recorded on the 4-sector mass spectrometer (Section 3.3.3), low energy FAB tandem mass spectra,[178] and previous assignments made by Sheil.[69] As discussed in Chapter 3, the tandem mass spectra of valinomycin molecule-ions may differ depending on the ionisation method employed. Ideally comparison would have been made of the MIKE spectrum shown in Figure 5.1 with a 4-sector tandem mass spectrum obtained by the same ionisation method, FD. Due to the poor signal-to-noise ratio observed for the FD 4-sector tandem mass spectrum, the comparison was not ideal and it was therefore necessary to also use the FAB 4-sector spectrum to make fragment ion assignments. In cases where two neighbouring peaks appear within 5 mass units of each other, separation of these peaks was not possible given the low resolution power of the MIKES technique. Translational energy losses measured from these peaks will be in error, since the expected value of the ESA potential is calculated from one mass assignment. Taking an average value of the mass of the two peaks is not a viable solution since decompositions to different

fragment ions are associated with different translational energy losses. Therefore in cases where neighbouring peaks of similar intensities were assigned, the fragment ion peaks were not included in the calculation of translational energy losses.

The fragment ions of valinomycin $[M+Na]^+$ ions which were chosen for investigation of the dependence of ΔE on collision gas pressure, have been arbitrarily denoted in Figure 5.1 by the letters *f* - *k*. Fragment ion *f* corresponds to the loss of a propyl side chain, C_3H_7, and to m/z 1090.6. Fragment ions *g*, *i* and *k* with m/z 962.6, 936.5 and 393.2 correspond with the sequence ions [(Hyv-Val-Lac-Val)$_2$-Hyv-Val + Na]$^+$, [(Hyv-Val-Lac-Val)$_2$-Hyv-Val + 2H + Na minus CO]$^+$ and [Hyv-Val-Lac-Val + Na]$^+$ respectively. Fragment ion *h*, m/z 948.6, corresponds to [(Hyv-Val-Lac-Val)$_2$-Hyv-Val + 2H + Na minus O]$^+$ and fragment ion *j*, m/z 779.5, with [(Hyv-Val-Lac-Val)$_2$ + O + Na]$^+$.

5.2.2 Pressure dependencies of ΔE for helium target gas

MIKE spectra recorded in the absence of collision gas for ESA potentials corresponding to decomposition of valinomycin $[M+Na]^+$ to fragment ions *f* - *k*, showed there to be negligible signal intensity resulting from metastable fragmentations at the scan rates used (0.5 - 1 V/s) and relative to the fragment ion currents when collision gas was present. A strong metastable contribution would have resulted in the measured values of ΔE being smaller than from purely CID processes. At low gas pressures fewer collisions occur and metastable decompositions would then dominate and provide the major contribution to the observed fragment ion peak resulting in the smallest values for ΔE. At higher gas pressures CID processes would be the major contributor and hence ΔE would be much larger. Thus it was important to choose fragment ion peaks with little metastable contribution, otherwise it would not have been possible to separate this pressure effect from one due to increasing numbers of collisions. Fortunately,

by its very nature FD is a soft ionisation technique and the internal energy uptake upon ionisation is relatively small (a few tenths of an eV) [170] compared with several eV with electron impact ionisation.[169] Few metastable fragmentations were observed for the large ions studied by FD-MIKES.

The values of ΔE for decomposition of valinomycin $[M+Na]^+$ to fragment ions *f* - *k* at various attenuations of helium collision gas are listed in Table 5.2. The incident ion energy in this case was 14.9 keV. Large values of ΔE were measured even at very low collision gas pressures where predominantly single collision conditions were expected. For example, at an attenuation of 10 %, ΔE = 35 eV for fragment ion *f* (m/z 1090.6). The effect of increasing the collision gas pressure resulted in no significant increase in ΔE for this fragment ion. At 95 % attenuation ΔE increased to 39 eV showing ΔE to be relatively independent of collision gas pressure.

For fragment ions *g* - *k*, ΔE values were unobtainable at the extremes of pressure due to low fragmentation efficiencies. At low gas pressures this was caused by an insufficient number of parent ions undergoing collision. At higher gas pressures, low fragmentation efficiencies were likely to have been due to the increased probability of ion losses as a result of to the larger numbers of collisions taking place. Similar trends, to those obtained for fragment ion *f*, for the variation of ΔE with collision gas pressure, were also observed for fragment ions *g* (m/z 962.6), *h* (m/z 948.6) and *i* (m/z 936.5). For these fragment ions ΔE was greater than 45 eV even at low attenuations and increased by only a few eV on increasing the gas pressure to correspond with attenuations of up to 90 %.

Fragment ions *j* (m/z 779.5) and *k* (m/z 393.2) showed more significant increases in ΔE over the same range of attenuations (40 - 90 %). For dissociations leading to fragment ion *j*, ΔE increased by 9 eV on increasing the attenuation from 40 % to 90 %. For fragment ion *k*, increasing the attenuation from

TABLE 5.2

Variation of translational energy losses ΔE with parent ion beam attenuation for CID of valinomycin $[M+Na]^+$ ions (incident ion energy = 14.9 keV) with helium target gas

Percentage attenuation	Translational energy losses ΔE (eV) for dissociation to fragment ions with mass-to-charge ratios of;					
	'f' m/z 1090.6	*'g'* m/z 962.6	*'h'* m/z 948.6	*'i'* m/z 936.5	*'j'* m/z 779.5	*'k'* m/z 393.2
10	35.0					
20	35.0					
30	36.3					
40	34.4	53.7	48.3	72.4	60.6	61.9
50	35.7	52.7	47.1	74.4	61.9	62.7
60	36.6	55.8	47.3	75.4	63.1	62.7
65						67.3
70	35.5	56.7	51.3	77.5	64.9	71.9
80	38.4	56.7	50.3	77.5	68.7	76.5
90	38.9	56.7	51.3	75.9	69.7	79.2
95	39.2					

40 % to 90 % resulted in an increase in ΔE of approximately 18 eV. In both cases, ΔE at 40 % attenuation, where the number of collisions expected to occur would be low, was still of the order of many tens of electronvolts in magnitude.

5.2.3 A theoretical prediction of the relationship between ΔE and transmission

Previously Neumann *et al.* [61] and Kim [78,79] have used the Poisson distribution to calculate the probability of different numbers of collisions occurring between ion and target. This will now be developed to describe the expected variation of ΔE with transmission.

The probability P of x number of collisions occurring can be described using the Poisson distribution function

$$P(x) = [\lambda^x e^{-\lambda}] / x! \qquad (5.1)$$

where λ is the mean number of collisions which occur for a given transmission. The probability that no collisions take place is given by $P(0)$, and Equation 5.1 reduces to

$$P(0) = e^{-\lambda} \qquad (5.2)$$

Assuming that the probability of no collision events occurring is equivalent to the transmission, then the value of λ (the mean number of collisions) can be found. The values of λ for transmissions of 0.04, 0.1, 0.2, ..., 0.9 are given in Table 5.3.

In an ideal case, all parent ions which have undergone collision lead to detectable fragment ions. Hence for 40 % transmission, the fragmentation efficiency n_f / n_0 would be 60 / 100, whereas in reality the fragmentation efficiency for the valinomycin spectrum shown in Figure 5.1 was 9 %. Assuming the probability of ion losses after each collision is the same, then P, the probability of detecting any ion (collided or un-collided), will be as follows:

TABLE 5.3

The average number of collisions occurring at a given transmission
(calculated using the Poisson function)

Transmission $P(0) = e^{-\lambda}$	Mean number of collisions, λ
0.04	3.2189
0.1	2.3026
0.2	1.6094
0.3	1.2040
0.4	0.9163
0.5	0.6931
0.6	0.5108
0.7	0.3567
0.8	0.2231
0.9	0.1054

Let P_d be the probability of detecting an ion after each collision event;

$$P = P(0).1 + P(1).P_d + P(2).P_d^2 + P(3).P_d^3 + \ldots\ldots \quad (5.3)$$

$$P = \sum_{x=0}^{\infty}\left\{\frac{\lambda^x e^{-\lambda}}{x!}(P_d)^x\right\} \quad (5.4)$$

$$P = \sum_{x=0}^{\infty}\left\{\frac{(\lambda P_d)^x e^{-\lambda}}{x!}\right\} \quad (5.5)$$

$$P = e^{-\lambda}\sum_{x=0}^{\infty}\left\{\frac{(\lambda P_d)^x}{x!}\right\} \quad (5.6)$$

$$P = e^{-\lambda} e^{\lambda P_d} \quad (5.7)$$

$$P = e^{\lambda(P_d - 1)} \quad (5.8)$$

In the valinomycin case, for every 100 incident ions at a transmission of 40 %, 40 + 9 ions are detected in total, and therefore

$$e^{\lambda(P_d - 1)} = 0.49 \quad (5.9)$$

$$\lambda (P_d - 1) = \ln 0.49 \quad (5.10)$$

since for 40 % transmission $\lambda = 0.9163$ (from Table 5.3)

$$0.9163 (P_d - 1) = \ln 0.49 \quad (5.11)$$

$$(P_d - 1) = -0.7785 \quad (5.12)$$

The probability of detecting an ion after one collision is therefore $P_d = 0.2215$.

To find the number of fragment ions contributing to each recorded peak which arose as a result of 1, 2, 3, ... collisions of the parent ions, the values for x were substituted into Equation 5.1 together with the values of λ given in

Table 5.3. For example, at 40 % transmission;

$$P(1) = 0.3665$$
$$P(2) = 0.1679$$
$$P(3) = 0.0513$$
$$P(4) = 0.0117$$
$$P(5) = 0.0022$$

The probability of detecting a fragment ion that arose as a result of a parent ion colliding x number of times, $P_d(x)$, was obtained by multiplying the value of $P(x)$ by P_d^x. The following values of $P_d(x)$ were obtained for the 40% transmission case, where $P_d = 0.2215$:

$$P_d(1) = P(1)\, P_d = 0.0811797$$
$$P_d(2) = P(2)\, P_d^2 = 0.0082375$$
$$P_d(3) = P(3)\, P_d^3 = 0.0005574$$
$$P_d(4) = P(4)\, P_d^4 = 0.0000281$$
$$P_d(5) = P(5)\, P_d^5 = 0.0000011$$

Hence,

$$\sum_{x=1}^{5} P_d(x) = 0.0900038$$

To find the percentage of 1, 2, 3, .. collision fragment ions making up a measured peak, the above P_d values were 'normalised'. The number of fragment ions arising from a single collision was therefore 0.0811797 / 0.0900038 x 100 = 90.19 %. The same treatment was applied for all transmissions listed in Table 5.3 and the final values are given in Table 5.4 and plotted in Figure 5.2. The above calculations estimate that single collisions predominate for collisions of valinomycin $[M+Na]^+$ ions, at an incident ion energy of 14.9 keV with helium target gas atoms. At attenuations below 60 %, a less than 10 % contribution to fragment ion peaks from multiple collisions was predicted.

To compare this theory with the experimental data, an average value of ΔE per collision would be required. Different fragment ions are associated with different translational energy losses, and therefore the theory would only be applicable to the average of ΔE for all fragment ions. In the present case, theory

TABLE 5.4

The percentage of ions contributing to the measured fragment ion peaks which arose as a result of 1, 2, 3, ... collisions of the incident ion

Transmission	Percentages					
	Number of collisions (x)					
	1	2	3	4	5	6
0.04	68.56	24.43	5.81	1.03	0.15	0.0017
0.1	76.66	19.55	3.32	0.42	0.043	0.0036
0.2	83.23	14.83	1.76	0.157	0.011	0.0006
0.3	87.26	11.63	1.03	0.069	0.0036	0.0001
0.4	90.19	9.15	0.62	0.03	0.001	
0.5	92.52	7.10	0.36	0.01		
0.6	94.45	5.34	0.2	0.0056		
0.7	96.11	3.79	0.1			
0.8	97.66	2.41	0.04			
0.9	98.85	1.15				

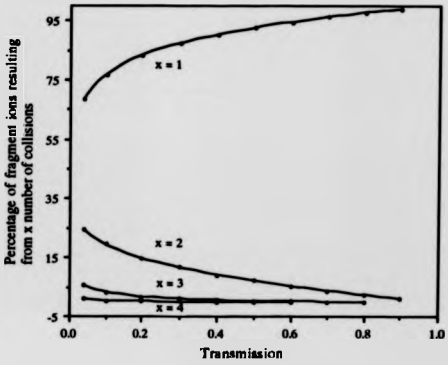

Figure 5.2 Percentage of ions contributing to each fragment ion peak which arose as a result of *x* number of collisions of the incident ion. (Calculated for a fragmentation efficiency of 9% - see text for details of calculations).

was fitted to the experimental data for individual fragment ions by calculating the value of ΔE per collision at the lowest collision gas pressure for which ΔE had been measured. The broad assumption was made that energy losses were the same for all collisions leading to a particular fragment ion. For decomposition to fragment ion *j* (m/z 779.5) of valinomycin, the value of ΔE at 60% transmission was 60.6 eV. The energy loss per collision was found as follows using the data from Table 5.4:

$$100\ \Delta E = (94.45\ \delta E) + 2\ (5.34\ \delta E) + 3\ (0.2\ \delta E) + 4\ (0.0056\ \delta E) \qquad (5.13)$$

$$6060 = 105.7524\ \delta E$$

$$\delta E = 57.3\ \text{eV}$$

This value of δE was then substituted back into similar versions of Equation 5.13 constructed for each transmission and for each fragment ion in turn.

5.2.4 Comparison of experimental results and theory

Figures 5.3 to 5.9 show plots of the translational energy lost by valinomycin $[M+Na]^+$ ions in collision with helium target gas atoms against parent ion beam attenuation for dissociation leading to fragment ions *f* - *k*. Attenuation was chosen rather than transmission, so that collision gas pressure was increasing from left to right when observing the graphs. Experimental data points are plotted with an estimate of error. The solid lines represent the theoretically predicted relationship between ΔE and gas pressure estimated using Poisson statistics (see Section 5.2.3).

For fragment ion *f* (m/z 1090.6), ΔE showed no significant increase as the gas pressure was increased (Figure 5.3). The theoretical relationship shows ΔE increasing to a greater extent than was observed experimentally. At attenuations above 40 % the theoretical and experimental data points begin to deviate. The experimental data show slight increases in ΔE as the gas pressure is increased.

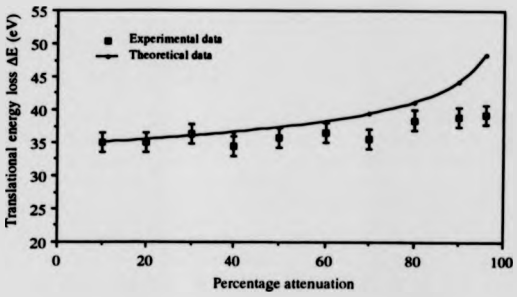

Figure 5.3 Variation of translational energy loss, ΔE, with collision gas pressure for CID of valinomycin $[M+Na]^+$ ions (m/z 1133.6) to fragment ion *f* (m/z 1090.6) with helium as target gas. E_l=14.9 keV.

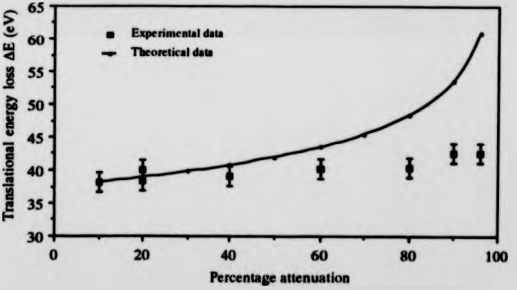

Figure 5.4 Variation of translational energy loss, ΔE, with collision gas pressure for CID of valinomycin $[M+Na]^+$ ions (m/z 1133.6) to fragment ion *f* (m/z 1090.6) with helium as target gas. E_l=8.1 keV.

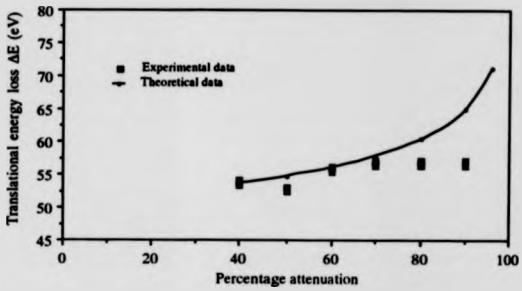

Figure 5.5 Variation of translational energy loss, ΔE, with collision gas pressure for CID of valinomycin $[M+Na]^+$ ions (m/z 1133.6) to fragment ion *g* (m/z 962.6) with helium as target gas. E_l=14.9 keV.

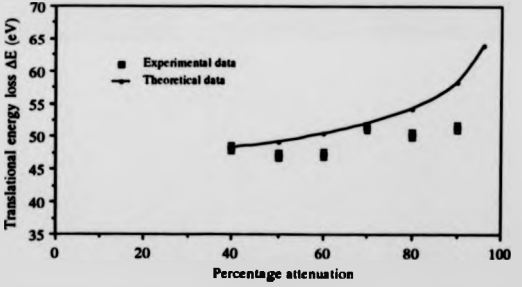

Figure 5.6 Variation of translational energy loss, ΔE, with collision gas pressure for CID of valinomycin $[M+Na]^+$ ions (m/z 1133.6) to fragment ion *h* (m/z 948.6) with helium as target gas. E_l=14.9 keV.

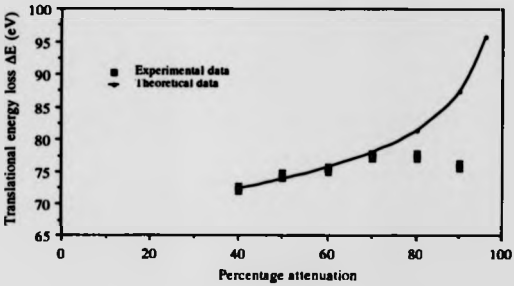

Figure 5.7 Variation of translational energy loss, ΔE, with collision gas pressure for CID of valinomycin $[M+Na]^+$ ions (m/z 1133.6) to fragment ion *i* (m/z 936.5) with helium as target gas. E_l=14.9 keV.

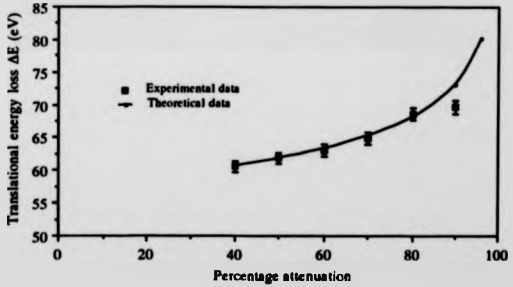

Figure 5.8 Variation of translational energy loss, ΔE, with collision gas pressure for CID of valinomycin $[M+Na]^+$ ions (m/z 1133.6) to fragment ion *j* (m/z 779.5) with helium as target gas. E_l=14.9 keV.

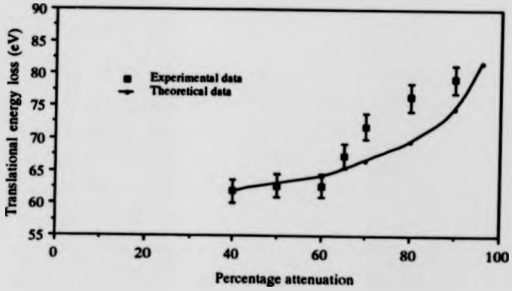

Figure 5.9 Variation of translational energy loss, ΔE, with collision gas pressure for CID of valinomycin $[M+Na]^+$ ions (m/z 1133.6) to fragment ion *k* (m/z 393.2)with helium as target gas. E_t=14.9 keV.

Given the magnitude of the experimental uncertainties these increases were not considered to be of particular significance. Similar results were also obtained with an incident ion energy of 8.1 keV and are shown in Figure 5.4. In this case the values of ΔE were marginally larger than those obtained with an incident ion energy of 14.9 keV.

Figures 5.5, 5.6 and 5.7 illustrate the results for fragment ions *g* (m/z 962.6), *h* (m/z 948.6) and *i* (m/z 936.5) respectively. The experimental data show only small increases in ΔE as collision gas pressure is increased. A much stronger relationship was predicted theoretically particularly for the higher gas pressures. Figures 5.5 and 5.7 for fragment ions *g* and *i* depict close agreement of experimental data with theory up to an attenuation of 70 %, above which the measured ΔE values increased no further. Theory predicts a much stronger dependence of ΔE on collision gas pressure than was revealed by experiment .

Figure 5.8 illustrates the results for fragment ion *j* (m/z 779.5). The experimental and theoretical data appear to agree quite closely except for the last experimental data point at 90 % attenuation which falls below the theoretical curve. Results for fragment ion *k* (m/z 393.2) contrast with those of the other fragment ions. In this case the experimental data points at attenuations above 60% lie above the theoretical curve (Figure 5.9). The experimentally observed relationship between ΔE and collision gas pressure for fragment ion *k* was stronger than predicted.

5.2.5 Pressure dependencies of ΔE for xenon target gas

The FD-MIKE spectrum of valinomycin $[M+Na]^+$ ions obtained using xenon collision gas is given in Figure 5.10. The parent ion beam attenuation was 60 % and the incident ion energy 14.9 keV. The general appearance of the spectrum was similar to that obtained when using helium as target (Figure 5.1), but the

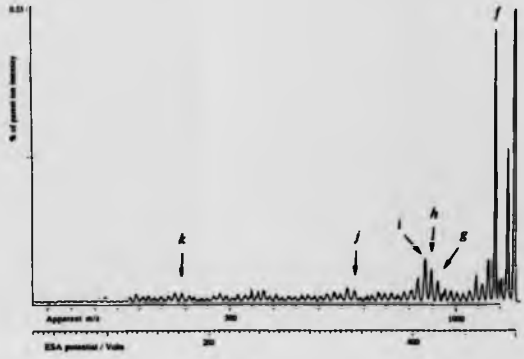

Figure 5.10 FD-MIKE spectrum of valinomycin $[M+Na]^+$ ions (m/z 1133.6); xenon target gas, 60 % parent ion beam attenuation, incident ion energy E_i = 14.9 keV

fragmentation efficiency with xenon was lower, 4.8 % compared with 9 %. A more detailed comparison of spectra obtained using different collision gases is given in Chapter 6.

The pressure dependencies of translational energy losses have been measured when xenon was used as target gas for fragment ions *f* (m/z 1090.6), *i* (m/z 936.5) and *k* (m/z 393.2), and are given in Table 5.5. ΔE values for fragment ions *f* and *i* were approximately a factor of two lower than those obtained with helium as target. The results for fragment ion *k* were anomalous, resulting in negative values for ΔE at all attenuations except 90 %. These data also showed considerable scatter. The data were recorded following those for fragment ion *f* and between measurements made for fragment ion *i*. This suggests that instrumental factors were not causing the 'error' and possible explanations are discussed later (Section 5.5). Figures 5.11, 5.12 and 5.13 show plots of ΔE versus attenuation for fragment ions *f*, *i*, and *k* respectively. The theoretical relationship estimated using Poisson statistics was re-calculated for the different fragmentation efficiency. A theoretical curve was not obtainable for fragment ion k (m/z 393.2) due to the negative value of ΔE at the lowest attenuation. For fragment ion *f* (m/z 1090.6) the theoretical relationship between ΔE and attenuation predicted an increase of 3 eV on increasing the attenuation from 10 % to 96 %. The experimental data were scattered about the theoretical curve, but showed no strong tendencies to deviate from this curve. Figure 5.12 shows the theoretically predicted rise in ΔE for fragment ion *i* to be 6 eV on increasing the attenuation from 10 to 96 %, whereas the experimental data showed very little change.

TABLE 5.5

Variation of translational energy losses with parent ion beam attenuation for CID of valinomycin $[M+Na]^+$ ions (incident ion energy = 14.9 keV) with xenon target gas

Percentage attenuation	Translational energy losses ΔE (eV) for dissociation to fragment ions with mass-to-charge ratios of;		
	'f' m/z 1090.6	*'j'* m/z 936.5	*'k'* m/z 393.2
10	14.4		
20	15.5		
30	13.2		
40	14.3	31.0	-5.1
50	15.8		
67.5	16.9		
65		30.8	
70	13.5,15.0		-4.2
76			-3.3
80	17.1		-7.9
90	14.2	30.5	3.5
96	15.5		

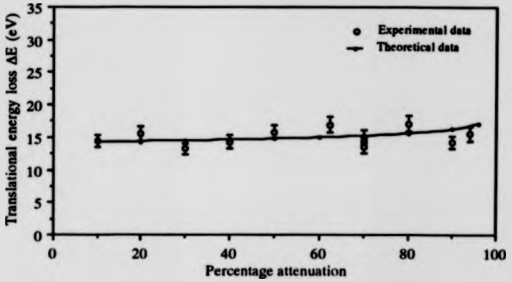

Figure 5.11 Variation of translational energy loss, ΔE, with collision gas pressure for CID of valinomycin $[M+Na]^+$ ions (m/z 1133.6) to fragment ion *f* (m/z 1090.6)with xenon as target gas. E_l=14.9 keV.

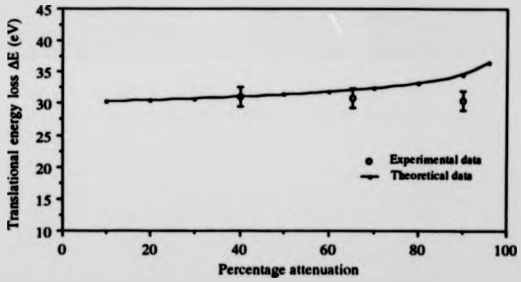

Figure 5.12 Variation of translational energy loss, ΔE, with collision gas pressure for CID of valinomycin $[M+Na]^+$ ions (m/z 1133.6) to fragment ion *i* (m/z 936.5)with xenon as target gas. E_l=14.9 keV.

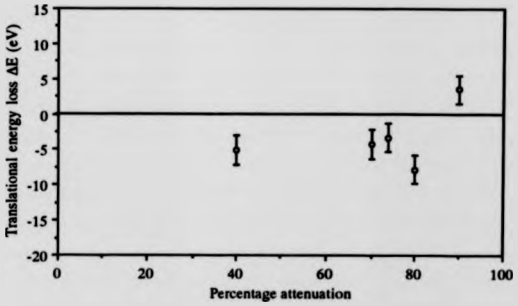

Figure 5.13 Variation of translational energy loss, ΔE, with collision gas pressure for CID of valinomycin $[M+Na]^+$ ions (m/z 1133.6) to fragment ion *k* (m/z 393.2)with xenon as target gas. E_I=14.9 keV.

5.3 RESULTS FOR VALINE-GRAMICIDIN A

5.3.1 MIKES of valine-gramicidin A

The FD-MIKE spectrum of $[M+K]^+$ molecule-ions of the peptide valine-gramicidin A (m/z 1920.2) is shown in Figure 5.14. The incident ion energy was 14.9 keV, the collision gas helium and an attenuation of 70 % was employed. The fragmentation efficiency in this case was 8.2 %. Valine-gramicidin A was considerably more difficult to field desorb than valinomycin. The emitter heating current at which ion beams were detectable was approximately 90 mA and the optimum EHC was between 100 and 110 mA. The majority of valinomycin FD experiments resulted in ion beams of a usable intensity but with valine-gramicidin A usable intense stable ion beams were the exception rather than the rule. Once a stable ion beam was obtained, it was usually more intense than could be achieved with valinomycin, providing > 250,000 parent ions/second reaching the detector prior to admission of target gas into the collision cell. Such ion beams could then be maintained for many hours. The optimum EHC was close to the EHC at which sample degradation occurred. Using potassium as the cation the optimum EHC was lowered by a few mA compared with using sodium. The advantages of cationisation by alkali cations for lowering the optimum EHC have been discussed in reference 145 and a model for field desorption has been proposed which explains this effect.[114,179] A further observation concerning this effect was that, after recording a spectrum over a period of hours, the $[M+Na]^+$ ion peak would become more intense as the $[M+K]^+$ ion decreased in intensity. At a slightly higher EHC, the $[M+H]^+$ ion could also be observed, but was short-lived due to depletion of the peptide sample. Generation of $[M+Na]^+$ molecule-ions from mixing the peptide sample with NaI salt, or $[M+H]^+$ ions in the absence of salt, was found to be unsuccessful for generating stable long-lived ion beams.

/

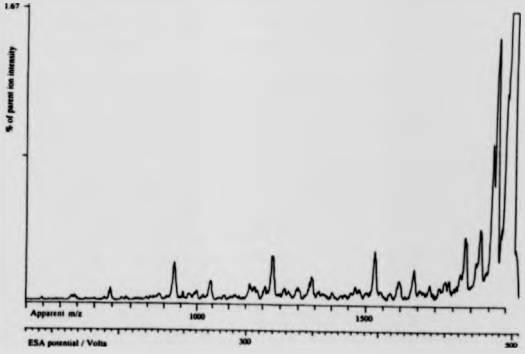

Figure 5.14 FD-MIKE spectrum of valine-gramicidin A $[M+K]^+$ ions (m/z 1920.2); helium target gas, 70 % parent ion beam attenuation, incident ion energy E_i = 14.9 keV

TABLE 5.6

Fragment ion mass assignments in the FD-MIKE spectrum of valine-gramicidin A $[M+K]^+$ ions (Figure 5.14). Incident ion energy = 14.9 keV and parent ion beam attenuated by 70% with helium target gas

V_m	Apparent m/z	Assigned mass (m_f) / Da	Fragment ion
		1903.20	Loss of OH or NH_3
409.829	1873.70	1876.10	Loss of C_3H_8 or $[z_{15} + K]^+$
406.392	1857.99	1861.13	Loss of C_2H_4NO
398.616	1822.43	1831.12	
389.669	1781.53	1789.09	$[y_{14}^{-2} + K]^+$
		1691.07	$[c_{14}^{+1} + K]^+$
358.128	1637.33	1645.04	$[a_{14}^{-1} + K]^+$
		1602.98	$[d_{14}^{-2} + K]^+$
		1576.93	$[x_{11}^{-2} + K]^+$
333.289	1523.77	1531.96	$[a_{13}^{-1} + K]^+$
		1345.88	$[a_{12}^{-1} + K]^+$
		1303.83	$[d_{12}^{-1} + K]^+$
268.267	1226.49	1232.79	$[a_{11}^{-1} + K]^+$
227.794	1041.45	1046.11	$[a_{10}^{-1} + K]^+$
		1004.67	$[d_{10}^{-1} + K]^+$
203.343	929.66	933.63	$[a_9^{-1} + K]^+$
162.823	744.41	747.55	$[a_8^{-1} + K]^+$

The number of dissociation channels available to valine-gramicidin A was greater than for valinomycin. Therefore, despite similar fragmentation efficiencies, the signal-to-noise ratios for individual fragment ion peaks were not as good. The spectrum characteristically contained a-type sequence ions which were relatively more intense than the other fragment ions, excepting the most intense fragment ions corresponding to side chain losses. Due to the lack of a 4-sector FD tandem mass spectrum the mass assignments of the fragment ion peaks in the MIKE spectrum, Table 5.6, have been made by comparison with the FAB-4-sector spectrum (Figure 3.2) and the tandem mass spectrum of the same molecule-ions formed by infrared laser desorption in a Fourier-transform ion cyclotron resonance mass spectrometer.[180] As discussed in Chapter 3, molecule-ions formed by different ionisation methods can produce different tandem mass spectra, and therefore these comparisons have their limitations.

The pressure dependencies of translational energy losses for valine-gramicidin A $[M+K]^+$ ions were studied for dissociation to the fragment ions corresponding to m/z 1876.1, 1232.8 and 933.6, since these were relatively intense in the MIKE spectrum.

5.3.2 Dependence of ΔE on collision gas pressure

The values of ΔE recorded at various attenuations of the parent ion beam of valine-gramicidin A $[M+K]^+$ with helium collision gas, for dissociations to fragment ions with m/z 1876.1, 1232.8 and 933.6 , are given in Table 5.7. Incident ion energies of 8.1 and 14.9 keV were used. The theoretical relationship between ΔE and attenuation was calculated with a fragmentation efficiency of 8.2 % for the 14.9 keV incident ion energy experiments and 1.9 % for the 8.1 keV experiments.

Figure 5.15 shows the results for the fragment ion with m/z 1876.1. The experimental data agree fairly closely with the theoretical curve and the

TABLE 5.7

Variation of translational energy losses with parent ion beam attenuation for CID of valine-gramicidin A $[M+K]^+$ ions with helium target gas

Percentage attenuation	Translational energy losses ΔE (eV) for dissociation to fragment ions with mass-to charge-ratios; (and incident ion energies E_i)				
	m/z 1876.1 E_i=14.9keV	m/z 1232.8 E_i=14.9keV	m/z 1232.8 E_i=8.1keV	m/z 933.6 E_i=14.9keV	m/z 933.6 E_i=8.1keV
96					78.6
90	53.6	85.2	84.8	56.5	73.7
85	51.6				
82					68.7
80				54.4	65.9
76			75.1		
75	49.2	75.0			
72.5					69.4
70	50.8			54.4	66.2
67		70.5			
63			66.9		
60	41.1		65.6	52.8	66.9
59				54.9	
56		70.0			
50	41.9	68.5	59.6		52.3
40	41.9	66.0	50.9	49.6	48.3
32			54.9		

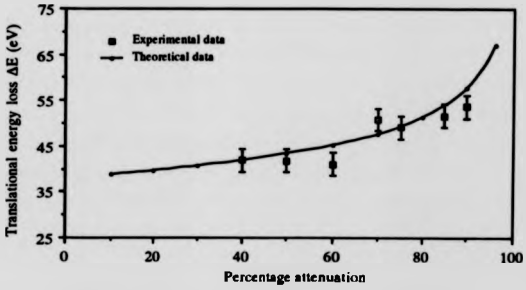

Figure 5.15 Variation of translational energy loss, ΔE, with collision gas pressure for CID of valine-gramicidin A $[M+K]^+$ ions (m/z 1920.2) to the m/z 1876.1 fragment ion with helium as target gas. E_l=14.9 keV.

experimentally observed increase in ΔE on increasing the attenuation from 40 to 90 % was approximately 12 eV. Similarly for the $[a_{11}^{-1} + K]^+$ fragment ion (m/z 1232.8) when an incident ion energy of 14.9 keV was used, the rise in ΔE was 19 eV (Figure 5.16). In this case, when the incident ion energy was 8.1 keV the experimental variation of ΔE with attenuation increased more rapidly than predicted by the theoretical model (Figure 5.17). Figure 5.18 shows a plot of the results for the $[a_9^{-1} + K]^+$ fragment ion of valine-gramicidin A recorded with an incident ion energy of 14.9 keV. ΔE increased by 7 eV on increasing the attenuation from 40 to 90 %. The theoretical curve shows a steeper increase in ΔE than was measured. In contrast the ΔE values measured for this fragment ion when the parent ion incident energy was 8.1 keV, showed an increase of 30 eV over the range of 40 - 96 % attenuation, an increase much greater than predicted (Figure 5.19).

5.4 RESULTS FOR CAESIUM IODIDE CLUSTER IONS $[Cs_2I_4]^+$

5.4.1 MIKES of $[Cs_2I_4]^+$

The MIKE spectrum of $[Cs_2I_4]^+$ (m/z 1172.145) molecule-ions formed by FAB is shown in Figure 5.20. The target gas used was helium, with the parent ion beam attenuated by 62 %. The incident ion energy in this case was 10.4 keV, which was the upper limit of the potential which could be held by the FAB ion source. The sensitivity of FAB experiments was reduced due to the inability of the FAB gun to hold a potential of more than 6 kV without electrically discharging. Therefore the intense ion currents generally associated with FAB of caesium iodide were not achieved and were a factor of at least two lower than the parent ion currents used in FD-MIKES experiments. Due to the limited number of dissociation pathways available to such cluster ions, the signal-to-noise ratio was reasonable despite the low intensity of the parent ion beam. The resolving

/

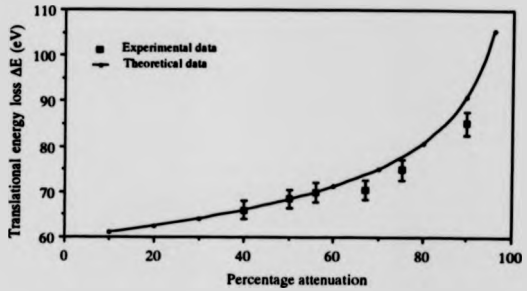

Figure 5.16 Variation of translational energy loss, ΔE, with collision gas pressure for CID of valine-gramicidin A $[M+K]^+$ ions (m/z 1920.2) to fragment ion $[a_{11}^{-1}+K]^+$ (m/z 1232.8) with helium as target gas. E_l=14.9 keV.

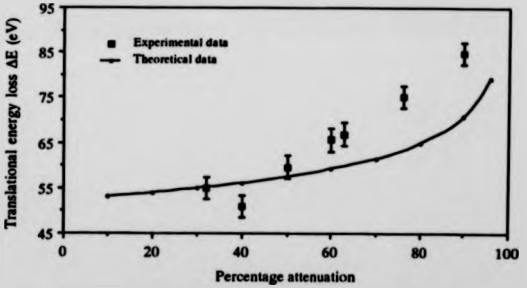

Figure 5.17 Variation of translational energy loss, ΔE, with collision gas pressure for CID of valine-gramicidin A $[M+K]^+$ ions (m/z 1920.2) to fragment ion $[a_{11}^{-1}+K]^+$ (m/z 1232.8) with helium as target gas. E_l=8.1 keV.

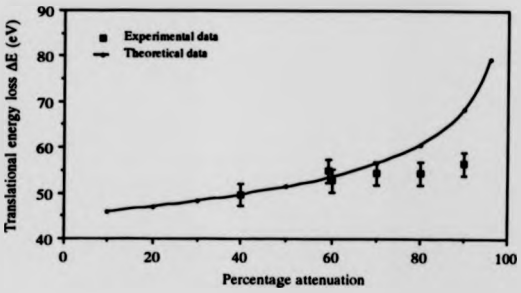

Figure 5.18 Variation of translational energy loss, ΔE, with collision gas pressure for CID of valine-gramicidin A $[M+K]^+$ ions (m/z 1920.2) to fragment ion $[a_9^{-1}+K]^+$ (m/z 933.6) with helium as target gas. E_l=14.9 keV.

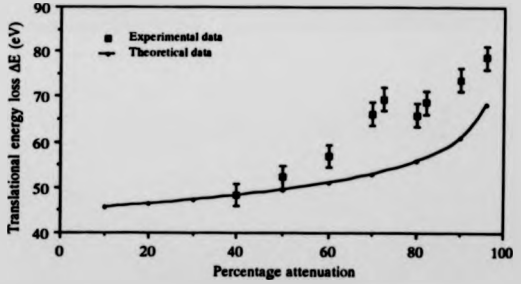

Figure 5.19 Variation of translational energy loss, ΔE, with collision gas pressure for CID of valine-gramicidin A $[M+K]^+$ ions (m/z 1920.2) to fragment ion $[a_9^{-1}+K]^+$ (m/z 933.6) with helium as target gas. E_l=8.1 keV.

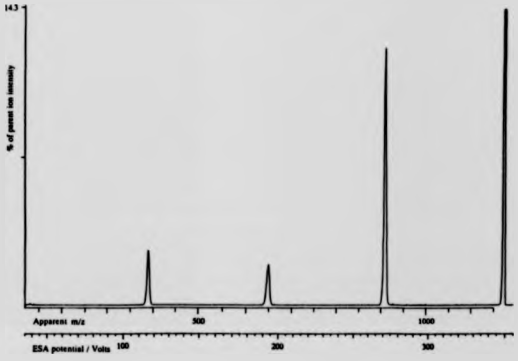

Figure 5.20 FAB-MIKE spectrum of $Cs_5I_4^+$ ions (m/z 1172.15); helium target gas, 60 % parent ion beam attenuation, incident ion energy E_I = 10.4 keV

slits of the instrument were opened to twice their usual values to obtain improved signal intensity. The isotope peaks of caesium iodide cluster ions are separated by two mass units and hence the decreased resolution was not problematic. Fragment ion peaks were separated by hundreds of mass units and therefore high resolving powers were not required for their separation. The fragmentation efficiency with $[Cs_5I_4]^+$ was 18.5 %, much greater than for the peptides described in the previous sections. The four possible fragment ion peaks arising from dissociation of $[Cs_5I_4]^+$ have m/z values of 132.9 (Cs^+), 392.7 (Cs_2I^+), 652.5 ($Cs_3I_2^+$) and 912.3 ($Cs_4I_3^+$). The Cs^+ fragment ion was of very low intensity relative to the parent ion and other fragment ions in this spectrum and hence was too weak to be used for a study of the relationship between ΔE and collision gas pressure. $[Cs_4I_3]^+$ was also excluded from the study since the contribution from metastable fragment ions was observed to be ~15 %.

5.4.2 Dependence of ΔE on helium collision gas pressure

The values of ΔE at various attenuations of helium and xenon collision gases for dissociation of $[Cs_5I_4]^+$ to $[Cs_3I_2]^+$ and $[Cs_2I]^+$ are given in Tables 5.8 and 5.9 respectively. Data for helium as target gas show the translational energy losses to be large, and of similar magnitudes to the results for valinomycin and valine-gramicidin A. The experimentally observed relationship between ΔE and collision gas pressure for both fragment ions showed ΔE to increase with increasing gas pressure. In the case of fragmentation leading to $[Cs_3I_2]^+$, increasing the attenuation from 20 % to 96 % resulted in an increase in the translational energy loss of 20 eV (Figure 5.21). Similarly for dissociation leading to $[Cs_2I]^+$, the translational energy loss increased by 25 eV (Figure 5.22). The theoretical relationship estimated for the dependence of ΔE on attenuation using the Poisson treatment described in Section 5.2.3, was adjusted for the fragmentation efficiency of 18.5 % and is shown as the solid line on the graphs. In both cases the experimental data agreed quite closely with the theoretical curve until very high

TABLE 5.8

Variation of translational energy losses with parent ion beam attenuation for CID of $[Cs_2I_4]^+$ ions (incident ion energy = 10.4 keV) with helium target gas

Percentage attenuation	Translational energy losses ΔE (eV) for $[Cs_2I_4]^+$ dissociating to fragment ions with m/z;	
	392.72	652.53
20	63.3	49.5
40	64.2	51.9
50	68.9	52.9
80	74.8	59.3
90	77.0	58.3
96	88.6	69.4

TABLE 5.9

Variation of translational energy losses with parent ion beam attenuation for CID of $[Cs_2I_4]^+$ ions (incident ion energy = 10.4 keV) with xenon target gas

Percentage attenuation	Translational energy losses ΔE (eV) for $[Cs_2I_4]^+$ dissociating to fragment ions with m/z;	
	392.72	652.53
30	-1.8	-0.2
40	-0.3	-0.5
60	-1.4	2.0
70	-1.3	-0.4
80	3.3	3.3
90	4.7	5.0

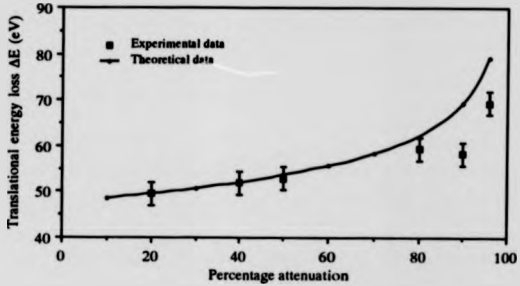

Figure 5.21 Variation of translational energy loss, ΔE, with collision gas pressure for CID of $[Cs_5I_4]^+$ ions (m/z 1172.15) to fragment ion $[Cs_3I_2]^+$ (m/z 652.5) with helium as target gas. E_i=10.4 keV.

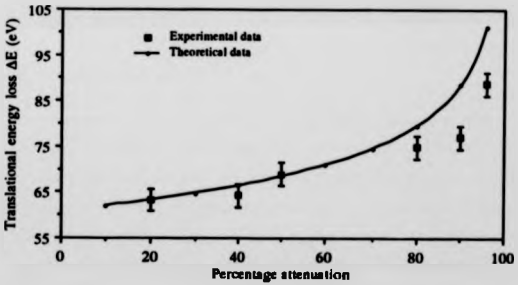

Figure 5.22 Variation of translational energy loss, ΔE, with collision gas pressure for CID of $[Cs_5I_4]^+$ ions (m/z 1172.15) to fragment ion $[Cs_2I]^+$ (m/z 392.7) with helium as target gas. E_i=10.4 keV.

gas preasures were reached. At high attenuations the experimental data fell marginally below the theoretical curve.

5.4.3 Dependence of ΔE on xenon collision gas pressure

Results for the dependency of translational energy loss on collision gas pressure when xenon was used as target gas are given in Table 5.9 for dissociation of $[Cs_5I_4]^+$ to fragment ions $[Cs_3I_2]^+$ and $[Cs_2I]^+$ respectively. These data are represented graphically in Figures 5.23 and 5.24. The magnitudes of the energy losses were small compared with those obtained with helium. Figures 5.23 and 5.24 show that at attenuations below 60 % the value of ΔE was close to zero and rose to ~5 eV at 90 % attenuation.

5.5 Discussion and conclusions

The results of the above investigations into the dependence of translational energy losses on collision gas pressure illustrate several important features concerning the dynamics of CID.

The translational energy losses vary for CID of the same parent ion dissociating to different fragment ions. Such a result was to be expected since different dissociation pathways are associated with differing critical energies. Consequently the amount of internal energy available to the activated incident ion will determine which dissociation pathways are accessible. The fragmentation pathways which can then be observed in the mass spectrometer will be governed by the dissociation rate constants. Since a portion of the translational energy loss results in internal energy of the incident ion, the ΔE values associated with individual fragment ions might be expected to reflect the different critical energies associated with their formation.

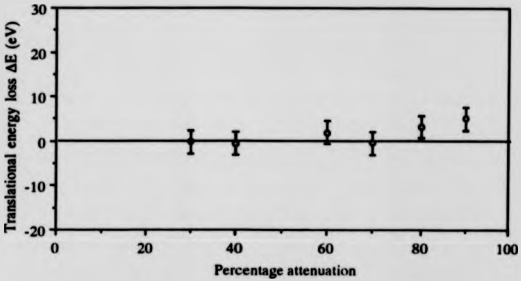

Figure 5.23 Variation of translational energy loss, ΔE, with collision gas pressure for CID of $[Cs_5I_4]^+$ ions (m/z 1172.15) to fragment ion $[Cs_3I_2]^+$ (m/z 652.5) with xenon as target gas. E_i=10.4 keV.

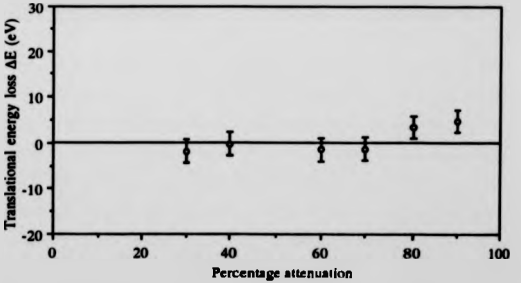

Figure 5.24 Variation of translational energy loss, ΔE, with collision gas pressure for CID of $[Cs_5I_4]^+$ ions (m/z 1172.15) to fragment ion $[Cs_2I]^+$ (m/z 392.7) with xenon as target gas. E_i=10.4 keV.

Secondly, in all experiments where helium was the target gas, the translational energy losses observed at very low gas pressures, where it is generally agreed that single collision conditions predominate, were still of the order of many tens of electronvolts in magnitude. This result contradicts that of Russell and co-workers [64] where the pressure dependence observed for $[(glycerol)_3 + H]^+$ dissociating to give $[(glycerol)_2 + H]^+$, showed the energy losses to reach zero at low gas pressures and only increase to the order of tens of eV at much higher gas pressures. On the basis of those results it was suggested that large energy losses were only obtained at high gas pressures and that collision-induced dissociation occurs via multiple collisions.[64] Alexander *et al.*[66] have observed ΔE to increase with increasing collision gas pressure for chlorophyll-*a*. On increasing the gas pressure from an attenuation of 15 % to 90 % the value of ΔE was shown to increase from 6 to 15 eV. All results presented in this chapter suggest that for large ions the energy losses associated with each collision between the incident ion and helium target gas atom are many tens of eV in magnitude. Hence if at higher gas pressures, such as those corresponding to 60 - 80 % attenuation which are routinely used in CID experiments, five or more collisions were taking place prior to dissociation to detectable fragment ions, then the measured ΔE would be expected to rise to many hundreds of eV. Such large increases were not observed for valinomycin, valine-gramicidin A or CsI_4^+. The results for these ions are consistent with the number of collisions occurring being low, and single collision conditions providing the dominant contribution to the fragment ion peaks. Collisions involving the loss of large amounts of translational energy are consistent with an impulsive model to describe the energy transfer in collisions of large ions and target gas atoms, and therefore with direct vibrational excitation of the incident ion.

Results which showed no significant increase in ΔE with increasing collision gas pressure, whereas theoretically a rise in ΔE was predicted, suggest

that fewer collisions are occurring on average than were expected. One possible explanation for such a result could be that as more collisions occur, and the internal energy of the ion is increased, higher energy decomposition pathways become available to the activated parent ion. For valinomycin, measured ΔE values which showed no significant increases with increasing attenuation, tended to be for dissociation pathways leading to higher mass fragment ions. The formation of low-mass fragment ions tends to be associated with higher energy processes than for high-mass fragment ions and also with larger values of ΔE.[68] Since ΔE is thought to reflect the internal energy uptake, then increased ΔE values for low-mass fragment ions are expected. The experimental results were consistent with a low number of collisions giving rise to higher mass fragment ions, and as the gas pressure became very high, increased numbers of collisions resulting in sufficient internal energy uptake for the formation of lower mass fragment ions. Deviations from the theoretical curve showing larger than expected ΔE values suggest that more collisions are occurring than expected or that sequential collisions are taking place. Sequential collisions have been used to explain the extremely large energy losses measured by Shell [68] for low-mass fragment ions formed by CID of valine-gramicidin A $[M+H]^+$ ions. As described in Section 1.4.2, energy losses measured for fragment ions formed from collisions of intermediate fragment ions are dependent on intermediate energy losses, and become amplified by the ratio m_1/m_f. Contributions of such large apparent energy losses to the measured fragment ion peak may result in a considerable shift or tailing of the peak to low energy. The incidence of sequential collisions was not taken into account in the theoretical model for the dependence of ΔE on collision gas pressure. Therefore stronger pressure dependencies of ΔE than predicted may be explained in this manner.

The complete MIKE spectra of valinomycin $[M+Na]^+$ ions recorded with 80% and 90% attenuations with helium collision gas are shown in Figure 5.25.

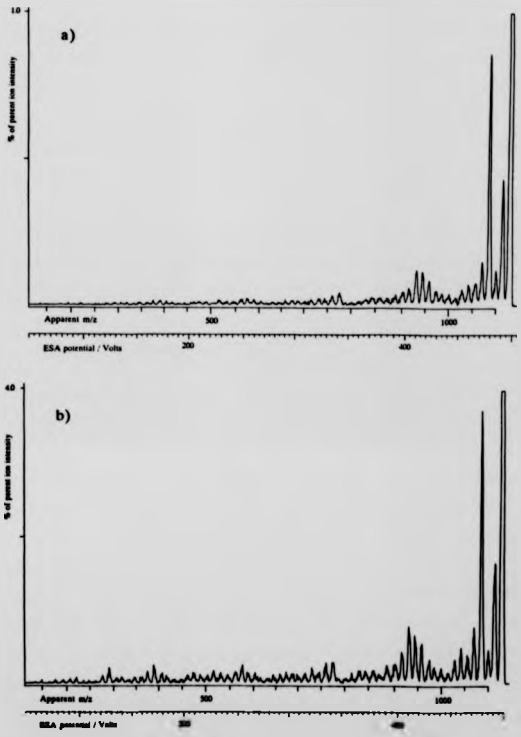

Figure 5.25 Comparison of the MIKE spectra of valinomycin $[M+Na]^+$ ions (m/z 1133.6) obtained with a) 60 % and b) 90 % attenuations with helium collision gas. (E_l = 14.9 keV)

Comparison of the spectra reveals that as the attenuation was increased, the intensity of low-mass fragment ions increased relative to high-mass fragment ions. A similar observation was made for the spectra of valine-gramicidin A $[M+K]^+$ ions with 70 % and 90 % beam attenuations with helium collision gas (Figure 5.26). Since low-mass fragment ions are scattered to a greater extent than high-mass fragment ions, the increase in their relative intensities is perhaps more significant than it appears at first sight. Curtis *et al.*[58] report similar results for a study of the variation of fragment ion abundances with collision gas pressure for a range of target gases. These results suggest that as the collision gas pressure is increased, fragmentation pathways leading to low-mass fragment ions become more populated, either by sequential collisions involving the higher mass fragment ions or by an increased amount of internal energy made available to the parent ion by multiple collisions.

A further assumption made in deriving the theoretical model for estimating the variation of ΔE with collision gas pressure, was that all collisions between the parent ion and target gas atoms lead to dissociation or ion losses. Hence all parent ions arriving at the detector were assumed to have undergone no collisions. When helium was used as target gas, the parent ion peak was observed to be asymmetrical with a considerable low-energy tail. This tailing of the low-energy side of the peak became more pronounced as the collision gas pressure was increased. Figure 5.27 shows the parent ion peaks of valinomycin $[M+Na]^+$ ions recorded at various attenuations with helium as target gas. Similar results have been reported previously for the peptide bombesin and have been attributed to parent ions colliding with gas atoms, losing translational energy but not decomposing within the experimental time scale.[61] In the case of xenon as target gas, the parent ion peak was more symmetrical for all attenuations. This suggests that either the energy losses with xenon were too

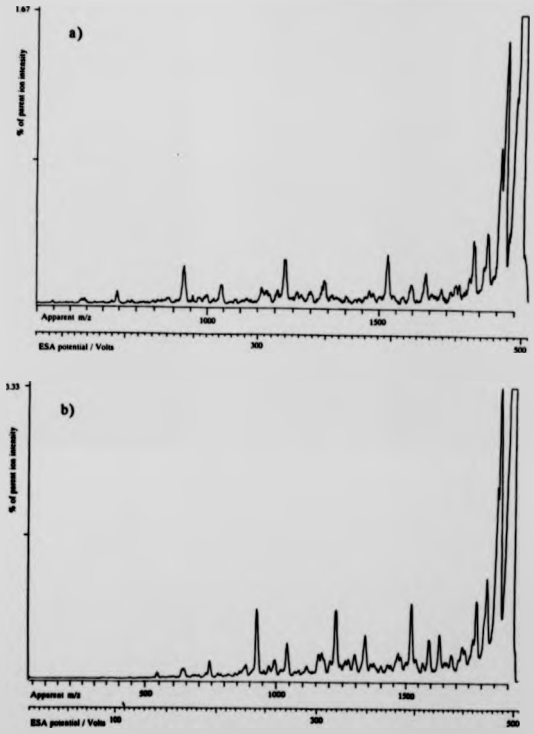

Figure 5.26 Comparison of the MIKE spectra of valine-gramicidin A $[M+K]^+$ ions (m/z 1920.2) obtained with a) 70 % and b) 90 % attenuations with helium collision gas. (E_i = 14.9 keV)

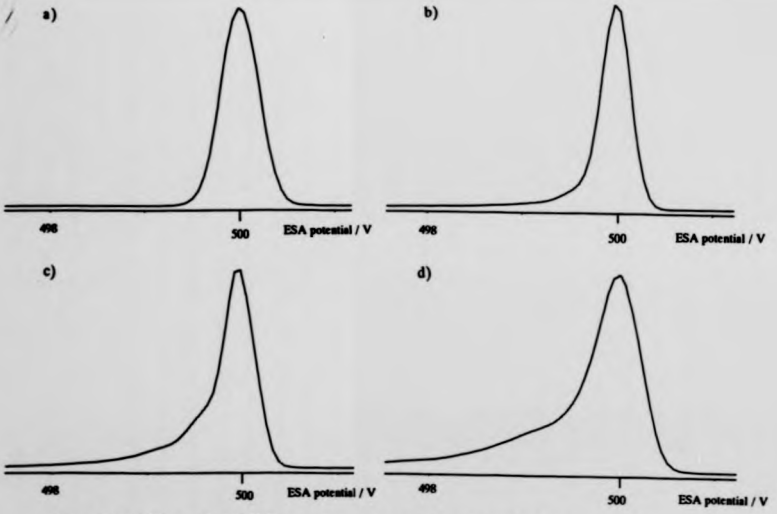

Figure 5.27 Valinomycin $[M+Na]^+$ parent ion peaks (E_i = 14.9 keV) recorded at attenuations of a) 0%, b) 40 %, c) 60% and d) 90 % with helium as target gas.

small to cause an appreciable low-energy tail, or that the input of internal energy was greater and sufficient to cause the majority of parent ions to fragment.

ΔE values for dissociation of valinomycin $[M+Na]^+$ ions dissociating to fragment ion *f* (m/z 1090.6) were shown to be slightly different for incident ion energies of 8.1 and 14.9 keV. Consider the energy losses corresponding with an attenuation of 10 %; for an incident ion energy of 14.9 keV, ΔE was 35 eV, and at E_l = 8.1 keV, ΔE was measured as 38 eV. If these values are entered into Equation 1.8 which relates ΔE to the internal energy uptake by the ion Q, via conservation of energy and momentum and treating the target and ions as wholes, then estimates for Q can be found. When E_l = 14.9 keV, Q was calculated to be 29.2 eV and for E_l = 8.1 keV, Q = 25.3 eV for the case when the scattering angle $\theta = 0^0$ where the internal energy uptake is at a maximum. Despite the larger energy loss value measured in the E_l = 8.1 keV case, the value estimated for Q is lower. Using the second model for momentum transfer, the impulsive collision theory developed by Uggerud and Derrick [54] (Equation 1.9) which considers the collision as involving only one atom in the ion and the target gas atom, the following values for Q were obtained. Considering the mass of the atom hit to be the average of the masses of the atoms in valinomycin, then for E_l = 14.9 keV the internal energy uptake was calculated to be 13.3 eV and a value of Q = 14.4 eV was obtained for E_l = 8.1 keV. In comparison with results obtained using Equation 1.8, the values of the internal energy uptake estimated using the ICT model are a factor of two lower. In the ICT case the internal energy uptakes were similar although the lower incident ion energy provided the slightly larger value of Q, in contrast to the simpler model. A larger value of internal energy taken up when the centre-of-mass collision energy was lower is difficult to rationalise. The observation that ΔE was larger at the lower incident ion energy contradicts the predictions of both momentum transfer models that ΔE should increase with increasing incident ion energy.

The values of ΔE obtained with xenon as target gas were lower than those obtained with helium. Figure 5.28 shows the variation of laboratory frame scattering angle with translational energy loss, calculated using Equation 1.8, for collisions between valinomycin $[M+Na]^+$ ions and helium and xenon target gas atoms. In this case the value of the internal energy uptake was assumed to be half the maximum value calculated for $\theta_i = 0^o$ which represents the mean of the distribution of internal energy uptakes. The top graph shows how the range of possible scattering angles is much larger for xenon than helium. The acceptance angle of the electric sector analyser of the large-scale mass spectrometer was approximately 1^o and, on the basis of Figure 5.28, all scattering angles calculated for collisions with helium result in detectable fragment ions, whereas only translational energy losses below 60 eV or above 5500 eV would result in detectable ions if xenon was used as target. Therefore large translational energy losses of tens of electronvolts would be expected for collisions with xenon, although the possible range which could be observed would be restricted by the acceptance angle of the ESA. For helium as target gas ΔE values up to ΔE = 210 eV should be detectable. Experimentally ΔE values were observed for valinomycin which were a factor of two lower for xenon as target compared with those obtained with helium, for dissociations leading to the fragment ions with m/z 1090.6 and 936.5. The results for dissociation to fragment ion *k* (m/z 393.2) were considerably different with negative values for ΔE being measured in the xenon case. A negative value for ΔE would represent a translational energy gain by the parent ion and would be a rather unusual and unexpected result. Without a more thorough investigation it is not possible to determine whether these measurements represent a real physical phenomenon or whether they are the product of some unexpected, and unaccounted for, experimental error. Figure 5.29 shows raw data plots of the m/z 393.2 fragment ion peak for helium and xenon as targets when the parent ion beam was attenuated by approximately 70 %. The

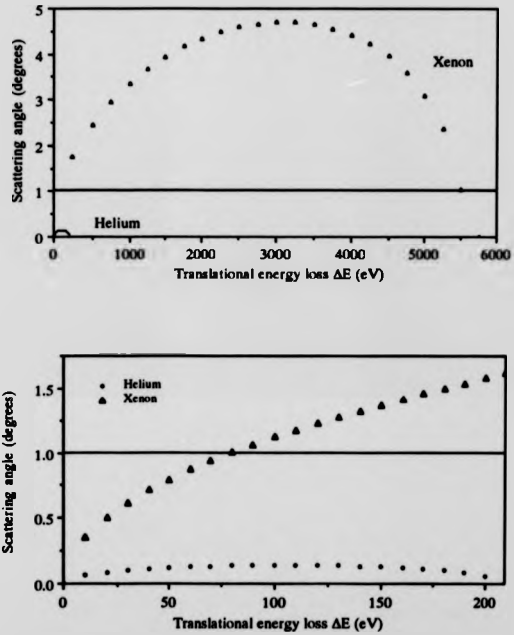

Figure 5.28 Calculated variation of laboratory frame scattering angle with translational energy loss (using Equation 1.8) for valinomycin $[M+Na]^+$ ions (m/z 1133.6) in collision with helium and xenon targets at E_l=14.9 keV.
Top - full range of scattering angles
Bottom - expanded scale

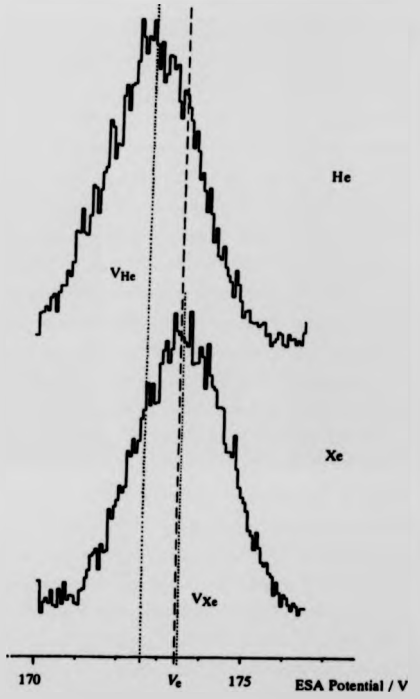

Figure 5.29 Raw data plots of the m/z 393.2 fragment ion peak [HyvValLacVal + Na]$^+$ of valinomycin [M+Na]$^+$ ions when helium and xenon were used as target gases (70 % and 73 % attenuation respectively) showing the shifts in fragment ion peak positions. The expected ESA voltage for transmission of the fragment ions is V_e and the measured peak centroids V_{He} and V_{Xe}.

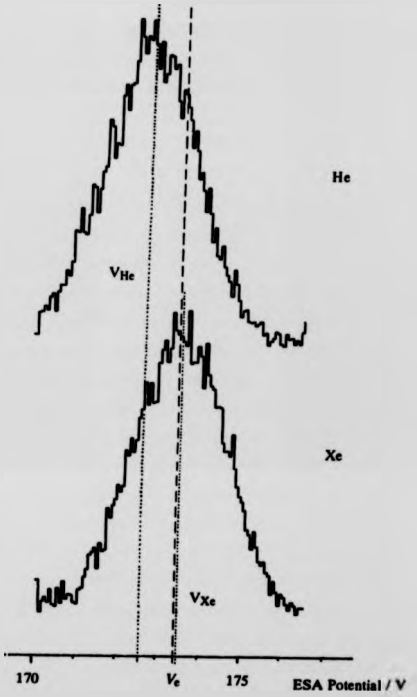

Figure 5.29 Raw data plots of the m/z 393.2 fragment ion peak [HyvValLacVal + Na]$^+$ of valinomycin [M+Na]$^+$ ions when helium and xenon were used as target gases (70 % and 73 % attenuation respectively) showing the shifts in fragment ion peak positions. The expected ESA voltage for transmission of the fragment ions is V_e and the measured peak centroids V_{He} and V_{Xe}.

shift from the ESA potential expected for transmission of the fragment ion peak is about 1 V lower in the case of helium as target, but with xenon the peak centroid appears slightly higher than the expected value but the deviation from V_e is only slightly larger than the estimate for experimental error (see Section 2.1.8 d). The measurement of the ΔE values for fragment ion *k* (m/z 393.2) were interspersed with the measurements for fragment ions *f* (1090.6) and *i* (m/z 936.5), where the energy losses were found to be a few tens of eV. When helium was used as target the energy losses measured for fragment ion *k* were larger than for the other two fragments. That the reverse should now be the case, may suggest that the results are not a consequence of instrumental error. One possible source of error may arise from the low resolution of the MIKES technique. Without an improved 4-sector FD mass spectrum, the possibility of contributions from neighbouring fragment ion peaks cannot be ruled out. Few measurements have been reported for energy losses of peptide ions during collision with heavy targets such as xenon. Bricker and Russell [62] report energy losses for chlorophyll A (m/z 892.5) dissociating to a fragment ion at m/z 614.2 of ~11 eV with krypton as target as compared to ~25 eV with helium. Similar results were reported by Alexander *et al.*[66] for the same fragmentation, with ΔE for xenon being similar to that obtained with krypton, ~11 eV. Alexander *et al*[181] have reported energy gains when heavy targets were used for CID of $[Cs_4I_3]^+$ to form the fragment ion $[Cs_3I_2]^+$. A detailed investigation found no source of experimental error, and speculation was made that two mechanisms may operate for CID. With light targets such as helium, conventional CID with large translational energy losses occurs, whereas it was suggested that with heavy targets such as Kr and Xe, superelastic collisions may take place involving an excited electronic state of the parent ion. Currently it is not possible, without further investigation, to determine whether the results obtained for valinomycin in collision with xenon may be of a similar origin to those described by Alexander *et al.*[181] for $[Cs_4I_3]^+$. Energy losses have been measured for $[Cs_5I_4]^+$ (Figures 5.23 and 5.24) and were very

small, but there was no evidence of negative values of the order of tens of eV like those reported for $[Ca_4I_3]^+$.[181]

Overall, the results of this chapter suggest that the numbers of collisions occurring between an ion and target are low. Under normal CID conditions of 60 - 70 % parent ion attenuation, predominantly single collisions are suggested to occur with large losses of translational energy involved per collision, although the number of collisions which give rise to a fragment ion may be dependent on the mass of the fragment.

Chapter 6 : TRANSLATIONAL ENERGY LOST BY LARGE IONS IN COLLISION-INDUCED DECOMPOSITION. II. Effect of increasing the centre-of-mass collision energy

6.1 AIMS AND INTRODUCTION

As the masses of incident ions become increasingly large, collision induced decomposition (CID) has been found to decrease in efficiency.[14] This is attributed to the decreasing centre-of-mass collision energy as the mass of the ion increases, when the incident ion energy is fixed. Methods of effecting an increase in the internal energy depositions into the ion are required to improve the CID efficiency. The centre-of-mass collision energy (thus the energy available to the molecule-ions for internal energy uptake) may be increased by: increasing the mass of the target gas, increasing the incident ion energy, or by a combination of these two. Successful increases in internal energy deposition would be expected to give rise to improved fragmentation efficiencies resulting in improved spectral quality and possibly to the formation of fragment ions which were not previously observable at the lower centre-of-mass collision energies. Measurement of the translational energy losses ΔE as a result of collision between the incident molecule-ions and target gas would be expected to give an indication of the variation in internal energy uptake Q.

The peptides methionine-enkephalin (RMM= 573.2), valinomycin (RMM = 1110.6) and valine-gramicidin A (RMM = 1881.2) have been used in an investigation of the effect of increasing the centre-of-mass collision energy on the general appearance of tandem mass spectra and on the translational energy lost by incident molecule-ions ΔE. The study was carried out on a large-scale

research mass spectrometer (see Section 2.1) using the MIKES technique and with field desorption employed to ionise samples. Laboratory frame collision energies (incident ion energies E_l) of between 8.1 and 25.1 keV were effected using FD emitter potentials of the same magnitudes. Use of emitter potentials of 20.0 and 25.1 kV frequently resulted in electrical discharges and subsequent breakage of emitter wires, hence few spectra were obtained for these higher collision energies. An emitter potential of 14.9 kV was found to provide fairly stable and relatively intense ion currents whereas the lower emitter potentials generally produced ion beams of lower intensity. Recording of spectra with sufficient fragment ion counts for measurement of translational energy losses was also problematic for the lower incident ion energies.

6.2 EFFECT OF INCREASING INCIDENT ION ENERGY

6.2.1 Methionine-enkephalin

Methionine-enkephalin (Met-enkephalin) is a pentapeptide with the amino acid sequence of Met-Phe-Gly-Gly-Tyr. Met-enkephalin was found to ionise relatively well by field desorption providing almost exclusively $[M+H]^+$ molecule-ions at an optimum emitter heating current of approximately 80 mA. At a parent ion energy of 10.4 keV, there was a negligible contribution to the overall FD-MIKE spectrum from metastable fragment ions.

Figure 6.1 shows the MIKE spectrum of Met-enkephalin $[M+H]^+$ ions obtained with an incident ion energy E_l = 10.4 keV. The target gas used was helium with a pressure which was sufficient to attenuate the parent ion beam by 60%. The measured ESA potentials, V_m, corresponding with the fragment ion peak centroids are listed in Table 6.1. The apparent masses, fragment ion peak assignments and exact masses, m_f, are also listed. The assignments have been made by comparison with the tandem mass spectra in references 60,88,163 and 182. Table 6.1 also lists the ESA potentials, V_o, which would have been required

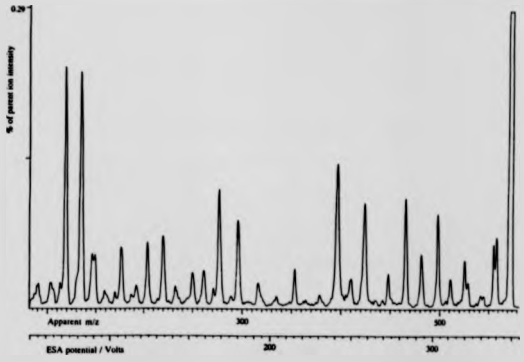

Figure 6.1 FD-MIKE spectrum of methionine-enkephalin $[M+H]^+$ ions (m/z 574.2); helium target gas, 60 % parent ion beam attenuation, incident ion energy E_i = 10.4 keV

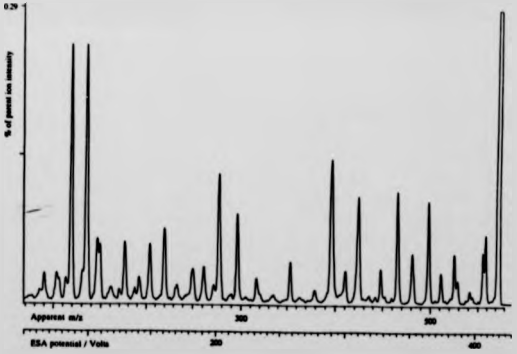

Figure 6.2 FD-MIKE spectrum of methionine-enkephalin $[M+H]^+$ ions (m/z 574.2); helium target gas, 60 % parent ion beam attenuation, incident ion energy E_i = 12.5 keV

TABLE 6.1

Translational energy losses measured in the FD-MIKE spectrum of methionine-enkephalin $[M+H]^+$ ions (m/z 574.2) with helium as target gas (Figure 6.1). Incident ion energy = 10.4 keV. Attenuation = 60 %.

V_m / V	Apparent m/z	Assigned mass (m_f) / Da	Fragment ion	V_a / V	ΔE / eV
-	-	91.05	$[\text{-}CH_2\text{-}C_6H_5]^+$	55.5	-
72.8	119.4	120.08	phenyl immonium ion	73.2	61.7
82.6	135.4	136.08	a_1	83.0	55.1
-	-	148.08	phenyl acyl ion $[H_2NCH(CH_2C_6H_5)CO^+]$	90.3	-
124.5	204.3	205.10	[GlyPhe + H minus CO]$^+$	125.0	43.3
134.3	220.3	221.09	b_1	134.8	36.1
159.4	261.4	262.12	internal acyl ion [GlyGlyPhe + H]$^+$	159.8	29.1
169.2	277.5	278.11	b_3	169.6	24.1
180.7	296.4	297.13	y_2^{+2}	181.2	24.8
215.6	353.6	354.15	y_3^{+2}	215.9	17.5
241.7	396.5	397.19	a_4	242.2	18.9
-	-	425.18	b_4	259.2	-
273.1	447.9	449.17	Loss of $\text{-}CH_2C_6H_4OH$ and H_2O	273.9	28.7
283.9	465.7	467.18	Loss of $CH_2C_6H_4OH$	284.8	32.5
293.4	481.3	482.17	Loss of $CH_3C_6H_5$	294.0	18.7
303.8	498.3	499.21	Loss of $CH_2CH_2SCH_3$	304.4	19.7
311.7	511.3	513.22	Loss of $\text{-}CH_2SCH_3$	312.9	39.4
320.3	525.4	526.23	Loss of SCH_3	320.8	17.5
338.8	555.7	556.22	Loss of H_2O	339.1	10.4
340.6	558.7	559.21	Loss of $\text{-}CH_3$	340.9	9.5

Fragmentation efficiency = 5.9 %
Total number of parent ion counts n_p = 233,938
Total number of fragment ion counts n_f = 34,329

TABLE 6.2

Translational energy losses measured in the FD-MIKE spectrum of methionine-enkephalin $[M+H]^+$ ions (m/z 574.2) with helium as target gas (Figure 6.2). Incident ion energy = 12.5 keV. Attenuation = 60 %.

V_m / V	Apparent m/z	Assigned mass (m_f) / Da	Fragment ion	V_c / V	ΔE / eV
66.3	90.6	91.05	$[\text{-}CH_2\text{-}C_6H_5]^+$	66.6	57.1
87.5	119.6	120.08	phenyl immonium ion	87.9	55.8
99.2	135.5	136.08	a_1	99.6	51.3
107.5	146.9	148.08	phenyl acyl ion $[H_2NCH(CH_2C_6H_5)CO^+]$	108.3	101.8
149.6	204.4	205.10	[GlyPhe + H minus CO]$^+$	150.1	40.4
161.2	220.4	221.09	b_1	161.8	39.3
191.3	261.4	262.12	internal acyl ion [GlyGlyPhe + H]$^+$	191.8	34.0
203.0	277.5	278.11	b_3	203.5	27.8
216.9	297.5	297.13	y_2^{+2}	217.4	26.2
258.6	353.5	354.15	y_3^{+2}	259.1	22.8
290.1	396.5	397.19	a_4	290.6	20.3
310.5	424.4	425.18	b_4	311.1	22.4
327.9	448.1	449.17	Loss of $\text{-}CH_2C_6H_4OH$ and H_2O	328.6	29.2
340.9	465.9	467.18	Loss of $CH_2C_6H_4OH$	341.8	33.6
352.2	481.5	482.17	Loss of $CH_3C_6H_5$	352.8	18.9
364.7	498.5	499.21	Loss of $CH_2CH_2SCH_3$	365.2	18.4
374.2	511.5	513.22	Loss of $\text{-}CH_2SCH_3$	375.5	43.3
384.5	525.5	526.23	Loss of SCH_3	385.0	17.5
406.7	555.9	556.22	Loss of H_2O	406.9	8.1
408.8	558.8	559.21	Loss of $\cdot CH_3$	409.1	10.3

Fragmentation efficiency = 6.2 %
Total number of parent ion counts, n_p = 449,239
Total number of fragment ion counts n_f = 69,520

to transmit fragment ions with the assigned masses had there been no loss of translational energy by the parent ions (calculated from Equation 1.3). ΔE values have been calculated using Equation 1.4, for dissociation of methionine-enkephalin $[M+H]^+$ ions to the various fragment ions. In some cases, fragment ion peaks may be observed in the spectra but the corresponding entries have not been made in the tables since valid measurements of V_m could not be made due to poor peak shapes.

The spectrum presented in Figure 6.1 for CID of Met-enkephalin $[M+H]^+$ ions, with an incident ion energy E_I = 10.4 keV and with helium as target gas, shows relatively intense fragment ions across the whole mass range. The fragmentation efficiency was found to be 5.9% and ΔE values have been calculated for almost all of the major fragment ions. The ΔE values ranged from 9.5 eV for a side-chain fragmentation corresponding to the loss of $\cdot CH_3$, to 61.7 eV for dissociation of the parent ion to form the phenyl immonium ion. In general the translational energy losses were a few tens of eV in magnitude. The estimated error in these ΔE values is ±6%.

The MIKE spectrum of Met-enkephalin $[M+H]^+$ ions obtained with an incident ion energy E_I = 12.5 keV and with 60% attenuation of the parent ion beam with helium target gas is shown in Figure 6.2. The measured ESA potentials for the fragment ion peaks and the corresponding values for ΔE are given in Table 6.2. In this case, the largest translational energy loss was measured for formation of the phenyl acyl ion, and corresponded to 101.8 eV. The MIKE spectrum was similar in appearance to that obtained when the incident ion energy was 10.4 keV, with no change in the fragmentation pathways observed. The fragmentation efficiency in this case was 6.2%, slightly higher than at the lower energy. The greater fragment ion current, in this case, is reflected in the improved quality of the spectrum compared with that obtained with E_I = 10.4 keV.

Figure 6.3 shows the FD-MIKE spectrum of Met-enkephalin $[M+H]^+$ ions obtained with an incident ion energy E_I = 14.9 keV and the parent ion beam attenuated by 60% with helium. The measured values of V_m and ΔE are given in Table 6.3. Compared with the spectrum recorded previously (with an incident ion energy of E_I = 12.5 keV), the fragmentation efficiency had marginally improved to 6.5%.

A comparison of the magnitudes of the ΔE values for the parent ions of Met-enkephalin with incident ion energies of 10.4, 12.5 and 14.9 keV, is represented graphically in Figure 6.4. For the purposes of clarity of the figure, the experimental errors are not shown on the graph but represent ±6% of the values of ΔE. In general ΔE increased with increasing incident ion energy. The increase was more significant when comparing the ΔE values for an incident ion energy of 14.9 keV with those obtained for 10.4 and 12.5 keV, than when comparing the two latter sets of data.

6.2.2 Valinomycin

The structure of the cyclic depsipeptide valinomycin has been shown earlier in Figure 3.4. The FD-MIKE spectrum of the $[M+Na]^+$ molecule-ions (m/z 1133.6) was presented in Figure 5.1, for an incident ion energy of 14.9 keV and 60% attenuation of the parent ion beam with helium collision gas. The fragment ion peaks in the MIKE spectrum were mass-assigned by comparison with the 4-sector tandem mass spectra of the $[M+Na]^+$ molecule-ions formed by FD and FAB (given in Figures 3.9 and 3.10 respectively). MIKE spectra have also been recorded for the $[M+Na]^+$ molecule-ions (m/z 1133.6) of valinomycin with laboratory frame collision energies of 8.1, 20.0 and 25.1 keV. These spectra are shown in Figures 6.5, 6.7 and 6.8 respectively. Each spectrum was obtained using helium as target gas with a pressure sufficient to attenuate the parent ion beam by approximately 60%. [The spectrum corresponding to an incident ion

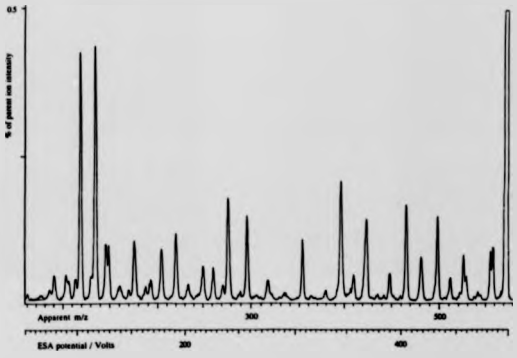

Figure 6.3 FD-MIKE spectrum of methionine-enkephalin $[M+H]^+$ ions (m/z 574.2); helium target gas, 60 % parent ion beam attenuation, incident ion energy E_i = 14.9 keV

TABLE 6.3

Translational energy losses measured in the FD-MIKE spectrum of methionine-enkephalin $[M+H]^+$ ions (m/z 574.2) with helium as target gas (Figure 6.3). Incident ion energy = 14.9 keV. Attenuation = 60 %.

V_m / V	Apparent m/z	Assigned mass (m_f) / Da	Fragment ion	V_a / V	ΔE / eV
-	-	91.05	$[\text{-}CH_2\text{-}C_6H_5]^+$	79.3	-
104.1	119.5	120.08	phenyl immonium ion	104.6	68.7
118.1	135.5	136.08	a_1	118.5	58.4
127.7	146.7	148.08	phenyl acyl ion $[H_2NCH(CH_2C_6H_5)CO^+]$	129.0	143.9
177.9	204.3	205.10	[GlyPhe + H minus CO]$^+$	178.6	61.4
192.0	220.4	221.09	b_1	192.6	43.9
227.7	261.4	262.12	internal acyl ion [GlyGlyPhe + H]$^+$	228.3	41.3
241.9	277.7	278.11	b_3	242.2	21.3
258.2	296.5	297.13	y_2^{+2}	258.8	32.0
307.9	353.5	354.15	y_3^{+2}	308.4	27.1
345.5	396.7	397.19	a_4	345.9	17.8
369.6	424.3	425.18	b_4	370.3	30.1
-	-	449.17	Loss of $\text{-}CH_2C_6H_4OH$ and H_2O	391.2	-
405.7	465.8	467.18	Loss of $CH_2C_6H_4OH$	406.9	44.2
419.1	481.2	482.17	Loss of $CH_3C_6H_5$	419.9	28.9
434.1	498.5	499.21	Loss of $CH_2CH_2SCH_3$	434.8	22.5
445.3	511.3	513.22	Loss of $\text{-}CH_2SCH_3$	446.9	57.0
457.6	525.4	526.23	Loss of SCH_3	458.3	22.6
484.1	555.9	556.22	Loss of H_2O	484.4	9.7
-	-	559.21	Loss of $\text{-}CH_3$	487.0	-

Fragmentation efficiency = 6.5 %
Total number of parent ion counts n_p = 726,188
Total number of fragment ion counts n_f = 118,907

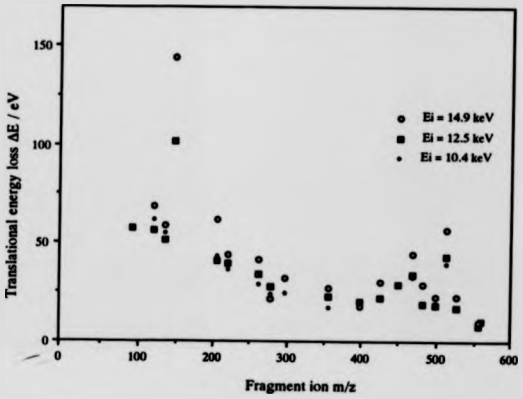

Figure 6.4 Variation of translational energy lost with incident ion energy E_i for $[M+H]^+$ ions of methionine-enkephalin (m/z 574.2) in collision with helium target gas atoms.

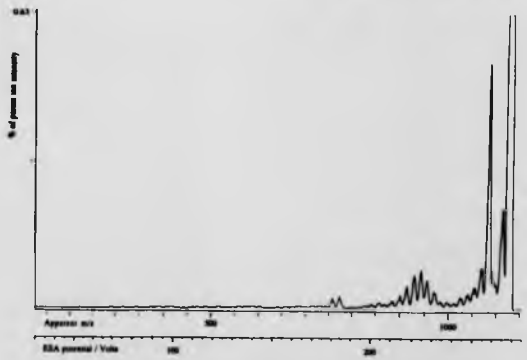

Figure 6.5 FD-MIKE spectrum of valinomycin [M+Na]+ ions (m/z 1133.6); helium target gas, 68 % parent ion beam attenuation, incident ion energy E_i = 8.1 keV

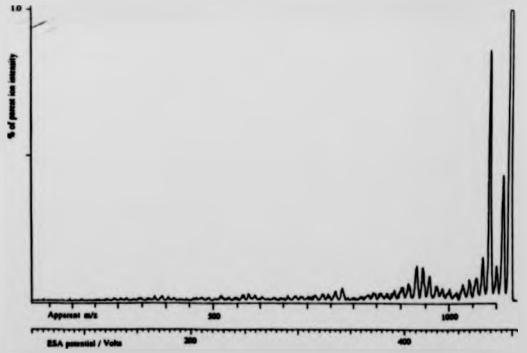

Figure 6.6 FD-MIKE spectrum of valinomycin [M+Na]+ ions (m/z 1133.6); helium target gas, 60 % parent ion beam attenuation, incident ion energy E_i = 14.9 keV

TABLE 6.4

Translational energy losses measured in the FD-MIKE spectrum of valinomycin $[M+Na]^+$ ions (m/z 1133.6) with helium as target gas (Figure 6.5). Incident ion energy = 8.1 keV. Attenuation = 68 %

V_m / V	Apparent m/z	Assigned mass (m_f) / Da	Fragment ion	V_e / V	ΔE / eV
265.0	1112.6	1118.60	Loss of CH_3	266.4	43.0
		1105.62	Loss of CO	263.3	
258.5	1085.2	1090.56	Loss of C_3H_7	259.7	39.9
254.5	1068.7	1075.54	Loss of either HCO_2 or $OCHCH_3$	256.2	51.1
		1061.60	$[(HVLV)_2VHV + Na]^+$	252.8	
		1047.58	$[(HVLV)_2VLV + Na + O]^+$	249.5	
		1033.57	$[(HVLV)_2VLV + Na]^+$	246.2	
227.6	955.5	962.53	$[(HVLV)_2HV + Na]^+$	229.2	59.1
224.5	942.8	948.53	$[(HVLV)_2HV + 2H + Na - O]^+$	225.9	49.0
221.3	929.2	936.51	$[(HVLV)_2HV + 2H + Na - CO]^+$	223.1	62.6
217.6	913.8	920.48	$[(HVLV)_2VL + 2H + Na - O]^+$	219.2	58.9
184.3	773.9	779.37	$[(HVLV)_2 + Na + O]^+$	185.6	56.3
180.8	759.0	763.38	$[(HVLV)_2 + Na]^+$	181.8	46.7
		393.20	$[HVLV + Na]^+$	93.7	
		294.13	$[HVL + Na]^+$	70.1	

Fragmentation efficiency = 4.7 %
Total number of parent ion counts n_p = 410,417
Total number of fragment ion counts n_f = 60,280

TABLE 6.5

Translational energy losses measured in the FD-MIKE spectrum of valinomycin $[M+Na]^+$ ions (m/z 1133.6) with helium as target gas (Figure 6.6). Incident ion energy = 14.9 keV. Attenuation = 60 %

V_m / V	Apparent m/z	Assigned mass (m_f) / Da	Fragment ion	V_c / V	ΔE / eV
491.9	1115.3	1118.60	Loss of CH_3	493.4	44.3
485.9	1101.6	1105.62	Loss of CO	487.6	54.2
479.7	1087.6	1090.56	Loss of C_3H_7	481.0	40.1
472.5	1071.4	1075.54	Loss of either HCO_2 or $OCHCH_3$	474.4	58.1
		1061.60	$[(HVLV)_2VHV + Na]^+$	468.2	
460.0	1042.9	1047.58	$[(HVLV)_2VLV + Na + O]^+$	462.0	67.4
—		1033.57	$[(HVLV)_2VLV + Na]^+$	455.9	
429.8	974.4	978.59		431.6	64.4
422.9	958.7	962.53	$[(HVLV)_2HV + Na]^+$	424.5	59.0
416.9	945.2	948.53	$[(HVLV)_2HV + 2H + Na - O]^+$	418.4	52.9
411.0	931.8	936.51	$[(HVLV)_2HV + 2H + Na - CO]^+$	413.1	74.5
404.0	916.0	920.48	$[(HVLV)_2VL + 2H + Na - O]^+$	406.0	72.4
342.1	775.6	779.36	$[(HVLV)_2 + Na + O]^+$	343.7	71.3
335.4	760.4	763.38	$[(HVLV)_2 + Na]^+$	336.7	58.8
259.8	589.0	592.32	$[(HVLV)HV + Na]^+$	261.2	82.8
		578.34	$[(HVLV)HV + 2H + Na - O]^+$	255.1	
		566.34	$[(HVLV)HV + 2H + Na - CO]^+$	249.8	
		409.19	$[(HVLV) + Na + O]^+$	180.5	
172.9	391.9	393.20	$[HVLV + Na]^+$	173.4	48.3
166.1	376.5	379.22	$[HVLV + 2H + Na - O]^+$	167.3	106.8
		294.13	$[HVL + Na]^+$	129.7	

Fragmentation efficiency = 8.5 %
Total number of parent ion counts n_p = 339,508
Total number of fragment ion counts n_f = 72,501

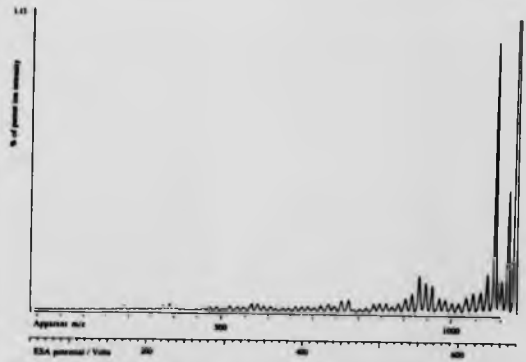

Figure 6.7 FD-MIKE spectrum of valinomycin $[M+Na]^+$ ions (m/z 1133.6); helium target gas, 60 % parent ion beam attenuation, incident ion energy E_i = 20.0 keV

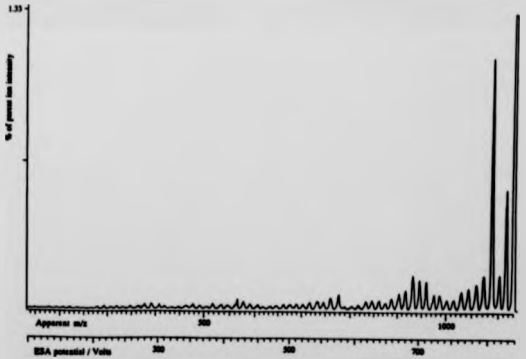

Figure 6.8 FD-MIKE spectrum of valinomycin $[M+Na]^+$ ions (m/z 1133.6); helium target gas, 60 % parent ion beam attenuation, incident ion energy E_i = 25.1 keV

TABLE 6.6

Translational energy losses measured in the FD-MIKE spectrum of valinomycin $[M+Na]^+$ ions (m/z 1133.6) with helium as target gas (Figure 6.7). Incident ion energy = 20.0 keV. Attenuation = 60 %

V_m / V	Apparent m/z	Assigned mass (m_f) / Da	Fragment ion	V_e / V	ΔE / eV
659.7	1116.3	1118.60	Loss of CH_3	661.1	41.6
651.6	1102.6	1105.62	Loss of CO	653.4	55.5
643.4	1088.7	1090.56	Loss of C_3H_7	644.5	34.3
633.9	1072.5	1075.54	Loss of either HCO_2 or $OCHCH_3$	635.7	55.9
		1061.60	$[(HVLV)_2VHV + Na]^+$	627.4	
617.2	1044.4	1047.58	$[(HVLV)_2VLV + Na + O]^+$	619.1	61.6
609.2	1030.7	1033.57	$[(HVLV)_2VLV + Na]^+$	610.9	55.6
		978.59		578.4	
567.4	960.1	962.53	$[(HVLV)_2HV + Na]^+$	568.9	51.0
559.5	946.7	948.53	$[(HVLV)_2HV + 2H + Na - O]^+$	560.6	37.8
551.5	933.1	936.51	$[(HVLV)_2HV + 2H + Na - CO]^+$	553.5	73.3
542.3	917.5	920.48	$[(HVLV)_2VL + 2H + Na - O]^+$	544.0	64.2
459.3	777.1	779.37	$[(HVLV)_2 + Na + O]^+$	460.6	57.7
450.2	761.7	763.38	$[(HVLV)_2 + Na]^+$	451.2	43.2
		592.32	$[(HVLV)HV + Na]^+$	442.9	
		578.34	$[(HVLV)HV + 2H + Na - O]^+$	435.8	
		566.34	$[(HVLV)HV + 2H + Na - CO]^+$	425.2	
290.6	491.7	492.27	$[(HVLV)V + Na]^+$	300.4	22.2
241.2	408.2	409.19	$[(HVLV) + Na + O]^+$	241.8	50.9
		393.20	$[HVLV + Na]^+$	232.4	
223.0	377.3	379.22	$[HVLV + 2H + Na - O]^+$	224.1	103.4
172.1	291.2	294.13	$[HVL + Na]^+$	173.8	198.5

Fragmentation efficiency = 9.8 %
Total number of parent ion counts n_p = 577,172
Total number of fragment ion counts n_f = 141,701

TABLE 6.7

Translational energy losses measured in the FD-MIKE spectrum of valinomycin $[M+Na]^+$ ions (m/z 1133.6) with helium as target gas (Figure 6.8). Incident ion energy = 25.1 keV. Attenuation = 60 %

V_m / V	Apparent m/z	Assigned mass (m_f) Da	Fragment ion	V_e / V	ΔE / eV
827.5	1116.8	1118.60	Loss of CH_3	828.9	39.9
817.4	1103.1	1105.62	Loss of CO	819.2	57.5
807.0	1089.0	1090.56	Loss of C_3H_7	808.1	35.0
795.1	1073.0	1075.54	Loss of either HCO_2 or $OCHCH_3$	796.9	59.6
785.1	1059.6	1061.60	$(HVLV)_2VHV + Na]^+$	786.6	47.8
774.4	1045.1	1047.58	$(HVLV)_2VLV + Na + O]^+$	776.2	58.9
764.2	1031.3	1033.57	$(HVLV)_2VLV + Na]^+$	765.9	54.2
752.9	1016.1	1017.50	$(HVLV)_2VHV + Na + CO]^+$	754.0	34.5
742.8	1002.4	1004.50		744.3	52.0
732.6	988.7	989.40		733.1	18.4
723.0	975.8	978.59	$(HVLV)_2HV + Na + O]^+$	725.1	72.4
712.0	960.8	962.53	$(HVLV)_2HV + Na]^+$	713.2	44.0
702.0	947.4	948.53	$(HVLV)_2HV + 2H + Na - O]^+$	702.8	29.4
692.0	933.8	936.51	$(HVLV)_2HV + 2H + Na - CO]^+$	693.9	71.6
680.1	917.9	920.48	$(HVLV)_2VL + 2H + Na - O]^+$	682.1	70.4
669.8	904.0	906.47	$(HVLV)_2V + Na + CO$ & $+ O]^+$	671.7	69.4
658.6	888.8	890.47	$(HVLV)_2V + Na + CO]^+$	659.8	48.0
648.7	875.4				
638.3	861.4	863.46	$(HVLV)_2H + Na]^+$	639.8	58.8
627.5	846.9	849.48	$(HVLV)_2H + 2H + Na - O]^+$	629.5	77.8
617.7	833.7	837.48	$(HVLV)_2V + 2H + Na - CO]^+$	620.6	114.5
576.3	777.7	779.37	$(HVLV)_2 + Na + O]^+$	577.5	53.1
564.8	762.2	763.38	$(HVLV)_2 + Na]^+$	565.7	37.9
554.7	748.8	749.43	$(HVLV)_2 + 2H + Na - CO]^+$	555.3	20.5
544.1	734.3	737.43	$(HVLV)VHV + Na + CO]^+$	546.4	106.3

TABLE 6.7 CONTINUED

Translational energy losses measured in the FD-MIKE spectrum of valinomycin $[M+Na]^+$ ions (m/z 1133.6) with helium as target gas (Figure 6.8). Incident ion energy = 25.1 keV. Attenuation = 60 %

V_m / V	Apparen m/z	Assigned mass (m_f) / Da	Fragment ion	V_e / V	ΔE / eV
531.9	717.9	719.38	$[(HVLV)HV + Na + O]^+$	533.1	52.4
511.2	689.9	691.39	$[(HVLV)VHV + Na]^+$	512.3	53.1
501.2	676.4	677.41	$[(HVLV)VHV + 2H + Na - O]^+$	501.9	35.7
491.0	662.7	664.34	$[(HVLV)VHL + Na]^+$	492.3	63.4
469.4	633.5	638.34	$[(HVLV)VHL + 2H + Na - CO]^+$	473.0	190.5
437.9	591.0	592.32	$[(HVLV)HV + Na]^+$	438.9	54.5
427.8	577.4	578.34	$[(HVLV)HV + 2H + Na - O]^+$	428.5	40.5
		566.34	$[(HVLV)HV + 2H + Na - CO]^+$	419.6	
405.5	547.2	550.31	$[(HVLV)VL + 2H + Na - O]^+$	407.8	142.0
384.6	519.0	520.26	$[(HVLV)V + Na + CO]^+$	385.5	59.0
375.0	506.0	508.26	$[(HVLV)V + Na + O]^+$	376.6	109.7
354.4	478.3	481.22	$[(HVLV)V + 2H + Na - O]^+$	356.6	151.0
302.5	408.2	409.19	$[(HVLV) + Na + O]^+$	303.2	60.7
290.9	392.7	393.20	$[HVLV + Na]^+$	291.4	35.2
279.9	377.7	379.22	$[HVLV + 2H + Na - O]^+$	281.0	99.4
237.0	319.9	321.18	$[VHV + Na]^+$	238.0	102.0
217.5	293.5	294.13	$[HVL + Na]^+$	217.9	54.6

Fragmentation efficiency = 10.6 %
Total number of parent ion counts n_p = 260,904
Total number of fragment ion counts n_f = 69,419

energy of 14.9 keV has been duplicated here, as Figure 6.6 (previously shown as Figure 5.1), for convenience when making comparisons among spectra.]

The spectrum obtained with E_i = 8.1 keV (Figure 6.5) resulted in a fragmentation efficiency of 4.7% and with a total number of fragment ion counts, n_f, of ~60,000. The fragment ion peaks were poorly resolved and the parent ion currents were too weak for the mass-resolving slits of the mass spectrometer to be reduced in width so as to improve the resolution. The lower mass peaks with m/z below 700 were of relatively low intensities, and were not well defined due to poor signal-to-noise ratios. Although the total number of fragment ion counts was comparable with those in the methionine-enkephalin spectra shown in Section 6.2.1, the greater number of dissociation channels available to the valinomycin parent ion resulted in individual fragment ion peaks with comparably worse signal-to-noise ratios. To obtain spectra with improved quality for this higher mass peptide, either more intense parent ion beams are required, or an improvement in the fragmentation efficiency such that the total fragment ion current increases and the resolution may also then be improved. Increasing the parent ion currents was not feasible whilst using FD as the ionisation method since the optimum FD conditions had already been met. Finding a means of improving the spectral quality by increasing the efficiency of fragmentation was the aim of the current investigation. Translational energy losses, ΔE, have been measured for the relatively more intense fragment ions in the spectrum and are given in Table 6.4. The abbreviations H, V and L have been used in the table for hydroxyisovaleric acid, valine and lactic acid residues respectively.

Increasing the incident ion energy to E_i = 14.9 keV (Figure 6.6) resulted in a spectrum with improved resolution due to the greater energy range. The fragmentation efficiency was found to have increased to 8.5%. Low-mass fragment ions were still of relatively low intensities but were more clearly

distinguished from the background chemical noise. Energy losses ΔE for dissociation of the parent ions to the higher mass fragment ions have been measured and are given in Table 6.5. Increasing the incident ion energy to 20.0 keV resulted in the spectrum shown in Figure 6.7. The fragmentation efficiency observed at this ion energy was 9.8%. The total number of fragment ion counts for this spectrum was ~140,000 and combined with the improved resolution at the higher incident ion energy resulted in a much improved spectrum compared with those obtained at E_i = 8.1 and 14.9 keV. Increasing the incident ion energy further to 25.1 keV, Figure 6.8, produced only a slight improvement over the 20.0 keV case, due to the lower total number of fragment ions counted, $n_f \approx 69{,}000$, despite the further improvement of the fragmentation efficiency to 10.6%. The values of ΔE are given in Table 6.6 for E_i = 20.0 keV and in Table 6.7 for E_i = 25.1 keV.

Figure 6.9 shows a plot of the translational energy losses versus fragment ion m/z for the spectra of valinomycin $[M+Na]^+$ ions obtained when the incident ion energies were 8.1, 14.9, 20.0 and 25.1 keV and the target gas was helium. The largest energy losses were measured for an incident ion energy of 14.9 keV.

6.2.3 Valine-gramicidin A

The MIKE spectrum of valine-gramicidin A $[M+K]^+$ ions formed by field desorption has been shown in Figure 5.14 and is shown again here for convenience in Figure 6.10. The collision gas was helium, with a pressure corresponding to an attenuation of the parent ion beam by 70%, and the incident ion energy was 14.9 keV. Fragment ion mass assignments were made by comparison with the 4-sector tandem mass spectrum obtained using fast atom bombardment as the ionisation method. The FD-MIKE spectrum shows a series of fragment ion peaks corresponding with the a-series of fragment ions, which are relatively more intense than many of the other fragment ions in the spectrum. Translational energy losses have been measured for the relatively more intense

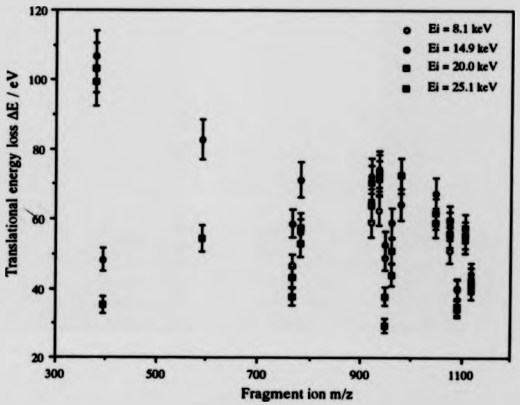

Figure 6.9 Variation of translational energy lost with incident ion energy E_i for $[M+Na]^+$ ions of valinomycin (m/z 1133.6) in collision with helium target gas atoms.

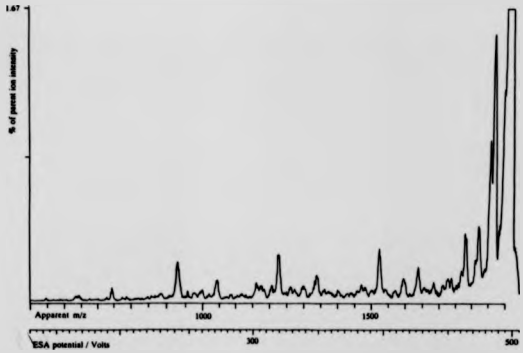

Figure 6.10 FD-MIKE spectrum of valine-gramicidin A $[M+K]^+$ ions (m/z 1920.2); helium target gas, 70 % parent ion beam attenuation, incident ion energy E_i = 14.9 keV

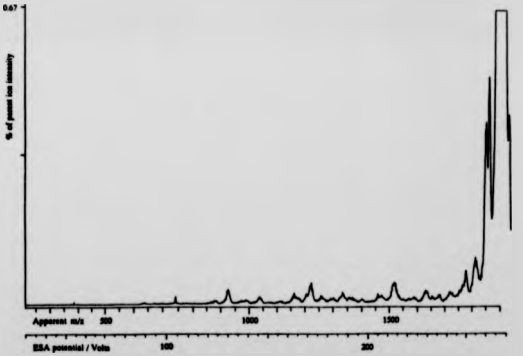

Figure 6.11 FD-MIKE spectrum of valine-gramicidin A $[M+K]^+$ ions (m/z 1920.2); helium target gas, 68 % parent ion beam attenuation, incident ion energy E_i = 8.1 keV

TABLE 6.8

Translational energy losses measured in the FD-MIKE spectrum of valine-gramicidin A $[M+K]^+$ ions (m/z 1920.2) with helium as target gas (Figure 6.10). Incident ion energy = 14.9 keV. Attenuation = 70 %

V_m / V	Apparent m/z	Assigned mass (m_f) / Da	Fragment ion	V_e / V	ΔE / eV
		1903.20	Loss of OH or NH_3	495.6	
486.9	1870.0	1876.10	Loss of C_3H_8 or $[z_{15} + K]^+$	488.5	48.7
		1861.13	Loss of C_2H_4NO	484.6	
474.8	1823.4	1831.12	$[a_{15}^{-2} + K]^+$	476.8	63.1
464.3	1783.0	1789.09	$[y_{14}^{-2} + K]^+$	465.9	51.0
		1691.07	$[c_{14}^{+1} + K]^+$	440.3	
426.7	1638.9	1645.04	$[a_{14}^{-1} + K]^+$	428.4	55.5
		1602.98	$[d_{14}^{-2} + K]^+$	417.1	
		1576.93	$[x_{11}^{-2} + K]^+$	410.6	
397.1	1525.1	1531.96	$[a_{13}^{-1} + K]^+$	398.9	66.4
		1345.88	$[a_{12}^{-1} + K]^+$	350.5	
		1303.83	$[d_{12}^{-1} + K]^+$	339.5	
319.7	1227.7	1232.79	$[a_{11}^{-1} + K]^+$	321.0	61.5
271.7	1043.4	1046.11	$[a_{10}^{-1} + K]^+$	272.4	39.2
		1004.67	$[d_{10}^{-1} + K]^+$	261.6	
242.2	930.3	933.63	$[a_9^{-1} + K]^+$	243.1	52.7
193.9	744.6	747.55	$[a_8^{-1} + K]^+$	194.7	58.8

Fragmentation efficiency = 8.2 %
Total number of parent ion counts n_p = 373,754
Total number of fragment ion counts n_f = 101,565

TABLE 6.9

Translational energy losses measured in the FD-MIKE spectrum of valine-gramicidin A $[M+K]^+$ ions (m/z 1920.2) with helium as target gas (Figure 6.11). Incident ion energy = 8.1 keV. Attenuation = 68 %

V_m / V	Apparent m/z	Assigned mass (m_f) / Da	Fragment ion	V_e / V	ΔE / eV
		1903.20	Loss of OH or NH_3	267.6	
262.6	1867.3	1876.10	Loss of C_3H_8 or $[z_{15} + K]^+$	263.8	38.0
261.1	1856.6	1861.13	Loss of C_2H_4NO	261.7	19.6
\		1831.12	$[a_{15}^{-2} + K]^+$	257.5	
250.3	1780.3	1789.09	$[y_{14}^{-2} + K]^+$	251.6	39.6
		1691.07	$[c_{14}^{+1} + K]^+$	237.8	
		1645.04	$[a_{14}^{-1} + K]^+$	231.3	
		1602.98	$[d_{14}^{-2} + K]^+$	225.3	
		1576.93	$[x_{11}^{-2} + K]^+$	221.7	
		1531.96	$[a_{13}^{-1} + K]^+$	215.4	
		1345.88	$[a_{12}^{-1} + K]^+$	189.2	
		1303.83	$[d_{12}^{-1} + K]^+$	183.3	
171.9	1222.4	1232.79	$[a_{11}^{-1} + K]^+$	173.3	68.3
		1046.11	$[a_{10}^{-1} + K]^+$	147.1	
		1004.67	$[d_{10}^{-1} + K]^+$	141.3	
130.4	927.6	933.63	$[a_9^{-1} + K]^+$	131.3	52.5
		747.55	$[a_8^{-1} + K]^+$	105.1	

Fragmentation efficiency = 1.9 %
Total number of parent ion counts n_p = > 1,000,000
Total number of fragment ion counts n_f = 67,289

fragment ions and are listed in Table 6.8. The ΔE values were many tens of electronvolts in magnitude. The fragmentation efficiency in the spectrum shown in Figure 6.10 was 8.2%.

Figure 6.11 shows the FD-MIKE spectrum obtained when the laboratory frame collision energy was 8.1 keV. Despite the very intense parent ion beams maintained during this experiment (> 1 million parent ion counts recorded in total) the quality of the spectrum obtained was poor due to the low fragmentation efficiency of 1.9%. The a-type sequence ions are relatively weak and correspond to broad asymmetrical peaks. Estimates of the translational energy lost by parent ions have been made for the more intense fragment ions and are listed in Table 6.9.

Figure 6.12 shows the FD-MIKE spectrum of valine-gramicidin A $[M+K]^+$ ions recorded when the incident ion energy was 12.5 keV. The fragmentation efficiency in this case was 6.3% which was significantly higher than for E_l = 8.1 keV. The general appearance of the spectrum was similar to that obtained when the incident ion energy was 14.9 keV (Figure 6.10). Translational energy losses have been measured for the major fragment ions and are listed in Table 6.10. MIKE spectra have also been recorded for incident ion energies of 20.0 and 25.1 keV and are shown in Figures 6.13 and 6.14 respectively. Translational energy losses have been measured for these spectra and are given in Tables 6.11 and 6.12. The fragmentation efficiencies increased further as the incident ion energy was increased. At E_l = 20.0 keV the fragmentation efficiency was 12.1% and at E_l = 25.1 keV increased to 14.8%.

The centre-of-mass collision energy increased from 16.8 eV to 52.2 eV as the laboratory frame collision energy was increased from 8.1 to 25.1 keV for valine-gramicidin A $[M+K]^+$ ions in collision with helium gas atoms. Such an increase in the energy available for internal energy uptake may be expected to be

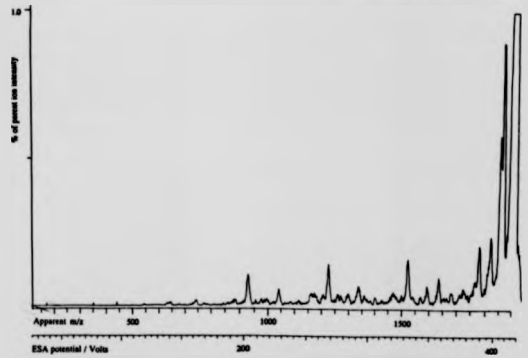

Figure 6.12 FD-MIKE spectrum of valine-gramicidin A $[M+K]^+$ ions (m/z 1920.2); helium target gas, 70 % parent ion beam attenuation, incident ion energy E_i = 12.5 keV

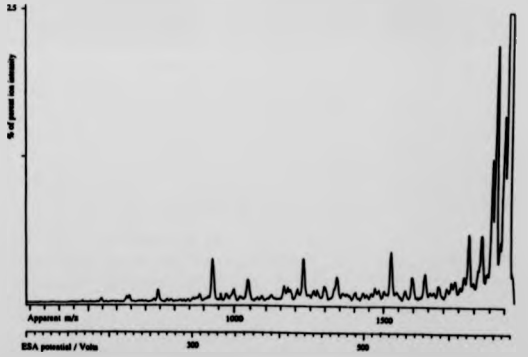

Figure 6.13 FD-MIKE spectrum of valine-gramicidin A $[M+K]^+$ ions (m/z 1920.2); helium target gas, 70 % parent ion beam attenuation, incident ion energy E_i = 20.0 keV

TABLE 6.10

Translational energy losses measured in the FD-MIKE spectrum of valine-gramicidin A $[M+K]^+$ ions (m/z 1920.2) with helium as target gas (Figure 6.12). Incident ion energy = 12.5 keV. Attenuation = 70 %

V_m / V	Apparent m/z	Assigned mass (m_f) / Da	Fragment ion	V_e / V	ΔE / eV
		1903.20	Loss of OH or NH_3	416.3	
409.8	1873.7	1876.10	Loss of C_3H_8 or $[z_{15} + K]^+$	410.4	16.1
406.4	1858.0	1861.13	Loss of C_2H_4NO	407.1	21.2
398.6	1822.4	1831.12		400.5	59.5
389.7	1781.5	1789.09	$[y_{14}^{-2} + K]^+$	391.3	53.0
		1691.07	$[c_{14}^{+1} + K]^+$	369.9	
358.1	1637.3	1645.04	$[a_{14}^{-1} + K]^+$	359.8	58.8
		1602.98	$[d_{14}^{-2} + K]^+$	350.4	
		1576.93	$[x_{11}^{-2} + K]^+$	344.9	
333.3	1523.8	1531.96	$[a_{13}^{-1} + K]^+$	335.1	67.0
		1345.88	$[a_{12}^{-1} + K]^+$	294.4	
		1303.83	$[d_{12}^{-1} + K]^+$	285.2	
268.3	1226.5	1232.79	$[a_{11}^{-1} + K]^+$	269.7	64.1
227.8	1041.5	1046.11	$[a_{10}^{-1} + K]^+$	228.8	55.9
		1004.67	$[d_{10}^{-1} + K]^+$	219.8	
203.3	929.7	933.63	$[a_9^{-1} + K]^+$	204.2	53.2
162.8	744.4	747.55	$[a_8^{-1} + K]^+$	163.5	52.7

Fragmentation efficiency = 6.3 %
Total number of parent ion counts n_p = 361,627
Total number of fragment ion counts n_f = 76,317

TABLE 6.11

Translational energy losses measured in the FD-MIKE spectrum of valine-gramicidin A $[M+K]^+$ ions (m/z 1920.2) with helium as target gas (Figure 6.13). Incident ion energy = 20.0 keV. Attenuation = 70 %

V_m / V	Apparent m/z	Assigned mass (m_f) / Da	Fragment ion	V_e / V	ΔE / eV
662.8	1899.4	1903.20	Loss of OH or NH_3	664.1	39.6
652.8	1870.9	1876.10	Loss of C_3H_8 or $[z_{15} + K]^+$	654.6	55.6
648.7	1859.1	1861.13	Loss of C_2H_4NO	649.4	22.3
		1831.12	$[a_{15}^{-2} + K]^+$	638.9	
622.4	1783.7	1789.09	$[y_{14}^{-2} + K]^+$	624.3	60.4
587.9	1684.7	1691.07	$[c_{14}^{+1} + K]^+$	590.1	74.9
572.0	1639.2	1645.04	$[a_{14}^{-1} + K]^+$	574.0	70.9
557.1	1596.7	1601.98	$[d_{14}^{-2} + K]^+$	559.0	65.8
548.6	1572.3	1576.93	$[x_{11}^{-2} + K]^+$	550.2	58.5
532.4	1525.7	1531.96	$[a_{13}^{-1} + K]^+$	534.5	81.5
		1345.88	$[a_{12}^{-1} + K]^+$	469.6	
453.6	1300.1	1303.83	$[d_{12}^{-1} + K]^+$	454.9	57.4
428.4	1227.8	1232.79	$[a_{11}^{-1} + K]^+$	430.2	80.3
364.1	1043.6	1046.11	$[a_{10}^{-1} + K]^+$	365.0	47.8
348.9	999.9	1004.67	$[d_{10}^{-1} + K]^+$	350.6	95.0
324.9	931.1	933.63	$[a_9^{-1} + K]^+$	325.8	53.3
259.8	744.6	747.55	$[a_8^{-1} + K]^+$	260.8	77.9

Fragmentation efficiency = 12.1 %
Total number of parent ion counts n_p = 515,226
Total number of fragment ion counts n_f = 207,050

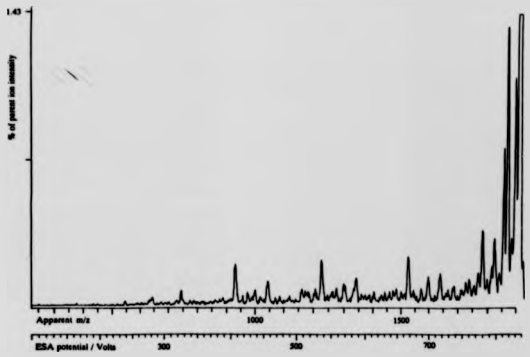

Figure 6.14 FD-MIKE spectrum of valine-gramicidin A $[M+K]^+$ ions (m/z 1920.2); helium target gas, 70 % parent ion beam attenuation, incident ion energy E_l = 25.1 keV

TABLE 6.12

Translational energy losses measured in the FD-MIKE spectrum of valine-gramicidin A $[M+K]^+$ ions (m/z 1920.2) with helium as target gas (Figure 6.14). Incident ion energy = 25.1 keV. Attenuation = 70 %

V_m / V	Apparent m/z	Assigned mass (m_f) / Da	Fragment ion	V_e / V	ΔE / eV
831.6	1901.0	1903.20	Loss of OH or NH_3	832.6	29.3
819.2	1872.5	1876.10	Loss of C_3H_8 or $[z_{15} + K]^+$	820.7	47.6
813.3	1859.2	1861.13	Loss of C_2H_4NO	814.2	26.1
799.0	1826.3	1831.12	$[a_{15}^{-2} + K]^+$	801.0	65.4
781.1	1785.5	1789.09	$[y_{14}^{-2} + K]^+$	782.7	50.2
		1691.07	$[c_{14}^{+1} + K]^+$	739.8	
717.6	1640.4	1645.04	$[a_{14}^{-1} + K]^+$	719.6	70.0
699.3	1598.5	1602.98	$[d_{14}^{-2} + K]^+$	700.8	54.8
688.6	1574.2	1576.93	$[x_{11}^{-2} + K]^+$	689.8	43.6
668.3	1527.7	1531.96	$[a_{13}^{-1} + K]^+$	670.2	70.3
		1345.88	$[a_{12}^{-1} + K]^+$	588.8	
		1303.83	$[d_{12}^{-1} + K]^+$	570.4	
537.5	1228.6	1232.79	$[a_{11}^{-1} + K]^+$	539.3	85.1
457.1	1044.8	1046.11	$[a_{10}^{-1} + K]^+$	457.6	31.5
		1004.67	$[d_{10}^{-1} + K]^+$	439.5	
407.8	932.3	933.63	$[a_9^{-1} + K]^+$	408.4	36.6
325.6	744.3	747.55	$[a_8^{-1} + K]^+$	327.0	107.7

Fragmentation efficiency = 14.8 %
Total number of parent ion counts n_p = 118,727
Total number of fragment ion counts n_f = 50,044

reflected in the fragmentation pathways available to the ion. Comparison of the MIKE spectra for this range of incident ion energies (Figures 6.10 to 6.14) showed no significant change in the nature of the fragmentations as the incident ion energy was increased although the relative abundances of the fragment ions showed some differences. The variation of ΔE with incident ion energy for this peptide in collision with helium has been plotted in Figure 6.15 for a number of fragmentation pathways. The data correspond to fragment ions for which energy loss values had been measured for each of the incident ion energies E_l = 8.1, 12.5, 14.9, 20.0 and 25.1 keV. The mean ΔE value 65.9 eV at an incident ion energy of 20.0 keV was larger than those for the other energies (62.4 eV measured for E_l = 25.1 keV, 54.2 eV for E_l = 14.9 keV and 52.6 eV for E_l = 12.5 keV). These differences are small when the magnitude of the experimental error is taken into consideration.

6.2.4 Discussion of results

The results presented in the previous three sections illustrate clearly the problem of decreasing efficiency of collision-induced decomposition as the mass of the incident ion is increased (for a fixed incident ion energy). Figure 6.16 shows a plot of the fragmentation efficiencies measured for collision-induced decomposition experiments with helium as target gas, for Met-enkephalin (m/z 574.2), valinomycin (m/z 1133.6) and valine-gramicidin A (m/z 1920.2). In the case of Met-enkephalin, increasing the incident ion energy from E_l = 10.4 keV to 14.9 keV resulted in only a slight improvement in the efficiency of fragmentation from 5.9% to 6.5%. For the heavier peptides increasing the incident ion energy had a more significant effect. For valinomycin the fragmentation efficiency increased from 4.7% to 10.6% as the incident ion energy was increased from 8.1 keV to 25.1 keV. A dramatic improvement was observed for valine-gramicidin A, where the fragmentation efficiency increased from 1.9% at E_l = 8.1 keV to 14.8%

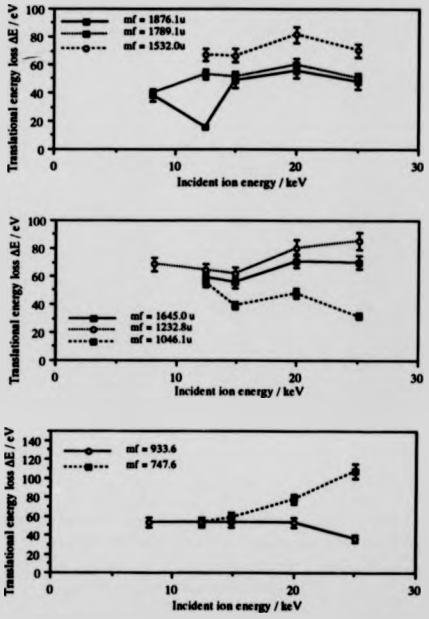

Figure 6.15 Variation of translational energy loss ΔE with incident ion energy E_i for decompositions of valine-gramicidin A $[M+K]^+$ ions (m/z 1920.2) to various fragment ions. Target gas = helium, ~70% attenuation.

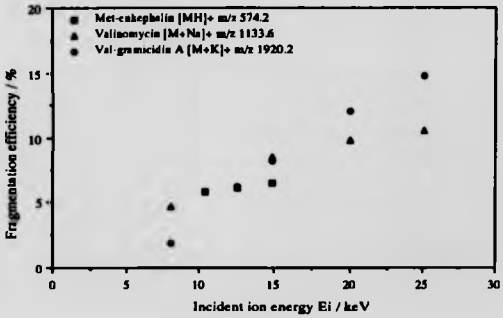

Figure 6.16 Variation of fragmentation efficiency with incident ion energy in the FD-MIKE spectra of methionine-enkephalin, valinomycin and valine-gramicidin A. Results are for helium target gas with a parent ion beam attenuation of 60 - 70%.

at E_l = 25.1 keV. These results may be explained in two ways: in terms of scattering effects, or by increased internal energy deposition as the incident ion energies (and hence centre-of-mass collision energies) were increased. Scattering effects are a combination of scattering due to collision and also scattering due to translational energy release. Scattering due to collision may be estimated using conservation of energy and momentum. It was shown in Section 5.5 that collisions between helium target gas atoms and valinomycin ions (m/z 1133.6), with an incident ion energy of 14.9 keV, should not lead to scattering angles greater than the acceptance angle of the electric sector of the large-scale mass spectrometer. The distribution of scattering angles from translational energy releases upon fragmentation, leads to discrimination effects in MIKES experiments (Section 2.1.8e). Rumpf *et al.*[133] have reported collection efficiencies for the large-scale mass spectrometer used in this work. The collection efficiencies are given as a ratio of the number of fragment ions collected to those which would have been collected in the absence of translational energy release. These ratios were based upon calculated ion trajectories and are reported for incident ion energies of 8 keV and 32 keV, for a range of translational energy releases and proportions of fragment ion to parent ion masses. The general trend is of improved collection efficiencies with increasing incident ion energy. Also greater improvements for the larger ions would also be predicted in this manner, since the fragment ions at low-mass are a much smaller proportion of the parent ion mass as its mass is increased, and it is for the smaller fragment to parent ion mass ratios that the collection efficiencies are lowest. Therefore two factors may be contributing to the observed improvements in fragmentation efficiencies in the present MIKES experiments: i) translational energy release, and ii) increased internal energy uptake. Since the possibility of increased internal energy uptake is of prime interest, a consideration must be made of the relative magnitudes of these two effects. The relative intensities of the $[a_{15}{}^{-2} + K]^+$, $[a_9{}^{-1} + K]^+$ and

$[a_8^{-1} + K]^+$ fragment ions relative to the fragment ion at m/z 1876.1 is shown in Figure 6.17. The relative intensities of the low-mass fragment ions compared with the high-mass fragment ions tended to increase with increasing incident ion energy, although the intensity of the $[a_{15}^{-2} + K]^+$ (m/z 1831.12) fragment ion relative to the m/z 1876.1 fragment ion appears to decrease at and above incident ion energies of 20.0 keV. Translational energy releases T for these fragment ions have been calculated using

$$T = \frac{m_i^2}{16 m_f m_n} \left(\frac{\Delta V}{V_i} \right)^2 eV \qquad (6.1)$$

where m_i, m_f and m_n are the masses of the incident ion, fragment ion and neutral fragment respectively. ΔV is the width of the fragment ion peak in ESA voltage units and V_i is the ESA voltage required to transmit the parent ions. The translational energy released for both valine-gramicidin A and valinomycin fragment ions were generally of the order of 0.1 eV. From the calculated collection efficiencies reported by Rumpf *et al.*[133] the fragment ion of valine-gramicidin A with m/z 747.6 would be expected to decrease in relative intensity to 57% of its measured value at 32 keV, when the incident ion energy was decreased to 8 keV. Similarly the relative intensities of the m/z 933.6 fragment ion would be expected to decrease to 63% of its original values as the incident ion energy was decreased from 32 keV to 8 keV, and for the fragment ion at m/z 1831.1, a decrease to 97% is estimated. The MIKE spectra of valine-gramicidin A recorded with incident ion energies of 25.1 and 8.1 keV have been plotted so that the height of the most intense fragment ion at m/z 1876.1 is the same in each case and the relative heights of the other fragment ions were considered for the two incident ion energies. At E_i = 8.1 keV the m/z 747 fragment ion was 11% of its height in the E_i = 25.1 keV spectrum. For the m/z 933 and m/z 1831 fragment ions the reductions in peak heights on decreasing the incident ion energy were to 29% and 80% of the original values respectively. These decreases in relative intensities

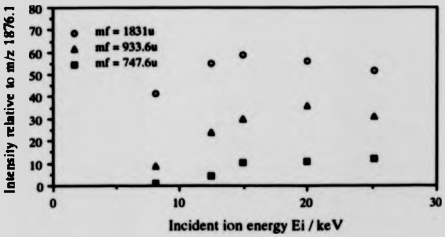

Figure 6.17 Intensities of fragment ions in the FD-MIKE spectra of valine-gramicidin A $[M+K]^+$ ions relative to the m/z 1876.1 fragment ion as 100. Results shown are for helium as collision gas providing a parent ion beam attenuation of ~70%.

were far greater than those predicted on the basis of discrimination effects caused by scattering due to translational energy releases. The same effect was observed if the comparisons were made when normalising the spectra such that the m/z 1831.1 fragment ion was the same height in each case, i.e. so that the same types of fragmentations, a-type ions, were considered relative to one another. Therefore the improvement in fragmentation efficiency was far greater than predicted from improvements in collection efficiency and is therefore likely to have been due to increased internal energy uptakes at the higher incident ion energies. These increases in internal energy deposition with increasing incident ion energy are consistent with the predictions of momentum transfer models for describing the collisions between large ions and target gas atoms. The translational energy loss ΔE would therefore have been expected to increase as the incident ion energy was increased. For all three peptides some evidence of increasing ΔE was observed as the incident ion energy was increased up to 14.9 keV. In the valinomycin case further increases in the incident ion energy appeared to result in decreased ΔE values and for the valine-gramicidin A the largest ΔE values were recorded for an incident ion energy of 20.0 keV and at E_i = 25.1 keV there appeared to be a fall-off in the size of ΔE

6.3 Effect of target-gas mass and attenuation

In the previous section (6.2), the collision-induced decomposition spectra of methionine-enkephalin $[M+H]^+$, valinomycin $[M+Na]^+$ and valine-gramicidin A $[M+K]^+$ ions have been measured using the MIKES technique when helium was used as target gas, for a range of incident ion energies. In all cases the parent ion beam attenuation was 60 - 70%. Increasing the incident ion energy was used as a means of increasing the available centre-of-mass collision energy, E_{cm}. Increasing the mass of the collision gas has a much more dramatic effect on E_{cm}.

For example, for valine-gramicidin A $[M+K]^+$ ions (m/z 1920.2) at an incident ion energy of 8.1 keV colliding with helium, E_{cm} is 16.8 eV, which on increasing the incident ion energy to 25.1 keV rises to a value of 52.2 eV. By switching the target gas to argon or xenon, E_{cm} could be increased to 164.3 eV and 514.7 eV respectively (for 8.1 keV incident ion energy). The results presented in the following sections show the effect of changing the target gas on the general appearance of the MIKE spectra and upon the magnitudes of translational energy losses (where ion currents were suitable). Increasing the available centre-of-mass collision energy by increasing the number of collisions was a further method of possibly increasing the internal energy uptake, with a view to increasing the efficiency of fragmentation. The variation of the general appearance of the spectra with target gas pressure has been studied. A detailed investigation of the effects of target gas pressure on the magnitudes of the translational energy lost by incident ions was presented in Chapter 5.

6.3.1 Valinomycin

Figure 6.18 shows FD-MIKE spectra of valinomycin $[M+Na]^+$ ions when the incident ion energy was 14.9 keV and the parent ion beam was attenuated by 60%. The top spectrum was obtained with xenon as target gas and can be compared with the spectrum obtained with helium, which is shown beneath it. [The helium spectrum was shown previously in Figure 6.6 and the data pertaining to it listed in Table 6.5.] Translational energy losses have been measured for the xenon case and are listed in Table 6.13. A general comparison of the appearance of the two spectra shows there to be a slight increase in the intensities of the low-mass fragments relative to the high-mass fragment ions when xenon was used as target relative to helium. The high-mass fragments are of similar relative intensities in the two spectra. The fragmentation efficiency with xenon as target was found to be lower than with helium (4.6% compared with 8.5%). A lower fragmentation efficiency with xenon is likely to be due to increased scattering

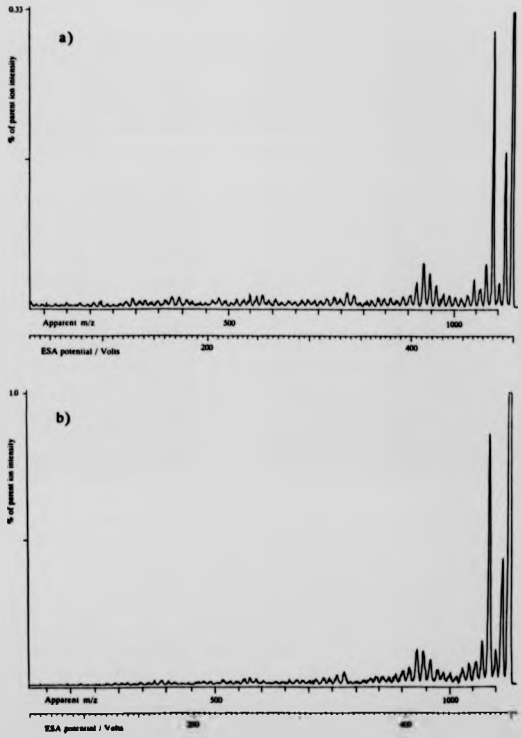

Figure 6.18 FD-MIKE spectra of valinomycin $[M+Na]^+$ ions (m/z 1133.6); 60 % parent ion beam attenuation, incident ion energy E_i = 14.9 keV a) xenon target gas b) helium target gas

TABLE 6.13

Translational energy losses measured in the FD-MIKE spectrum of valinomycin [M+Na]$^+$ ions (m/z 1133.6) with xenon as target gas (Figure 6.18a). Incident ion energy = 14.9 keV. Attenuation = 60 %

V_m / V	Apparent m/z	Assigned mass (m_f) / Da	Fragment ion	V_c / V	ΔE / eV
492.8	1117.2	1118.60	Loss of CH_3	493.4	18.3
486.6	1103.2	1105.62	Loss of CO	487.6	33.4
480.6	1089.7	1090.56	Loss of C_3H_7	481.0	12.5
473.7	1073.9	1075.54	Loss of either HCO_2 or $OCHCH_3$	474.4	22.9
		1061.60	$(HVLV)_2VHV + Na]^+$	468.2	
461.4	1046.2	1047.58	$(HVLV)_2VLV + Na + O]^+$	462.0	19.9
424.0	961.2	962.53	$(HVLV)_2HV + Na]^+$	424.5	20.1
418.0	947.8	948.53	$(HVLV)_2HV + 2H + Na - O]^+$	418.4	12.1
412.2	934.6	936.51	$(HVLV)_2HV + 2H + Na - CO]^+$	413.1	29.9
405.3	918.9	920.48	$(HVLV)_2VL + 2H + Na - O]^+$	406.0	25.5
343.3	778.5	779.37	$(HVLV)_2+ Na + O]^+$	343.7	17.4
336.5	762.9	763.38	$(HVLV)_2 + Na]^+$	336.7	8.6
173.7	393.9	393.20	$[HVLV + Na]^+$	173.4	-26.0
		294.13	$[HVL + Na]^+$	129.7	

Fragmentation efficiency = 4.6 %
Total number of parent ion counts n_p = 267,417
Total number of fragment ion counts n_f = 30,787

with the more massive target. The increased relative intensity of low-mass fragment ions suggests that more internal energy was being taken up in the xenon case. The translational energy losses measured for the more intense fragment ions were at least a factor of two lower with xenon as compared with helium.

Figure 6.19 shows the FD-MIKE spectra of valinomycin $[M+Na]^+$ ions obtained with xenon (Fig. 6.19a) and helium (Fig. 6.19b) target gases with a parent ion beam attenuation of 90%. The fragmentation efficiency was 2.9% in the xenon case, as compared to 6.0% with helium. The fragmentation pathways were similar and the intensities of the low-mass fragment ions relative to the high-mass fragment ions were similar in the two spectra. Translational energy losses measured for the more intense fragment ions are listed in Table 6.14 for the spectrum obtained with xenon as target gas and in Table 6.15 for helium. The measured energy losses were a factor of a least two lower in the case of xenon compared with helium. Comparison of the energy loss values for xenon target gas with parent ion beam attenuations of 90% (Table 6.15) and 60% (Table 6.13) shows there to have been little variation despite the variation in gas pressure.

Figures 6.20a and 6.20b show the FD-MIKE spectra obtained with helium as target gas with attenuations of 80% and 40% respectively. Comparison of these spectra with those obtained at 90% (Figure 6.19b) and 60% (Figure 6.18b) attenuations shows a trend of increasing intensities of low-mass fragment ions compared with high-mass fragment ions. Translational energy losses ΔE are reported for these spectra in Tables 6.16 and 6.17. The ΔE values show some tendency to be larger for the higher gas pressures although in the majority of cases the variations are within the estimate of experimental error (~10% of the value). A detailed study of the variation of translational energy loss ΔE with target gas pressure has been reported in Chapter 5 where fragment ion peaks

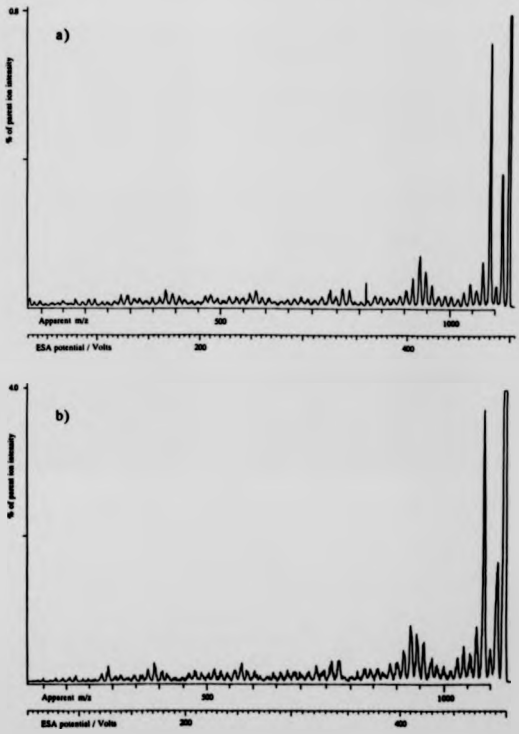

Figure 6.19 FD-MIKE spectra of valinomycin $[M+Na]^+$ ions (m/z 1133.6); 90 % parent ion beam attenuation, incident ion energy E_i = 14.9 keV
a) xenon target gas b) helium target gas

TABLE 6.14

Translational energy losses measured in the FD-MIKE spectrum of valinomycin $[M+Na]^+$ ions (m/z 1133.6) with xenon as target gas (Figure 6.19a). Incident ion energy = 14.9 keV. Attenuation = 90 %

V_m / V	Apparent m/z	Assigned mass (m_f) / Da	Fragment ion	V_e / V	ΔE / eV
492.7	1117.2	1118.60	Loss of CH_3	493.4	19.2
486.4	1102.8	1105.62	Loss of CO	487.6	37.8
480.6	1089.7	1090.56	Loss of C_3H_7	481.0	12.0
473.6	1073.8	1075.54	Loss of either HCO_2 or $OCHCH_3$	474.4	23.6
467.3	1059.5	1061.60	$(HVLV)_2VHV + Na]^+$	468.2	30.1
461.1	1045.4	1047.58	$(HVLV)_2VLV + Na + O]^+$	462.0	30.7
423.7	960.7	962.53	$(HVLV)_2HV + Na]^+$	424.5	27.7
418.1	947.9	948.53	$(HVLV)_2HV + 2H + Na - O]^+$	418.4	9.8
412.3	934.7	936.51	$(HVLV)_2HV + 2H + Na - CO]^+$	413.1	28.6
405.4	919.1	920.48	$(HVLV)_2VL + 2H + Na - O]^+$	406.0	23.1
343.3	778.5	779.37	$(HVLV)_2 + Na + O]^+$	343.7	17.4
336.4	762.8	763.38	$(HVLV)_2 + Na]^+$	336.7	11.7
		393.20	$[HVLV + Na]^+$	173.4	
		294.13	$[HVL + Na]^+$	129.7	

Fragmentation efficiency = 2.9 %
Total number of parent ion counts n_p = 115,393
Total number of fragment ion counts n_f = 33,464

TABLE 6.15

Translational energy losses measured in the FD-MIKE spectrum of valinomycin $[M+Na]^+$ ions (m/z 1133.6) with helium as target gas (Figure 6.19b). Incident ion energy = 14.9 keV. Attenuation = 90 %

V_m / V	Apparent m/z	Assigned mass (m_f) / Da	Fragment ion	V_s / V	ΔE / eV
491.8	1115.0	1118.60	Loss of CH_3	493.4	48.0
		1105.62	Loss of CO	487.6	
479.8	1087.8	1090.56	Loss of C_3H_7	481.0	37.5
472.4	1071.1	1075.54	Loss of either HCO_2 or $OCHCH_3$	474.4	61.3
		1061.60	$(HVLV)_2VHV + Na]^+$	468.2	
460.0	1042.9	1047.58	$(HVLV)_2VLV + Na + O]^+$	462.0	67.4
		1033.57	$(HVLV)_2VLV + Na]^+$	455.9	
422.7	958.5	962.53	$(HVLV)_2HV + Na]^+$	424.5	62.8
417.0	945.5	948.53	$(HVLV)_2HV + 2H + Na - O]^+$	418.4	47.8
411.1	932.2	936.51	$(HVLV)_2HV + 2H + Na - CO]^+$	413.1	69.4
404.4	916.8	920.48	$(HVLV)_2VL + 2H + Na - O]^+$	406.0	59.9
342.1	775.7	779.37	$(HVLV)_2 + Na + O]^+$	343.7	70.7
335.6	761.0	763.38	$(HVLV)_2 + Na]^+$	336.7	47.1
260.0	589.6	592.32	$[(HVLV)HV + Na]^+$	261.2	69.4
254.2	576.5	578.34	$[(HVLV)HV + 2H + Na - O]^+$	255.1	48.8
247.9	562.1	566.34	$[(HVLV)HV + 2H + Na - CO]^+$	249.8	111.3
179.2	406.4	409.19	$[(HVLV) + Na + O]^+$	180.5	102.7
172.6	391.3	393.20	$[HVLV + Na]^+$	173.4	72.1
166.2	376.7	379.22	$[HVLV + 2H + Na - O]^+$	167.3	98.6
		294.13	$[HVL + Na]^+$	129.7	

Fragmentation efficiency = 6.0 %
Total number of parent ion counts n_p = 69,932
Total number of fragment ion counts n_f = 41,959

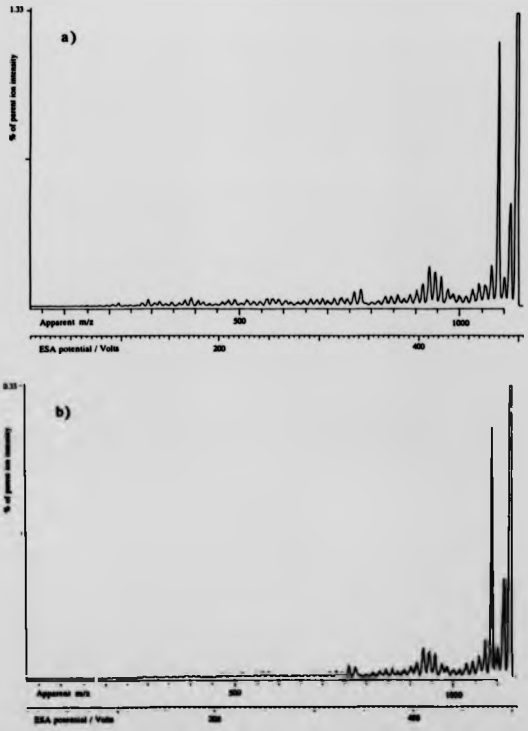

Figure 6.20 FD-MIKE spectra of valinomycin [M+Na]+ ions (m/z 1133.6); helium target gas, incident ion energy E_i = 14.9 keV a) 80 % attenuation b) 40 % attenuation

TABLE 6.16

Translational energy losses measured in the FD-MIKE spectrum of valinomycin $[M+Na]^+$ ions (m/z 1133.6) with helium as target gas (Figure 6.20a). Incident ion energy = 14.9 keV. Attenuation = 80 %

V_m / V	Apparent m/z	Assigned mass (m_f) / Da	Fragment ion	V_c / V	ΔE / eV
491.8	1115.1	1118.60	Loss of CH_3	493.4	46.2
485.8	1101.4	1105.62	Loss of CO	487.6	56.8
479.9	1088.0	1090.56	Loss of C_3H_7	481.0	35.4
472.7	1071.7	1075.54	Loss of either HCO_2 or $OCHCH_3$	474.4	53.3
		1061.60	$(HVLV)_2VHV + Na]^+$	468.2	
		1047.58	$(HVLV)_2VLV + Na + O]^+$	462.0	
423.1	959.2	962.53	$(HVLV)_2HV + Na]^+$	424.5	51.2
417.1	945.6	948.53	$(HVLV)_2HV + 2H + Na - O]^+$	418.4	46.0
411.1	932.2	936.51	$(HVLV)_2HV + 2H + Na - CO]^+$	413.1	69.6
404.3	916.6	920.48	$(HVLV)_2VL + 2H + Na - O]^+$	406.0	63.0
342.6	776.8	779.37	$(HVLV)_2 + Na + O]^+$	343.7	48.9
335.4	760.5	763.38	$(HVLV)_2 + Na]^+$	336.7	56.1
172.6	391.4	393.20	$[HVLV + Na]^+$	173.4	69.0
128.8	292.0	294.13	$[HVL + Na]^+$	129.7	108.1

Fragmentation efficiency = 6.7 %
Total number of parent ion counts n_p = 231,122
Total number of fragment ion counts n_f = 77,426

TABLE 6.17

Translational energy losses measured in the FD-MIKE spectrum of valinomycin $[M+Na]^+$ ions (m/z 1133.6) with helium as target gas (Figure 6.20b). Incident ion energy = 14.9 keV. Attenuation = 40 %

V_m / V	Apparent m/z	Assigned mass (m_f) / Da	Fragment ion	V_e / V	ΔE / eV
492.0	1115.5	1118.60	Loss of CH_3	493.4	40.8
486.0	1102.0	1105.62	Loss of CO	487.6	48.9
479.9	1088.0	1090.56	Loss of C_3H_7	481.0	34.7
473.0	1072.3	1075.54	Loss of either HCO_2 or $OCHCH_3$	474.4	44.6
		1061.60	$[(HVLV)_2VHV + Na]^+$	468.2	
		1047.58	$[(HVLV)_2VLV + Na + O]^+$	462.0	
423.0	959.2	962.53	$[(HVLV)_2HV + Na]^+$	424.5	52.2
417.2	945.9	948.53	$[(HVLV)_2HV + 2H + Na - O]^+$	418.4	41.5
410.9	931.7	936.51	$[(HVLV)_2HV + 2H + Na - CO]^+$	413.1	76.3
404.6	917.4	920.48	$[(HVLV)_2VL + 2H + Na - O]^+$	406.0	50.9
342.4	776.3	779.37	$[(HVLV)_2 + Na + O]^+$	343.7	59.0
335.6	760.9	763.38	$[(HVLV)_2 + Na]^+$	336.7	49.2
		393.20	$[HVLV + Na]^+$	173.4	
		294.13	$[HVL + Na]^+$	129.7	

Fragmentation efficiency = 5.7 %
Total number of parent ion counts n_p = 276,842
Total number of fragment ion counts n_f = 26,300

were investigated individually to provide much improved peak shapes resulting in reduced errors.

6.3.2 Valine-gramicidin A

Figure 6.21 shows the tandem mass spectra of valine-gramicidin A $[M+K]^+$ ions measured using the MIKES technique when the target gases were helium (Fig. 6.21a and shown previously in Fig. 6.11) and argon (Fig. 6.21b). In both cases the incident ion energy was 8.1 keV. The argon spectrum was obtained with a parent ion beam attenuated by 90% and the helium spectrum with 70% attenuation. The total number of fragment ion counts was similar in the two spectra. The fragmentation pathways appear not to differ on changing the target from helium to argon. A comparison of the relative intensities of the fragment ions in the two spectra would not be useful due to the differences in collision gas pressure. An interesting feature of the spectra is the apparently improved resolution in the argon spectrum. With argon as target gas the fragment ion peak at m/z 1903 is resolved from the parent ion peak, whereas this is not the case with helium as target gas. The two fragment ions at m/z 1876 and m/z 1861 are also resolved better with argon, as compared with helium. Other fragment ion peaks appear to be less broad with argon. Translational energy losses measured for the spectrum obtained with argon as target are given in Table 6.18 and in the helium case have been reported previously in Table 6.9. In general, the energy losses are much smaller when argon is employed as target and therefore the distribution of ΔE values is expected to be smaller, resulting in an improvement in resolution.

Spectra have also been obtained using xenon as target and are shown in Figure 6.22. The incident ion energy was 8.1 keV and parent ion beams were attenuated by 40% (Fig. 6.22a) and 90% (Fig. 6.22b). The total number of fragment ion counts was approximately a factor of three lower than for the spectra

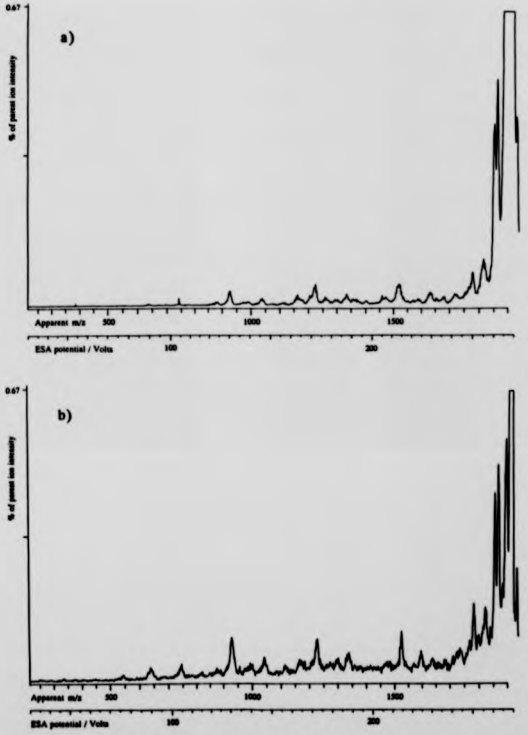

Figure 6.21 FD-MIKE spectra of valine-gramicidin A $[M+K]^+$ ions (m/z 1920.2); incident ion energy E_i = 8.1 keV a) helium, 70 % attenuation b) argon, 90 % attenuation

TABLE 6.18

Translational energy losses measured in the FD-MIKE spectrum of valine-gramicidin A $[M+K]^+$ ions (m/z 1920.2) with argon as target gas (Figure 6.21). Incident ion energy = 8.1 keV. Attenuation = 90 %

V_m / V	Apparent m/z	Assigned mass (m_f) / Da	Fragment ion	V_e / V	ΔE / eV
267.2	1900.4	1903.20	Loss of OH or NH_3	267.6	11.8
263.2	1871.9	1876.10	Loss of C_3H_8 or $[z_{15} + K]^+$	263.8	18.2
261.5	1859.6	1861.13	Loss of C_2H_4NO	261.7	6.5
		1831.12	$[a_{15}^{-2} + K]^+$	257.5	
251.1	1785.9	1789.09	$[y_{14}^{-2} + K]^+$	251.6	14.3
		1691.07	$[c_{14}^{+1} + K]^+$	237.8	
		1645.04	$[a_{14}^{-1} + K]^+$	231.3	
		1602.98	$[d_{14}^{-2} + K]^+$	225.3	
		1576.93	$[x_{11}^{-2} + K]^+$	221.7	
214.6	1526.4	1531.96	$[a_{13}^{-1} + K]^+$	215.4	29.3
		1345.88	$[a_{12}^{-1} + K]^+$	189.2	
		1303.83	$[d_{12}^{-1} + K]^+$	183.3	
		1232.79	$[a_{11}^{-1} + K]^+$	173.3	
		1046.11	$[a_{10}^{-1} + K]^+$	147.1	
		1004.67	$[d_{10}^{-1} + K]^+$	141.3	
130.9	931.0	933.63	$[a_9^{-1} + K]^+$	131.3	22.8
		747.55	$[a_8^{-1} + K]^+$	105.1	

Fragmentation efficiency = 2.5%
Total number of parent ion counts n_p = 274,000
Total number of fragment ion counts n_f = 68,500

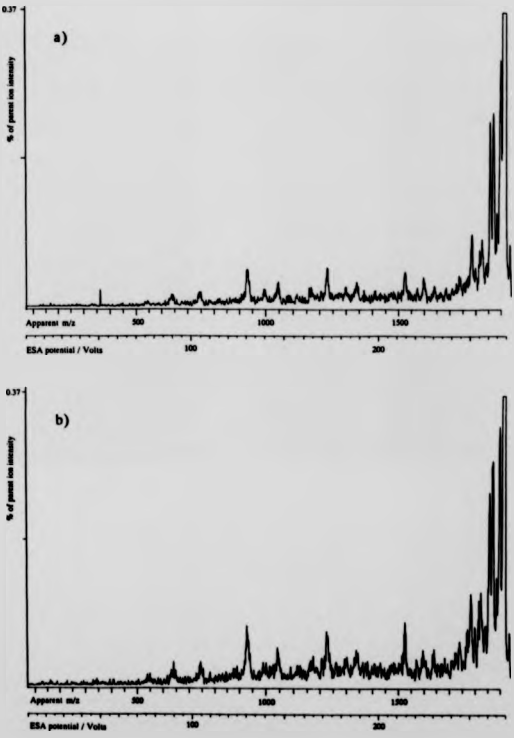

Figure 6.22 FD-MIKE spectra of valine-gramicidin A $[M+K]^+$ ions (m/z 1920.2); incident ion energy E_i = 8.1 keV, xenon target gas a) 40 % attenuation b) 90 % attenuation

TABLE 6.19

Translational energy losses measured in the FD-MIKE spectrum of valine-gramicidin A $[M+K]^+$ ions (m/z 1920.2) with xenon as target gas (Figure 6.22a). Incident ion energy = 8.1 keV. Attenuation = 40 %

V_m / V	Apparent m/z	Assigned mass (m_f) / Da	Fragment ion	V_e / V	ΔE / eV
267.3	1901.2	1903.20	Loss of OH or NH_3	267.6	8.5
263.3	1872.6	1876.10	Loss of C_3H_8 or $[z_{15} + K]^+$	263.8	15.0
261.5	1859.6	1861.13	Loss of C_2H_4NO	261.7	6.6
		1831.12	$[a_{15}^{-2} + K]^+$	257.5	
251.1	1786.1	1789.09	$[y_{14}^{-2} + K]^+$	251.6	13.6
		1691.07	$[c_{14}^{+1} + K]^+$	237.8	
		1645.04	$[a_{14}^{-1} + K]^+$	231.3	
		1602.98	$[d_{14}^{-2} + K]^+$	225.3	
		1576.93	$[x_{11}^{-2} + K]^+$	221.7	
214.7	1526.8	1531.96	$[a_{13}^{-1} + K]^+$	215.4	27.3
		1345.88	$[a_{12}^{-1} + K]^+$	189.2	
		1303.83	$[d_{12}^{-1} + K]^+$	183.3	
		1232.79	$[a_{11}^{-1} + K]^+$	173.3	
		1046.11	$[a_{10}^{-1} + K]^+$	147.1	
		1004.67	$[d_{10}^{-1} + K]^+$	141.3	
		933.63	$[a_9^{-1} + K]^+$	131.3	
		747.55	$[a_8^{-1} + K]^+$	105.1	

Fragmentation efficiency = 5.6 %
Total number of parent ion counts n_p = 228,236
Total number of fragment ion counts n_f = 21,302

TABLE 6.20

Translational energy losses measured in the FD-MIKE spectrum of valine-gramicidin A $[M+K]^+$ ions (m/z 1920.2) with xenon as target gas (Figure 6.22b). Incident ion energy = 8.1 keV. Attenuation = 90 %

V_m / V	Apparent m/z	Assigned mass (m_f) / Da	Fragment ion	V_e / V	ΔE / eV
267.3	1900.7	1903.20	Loss of OH or NH_3	267.6	10.7
263.4	1873.0	1876.10	Loss of C_3H_8 or $[z_{15} + K]^+$	263.8	13.3
261.7	1861.1	1861.13	Loss of C_2H_4NO	261.7	0.1
		1831.12	$[a_{15}^{-2} + K]^+$	257.5	
251.2	1786.6	1789.09	$[y_{14}^{-2} + K]^+$	251.6	11.2
		1691.07	$[c_{14}^{+1} + K]^+$	237.8	
		1645.04	$[a_{14}^{-1} + K]^+$	231.3	
		1602.98	$[d_{14}^{-2} + K]^+$	225.3	
		1576.93	$[x_{11}^{-2} + K]^+$	221.7	
214.9	1528.6	1531.96	$[a_{13}^{-1} + K]^+$	215.4	17.8
		1345.88	$[a_{12}^{-1} + K]^+$	189.2	
		1303.83	$[d_{12}^{-1} + K]^+$	183.3	
		1232.79	$[a_{11}^{-1} + K]^+$	173.3	
		1046.11	$[a_{10}^{-1} + K]^+$	147.1	
		1004.67	$[d_{10}^{-1} + K]^+$	141.3	
		933.63	$[a_9^{-1} + K]^+$	131.3	
		747.55	$[a_8^{-1} + K]^+$	105.1	

Fragmentation efficiency = 2.0 %
Total number of parent ion counts n_p = 100,515
Total number of fragment ion counts, n_f = 20,103

obtained with helium and argon target gases, which were shown in Figure 6.21. Hence the signal-to-noise ratios are much lower and the relative intensities of the fragment ion peaks less reliable. There does appear to be an increase in the relative intensities of the low-mass fragment ions compared to the high-mass fragment ions when the collision gas pressure was increased. Translational energy losses have been measured for some of the more relatively intense fragment ions with the more asymmetrical peak shapes. These are reported in Table 6.19 for the case of 40% attenuation and Table 6.20 for the spectrum obtained with 90% attenuation of the parent ion beam. The ΔE values are similar given the magnitudes of experimental error for the less than ideal peak shapes and are also similar to the ΔE values obtained at the same incident ion energy for argon (Table 6.18). The resolution of the various fragment ion peaks also appears to be improved, compared to when helium was employed as target. The fragmentation efficiency was 2.0% when the parent ion beam was attenuated by 90% with xenon and was 5.6% for 40% attenuation with helium.

Comparisons of the MIKE spectra recorded for CID of valine-gramicidin A $[M+K]^+$ ions with helium and argon as collision gases are shown in Figures 6.23 and 6.24 for incident ion energies of 12.5 and 14.9 keV respectively. In each case the parent ion beam attenuation was approximately 70%. Translational energy losses have been measured for the argon case and are given in Tables 6.21 and 6.22 for E_l = 12.5 and E_l = 14.9 keV respectively. Translational energy losses for the helium case were given previously in Tables 6.10 and 6.12. When the incident ion energy was 12.5 keV, the intensities of the low-mass fragment ions relative to the higher mass fragment ions was increased when argon was used as target compared with helium. For example, the relative heights of the fragment ion peaks at m/z 747.5, 648.4 and 549.5 are higher in the argon spectrum than in the helium spectrum. A similar effect was observed when the incident ion energy was 14.9 keV but was not as significant as in the E_l = 12.5 keV case.

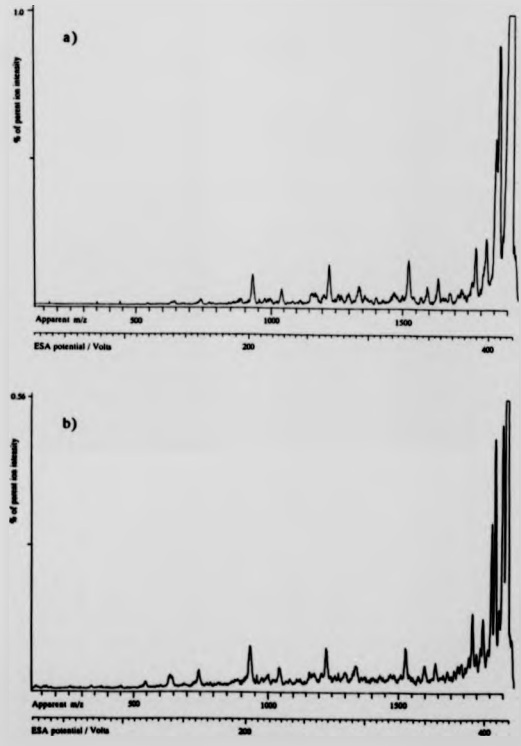

Figure 6.23 FD-MIKE spectra of valine-gramicidin A $[M+K]^+$ ions (m/z 1920.2); incident ion energy E_l = 12.5 keV, ~70 % attenuation
a) helium target gas b) argon target gas

TABLE 6.21

Translational energy losses measured in the FD-MIKE spectrum of valine-gramicidin A $[M+K]^+$ ions (m/z 1920.2) with argon as target gas (Figure 6.23b). Incident ion energy = 12.5 keV. Attenuation = 70 %

V_m / V	Apparent m/z	Assigned mass (m_f) / Da	Fragment ion	V_c / V	ΔE / eV
416.0	1901.9	1903.20	Loss of OH or NH_3	416.3	8.4
409.7	1873.2	1876.10	Loss of C_3H_8 or $[z_{15} + K]^+$	410.4	19.6
406.8	1860.0	1861.13	Loss of C_2H_4NO	407.1	7.9
399.7	1827.2	1831.12		400.5	27.2
390.8	1786.7	1789.09	$[y_{14}^{-2} + K]^+$	391.3	16.9
		1691.07	$[c_{14}^{+1} + K]^+$	369.9	
359.2	1642.1	1645.04	$[a_{14}^{-1} + K]^+$	359.8	22.6
		1602.98	$[d_{14}^{-2} + K]^+$	350.4	
		1576.93	$[x_{11}^{-2} + K]^+$	344.9	
334.3	1528.3	1531.96	$[a_{13}^{-1} + K]^+$	335.1	29.8
		1345.88	$[a_{12}^{-1} + K]^+$	294.4	
		1303.83	$[d_{12}^{-1} + K]^+$	285.2	
269.0	1229.8	1232.79	$[a_{11}^{-1} + K]^+$	269.7	30.2
		1046.11	$[a_{10}^{-1} + K]^+$	228.8	
		1004.7	$[d_{10}^{-1} + K]^+$	219.8	
204.0	932.8	933.6	$[a_9^{-1} + K]^+$	204.2	11.1
163.1	745.5	747.6	$[a_8^{-1} + K]^+$	163.5	34.3

Fragmentation efficiency = 8.2 %
Total number of parent ion counts n_p = 380,487
Total number of fragment ion counts n_f = 104,000

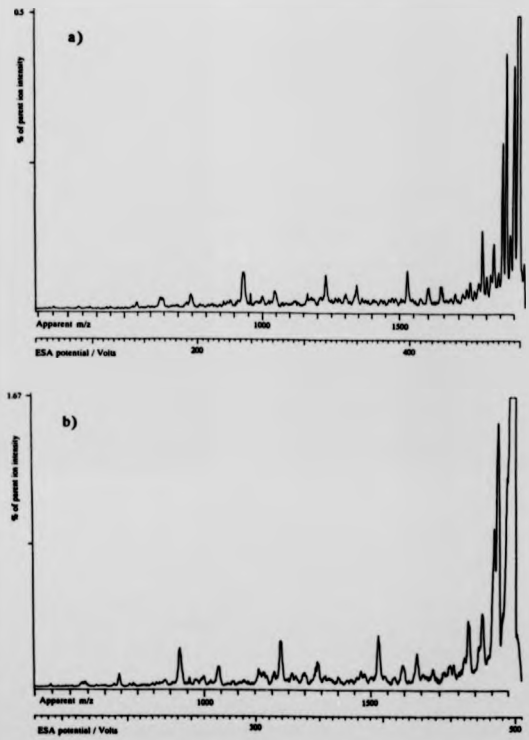

Figure 6.24 FD-MIKE spectra of valine-gramicidin A $[M+K]^+$ ions (m/z 1920.2); incident ion energy E_i = 14.9 keV, 70 % attenuation
a) argon target gas b) helium target gas

TABLE 6.22

Translational energy losses measured in the FD-MIKE spectrum of valine-gramicidin A $[M+K]^+$ ions (m/z 1920.2) with argon as target gas (Figure 6.24a). Incident ion energy = 14.9 keV. Attenuation = 70 %

V_m / V	Apparent m/z	Assigned mass (m_f) / Da	Fragment ion	V_e / V	ΔE / eV
495.3	1902.2	1903.20	Loss of OH or NH_3	495.6	8.3
488.0	1874.2	1876.10	Loss of C_3H_8 or $[z_{15} + K]^+$	488.5	15.0
484.5	1860.6	1861.13	Loss of C_2H_4NO	484.6	4.5
476.1	1828.4	1831.12	$[a_{15}^{-2} + K]^+$	476.8	21.8
465.4	1787.3	1789.09	$[y_{14}^{-2} + K]^+$	465.9	15.1
		1691.07	$[c_{14}^{*-1} + K]^+$	440.3	
		1645.04	$[a_{14}^{-1} + K]^+$	428.4	
		1602.98	$[d_{14}^{-2} + K]^+$	417.1	
		1576.93	$[x_{11}^{-2} + K]^+$	410.6	
398.3	1529.5	1531.96	$[a_{13}^{-1} + K]^+$	398.9	23.8
	1345.9	1345.88	$[a_{12}^{-1} + K]^+$	350.5	
		1303.83	$[d_{12}^{-1} + K]^+$	339.5	
320.5	1231.0	1232.79	$[a_{11}^{-1} + K]^+$	321.0	22.2
		1046.11	$[a_{10}^{-1} + K]^+$	272.4	
		1004.67	$[d_{10}^{-1} + K]^+$	261.6	
243.1	933.5	933.63	$[a_9^{-1} + K]^+$	243.1	2.1
		747.55	$[a_8^{-1} + K]^+$	194.7	

Fragmentation efficiency = 6.8 %
Total number of parent ion counts n_p = 551,471
Total number of fragment ion counts n_f = 125,000

Figure 6.25 shows a comparison of the FD-MIKE spectra obtained for valine-gramicidin A $[M+K]^+$ ions with an incident ion energy of 14.9 keV when the target gas was helium and the parent ion beam attenuated to 90% and 70%. Translational energy losses for the 70% attenuation case have been reported previously in Table 6.8 and the values for the 90% case are given in Table 6.23. When making a comparison of the general appearance of the two spectra, the differing total number of fragment ion counts should be considered. In the spectrum where the parent ion beam was attenuated by 90%, the values of n_f were greater than three times the value for the 70% attenuation spectrum. The fragment ion peaks in the former spectrum were of improved shape and definition than in the latter. The intensities of the a-series sequence ions, relative to the most intense fragment ion peak at m/z 1876.1, increased when the target gas pressure was increased. Figure 6.26 shows a plot of the ratio of the fragment ion peak intensities in the spectrum obtained with 90% attenuation of the parent ion beam to that at 70% attenuation. The fragment ion intensities were normalised so that the peak-height of the $[a_{15}^{-2} + K]^+$ fragment ion at m/z 1831.1 was the same in each case. The graph shows how the intensity of the lower mass fragment ions was increased relative to the high-mass fragment ions when a higher target gas pressure was employed.

6.3.3 Caesium iodide cluster ions

Translational energy losses have been measured for collision-induced decomposition of the caesium iodide cluster ions $[Cs_3I_4]^+$ (m/z 1172.1) formed by FAB when helium, deuterium and argon were employed as target gases. In all cases the incident ion energy was 10.4 keV and the parent ion beam was attenuated by 60%.

MIKE spectra have been recorded for CID of $[Cs_3I_4]^+$ ions with helium, deuterium and argon gases as targets and are shown in Figure 6.27 with the

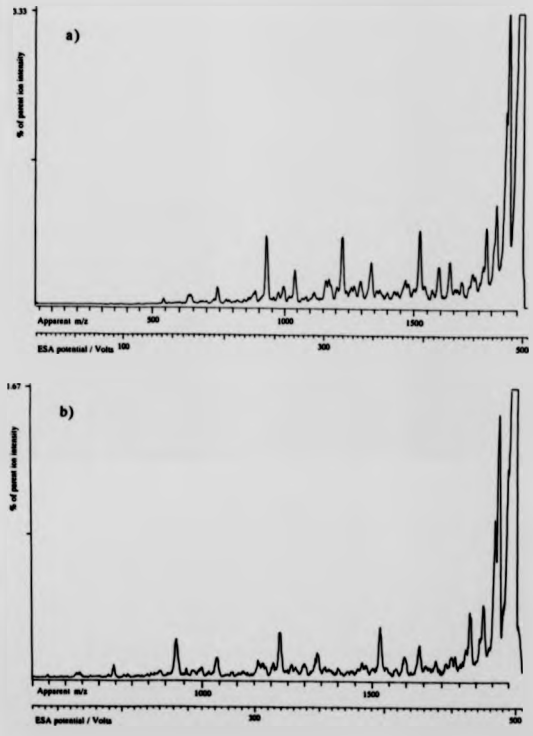

Figure 6.25 FD-MIKE spectra of valine-gramicidin A $[M+K]^+$ ions (m/z 1920.2); incident ion energy E$_l$ = 14.9 keV, helium target gas a) 90 % attenuation b) 70 % attenuation

TABLE 6.23

Translational energy losses measured in the FD-MIKE spectrum of valine-gramicidin A $[M+K]^+$ ions (m/z 1920.2) with helium as target gas (Figure 6.25a). Incident ion energy = 14.9 keV. Attenuation = 90 %

V_m / V	Apparent m/z	Assigned mass (m_f) / Da	Fragment ion	V_e / V	ΔE / eV
		1903.20	Loss of OH or NH_3	495.6	
486.6	1868.8	1876.10	Loss of C_3H_8 or $[z_{15} + K]^+$	488.5	58.5
		1861.13	Loss of C_2H_4NO	484.6	
473.6	1818.9	1831.12	$[a_{15}^{-2} + K]^+$	476.8	99.9
463.7	1780.7	1789.09	$[y_{14}^{-2} + K]^+$	465.9	69.9
		1691.07	$[c_{14}^{+1} + K]^+$	440.3	
426.0	1635.9	1645.04	$[a_{14}^{-1} + K]^+$	428.4	82.6
415.0	1593.9	1602.98	$[d_{14}^{-2} + K]^+$	417.1	75.4
		1576.93	$[x_{11}^{-2} + K]^+$	410.6	
396.7	1523.6	1531.96	$[a_{13}^{-1} + K]^+$	398.9	81.5
348.1	1345.9	1345.88	$[a_{12}^{-1} + K]^+$	350.5	99.8
		1303.83	$[d_{12}^{-1} + K]^+$	339.5	
319.3	1226.2	1232.79	$[a_{11}^{-1} + K]^+$	321.0	79.7
271.3	1042.1	1046.11	$[a_{10}^{-1} + K]^+$	272.4	58.0
		1004.67	$[d_{10}^{-1} + K]^+$	261.6	
242.1	929.7	933.63	$[a_9^{-1} + K]^+$	243.1	63.1
		747.55	$[a_8^{-1} + K]^+$	194.7	

Fragmentation efficiency = 6.0 %
Total number of parent ion counts n_p = 661,150
Total number of fragment ion counts n_f = 396,690

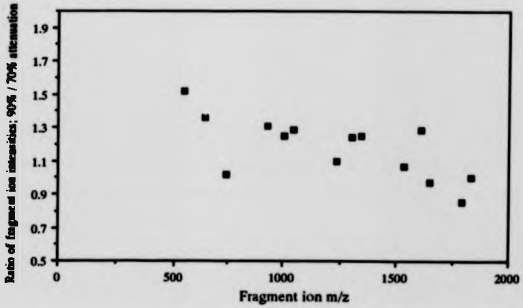

Figure 6.26 Ratios of the fragment ion intensities in the MIKE spectra of valine-gramicidin A $[M+K]^+$ ions when the parent ion beams were attenuated by 90% and 70% with helium as target gas. Intensities were normalised such that the m/z 1831.1 $[a_{15}^{-H_2O} + K]^+$ fragment ion was the same height in each case.

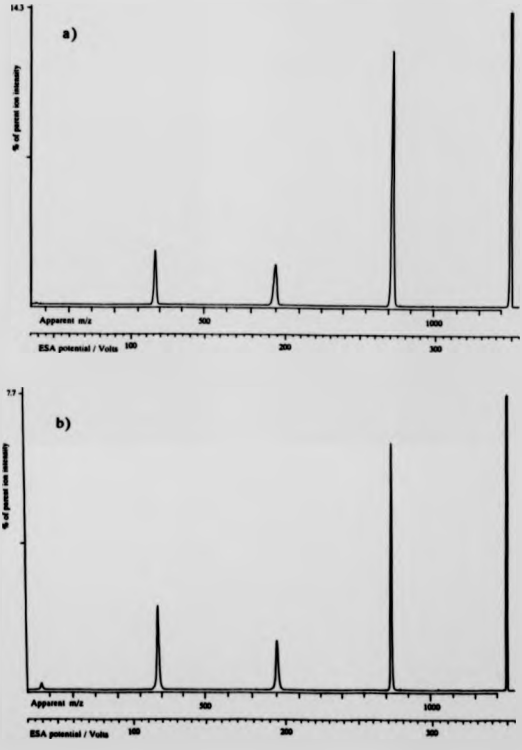

Figure 6.27 FAB-MIKE spectra of $[Cs_2I_4]^+$ ions (m/z 1172.1); incident ion energy E_l = 10.4 keV, 60 % attenuation, target gases: a) helium b) argon c) deuterium

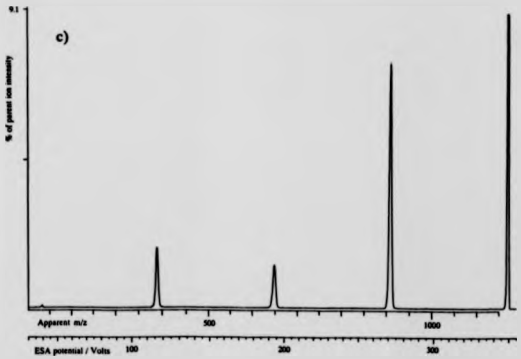

Figure 6.27 continued

TABLE 6.24

Translational energy losses measured in the FD-MIKE spectrum of $[Cs_5I_4]^+$ ions (m/z 1172.1) with helium as target gas (Figure 6.27a). Incident ion energy = 10.5 keV. Attenuation = 60 %

V_m / V	Apparent m/z	Assigned mass (m_f) / Da	Fragment ion	V_e / V	ΔE / eV
271.9	910.7	912.34	$[Cs_4I_3]^+$	272.4	18.5
193.9	649.5	652.53	$[Cs_3I_2]^+$	194.8	49.0
116.4	389.0	392.72	$[Cs_2I]^+$	117.3	73.1
		132.91	Cs^+	39.7	

Fragmentation efficiency = 18.5 %
Total number of parent ion counts n_p = 150,019
Total number of fragment ion counts n_f = 69,474

TABLE 6.25

Translational energy losses measured in the FD-MIKE spectrum of $[Cs_5I_4]^+$ ions (m/z 1172.1) with argon as target gas (Figure 6.27b). Incident ion energy = 10.5 keV. Attenuation = 60 %

V_m / V	Apparent m/z	Assigned mass (m_f) / Da	Fragment ion	V_e / V	ΔE / eV
272.4	912.2	912.34	$[Cs_4I_3]^+$	272.5	1.5
194.8	652.4	652.53	$[Cs_3I_2]^+$	194.9	2.6
117.2	392.6	392.72	$[Cs_2I]^+$	117.3	3.1
39.7	132.8	132.91	Cs^+	39.7	5.1

Fragmentation efficiency = 10.8 %
Total number of parent ion counts n_p = 250,271
Total number of fragment ion counts n_f = 67,654

TABLE 6.26

Translational energy losses measured in the FD-MIKE spectrum of $[Cs_5I_4]^+$ ions (m/z 1172.1) with deuterium as target gas (Figure 6.27c). Incident ion energy = 10.5 keV. Attenuation = 60 %

V_m / V	Apparent m/z	Assigned mass (m_f) / Da	Fragment ion	V_e / V	ΔE / eV
271.9	910.6	912.34	$[Cs_4I_3]^+$	272.4	20.0
194.0	649.5	652.53	$[Cs_3I_2]^+$	194.8	47.8
116.7	390.7	392.72	$[Cs_2I]^+$	117.3	53.4
39.6	132.5	132.91	Cs^+	39.7	30.4

Fragmentation efficiency = 13.9 %
Total number of parent ion counts n_p = 234,364
Total number of fragment ion counts n_f = 81,454

translational energy losses ΔE reported in Tables 6.24, 6.25 and 6.26 respectively. These data have also been presented as a plot of ΔE versus fragment ion mass, Figure 6.28. ΔE values were similar with helium and deuterium as targets and were an order of magnitude smaller with argon. This is in line with the results of Sheil[69] and Alexander *et al.*[66] who showed the magnitudes of ΔE to be dependent on target gas mass, rather than ionisation energy as was previously suggested by Bricker and Russell,[62] since the mass of helium is similar to that of deuterium but the ionisation energy for deuterium is similar to that of argon. The relative intensities of the fragment ions in the spectra are similar in the cases of the two lighter targets, but with argon the intensity of the Cs^+ fragment ion peak was increased.

6.3.4 Discussion of results

The preceding sections have shown comparisons of the MIKE spectra for valinomycin, valine-gramicidin A and $[Cs_3I_4]^+$ molecule-ions, when the target gas mass was varied and also for different target gas pressures. Overall the results have shown that despite increasing the centre-of-mass collision energy by a factor of 10 or 30, on changing the target from helium to argon or xenon, the nature of the fragmentations induced by collisional activation remained the same. Evidence was found that the intensities of these fragment ions relative to each other were influenced to some extent by the choice of target gas. The overall intensities of the fragment ions relative to the incident parent ion beam, as described by the fragmentation efficiency, was lower with xenon or argon compared to helium. The greater ion losses when heavier targets were employed presumably reflects the greater range of possible scattering angles. This was illustrated in Figure 6.28, where calculations of the range of scattering angles were made for helium and xenon in collision with an ion of mass 1133.6 Da. These calculations were based upon a simple model for energy transfer described by

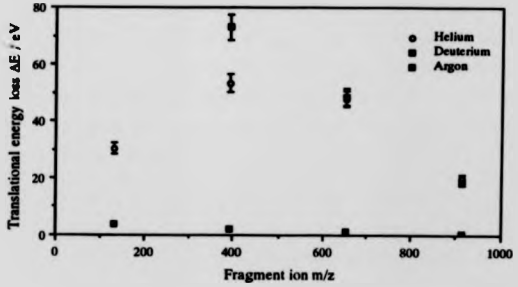

Figure 6.28 Variation of translational energy losses with target gas mass for fragment ions of $[Cs_5I_4]^+$ (m/z 1172.1).

conservation of energy and momentum (Equation 1.8). It was shown how, for a fixed acceptance angle of an electric sector analyser of 1°, only a fraction of the possible ion current could be sampled with xenon as target, whereas when helium was employed no ions were scattered above 0.25° and hence ion losses through scattering should be negligible after a single collision with helium. This is also consistent with ion trajectory calculations made by Uggerud and Derrick [54] which showed the range of possible scattering angles for helium to have a maximum value of θ less than 0.3° whereas the maximum values for argon and xenon targets were ~1.6° and ~3° respectively.

Comparisons of the MIKE spectra of valinomycin $[M+Na]^+$ ions with an incident ion energy was 14.9 keV and parent ion beam attenuated by 60% (Figure 6.18) showed the intensities of the low-mass fragment ions to increase relative to high-mass fragments, if xenon was used as target in preference to helium. When the collision gas pressure was raised to give a parent ion beam attenuation of 90% (Figure 6.19), the relative intensities of low- to high-mass fragment ions were similar with both xenon and helium. Low-mass fragment ions are generally associated with larger translational energy losses by the parent ions and the energy requirement for their formation is assumed to be greater (since larger ΔE values are assumed to reflect increased internal energy uptakes). When xenon was used as target under single collision conditions, a greater internal energy was taken up by the parent ions due to the increased amount of centre-of-mass collision energy available, resulting in an increased abundance of the low-mass fragment ions relative to the high-mass fragment ions. When higher gas pressures were used however, such that there was an increasing contribution from multiple and sequential collisions, the relative abundances of the fragment ions with helium and xenon as targets were similar. This suggests that when more collisions occur with xenon the range of scattering angles becomes increasingly large resulting in increased ion losses, whereas with helium an

increased number of collisions may still result in detectable fragment ions. The multiple or sequential collisions with helium may then impart a similar amount of internal energy to the ions as with a single collision with xenon.

Similar increases in fragment ion relative intensities were observed for the peptide valine-gramicidin A. When the incident ion energy was 8.1 keV and the parent ion current was attenuated by 40% with xenon (Figure 6.22a) and 70% with helium (Figure 6.21a), the relative intensities of low-mass fragment ions compared with high-mass fragment ions was higher with xenon as target despite the lower gas pressure in this case. The results of Chapter 5 suggest that at both these attenuations single collisions would be the dominant process. Similar results were obtained with incident ion energies of 12.5 keV (Figure 6.23) and 14.9 keV (Figure 6.24), where the parent ions were attenuated by 70% with helium and argon. The increases in abundances of low-mass fragment ions achieved by switching from helium to argon as target gas, were greater at the lower incident ion energy of 12.5 keV. In the E_l = 14.9 keV case, the increase in intensity of the low-mass fragment ions was only noticeable if compared with a high-mass fragmentation which had involved a side-chain loss. Comparisons with a high-mass a-series sequence ion revealed little change. Sequence ions which correspond with cleavages of the peptide backbone are likely to demand more internal energy than a simpler side chain loss. For valine-gramicidin A this is illustrated by the most dominant peaks in the MIKE spectra corresponding with side-chain losses which are presumably more facile processes for this ion. Hence the use of heavier targets appears to result in a general increase in the abundances of all sequence-type ions relative to side-chain losses, presumably due to an increase in the internal energy available for these higher energy dissociation pathways.

With both the peptide ions and the caesium iodide cluster ions, translational energy losses measured with argon or xenon as target were smaller in magnitude

than when helium was used. One explanation may be the increased range of scattering angles of the incident ion when heavier target gases are used. Alternatively, the lower energy losses may be explained using an impulsive collision theory (ICT).[54] Table 6.27 shows the translational energy losses measured for valine-gramicidin A $[M+K]^+$ ions when the incident ion energy was 12.5 keV for collision with helium and argon gas atoms. Internal energy uptakes have been calculated using ICT (Equation 1.9). For valine-gramicidin A the mass of the atom within the ion which is directly involved in the collision was taken to be the average mass of the atoms within the ion (m_a = 6.8 Da), since collisions would be expected to involve a random distribution of the possible orientations of the ions. In general, the estimated internal energy uptakes are similar, to within a few eV, with either helium or argon as targets despite the translational energy losses being on average a factor of two lower with argon compared with helium. The ICT model is based upon conservation of energy and momentum and predicts that the recoil energies of heavier targets gas atoms will be lower. Only a portion of the translational energy loss of the incident ion, results in internal energy uptake of the ion and some of the remainder is imparted as translational energy of the target gas atom. Larger ΔE values for collisions with lighter targets might therefore be explained by larger recoil energies since the internal energy uptakes are predicted to be similar for either helium or argon as targets. The MIKE spectra of valinomycin and valine-gramicidin A ions showed similar fragmentation pathways with either heavy or light targets but with some slight differences in the relative abundances of the fragment ions. These experimental results suggest that whilst the internal energy uptakes do differ to some extent with the mass of the target gas, the differences are not sufficient to change the types of fragmentations which are observed.

The results for the $[Cs_3I_4]^+$ ions also showed evidence for increased internal energy uptake when argon was used as target in preference to helium or

Table 6.27

Internal energy uptakes calculated using an impulsive collision theory (ICT) for collisions between valine-gramicidin A $[M+K]^+$ ions and helium and argon target gas atoms (Incident ion energy = 12.5 keV)*

Assigned mass (m_f) / Da	Fragment ion	ΔE (eV) He	Q (eV) He	ΔE (eV) Ar	Q (eV) Ar
1876.10	Loss of C_3H_8 or $[z_{15} + K]^+$	16.1	6.0	19.6	16.8
1861.13	Loss of C_2H_4NO	21.2	7.9	7.9	6.8
1831.12	$[a_{15}^{-2} + K]^+$	59.5	22.1	27.2	23.4
1789.09	$[y_{14}^{-2} + K]^+$	53.0	19.7	16.9	14.6
1645.04	$[a_{14}^{-1} + K]^+$	58.8	21.9	22.6	19.4
1531.96	$[a_{13}^{-1} + K]^+$	67.0	24.9	29.8	25.7
1232.79	$[a_{11}^{-1} + K]^+$	64.1	23.8	30.2	26.0
933.63	$[a_9^{-1} + K]^+$	53.2	19.8	11.1	9.6
747.55	$[a_8^{-1} + K]^+$	52.7	19.6	34.3	29.5

Table 6.28

Internal energy uptakes calculated using an impulsive collision theory (ICT) for collisions between $[Cs_5I_4]^+$ ions and helium and argon target gas atoms (Incident ion energy = 10.4 keV)*

Assigned mass (m_f)	Fragment ion	ΔE (eV) He	Q (eV) He	ΔE (eV) Ar	Q (eV) Ar
912.34	$[Cs_4I_3]^+$	18.5	0.6	1.5	0.4
652.53	$[Cs_3I_2]^+$	49.0	1.6	2.6	0.7
392.72	$[Cs_2I]^+$	73.1	2.3	3.1	0.8
132.91	Cs^+			5.1	1.3

* See text for details of calculations

deuterium. This was shown by the increased relative intensity of the Cs^+ fragment ion with argon as target. Translational energy losses were at least a factor of ten lower with argon as target as compared with helium, whereas a similar comparison for valine-gramicidin A gave a factor of approximately two. The magnitudes of the ΔE values with helium as target were similar for the peptide ions and caesium iodide cluster ions. Valine-gramicidin A has many more internal degrees of freedom than the $[Cs_5I_4]^+$ (822 compared to 21) and on the basis of quasi-equilibrium theory the peptide ion would require a greater amount of internal energy to dissociate at any given rate. Internal energy uptakes have been calculated from the measured ΔE values using ICT for $[Cs_5I_4]^+$ ions (m_a = 130.2 Da) and are listed in Table 6.28. With helium and argon as targets, the calculated internal energy uptakes are an order of magnitude smaller than those calculated for valine-gramicidin A, in line with the predictions made above of lower energy requirements for dissociation of the cluster ions. Compared with the peptide ion, lower internal energy uptakes calculated by ICT for the $[Cs_5I_4]^+$ with helium, are a consequence of a greater recoil energy of the helium atoms off the much heavier atoms of caesium and iodine. In contrast, the simple energy and momentum transfer model which considers the whole ion colliding with the target gas atom, would predict similar internal energy uptakes for a heavy atom cluster ion and a peptide ion when the ΔE values are similar (when the masses of the two ions are similar, and for collisions with helium). Given that the cluster ions have far fewer internal degrees of freedom, a similar internal energy uptake would be expected to result in much more extensive fragmentation than for the peptide ions. Although the fragmentation efficiencies were higher for the cluster ions than for peptide ions, the values were not too dissimilar. In this case, the ICT model appears to provide a more realistic model for describing the collisions of large ions.

Chapter 7 : DEPENDENCE OF DECOMPOSITION RATES ON THE SIZE OF MOLECULE-IONS

7.1 INTRODUCTION

Statistical rate theories, such as quasi-equilibrium theory (QET), predict that for a fixed range of internal energies the rates of dissociation of ions decrease with increasing number of internal modes (see Section 1.2). As the internal energy becomes distributed over a larger number of vibrational modes the energy per mode decreases, and hence the rates of dissociation decrease. To investigate the magnitudes of these effects, microcanonical rate constants have been calculated on the basis of QET using Equation 1.1 for various sizes of polystyrene molecules, up to 1874 Da, and for the peptide methionine-enkephalin (RMM = 573.2). Vibrational frequencies required for the determination of the rates were calculated using classical mechanics with the aid of a computer program. The variation of QET rate constants with internal energy has been investigated for molecules of various sizes and for a range of critical energies. The polystyrene results are used as a model for explaining the CID behaviour of peptides. Peptides may be considered as biological polymers and hence the model should prove to be a reasonable one, but comparisons of results with those obtained for methionine-enkephalin will be used to confirm this. Table 7.1 lists the numbers of internal modes for the various polystyrene oligomers and also for the peptides for which the CID energetics have been studied in previous chapters. The restraints that the calculated dissociation rates impose upon the experimentally observable fragmentations are discussed with reference to the magnitudes of internal energy uptakes estimated in Chapter 6.

Table 7.1

The number of fundamental vibrational frequencies associated with various molecules

Molecule	RMM	Number of internal modes (3N-6)
Methionine-enkephalin	573.2	222
Valinomycin	1110.6	498
Valine-gramicidin A	1881.2	822
Polystyrene-3-mer	314.2	144
Polystyrene-6-mer	628.4	288
Polystyrene-9-mer	938.6	432
Polystyrene-12-mer	1250.8	576
Polystyrene-15-mer	1563.0	720
Polystyrene-18-mer	1875.1	864
Polystyrene-21-mer	2187.3	1008
Polystyrene-24-mer	2499.5	1152

7.2 CALCULATION OF VIBRATIONAL FREQUENCIES

Vibrational frequencies for use with the QET calculations were determined with the aid of the computer program 'vib' described in Section 2.6.1. The program uses classical mechanics via the GF-matrix method [156,157] to calculate the vibrational frequencies from the cartesian co-ordinates and force constants associated with the possible vibrations of a given molecule. Input data consisted of the cartesian coordinates of the atoms within the test molecule and then various definitions of the internal coordinates. These definitions of internal coordinates were made by manually considering all possible bending, stretching and torsion modes within the molecule, and then by dividing these into various subgroups. Finally the force constants associated with the various vibrations were listed. In the case of the polystyrene molecules the input data had been compiled by Uggerud, [155] although some modification was necessary to the force constants and to the 'vib' program prior to determination of the vibrational frequencies. In the case of methionine-enkephalin, the input was derived from the x-ray crystallographic data obtained from the Cambridge Crystallographic Data Centre [183,184] and the crystal structure of the molecule is shown in Figure 7.1. Force constants used when compiling the input data for the vibrational analysis program were estimated from various compilations of force constants which have been made for small molecules.[185-189]

Calculation of the vibrational frequencies for polystyrene 3 - 24 mers (i.e 3 - 24 repeating styrene molecules) resulted in calculation of the correct number of internal modes for molecules smaller than the 18-mer. For the 18-mer an incomplete set of vibrational frequencies was obtained, (861 rather than 864), despite refinements made to the tolerances of the various matrices in the computer program. In this case, the calculated vibrational frequencies were used in QET calculations with the addition of three extra frequencies at higher

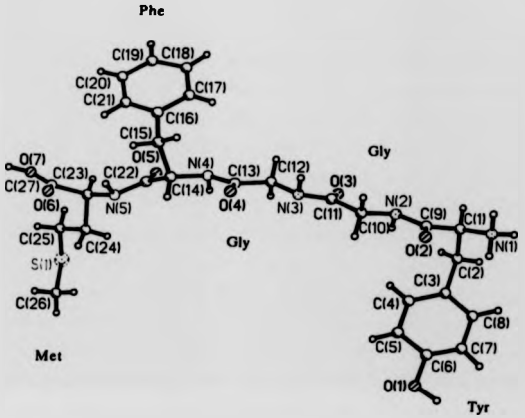

Figure 7.1 Structure of methionine-enkephalin

wavenumber values, where they would be expected to have a lesser influence on the overall outcome of the rate constants. For larger polystyrene molecules, 21- and 24-mers, the short-fall in frequencies was much greater and hence the input to the QET calculations would have been too unreliable. The problems of fewer than required numbers of internal modes being calculated are thought to be a consequence of a numerical problem associated with diagonalisation within the 'vib' program of the much larger matrices involved as the molecular size increases. For the program to be used for these larger molecules more sophisticated numerical methods may be required which would involve a number of major changes within the computer program. For methionine-enkephalin only 218 of the required 222 vibrational frequencies were attainable. Since complete sets of frequencies were obtained for the polystyrene 3- and 6-mers, which had similar numbers of internal modes to the peptide, the problem with too few internal modes was thought to be related to the input data rather than a problem with the program itself. Refinements of the input did little to improve upon the 218 frequencies and the source of the error has not been found. Therefore the shortfall was corrected as in the polystyrene 18-mer case, by the addition of extra frequencies in the region of 3000 cm^{-1}. The exact magnitudes of these additional frequencies on the QET calculations had no significant effect on the overall trends that were to be identified (see Section 7.3). The full set of fundamental vibrational frequencies calculated for methionine-enkephalin are given in Table 7.2

7.3 QET CALCULATIONS

The variation of rate constants $k(E)$ with internal energy E and critical energy E_o have been calculated for a range of polystyrene molecules and for methionine-enkephalin. The vibrational frequencies of the reactant were calculated by normal mode analysis as described in the previous section. For the transition state frequencies the reactant frequencies were used with the removal of one frequency

TABLE 7.2

Calculated vibrational frequencies for methionine-enkephalin in cm^{-1}.

45	50.9	53.8	58.8	59.9	65.8	72.5	79.5	89	90.9
98	104.2	110.2	114.4	127.4	145.8	147.1	148.4	159.5	172.5
177.3	183.3	186.6	195.7	201.5	202.5	219.4	225.7	231.9	243.1
246.1	252.2	260.8	265.4	273	274.1	279.9	287.9	293.7	309.8
314.7	321.5	327.1	330	360	361.4	364.3	385.1	385.8	388
397	402	412.9	414.6	423.1	439.1	458.1	459.8	461.4	467.4
475.7	479.7	484.1	484.2	495.1	499.4	510	519	525.2	550.8
554.6	579.4	583.1	593.1	594	622.4	632.3	636.7	651.9	664.2
672.9	686.9	702.9	706.1	719.6	724.5	726.9	739.7	783.5	786
792.1	792.5	807.3	828.4	858.9	869.8	876.4	892.5	912.9	929.9
936.8	947.8	949.8	960.8	967.6	995.3	996.7	1015.1	1019.6	1023.1
1043.6	1071.6	1088.3	1100	1121.8	1132.5	1133.8	1140.8	1161.3	1164.7
1169.8	1189.3	1210.4	1229.7	1243.2	1258.3	1283.1	1290.9	1302.4	1313.6
1330.8	1347.8	1354.6	1360.5	1364.7	1424.2	1450.9	1459	1471.8	1486.3
1504.1	1509.2	1514.5	1523.5	1558.2	1602	1680.1	1691.4	1698.2	1699
1699.5	1717.4	1720.9	1722.3	1743.6	1758.4	1800	1812.5	1860.5	1913.3
2017.2	2066.4	2099	2242.6	2306.4	2386	2484.8	2532.6	2598.5	2831.3
2841.1	2856.6	2862.8	2877.5	2884.4	2886.7	2900.8	2926.5	3027.8	3060.8
3061.8	3062.1	3062.2	3065.1	3137.3	3258	3371.4	3397.5	3716.5	3752
3836.7	4003.1	4013.5	4013.5	4094.4	4195.2	4367.7	4403.8	4422.9	4509.5
4725.5	4849.3	4978.0	5114.1	5401.4	5465.6	6151.9	6824.4		

which corresponded with the reaction co-ordinate. In each case, a frequency of ~1485 cm^{-1} was removed to correspond to the cleavage of a CC bond in the backbone of the molecules and no other adjustments to the vibrational frequencies have been made. The computer program RRKM7 used in these QET calculations in listed in Appendix 1. A second QET program (given by Allison[190]) was also available and gave similar values for $k(E)$ and used a similar amount of computer time. The use of RRKM7 in preference to the other program was a matter of personal choice.

Figure 7.2 shows plots of $\log_{10}k(E)$ against the internal energy E above E_o for the polystyrene 6-mer and for the peptide methionine-enkephalin. The number of internal modes for the polystyrene 6-mer was 288 compared with 222 for the peptide and similar dependencies of the rate constants on internal energy E and on critical energy E_o would therefore be expected. Comparison of the graphs for the two molecules reveals similar results which suggests that the use of polystyrene as a model for the larger peptides should prove reliable. Curve a is the $\log_{10}k(E)$ versus E curve corresponding to a critical energy of 0.1 eV, curve b to 2.0 eV and curve c to 4.0 eV. For fragmentation to be observed within the time-scale of a CID experiment, a rate constant is required of approximately 10^6 s^{-1} or faster. Figure 7.3 shows an expanded view of the y-axis of the $\log_{10}k(E)$ versus E curves for methionine-enkephalin shown in Figure 7.2, with the addition of curves calculated for critical energies of 0.5, 1.0 and 3.0 eV. For a reaction pathway which requires a critical energy of 0.1 eV an internal energy E above E_o of 0.07 eV gives rate constants which would result in fragmentation occurring within the experimental time-scale i.e. the curve rises above $\log_{10}k(E) = 6$. As the energy barrier to the reaction is increased the energy required above E_o becomes increasingly large. For example, with a critical energy of 4.0 eV the total internal energy required for dissociation to be sufficiently fast for observation in the mass spectrometer is predicted to be in excess of 39 eV ($E_o + E$). Typical

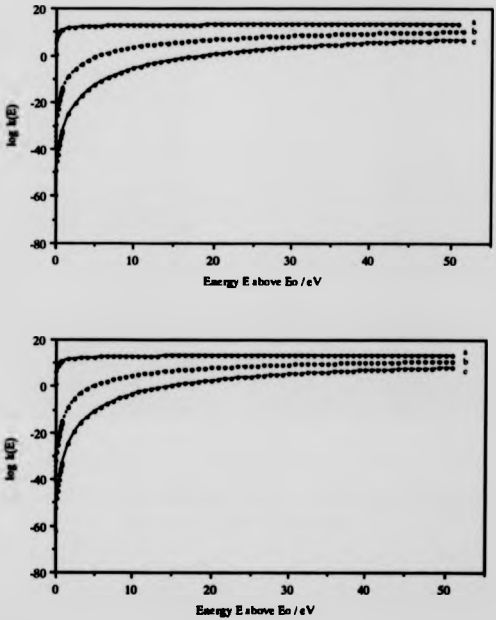

Figure 7.2 Comparison between the QET $\log_{10}k(E)$ versus E curves calculated for the polystyrene 6-mer (top) and methionine-enkephalin (bottom). Curves a, b and c correspond to critical energies E_o of 0.1, 2.0 and 4.0 eV.

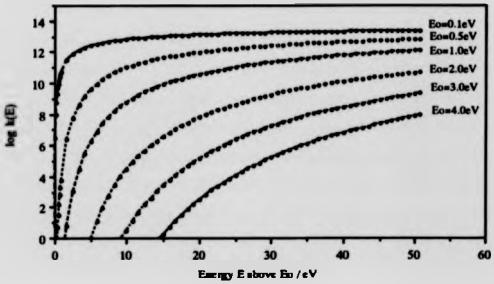

Figure 7.3 Plot of QET $\log_{10}k(E)$ versus E curves for methionine-enkephalin calculated with a range of critical energies.

bond dissociation energies for the cleavage of CC or CN bonds in the backbone of a large uncharged molecule are of the order 1 - 3 eV. On the basis of QET calculations for these critical energies, internal energy uptakes Q (E_o + E) of in excess of 15 eV would be needed for the required dissociation rates. Figure 7.4 shows a similar plot of $\log_{10}k(E)$ versus energy above E_o for the polystyrene 18-mer, the largest molecule studied. The top graph shows the full range of calculated $\log_{10}k(E)$ values and the lower graph an expanded view of the region between $\log_{10}k(E)$ = -20 and 20. When the critical energy is 0.1 eV the calculated rates are greater than 10^6 s^{-1} for values of E greater than 0.3 eV; at a value of E_o = 1.0 eV this increases to 17 eV. For further increases of the critical energy the rates are below this 10^6 s^{-1} threshold, and hence fragmentation would be too slow for observation on the experimental time-scale. Calculations with values of E above 20 - 25 eV were not possible since the density of states became too large for evaluation with the present version of the QET program. Both the reactant and transition state densities reached values of the order of 10^{309} whereupon the program terminated.

Figures 7.5 to 7.10 show how the QET $\log_{10}k(E)$ versus E curves vary with increasing mass for the polystyrene 6- to 18-mers for a fixed value of E_o. Figures 7.6 to 7.10 show two plots, the first illustrating the complete set of $\log_{10}k(E)$ versus E curves and the lower graph in each case showing a magnified view in the region of interest. Comparison of Figures 7.5 to 7.10 shows how for a fixed value of E_o the $\log_{10}k(E)$ versus E curves rise less steeply as the mass of the molecule is increased. Hence to attain a certain rate, as the mass of the molecule is increased more internal energy is required. When the critical energy is 0.1 eV (Figure 7.5) the $\log_{10}k(E)$ versus E curves for the polystyrene 6-, 12-, and 18-mers are relatively similar, with the rates reaching values in excess of 10^6 s^{-1} when the internal energy above E_o is ~0.4 eV. As the critical energy is raised the three $\log_{10}k(E)$ versus E curves become increasingly separated. At E_o=1.0eV

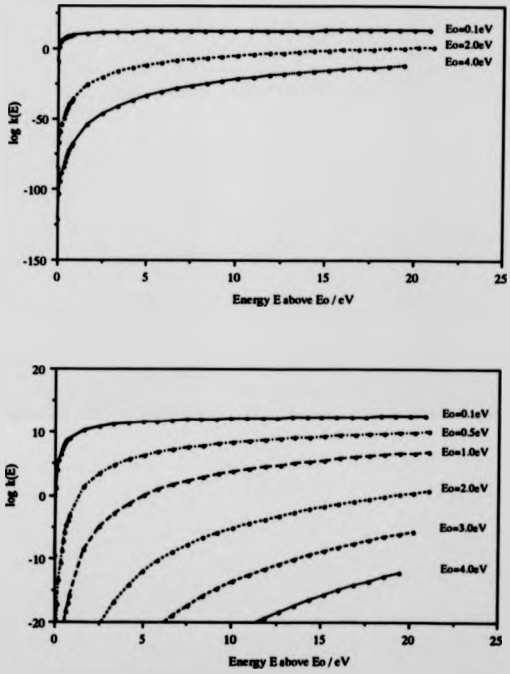

Figure 7.4 QET $\log_{10}k(E)$ versus E curves for the polystyrene 18-mer; calculated with a range of critical energies.

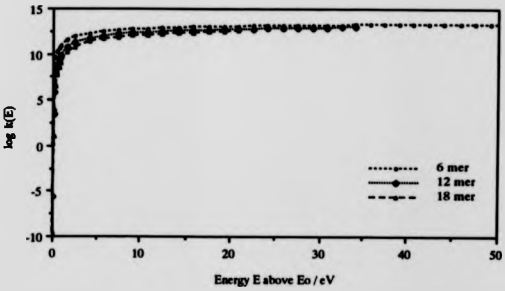

Figure 7.5 QET $\log_{10}k(E)$ versus E curves for polystyrene 6-, 12-, and 18-mers calculated for a critical energy E_0 of 0.1 eV.

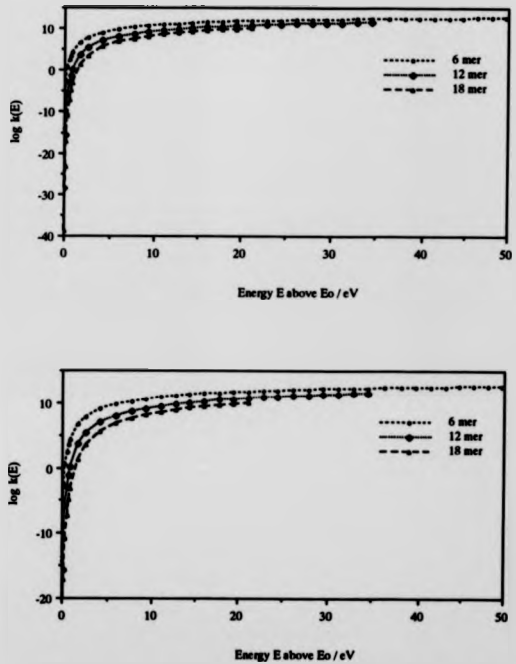

Figure 7.6 QET $\log_{10}k(E)$ versus E curves for polystyrene 6-, 12-, and 18-mers calculated for a critical energy E_o of 0.5 eV. Lower plot shows a magnified view of the top graph for the range $\log_{10}k(E)$ = 15 to -20.

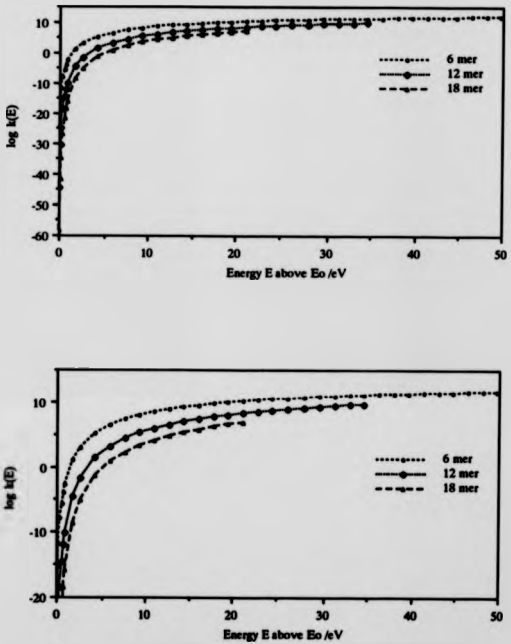

Figure 7.7 QET $\log_{10}k(E)$ versus E curves for polystyrene 6-, 12-, and 18-mers calculated for a critical energy E_o of 1.0 eV. Lower plot shows a magnified view of the top graph for the range $\log_{10}k(E)$ = 15 to -20.

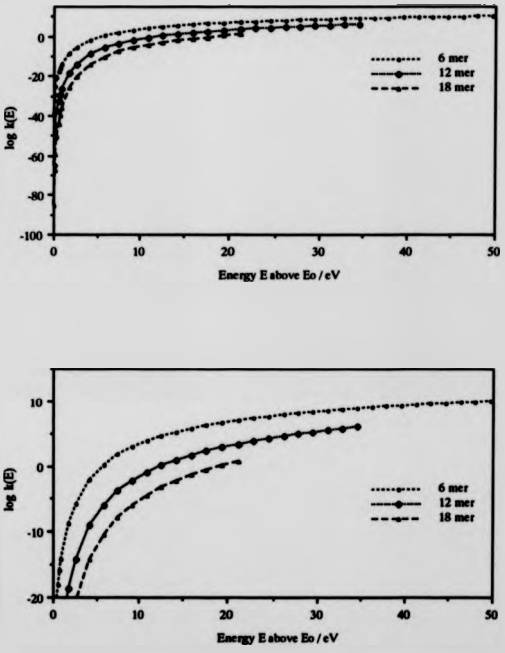

Figure 7.8 QET $\log_{10}k(E)$ versus E curves for polystyrene 6-, 12-, and 18-mers calculated for a critical energy E_o of 2.0 eV. Lower plot shows a magnified view of the top graph for the range $\log_{10}k(E)$ = 15 to -20.

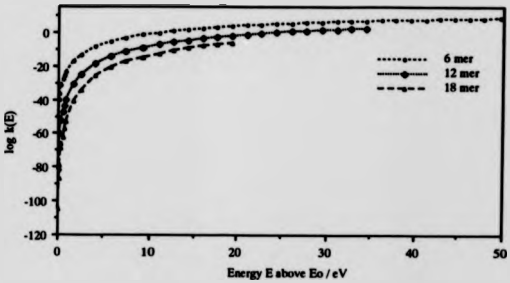

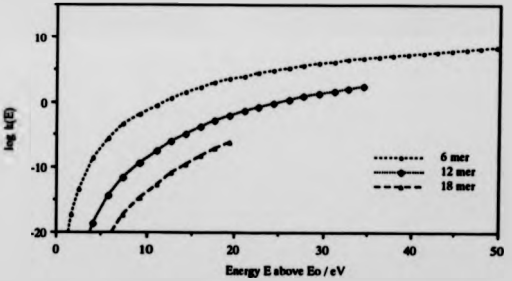

Figure 7.9 QET $\log_{10}k(E)$ versus E curves for polystyrene 6-, 12-, and 18-mers calculated for a critical energy E_o of 3.0 eV. Lower plot shows a magnified view of the top graph for the range $\log_{10}k(E)$ = 15 to -20.

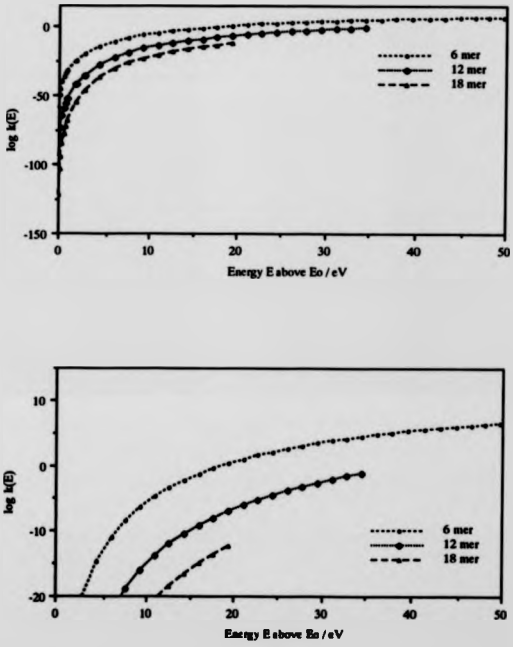

Figure 7.10 QET $\log_{10}k(E)$ versus E curves for polystyrene 6-, 12-, and 18-mers calculated for a critical energy E_o of 4.0 eV. Lower plot shows a magnified view of the top graph for the range $\log_{10}k(E)$ = 15 to -20.

(Figure 7.7) the curve for the 6-mer reaches a rate of 10^6 s^{-1} when E = 5.5 eV, and correspondingly E = 11 eV for the 12-mer and 17 eV for the 18-mer. For higher critical energies the rate constants calculated for the larger molecules become very small, even when internal energies are reasonably large. For example at E = 20 eV and a critical energy of 2.0 eV the calculated rate for the 18-mer is $10^{0.37}s^{-1}$, for E_0 = 3.0 eV this becomes $10^{-5.8}$ s^{-1}, and at E_0 = 4.0 eV the rate was found to be 10^{-12} s^{-1}. Such rates would be too slow for fragmentation to be observed within the experimental time-scale.

7.4 DISCUSSION AND CONCLUSIONS

The microcanonical rate constants calculated by QET for various polystyrene molecules illustrate the effect of increasing molecular size on the rates of dissociation. For a fixed critical energy and a given value for the internal energy content, the times taken for dissociation become increasingly long as the mass of the molecules increases, i.e. the lower energy per vibrational mode of the molecule results in much slower rates. The total internal energy of an ion prior to dissociation in a tandem mass spectrometry experiment is made up of:

i) the internal energy deposited in the ion by the desorption / ionisation process,

ii) the thermal energy of the molecule, E_T, which may be estimated from E_{aRT} = (3N-6)RT,

iii) the internal energy uptake due to collisional activation,

and it is point iii) which is of principle interest here. The internal energy uptake during FD is thought to range from a few tenths of an eV to a few eV.[170] The thermal energy content of a molecule may be estimated from E_{aRT} = (3N-6)RT and for the peptide valine-gramicidin A would be 2734 kJ/mol (28 eV) at a temperature of 400 K. This temperature is that estimated for a 25μm diameter

field desorption emitter with a heating current of 90 mA. A 25 μm diameter FD emitter requires approximately a factor of six times the heating current of a 10 μm diameter emitter and for the latter with a heating current of 15 mA a temperature of between 343 K and 373 K is reported.[145] Thermal energy calculated on the basis of (3N-6)RT has been shown to be overestimated by a factor of up to 6.[191] Turecek [191] calculated thermal energies of alkanes by integration of molar heat capacities and found good agreement with experimental data. For cholesterol at 520 K the thermal energy was found to be 2.6 eV whereas previous estimates on the basis of (3N-6)RT were 10 eV.[192] The ratio of the thermal energies calculated by heat capacities (E_H) and by (3N-6)RT, (E_{nRT}), was found to be 0.21 at 400 K for various ethylene-glycol oligomers and to vary very little with increasing numbers of internal degrees of freedom. On the basis of this ratio, a more realistic estimate of the thermal energy for valine-gramicidin A might be 5.9 eV (28eV x 0.21). Hence the total internal energy of a large ion prior to collisional with a target gas may be of the order of a few eV. At an internal energy of 5 eV, the rates of dissociation of the polystyrene 18-mer, and hence similarly for valine-gramicidin A, were of the order of 1 s^{-1} for a critical energy of 1.0 eV, and 10^{-10} s^{-1} for E_0 = 2.0 eV. These rates are consistent with experimental observations since very few metastable ions are observed in the FD-MIKE spectrum of valine-gramicidin A. In order to achieve rates sufficiently fast for dissociation to take place within the experimental time-scale, QET predicts that for a critical energy of 1.0 eV, a further 10 eV or more of internal energy would be required from collisional activation. Gross *et al.*[193] have estimated that remote charge-site fragmentation in cationised fatty alcohols requires 1.3 - 1.9 eV for bond breakage. Hence if charge remote fragmentations in peptides have similar critical energies of ~2.0 eV, an ion with 500 internal modes (for example valinomycin (RMM = 1110.6)) would require in excess of 30 eV for dissociation to take place sufficiently fast to be observed by mass spectrometry. Correspondingly for larger ions, much greater internal energies would be required possibly up to hundreds of

eV. Charge-remote fragmentations are observed in the tandem mass spectra of peptides (see Sections 3.2 and 3.3) which, on the basis of QET calculations, suggests that many tens of eV of internal energy are taken up during CID, since the thermal energy and energy deposited upon ionisation are likely to account for only a few eV of the total internal energy requirement. In Chapter 6, internal energy uptakes Q of valine-gramicidin A were calculated from the translational energy lost during CID using an impulsive collision theory (ICT) [54] based on conservation of energy and momentum. Q was estimated to be of the order of tens of eV in magnitude and this appears to agree with the estimate based upon QET calculations, although the latter tend to predict larger energy requirements - possibly hundreds of eV for larger ions at critical energies of above 2.0 eV. Previously Schlag [26] also suggested that faster than QET rates were required to describe the dissociations of large ions. If this were to be the case, then statistical redistribution of internal energy may not be taking place prior to dissociation. QET makes the assumptions that the activation and dissociation steps are separated in time, and that the internal energy taken up in the collision is statistically redistributed over all vibrational modes of the molecule. For collisions of large ions where transfers of large amounts of energy and momentum are thought to take place, the internal energy transferred and dissociation may be localised at the collision site.

Chapter 8 : CONCLUSION

Concern has been expressed about the decreasing efficiency of collision-induced decomposition (CID) for providing structural information as the masses of incident ions become increasingly large. In order to improve the internal energy uptake by these large ions it is important to gain some understanding of the mechanism of CID. The translational energy losses ΔE of parent ions in collision with target gas atoms have been used as an indication of the variation of the internal energy uptake when a number of factors are changed, such as collision energy, collision gas pressure and target gas mass. Both molecule-ions of peptides and caesium iodide cluster ions with keV incident ion energies lose several tens of eV of translational energy in collisions with helium target gas atoms. Investigations of the pressure dependence of these energy losses has shown that energy losses of these magnitudes occurred even at very low gas pressure. These results suggest that, under normal CID conditions of 60 - 80% attenuation, the numbers of collisions occurring between the ion and target are low and that the energy lost in each of these collisions is large (tens of eV). Hence multiple collisions are not expected to play a major role in CID of large ions.

Increases in incident ion energies provided the best means of increasing internal energy deposition for the MIKES experiments. Dramatic improvements in the fragmentation efficiency of CID was observed for valine-gramicidin A $[M+K]^+$ ions on increasing the incident ion energy from 8 keV to 25 keV. Increased internal energy uptakes at higher incident ion energies are consistent with energy uptake via direct momentum transfer. Increases in target gas mass and gas pressure resulted in increased ion losses although some evidence of

increased internal energy uptake was observed via the increase in the relative abundances of low-mass fragment ions. Even at higher incident ion energies a major proportion of the parent ion current results in ion losses despite the use of helium as target for which scattering of ions should not be outside the acceptance angle of the electric sector. In general, smaller values of ΔE were measured when heavier targets were used. In the cases of peptide ions ΔE values decreased by a factor of approximately two on changing the target from helium to argon, whereas for cluster ions (where the values of ΔE with helium were of a similar magnitude) changing the target to argon resulted in an order of magnitude decrease in ΔE. These results were explained using an impulsive collision theory (ICT) which predicted smaller energy uptakes for the cluster ions than for the peptides with both helium and argon targets. The fragmentation efficiencies were fairly similar for the peptides and cluster ions suggesting that, given the lower numbers of degrees of freedom in the cluster, the internal energy uptakes should be quite different.

The use of collision energies of hundreds of eV on a hybrid instrument when helium was employed as target, gave tandem mass spectra which closely resembled those obtained on a four-sector mass spectrometer when using helium as target. Differences which were present have been explained using an impulsive collision theory, with the most efficient energy transfer taking place with helium rather than argon. The improvements in the hybrid spectra achieved by using higher collision energies of hundreds rather than tens of eV, suggest that if keV collision energies could be attained in hybrids or triple quadrupole tandem mass spectrometers, then their performances could compare much more favourably with sector tandem instruments.

Dissociation rate constants calculated using quasi-equilibrium theory were very small for large ions and many tens or hundreds of eV of internal energy were found to be required for dissociation to take place on the time-scale of the CID

experiment. Although internal energy uptakes calculated by ICT, from the translational energy losses of large ions, were tens of eV in magnitude, on the basis of QET this would not be sufficient for dissociation to take in the experimental time-scale. QET assumes that energy is randomised and would result in fractions of an eV of internal energy per vibrational mode. Hence the question is raised of whether energy is totally randomised prior to dissociation or whether energy and fragmentation are localised at the site of collision.

Overall the investigations of the dynamics of CID are consistent with large amounts of energy being transferred in each collision and therefore with direct momentum transfer via vibrational excitation. An impulsive collision theory, which applies conservation of energy and momentum to the collision between the target gas atom and a single atom within the ion, goes some way toward explaining the experimental results. It is clear, however, that much is still unknown about the mechanisms of CID.

References

1 a) H. M. Rosenstock and C. E. Melton, *J. Chem. Phys.* **26**, 314 (1957).

b) W. F. Haddon and F. W. McLafferty, *J. Am. Chem. Soc.* **90**, 4745 (1968).

c) K. R. Jennings, *Int. J. Mass Spectrom. Ion Phys.* **1**, 227 (1968).

2 H. D. Beckey, *Adv. Mass Spectrom* **2**, 1 (1963).

3 M. Barber, R. S. Bordoli, R. D. Sedgewick, A. N. Tyler, *J. Chem. Soc., Chem. Commun.* 325 (1981).

4 D. F. Torgeson, R. P. Skrowronski, R. D. MacFarlane, *Biochem. Biophys. Res. Commun.* **60**, 616 (1974).

5 K. L. Busch, G. L. Glish and S. A. McLuckey, *Mass Spectrometry/Mass Spectrometry*, VCH, New York (1988).

6 K. B. Tomer, *Mass Spectrom. Rev.* **8**, 483 (1989).

7 K. B. Tomer, *Mass Spectrom. Rev.* **8**, 445 (1989).

8 A. E. Ashcroft and P. J. Derrick, in *Mass Spectrometry of Pepsides*, ed. by D. M. Desiderio, CRC Press, Boca Raton, Florida (1990).

9 K. Biemann, *Biomed. Environ. Mass Spectrom.* **16**, 99 (1988).

10 M. Hamdan and O. Curcuruto, *Int. J. Mass Spectrom. Ion Proc.* **108**, 93 (1991).

11 J. B. Fenn, M. Mann, C. -K. Meng, S. -F. Wong and C. M. Whitehouse, *Science* **246**, 64 (1989).

12 J. B. Fenn, M. Mann, C. -K. Meng and S. -F. Wong, *Mass Spectrom. Rev.* **9**, 37 (1990).

13 M. Karas, A. Ingendoh, U. Bahr, F. Hilenkamp, *Biomed. Environ. Mass Spectrom.* **18**, 841 (1989).

14 See for example ; M. L. Gross, K. B. Tomer, R.L. Cerny and D. E. Giblin, in *Mass Spectrometry in the Analysis of Large Molecules*, ed. by C. J. McNeal, p. 171, John Wiley and Sons, Chichester (1986).

15 A. K. Shukla. K. Qulan, S. L. Howard, S. G. Anderson, K. W. Sohlberg and J. H. Futrell, *Int. J. Mass Spectrom. Ion Proc.* **92**, 147 (1989).

16 K. Levsen and H. Schwarz, *Mass Spectrom. Rev.* **2**, 77 (1983).

17 M. S. Kim, *Org. Mass Spectrom.* **26**, 565 (1991).

18 J. Bordas-Nagy and K. R. Jennings, *Int. J. Mass Spectrom. Ion Proc.* **100**, 105 (1990).

19 C. D. Bradley and P. J. Derrick, *Mass Spectrom. Rev.* in preparation.

20 W. Forst, *Theory of Unimolecular Reactions*, Academic Press, New York (1973).

21 P. J. Robinson, K. A. Holbrook, *Unimolecular Reactions*, John Wiley and Sons, London, (1972).

22 H. M. Rosenstock, M. B. Wallenstein, A. L. Wahrhaftig and H. Eyring, *Proc. Natl. Acad. Sci. U. S.* **38**, 667 (1952).

23 R. A. Marcus and O. K. Rice, *J. Phys. Coll. Chem.* **55**, 894 (1951).

24 F. W. McLafferty and H. D. R. Schuddemage, *J. Am. Chem. Soc.* **91**, 1886 (1969).

25 a) J. D. Rynbrandt and B. S. Rabinovitch, *J. Chem. Phys.* **41**, 280 (1964).

b) J. D. Rynbrandt and B. S. Rabinovitch, *J. Chem. Phys.* **42**, 1624 (1965).

26 E. W. Schlag and R. D. Levine, *Chem Phys. Lett.* **163**, 523 (1989).

27 D. L. Bunker and F-M. Wang, *J. Am. Chem. Soc.* **99**, 7457 (1977).

28 A. G. Craig and P. J. Derrick, *J. Am. Chem. Soc.* **107**, 6707 (1985).

29 J. A. Loo, C. G. Edmonds and R. D. Smith, *Anal. Chem.* **63**, 2488 (1991).

30 A. L. Rockwood, M. Busman and R. D. Smith, *Int. J. Mass Spectrom. Ion Proc.* in press.

31 See for example; T. Wachs and F. W. McLafferty, *Int. J. Mass Spectrom. Ion Phys.* **23**, 243 (1977).

32 R. G. Cooks, J. H. Beynon, R. M. Caprioli and G. R. Lester, *Metastable Ions*, Elsevier, Amsterdam (1973).

33 C. A. McDowell, *Mass Spectrometry*, McGraw-Hill, New York (1963).

34 J. H. Beynon, M. Bertrand E. G. Jones and R. G. Cooks, *J. Chem. Soc. Chem. Commun.* 341 (1972).

35 F. W. McLafferty, P. F. Bente III, R. Kornfield, S. -C. Tsai and I. Howe, *J. Am. Soc. Mass Spectrom.* **95**, 2120 (1973).

36 R. G. Cooks, L. Hendricks and J. H. Beynon, *Org. Mass Spectrom.* **10**, 625 (1975).

37 R. G. Cooks, *Collision Spectroscopy*, Plenum Press, New York (1978).

38 H. Yamaoka, D. Pham and J. Durup, *J. Chem. Phys.* **51**, 3465 (1969).

39 H. S. W. Massey, *Rep. Prog. Phys.* **12**, 248 (1949).

40 H. S. W. Massey and E. H. S. Burhop, *Electronic and Ionic Impact Phenomena*, Oxford University Press, Oxford (1952).

41 J. B. Hasted, *Proc. R. Soc. London Ser. A* **205**, 421 (1951).

42 J. Fayeton, A. Pernot, P. Fournier and M. Barat, *Le Journal de Physique* **32**, 743 (1971).

43 R. K. Boyd, E. E. Kingston, A. G. Brenton and J. H. Beynon, *Proc. R. Soc. Lond. A* **392**, 59 (1984).

44 B. H. Mahan, *J. Chem. Phys.* **52** (10), 5521 (1970).

45 A. Russek, *Physica* **48**, 165 (1970).

46 a) J. L. Franklin, *Ion-Molecule Reactions*, Plenum Press, New York (1972).

b) P. Ausloos (Ed.), *Interactions Between Ions and Molecules, NATO Advanced Study Institute, Ser. B: Physics*, Vol. 6, Plenum Press, New York (1975).

c) M. T. Bowers, *Gas Phase Ion Chemistry*, Academic Press, New York (1979).

d) P. Ausloos (Ed.), *Kinetics of Ion-Molecule Reactions, NATO Advanced Study Institute, Ser. B: Physics*, Vol. 40, Plenum Press, New York (1979).

47 G. Gioumousis and D. P. Stevenson, *J. Chem. Phys.* **29**, 294 (1958).

48 a) T. F. Moran, W. H. Hamill, *J. Chem. Phys.* **29**, 294 (1958).

b) S. K. Gupta, E. G. Jones, A. G. Harrison and J. J. Myher, *Can. J. Chem.* **45**, 3107 (1967).

49 T. E. Su and M. T. Bowers, *J. Chem. Phys.* **58**, 3027 (1973).

50 T. E. Su, C. F. Su, M. T. Bowers, *J. Chem. Phys.* **69**, 2243 (1978).

51 J. C. Light and J. Lin, *J. Chem. Phys.* **43**, 3209 (1965).

52 R. A. Barker, D. P. Ridge, *J. Chem. Phys.* **64**, 4411 (1976).

53 E. T. -Y. Hsieh and A. W. Castleman, *Int. J. Mass Spectrom. Ion Phys.* **40**, 295 (1981).

54 E. Uggerud and P. J. Derrick, *J. Phys. Chem.* **95**, 1430 (1991).

55 R. K. Boyd, *Int. J. Mass Spectrom. Ion Proc.* **78**, 243 (1987).

56 J. A. Laramée, D. Cameron and R. G. Cooks, *J. Am. Chem. Soc.* **103**, 12 (1981).

57 C. E. D. Ouwerkerk, S. A. McLuckey, K. J. Kistemaker and A. J. H. Boerboom, *Int. J. Mass Spectrom. Ion Proc.* **56**, 11 (1984).

58 J. M. Curtis, L. S. Rong, R. M. Milberg and K. L. Rinehart, paper presented at the 36th ASMS Conference on Mass Spectrometry and Allied Topics, San Francisco (1988).

59 J. Bordas-Nagy, D. Despeyroux and K. R. Jennings, paper presented at the 12th International Mass Spectrometry Conference, book of abstracts p. 209, Amsterdam (1991).

60 G. M. Neumann and P. J. Derrick, *Org. Mass Spectrom.* **19** (4), 165 (1984).

61 G. M. Neumann, M. M. Sheil and P. J. Derrick, *Z. Naturforsch*, **39a**, 584 (1984).

62 D. L. Bricker and D. H. Russell, *J. Am. Chem. Soc.* **108**, 6174 (1986).

63 R. Guevremont and R. K. Boyd, *Rapid Commun. Mass Spectrom.* **2** (1), 1 (1988).

64 D. H. Russell, paper presented at the 37th ASMS Conference on Mass Spectrometry and Allied Topics, Miami Beach, Florida, (1989).

65 D. H. Russell and D. L. Bricker, *Anal. Chim. Acta* **178**, 117 (1985).

66 A. J. Alexander, P. Thibault and R. K. Boyd, *J. Am. Chem. Soc.* **112**, 2484 (1990).

67 C. D. Bradley, J. M. Curtis, M. M. Sheil and P. J. Derrick, *J. Chem. Soc. Faraday*, in preparation

68 M. M. Sheil and P. J. Derrick, *Org. Mass Spectrom.* **23**, 429 (1988).

69 M. M. Sheil, Ph. D. thesis, University of New South Wales, Australia (1987).

70 G. M. Neumann, Ph. D. thesis, La Trobe University, Australia (1983).

71 R. G. Gilbert, M. M. Sheil and P. J. Derrick, *Org. Mass Spectrom.* **20**, 430 (1985).

72 B. Spengler, D. Kirsch and R. Kaufmann, paper presented at the 12th International Mass Spectrometry Conference, book of abstracts p. 292, Amsterdam (1991).

73 S. E. Kupriyanov and A. A. Perov, *Z. Tech. Fiz.* **33**, 823 (1963).

74 P. J. Todd and F. W. McLafferty, *Int. J. Mass Spectrom. Ion Proc.* **38**, 371 (1981).

75 C. D. Bradley and P. J. Derrick, *Org. Mass Spectrom.* **26**, 395 (1991).

76 Personal communication.

77 R. E. Tecklenburg, L. S. Hann and D. H. Russell, *Int. J. Mass Spectrom. Ion Proc.* **87**, 111 (1989).

78 M. S. Kim, *Int. J. Mass Spectrom. Ion Phys.* **50**, 189 (1983).

79 M. S. Kim, *Int. J. Mass Spectrom. Ion Phys.* **51**, 279 (1983).

80 S. A. Martin, R. S. Johnson, C. E. Costello and K. Biemann, In "The Analysis of Peptides and Proteins by Mass Spectrometry," Ed. C. J.McNeal, John Wiley and Sons, Chichester, 1988, p. 135.

81 R. S. Johnson, S. A. Martin and K. Biemann, *Int. J. Mass Spectrom. Ion Proc.* **86**, 137 (1988).

82 C. Wesdemiotis, M. M. Cordero and M. J. Polce, paper presented at the 39th ASMS Conference on Mass Spectrometry and Allied Topics, Nashville (1991).

83 D. J. Douglas, *J. Phys. Chem.* **86**, 185 (1982).

84 J. C. Light, *Discuss. Faraday Soc.* **44**, 14 (1967).

85 W. Eastes and J. P. Toennies, *J. Chem. Phys.* **70**, 1644 (1979).

86 L. Poulter and L. C. E. Taylor, *Int. J. Mass Spectrom. Ion Proc.* **91**, 183 (1989).

87 A. J. Alexander, P. Thibault, R. K. Boyd, J. M. Curtis and K. L. Rinehart, *Int. J. Mass Spectrom. Ion Proc.* **98**, 107 (1990).

88 M. F. Bean, S. A. Carr, G. C. Thorne, M. H. Reilly and S. J. Gaskell, *Anal. Chem.* **63**, 1473 (1991).

89 A. J. Alexander, P. Thibault and R. K. Boyd, *Rapid. Commun. Mass Spectrom.* **3**, 30 (1989).

90 H. D. Beckey, G. Hoffman, K. Maurer and H. U. Winkler, *Adv. Mass Spectrom.* **5**, 626 (1971).

91 H. U. Winkler and H. D. Beckey, *Biochem. Biophys. Res. Commun.* **46**, 391 (1972).

92 H. U. Winkler, R. J. Beuhler and L. Friedman, *Biomed. Mass Spectrom.* **3**, 201 (1972).

93 S. Ansante-Poku, G. W. Wood, G. Perseo, B. Danieli and R. Rubino, *Biomed. Mass Spectrom.* **2**, 121 (1975).

94 H. -R. Schulten, *Int. J. Mass Spectrom. Ion Phys.* **32**, 97 (1979).

95 R. Weber and K. Levsen, *Biomed. Mass Spectrom.* **7**, 314 (1980).

96 T. Matsuo, H. Matsuda, I. Katakuse, Y. Shimonishi, Y. Maruyama, T. Higuchi and E. Kubota, *Anal. Chem.* **53**, 416 (1981).

97 S. J. Gaskell (Ed.), *Mass Spectrometry in Biomedical Research*, John Wiley and Sons, Chichester (1986).

98 C. J. McNeal (Ed.), *The Analysis of Peptides and Proteins by Mass Spectrometry*, John Wiley and Sons, Chichester (1988).

99 D. M. Desiderio (Ed.), *Mass Spectrometry of Peptides*, CRC Press, Boca Raton, Florida (1990).

100 J. A. Loo, C. G. Edmonds and R. D. Smith, *Science* **248**, 201 (1990).

101 P. Roepstorff and J. H. Fohlman, *Biomed. Environ. Mass Spectrom.* **11** (11), 601 (1984).

102 R. S. Johnson and K. Biemann, *Biomed. Environ. Mass Spectrom.* **18**, 945 (1989).

103 D. Zidarov, P. Thibault, M. J. Evans and M. Bertrand *Biomed. Environ. Mass Spectrom.* **19**, 13 (1990).

104 R. Feng, F. Bouthillier, Y. Konishi and M. Cygler, Presented at 39th Annual Conference on Mass Spectrometry and Allied Topics, book of abstracts p. 1159, Nashville (1991).

105 M. Karas, U. Bahr, A. Igendoh and F. Hillenkamp, *Angew. Chem. Int. Ed. Engl.* **6**, 28 (1989).

106 P. G. Cullis, G. M. Neumann, D. E. Rogers and P. J. Derrick, *Adv. Mass Spectrom.* **8**, 1729 (1980).

107 Edwards High Vacuum International, Manor Royal, Crawley, West Sussex, RH1 2LW, U. K. Model numbers;

a) Diffstak 160/170 C
b) Cryo cooled diffstak CR160/700 M (collision cell)
c) Diffstak 63/150 M

108 Edwards High Vacuum International, Manor Royal, Crawley, West Sussex, RH1 2LW, U. K. Model numbers;

a) Two stage rotary pump E3M40 (source, collision cell and ESA)
b) Rotary pump EDM12 (pre-magnetic sector)
c) Rotary pump ES200 (post-magnetic sector and pre- and post-collision cell)
d) Rotary pump ES330 (detector)
e) Rotary pump ED330

109 Edwards High Vacuum International, Manor Royal, Crawley, West Sussex, RH1 2LW, U. K. Model numbers;

a) Ionisation guage head IGSG
b) Guage Ion 7

110 Edwards High Vacuum International, Manor Royal, Crawley, West Sussex, RH1 2LW, U. K. Model numbers;

a) Pirani guage head PR10S
b) Pirani guage head PR10K (collision cell)
c) Pirani guage head PR25K
d) Pirani guage PR11
e) Pirani guage PR10
f) Pirani guage PR14

111 Du Pont Chemical Company, Plastic products and resins department, Vespel marketing section, Wilmington, Delaware 19898, U. S. A.

112 Spellman High Voltage Electronics Corporation, 7 Fairchild Avenue, Plainview NY11803, U. S. A. Model numbers; RHSR series.

113 Ion Tech Ltd., 2 Park Street, Teddington, Middlesex, TW11 OLT, U. K. Model numbers; Fine beam fast atom saddle field gas gun FAB11N and B50 power supply.

114 S. C. Davis, Ph. D Thesis, University of New South Wales, Australia, 1988.

115 The Materials Business, Corning Glass Works, Corning, New York 14830, U. S. A.

116 J. H. J. Dawson, Sydney, Australia (1985).

117 M. G. Darcy, D. E. Rogers and P. J. Derrick, *Int. J. Mass Spectrom. Ion Phys.* 27, 335 (1978).

118 D. E. Rogers, Ph. D. Thesis, La Trobe University, Australia (1980).

119 Alpha Scientific Inc., 25393 Huntwood Avenue, Hayward, California 94544, U. S. A. Model number; 3038M current regulated power supply 80A@60 V DC.

120 P. G. Cullis, Ph. D. Thesis, University of New South Wales, Australia (1984).

121 Granville-Phillips Company, 5675 East Arapahoe Avenue, Boulder, Colorado 80803, U. S. A. Model number; series 203 variable leak.

122 Swagelock Company, Solon, Ohio 44139, U. S. A. Model number; Quickconnect series QC6.

123 R. F. Herzog, *Z. Naturforsch. Teil A* 10, 887 (1955).

124 H. Matsuda, *Int. J. Mass Spectrom. Ion Phys.* 22, 95 (1976).

125 John Fluke Manufacturing Corporation, P. O. Box 43210, Mountlake Terrace, Washington, 98043, U. S. A. Model number; 415B.

126 ETP Oxford Pty. Ltd., P. O. Box 105, Ermington, New South Wales, Australia. Model number; AEM-1000.

127 Digital Equipment Corporation, Australia P.O. Box 384, Chatswood N.S.W. 2067
a) Model numbers;
b) PDP11-LSI11/23 BC
c) RLV22-AK (hard disks)
FPF11 (floating point processor)

128 Watanabe Instruments Corporation, 3-19-6 Nishi-shinagawa, Shinagawa-ku, Tokyo, Japan. Model number; WX4671.

129 J. R. Chapman, *Practical Organic Mass Spectrometry*, John Wiley and Sons, Chichester (1985).

130 a) H. Hintenberger and L. A. König, *Z. Naturforsch* **12a**, 773 (1957).

b) H. Hintenberger and L. A. König, in *Advances in Mass Spectrometry*, ed. by J. H. Waldron, p. 16, Pergamon Press, New York (1959)

c) H. Hintenberger and L. A. König, *Z. Naturforsch* **11a**, 1039 (1956).

d) H. Hintenberger and L. A. König, *Z. Naturforsch* **12a**, 140 (1957).

131 M. J. Lacey, C. G. MacDonald, K. F. Donchi and P. J. Derrick, *Org. Mass Spectrom.* **16**, 351 (1981).

132 A. J. Alexander, P. Thibault, R. Guevremont and R. K. Boyd, *Rapid Commun. Mass Spectrom.* **2**, 79 (1988).

133 B. A. Rumpf, C. E. Allison and P. J. Derrick, *Org. Mass Spectrom.* **21**, 295 (1986).

134 Kratos Analytical, Barton Dock Road, Urmston, Manchester, U. K.

135 S. C. Davis, G. M. Neumann and P. J. Derrick, *Anal. Chem.* **59**, 1360 (1987).

136 J. H. Beynon , F. M. Harris, B. N. Green and R. H. Bateman, *Org. Mass Spectrom.* **17**, 55 (1982).

137 R. K. Boyd and J. H. Beynon, *Org. Mass Spectrom.* **12**, 163 (1977).

138 K. R. Jennings and R. S. Mason, in *Tandem Mass Spectrometry*, ed. by F. W. McLafferty, John Wiley and Sons, Chichester (1983).

139 R. K. Boyd, D. J. Harvan and J. R. Haas, *Int. J. Mass Spectrom. Ion Proc.* **68**, 273 (1985).

140 Data General Corporation, Westboro, Massachusetts 01580, U.S.A. Model number; Data General DG30

141 Sun Microsystems Limited, Citygate Cross Street, Sale, Cheshire M33 4BT, U. K. Model number; Sparc station IPC.

142 Macpromass, Version 1.05, 1989, T. D. Lee and S. Vemuri, Division of Immunology, Beckman Research Institute of the City of Hope, 1450 East Duarte Road, Duarte CA 91010, U. S. A.

143 T. D. Lee and S. Vemuri, *Biomed. Environ. Mass Spectrom.* **19**, 639 (1990).

144 H. D. Beckey, *Int. J. Mass Spectrom. Ion Phys.* **2**, 500 (1969).

145 L. Prokai, *Field Desorption Mass Spectrometry*, Marcel Dekker, New York (1990).

146 H. D. Beckey, *Principles of Field Ionization and Field Desorption Mass Spectrometry*, Pergamon Press, Oxford (1977).

147 H. D. Beckey, E. Hilt and H. -R. Schulten, *J. Phys. E. Sci.* **6**, 1043 (1973).

148 Mass Spectrometry Enterprises, 23 New Mount Street, Manchester, M4 4DE, U. K. Reference number; emitter base KR4.

149 Advent Research Materials Limited, Blyth Road Industrial Estate, Halesworth, Suffolk, IP19 8DD, U. K. Reference number; W 557318.

150 Aldrich Chemical Company Limited, The Old Brickyard, New Road, Gillingham, Dorset SP8 4JL, U. K.

151 Brandenburg Limited, 939 London Road, Thornton Heath, Surrey, CR4 6JE, U. K. Model number; Alpha series II.

152 DI-AN Micro Systems Limited, Mersey House, Battersea Road, Heaton Mersey Industrial Estate, Stockport, Cheshire, SK4 3EA, U. K. Model number; DM5541.

153 T. -W. D. Chan, A. W. Colburn, D. S. Alderdice and P. J. Derrick *Int. J. Mass Spectrom. Ion Proc.* **107**, 491 (1991).

154 Sigma Chemical Company Limited, Fancy Road, Poole, Dorset, BH17 7NH, U. K.

155 E. Uggerud, Department of Chemistry, University of Oslo, P. O. Box 1033, Blindern, N-0315 Oslo 3, Norway.

156 E. B. Wilson Jr., J. C. Decius and P. C. Cross, *Molecular vibrations*, McGraw Hill, New York (1955).

157 L. A. Woodward, *Introduction to the theory of molecular vibrations and vibrational spectroscopy*, Oxford University Press, Oxford (1972).

158 S. Nordholm, Chalmers, Göteborg, Sweden.

159 J. H. Beynon and J. R. Gilbert, *Application of Transition State Theory to Unimolecular Reactions*, John Wiley and Sons, Chichester (1984).

160 T. Beyer and D. F. Swinehart, *Commun. Assoc. Comput. Machin.* **16**, 379 (1973).

161 K. B. Tomer, L. J. Deterding and C. Guenat, *Biol. Mass Spectrom.* **20**, 121 (1991).

162 D. H. Russell, E. S. McGlohan and L. M. Mallis, *Anal. Chem.* **60**, 1818 (1988).

163 R. P. Grese, R. L. Cerny and M. L. Gross, *J. Am. Chem. Soc.* **111**, 2835 (1989).

164 L. M. Teesch and J. A. Adams, *J. Am. Chem. Soc.* **112**, 4110 (1990).

165 W. Kulik, W. Heerma and J. K. Terlouw, *Rapid Commun. Mass Spectrom.* **3**, 276 (1989).

166 D. Renner and G. Spiteller, *Biomed. Environ. Mass Spectrom.* **15**, 75 (1988).

167 R. S. Johnson, S.A. Martin, K. Biemann, J. T. Stults and J. T. Watson, *Anal. Chem.* **59**, 2261 (1987).

168 F. W. McLafferty, *Anal. Chem.* **31**, 2072 (1959).

169 F. H. Field and J. R. Franklin, *Electron Impact Phenomena*, Academic Press, New York (1970).

170 W. Brand and K. Levsen, *Int. J. Mass Spectrom Ion Phys.* **35**, 1 (1980).

171 J. M. Curtis, C. D. Bradley, P. J. Derrick and M. M. Sheil, *Org. Mass Spectrom.* In press, due for publication April 1992.

172 M. M. Sheil, M. Guilhaus and P. J. Derrick, *Org. Mass Spectrom.* **25**, 671 (1990).

173 R. P. Grese and M. L. Gross, *J. Am. Chem. Soc.* **112**, 5098 (1990).

174 B. C. Das, P. Varenne and A. Taylor, *J. Antibiotics* **32**, 569 (1979).

175 L. M. Mallis and D. H. Russell, *Anal. Chem.* **58**, 1076 (1986).

176 S. C. Davis and B. Wright, *Rapid Commun. Mass Spectrom.* **4**, 186 (1990).

177 C. D. Bradley, J. M. Curtis, P. J. Derrick and B. Wright, *Anal. Chem.* submitted for publication.

178 M. Barber, M. Morris, L. Tetler, M. Woods, J. Monaghan and W. E. Morden, paper presented at the British Mass Spectrometry Society Meeting, Nottingham (1989).

179 S. C. Davis, V. Natoli, G. M. Neumann and P. J. Derrick, *Int. J. Mass Spectrom. Ion Proc.* **78**, 17 (1987).

180 R. B. Cody, I. J. Amster, F. W. McLafferty, *Proc. Natl. Acad. Sci. USA*, **82**, 6367 (1985).

181 A. J. Alexander, P. Thibault and R. K. Boyd, *Rapid Commun. Mass Spectrom.* **3**, 267 (1989).

182 L. C. E. Taylor, D. Hazelby and D. Wakefield, *Int. J. Mass Spectrom. Ion Phys.* **46**, 407 (1983).

183 Cambridge Crystallographic Data Centre, Cambridge, CB2 1EW, U. K.. Reference code FABJIB

184 J. F. Griffin, D. A. Langs, G. D. Smith, T. L. Blundell, I. J. Tickle and S. Bedarkar, *Proc. Natl. Acad. Sci. USA*, **83**, 3272 (1986).

185 J. H. Schachtschneider and R. G. Snyder, *Spectrochimica Acta* **19A**, 117 (1963).

186 G. Herzberg, *Molecular Spectroscopy and Molecular Structure. II Spectra of Diatomic Molecules*, D. Van Nostrand Company, Canada (1945).

187 W. Gordy, *J. Chem. Phys.* **14**, 305 (1946).

188 J. Jakes and S. Krimm, *Spectrochimica Acta* **27A**, 19 (1971).

189 M. Ohsaku, Y. Shiro and H. Murata, *Bull. Chem. Soc. Japan* **46**, 1399 (1973).

190 C. E. Allison, Ph. D. thesis, University of New South Wales, Australia (1986).

191 F. Turecek, *Org. Mass Spectrom.* **26**, 1074 (1991).

192 A. Amirav, *Org. Mass Spectrom.* **26**, 1 (1991).

193 J. Adams and M. L. Gross, *J. Am. Chem. Soc.* **108**, 6915 (1986).

This thesis was prepared in accordance with the University of Warwick Department of Chemistry guidelines (October 1989).

Appendix 1 : Listing of computer program RRKM7

```
C     A RRKM PROGRAM FOR NONLINEAR MOLECULES AND ACTIVATED
C     COMPLEXES ALLOWING FOR VIBRATIONAL STATES ONLY (ROTATIONS
C     NEGLECTED).
C
C     THIS PROGRAM IS SUITABLE FOR J=0 REACTIONS WITH J-CONSERVATION
C     ACCOUNTED FOR. PROVISION FOR RHO(E) SMOOTHING EXISTS TO APPROACH
C     AN ERGODIC SPECTRUM FOR THE REACTANT.
C
C     original program from Sture Nordholm, Chalmers, Goeteborg.
C     revised unix version for large scale calculations by
C     Einar Uggerud, Department of Chemistry, University of
C     Oslo.   Warwick 19. May 1988.
C     eu190588
C     Further amendments made by Caroline Bradley 1989-91.
C*****************************************************************
C     THE INPUT SHOULD BE IN THE FOLLOWING FORMAT
C     LINE 1    NAME OF THE OUTPUT FILE FOR THE ENERGY AND RATE
C               CONSTANT DATA. OTHER DATA INCLUDING DENSITY OF
C               STATES WILL BE SENT TO THE TERMINAL UNLESS
C               OTHERWISE DIRECTED
C     LINE 2    VALUES FOR;
C        NN     THE NUMBER OF ENERGY STEPS TO THE CRITICAL ENERGY
C        NM     TOTAL NUMBER OF ENERGY STEPS
C        T      TEMPERATURE IN KELVIN
C        EO     THE CRITICAL ENERGY IN cm-1
C        WCC    COLLISION FREQUENCY IN s-1
C        NSS    =0 FOR RHO SMOOTHING OFF
C               =1 FOR RHO SMOOTHING ON
C     LINE 3    ES - ENERGY INTERVAL FOR SMOOTHING OF k(E)    CURVE
C     LINE 4    KN = 1 FOR QUANTUM MECHANICAL k(E)
C               = 0 FOR CLASSICAL k(E)
C     LINE 5    NUMBER OF REACTANT FREQUENCIES
C     LINE 6    REACTANT VIBRATIONAL FREQUENCIES IN ASCENDING ORDER
C               ON LINES 1-100. FOLLOWED BY NF-1 TRANSITION STATE
C               FREQUENCIES, LINES 101-200. EXCESS LINES READ 0.D0
C*****************************************************************
C     Other variables used in the program are defined as follows.
C     F(I)  THE Ith FREQUENCY
C     F(1) to F(1400) are reactant frequencies
C     F(1401) to F(2800) are activated complex frequencies
C     RHO   Density of states for the reactant
C     W     Density of states for the transition state
C     EMAX  Maximum energy to be calculated
C     DE    Internal energy
C     KA    Rate constant
C     DKL   Log10 of rate constant
C
C
C*****************************************************************
C
      PROGRAM RRKM
      IMPLICIT double precision(A-H,O-Z)
      double precision RHO(0:80000),W(0:80000),AK(0:80000),PT(0:80000)
      double precision RHB(0:80000),DKL(0:80000),AKL(0:80000)
      double precision F(2800),WW(40),EKW(40)
```

```
      real tarray(2)
      character tab
      character*12 filnavn
      ellenti=log(10.0)
C
C     READ IN THE VARIABLES
C
      READ(5,111) filnavn
111   FORMAT(a12)
      OPEN(7,file=filnavn,status='unknown',form='formatted',
     1     access='sequential')
      TAB = '  '
      READ(5,*) NN,NM,T,E0,WCC,NSS
      READ(5,*) ES
      READ(5,*) KN
      READ(5,*) NF
      READ(5,*) (F(I),I=1,NF)
      READ(5,*) (F(I),I=1401,1399+NF)
10    FORMAT(D16.6)
20    CONTINUE
C     WRITE(6,*) 'REACTANT FREQUENCIES'
C     WRITE(6,10) (F(I),I=1,NF)
C     WRITE(6,*) 'ACTIVATED COMPLEX FREQUENCIES'
C     WRITE(6,10) (F(I),I=1401,1399+NF)
C
C     OBTAIN ENERGY STEP LENGTH
      DE=E0/NN
C     CALCULATE THE NUMBER OF ENERGY INTERVALS REQUIRED
C     FOR SMOOTHING k(E)
      NES=IDNINT(ES/DE)
C
C     OBTAIN DENSITY OF REACTANT STATES RHO BY DIRECT COUNT.
C     INITIALIZE RHO. NOTE THAT RHO(E)=RHO(K)/DE.
C
      DO 30 K=0,NM
      RHO(K)=0.D0
30    CONTINUE
C     FOLD IN VIBRATIONS CONSECUTIVELY.
      RHO(0)=1.D0
      EMAX=NM*DE
      DO 40 K=1,NF
C     THE FREQUENCY IS DISCRETIZED BELOW.
      NR=IDNINT(F(K)/DE)-1
      F(K)=(NR+1)*DE
      DO 50 I=0,NR
      LMAX=IDINT(EMAX/F(K))
      RHH=RHO(I)
      DO 60 J=1,LMAX
      L=IDNINT((I*DE+J*F(K))/DE)
      RHO(L)=RHO(L)+RHH
      RHH=RHO(L)
60    CONTINUE
50    CONTINUE
40    CONTINUE
62    CONTINUE
      DO 65 I=1,NM
      RHH(I)=RHO(I)
65    CONTINUE
C
C     APPLY RHO SMOOTHING IF REQUIRED ie NSS=1
C
      IF(NSS.EQ.0) GO TO 120
      KK=0
```

```
 70   KK=KK+1
C     APPLY SIMPLE 1-1-1 NEAREST NEIGHBOUR SMOOTHING.
      RR1=RHB(0)
      DO 80 I=1,NM-1
      RR2=RHB(I)
      RR3=RHB(I+1)
      RHB(I)=(RR1+RR2+RR3)/3.D0
      RR1=RR2
 80   CONTINUE
      IF(KK.LT.NES) GO TO 70
120   IF(NSS.EQ.2) GO TO 240
C
C     CALCULATE CLASSICAL KA(E) IF REQUIRED ie KN=0
C
      IF(KN.EQ.1) GO TO 138
C     CALCULATE QM ZERO POINT ENERGY AND FREQUENCY RATIO.
      EZP=0.D0
      FR=1.D0
      DO 122 I=1,NF
      EZP=EZP+F(I)/2
      FR=FR*F(I)
      IF(I.GE.NF) GO TO 122
      FR=FR/F(I+1400)
122   CONTINUE
C
C     OBTAIN VIBRATIONAL DENSITY OF STATES OF THE ACTIVATED COMPLEX.
C     F(1401) TO F(2800) ARE ACTIVATED COMPLEX FREQUENCIES.
C
138   CONTINUE
      W(0)=1.D0
      DO 139 I=1,NM-NN+1
      W(I)=0.D0
139   CONTINUE
      DO 140 K=1401,NF+1399
      NR=IDNINT(F(K)/DE)-1
      F(K)=(NR+1)*DE
      DO 150 I=0,NR
      LMAX=IDINT((EMAX-E0)/F(K))
      RHH=W(I)
      DO 160 J=1,LMAX
      L=IDNINT((I*DE+J*F(K))/DE)
      W(L)=W(L)+RHH
      RHH=W(L)
160   CONTINUE
150   CONTINUE
140   CONTINUE
C     FOLD IN INTEGRATION TO FIND W(E).
      KMAX=NM-NN
      DO 200 K=1,KMAX
      W(K)=W(K)+W(K-1)
200   CONTINUE
240   CONTINUE
C
C     CALCULATE AK(E) AND PT(E) .
C
      DO 300 I=0,KMAX
      IF(KN.EQ.1) THEN
      AK(I)=0.D0
      DKL(I)=0.D0
      IF(RHB(I+NN).LE.1.D-20) GO TO 300
      AK(I)=2.897925D10*W(I)*DE/RHB(I+NN)
      DKL(I)=DLOG(AK(I))/ELLENTI
      ELSE
```

```
      AK(I)=FR*(I*DE/((NN+I)*DE+EZP))**(NF-1)*2.997925D10
      DKL(I)=DLOG(AK(I))/ELLENTI
      ENDIF
300   CONTINUE
      write(6,312) (L,DKL(L),L=0,KMAX,50)
      WRITE(6,304)
312   FORMAT(1x,i10,5x,f10.5)
304   FORMAT(4X,'L',11X,'RHO',13X,'W',12X,'AK',12X,'RHB')
      WRITE(6,305) (L,RHO(L+NN),W(L),AK(L),RHB(L+NN),L=0,KMAX,50)
305   FORMAT(16,4D16.6)
      fac=1.1961D-02
      DET=DE
      DEE=fac*DET
      DO 630 I=1,KMAX
630   AKL(L)=dlog10(AK(L))
      WRITE(7,650) ((I-1)*DEE,AKL(I),I=1,380,20)
650   FORMAT(2f9.2)
      WRITE(7,670) ((I-1)*DEE,AKL(I),I=400,kmax,400)
670   FORMAT(2f9.2)
c     700 CONTINUE
c     CLOSE(2)
      CLOSE(7)
C     CLOSE(8)
C     CLOSE(9)
      tid=etime(tarray)
      write(6,701) tid
701   format(1X,'total  time = ',D16.6)
      write(6,702) tarray(1)
702   format(1X,'user  time = ',D16.6)
      write(6,703) tarray(2)
703   format(1X,'system time = ',D16.6)
      STOP
      END
```